RIMs and RIM interacting proteins: localization and function under physiological and pathophysiological conditions

Dissertation

zur Erlangung des Doktorgrades (Dr. rer. Nat.)

der

Mathematisch-Naturwissenschaftlichen Fakultät der

Rheinischen Friedrich-Wilhelms-Universität Bonn

Vorgelegt von

Tobias Mittelstaedt

aus Aachen

Bonn 2010

Zusammenfassung

Die Exozytose synaptischer Vesikel findet an einem spezialisierten Bereich der präsynaptischen Nervenendigung statt. Eine Schlüsselkomponente des Proteinnetzwerkes dieses Aktive Zone genannten Bereiches sind die großen Multidomänenproteine RIM1 und RIM2. Als Adapterproteine interagieren sie simultan mit einer Vielzahl anderer an der Aktiven Zone angereicherter Proteine und verbinden diese unter anderem mit spannungsabhängigen Kalziumionenkanälen und synaptischen Vesikelproteinen. Neben der kompletten α-Variante von RIM1 und -2 existieren im Gehirn zwei weitere, kürzere RIM Isoformen (β und γ), die von den vier Genen RIM1-4 exprimiert werden (1α, 1β, 2α, 2β, 2γ, 3γ, 4γ). Von diesen verschiedenen RIM Isoformen war RIM1α das einzige, das zu Beginn dieses Projektes bereits detailliert erforscht war. Mit RIM1α defizienten Mäusen konnte gezeigt werden, dass RIM1α zur Induktion von Formen präsynaptischer Kurz- und Langzeitplastizität erforderlich ist. Pathologische Veränderungen der Effizienz dieser synaptischen Plastizität und Reizweiterleitung wurden in den letzten Jahren mit vielen neurologischen Erkrankungen in Verbindung gebracht, und scheinen z. B. zur Entstehung von Epilepsie beizutragen.

In dieser Arbeit sollten daher (1) die gemeinsamen und sich voneinander unterscheidenden Funktionen der verschiedenen α-RIM Proteine im normalen wie auch epileptischen Gehirn, sowie (2) die Veränderungen des präsynaptischen Proteinnetzwerkes im Verlauf der Epileptogenese untersucht werden.

(1) Zur Analyse der α-RIM Isoformen wurden Mäuse verwendet, denen entweder das RIM2α Protein oder sowohl RIM1α als auch -2α fehlten. Während RIM2α-defiziente Mäuse keinen physiologisch messbaren Phänotyp zeigten, erwies sich das Fehlen beider RIM-α Proteine als postnatal lethal. Dabei konnte gezeigt werden, dass sich zwar intakte synaptische Strukturen ausbildeten, die spannungs- bzw. Ca^{2+}-abhängige Neurotransmitterfreisetzung jedoch stark beeinträchtigt war.

(2) Zur Charakterisierung des präsynaptischen Proteinnetzwerkes wurden zunächst neuronalen Expressionsmuster an der Aktiven Zone angereicherter Proteine untersucht. Dabei konnte ein neues Mitglied der RIM-BP Familie beschrieben werden. Mit Hilfe eines Tiermodells für chronische Temporallappenepilepsie wurde dann die Expression der Proteinfamilien in verschiedenen hippokampalen Subregionen im Verlauf der Epileptogenese auf mRNA- und Proteinebene analysiert. Es konnte eine Vielzahl von Proteinen identifiziert werden, deren Expression durch die pathologisch gesteigerte synaptische Aktivität des primären epileptischen Anfalls, sowie auch im weiteren Verlauf der Epileptogenese signifikant verändert war.

Diese Arbeit trägt somit zum erweiterten Verständnis des präsynaptischen Vesikelfusionsapparates bei und liefert neue Erkenntnisse über die mögliche Funktion an der Aktiven Zone angereicherter Proteinfamilien in Reaktion auf gesteigerte synaptische Aktivität sowie während der Entstehung chonischer Epilepsie.

Table of Contents

Figures

Tables

Abbreviations

AB	antibody
AHS	Ammons' horn sclerosis
AMPA	α-amino-3-hydroxy-5-methyl-4-isoxazolepropionic acid
AMPAR	AMPA receptor
AON	anterior olfactory nucleus
APT	anterior pretectal nucleus
ATP	adenosine tri-phosphate
AZ	active zone
BG	basal ganglia
CA	cornu ammonis
cAMP-GEFII	guanine nucleotide-exchange factor II
CAZ	cytomatrix at the active zone
CB	cerebellum
cbw	cerebellar white matter
CC	coiled-coil domain
cDNA	complementary DNA
CO	colliculus
C-terminus	carboxyl terminus
CX	cortex
DAB	3,3'-Diaminobenzidine
dATP	deoxyadenosine triphosphate
DC	diencephalon
DNA	deoxyribonucleic acid
DG	dentate gyrus
DKO	double knockout
E18.5	embryo at day 18.5 after fertilization
EDTA	ethylenediaminetetraacetic acid
EGFP	enhanced green fluorescent protein
EPL	external plexiform layer
EST	expressed sequence tag
FNIII	Fibronectin III domain
FW	forward
GC	cerebellar granule cell layer
GFAP	Glial fibrillary acidic protein
GFP	green fluorescent protein
GL	glomerular layer
GRL	granule cell layer
GrO	granule layer of the olfactory bulb
HC	hippocampus
HE	Haematoxylin & Eosin staining
hGFAP	human GFAP
HI	hilus
HY	hypothalamic nuclei
IC	inferior colliculi
ICj	islands of Caleja
i.p.	intraperitoneal
ISH	in situ hybridization

kDa	kilo Dalton
KO	knockout
MB	midbrain
MCL	mitral cell layer
MeA	medial amygdaloid nucleus
MeAD	anterio-dorsal medial amygdaloid nucleus
mGluR	metabotropic glutamate receptors
MHb	medial habenular nucleus
Mi	mitral cells
ML	molecular layer
MO	medulla oblongata
mRNA	messenger RNA
MUN	Munc homology-domain
NMDA	N-methyl-D-aspartic acid
NMDAR	NMDA receptor
NMJ	neuro-muscular junction
N-terminus	amino-terminus
OB	olfactory bulb
Oligo	oligonucleotide
P28	day 28 after (post) birth
PAGE	polyacrylamide gel electrophoresis
PBS	phosphate buffered saline
PC	Purkinje cell
PCL	Purkinje cell layer
PCR	polymerase chain reaction
PDZ	PDZ-protein binding domain
PFA	paraformaldehyde
PKA	protein kinase A
Pn	pontine nucleus
PT	posterior thalamus
q-rtPCR	quantitative real time RT-PCR
REV	reverse
RIM	Rab interacting molecule
RNA	ribonucleic acid
RRP	rapidly-releasable pool
RT-PCR	reverse transcription PCR
SAM	sterile-α-motif interaction domain
SC	superior colliculi
s.c.	subcutaneous
SDS	sodiumdodecylsulfate
SE	Status epilepticus
SEM	standard error of the mean
SH3	Src homology 3 domain
SN	substantia nigra
SNAP	synaptosome associated protein
SNARE	soluble N-ethylmaleimide-sensitive factor (NSF) attachment protein receptors
Sr	stratum radiatum
SRP	slowly releasable pool
SSC	saline sodium citrate buffer
Stdev	standard deviation
sTn	subthalamic nucleus

STR	striatum
Syt	Synaptotagmin
TH	thalamus
TLE	temporal lobe epilepsy
TMD	transmembrane domain.
VCP	valosin containing protein
VP	ventral pallidum
WM	white matter regions
wt	wild type
ZI	zona incerta

URLs

BLAST	http://blast.ncbi.nlm.nih.gov/Blast.cgi
ClustalW	http://www.ebi.ac.uk.clustalw/index.html
Dialign	http://bibiserv.techfak.uni-bielefeld.de/dialign/
ENSEMBL	http://www.ensembl.org/
NCBI	http://www.nlm.nih.gov/
Phyml	http://atgc.lirmm.fr/phyml/
Sequence manipu-lation suite	http://www.ualberta.ca/~stothard/javascript/ident_sim.html
T-coffee	http://tcoffee.vital-it.ch/cgi-bin/Tcoffee/tcoffee_cgi/index.cgi
TIGR	http://www.tig.org/

1 Introduction

The human brain consists of at least 100 billion neurons, interconnected by a complex network of neuronal contacts. At these contact-sites, the synapses, information is passed on from one neuron to another. The most important mode of interneuronal communication, the fast, unidirectional synaptic transmission, is mediated by diffusion of secreted transmitter substances from the presynapse to postsynaptic receptors, located on the opposite side of the synaptic cleft.

The exocytosis of neurotransmitter filled vesicles at the presynaptic membrane is thought to be the fastest, most tightly regulated, and most spatially accurate membrane fusion event occurring in mammalian cells. The coupling of the electrical stimulus of an incoming action potential to the fusion of synaptic vesicles with the plasma membrane occurs within 1 ms (reviewed in Borst & Sakmann 1996, Sabatini & Regehr 1996). This process is highly dependent on the cytosolic Ca^{2+} concentration and spatially restricted to designated release cites at the presynaptic plasma membrane, the active zone (Schneggenburger & Neher 2005).

1.1 The Synaptic Vesicle Cycle
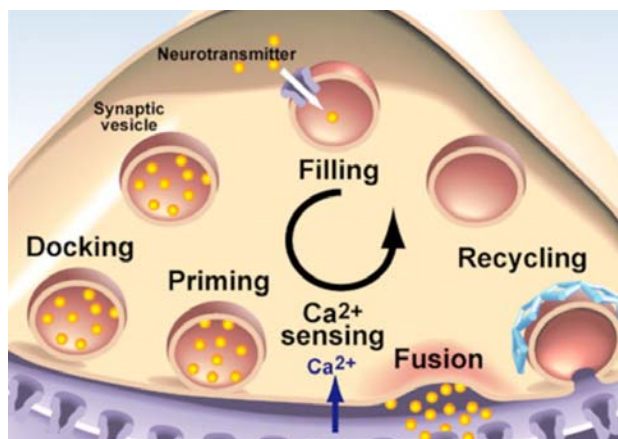
Figure 1.1: The synaptic vesicle cycle (from Weimer & Jorgensen 2003).

In order to maintain the high speed and accuracy of synaptic vesicle fusion, sufficient amounts of neurotransmitter-filled vesicles have to be available in the presynaptic nerve terminals at all times. Therefore, synaptic vesicles are recycled locally, a process called the "synaptic vesicle cycle" (**Fehler! Verweisquelle konnte nicht gefunden werden.**, see Südhof, 2004). The cycle resembles other cellular membrane-fusion processes and can be divided into five phases: (1) filling of synaptic vesicles with neurotransmitter, (2) docking and (3) priming at the presynaptic active zone, (4) fusion and (5) recycling through endocytosis, that itself can be further divided into several steps. (1) First, vesicular neurotransmitter – transporters

use a proton-electrochemical gradient generated by the vacuolar H^+-ATPase to fill synaptic vesicles with transmitter molecules (Liu et al. 1999). (2) Subsequently, the vesicles are directed towards the active zone, putatively via the vesicle-bound protein Synapsin that interacts with the synaptic Actin cytoskeleton (Siksou et al. 2009). (3) After docking at the active zone, the vesicles are rendered fusion-competent by a process called priming (Rizo & Rosenmund 2008). This maturation process involves interactions of the SNARE proteins, Syntaxin (target-/ t-SNARE), SNAP-25 and Synaptobrevin (vesicular-/ v-SNARE), with several effectors that are essential for fast Ca^{2+}-triggered release at the active zone (Figure 1.2). Required components for Ca^{2+}-triggered release are the SNARE-binding protein Munc18-1 (Deak et al. 2009), the putative Ca^{2+}- sensor Synaptotagmin-1 (Xu et al. 2009), as well as RIM1 and the priming protein Munc13, both central components of the protein network at the active zone (Betz et al. 2001, Schoch et al. 2002, Varoqueaux et al. 2002). Besides these essential proteins several other interaction partners of the pre-fusion complex have been described: Complexin interacts with the SNARE four helix bundle (Chen et al. 2002) to increase the performance of Ca^{2+}-triggered release and in the same time inhibits spontaneous fusion events ("minis") (Cai et al. 2008, Maximov et al. 2009), Tomosyn interferes with the priming process through its Syntaxin interaction, and further reduces priming efficiency by oligomerization of cis-SNARE complexes (Ashery et al. 2009).

Figure 1.2: Proteins involved in docking, priming and fusion of synaptic vesicles at the active zone.

(4) The fusion of synaptic vesicles is triggered by action potentials arriving at the synapse and subsequent depolarization of the membrane. The reversal of the electrical gradient across the presynaptic membrane leads to an opening of voltage gated Ca^{2+}-channels, allowing Ca^{2+} to enter the synapse and build up Ca^{2+}-microdomains in the immediate vicinity to the release machinery (Bucurenciu et al. 2008, Llinas et al. 1992). Synaptotagmin 1, which is present on synaptic vesicles and is associated with the fusion complex after priming, can bind five Ca^{2+}-ions with its two C2 domains, thereby increasing its affinity to phosphatidylinositol 4,5-bisphosphate (PIP_2) in the adjacent presynaptic membrane (Paddock et al. 2008). The following steps involving the SNARE complex as well as the accessory proteins described above (Figure 1.2) allow the vesicle to overcome the energy-barrier between vesicular and presynaptic membrane and form a fusion pore to release the transmitter substance into the synaptic cleft. (5) Although disputed for more than 15 years (Alvarez de Toledo et al. 1993, Balaji & Ryan 2007, Harata et al. 2006), recent data supports the view that the vesicle can subsequently be recycled following different pathways (Chen et al. 2008, Zhang et al. 2009). On the one hand, local SV reuse ("kiss-and-run") can take place at the AZ. Thereby SVs retrieve 0.5 – 1 second after transient fusion and transmitter-release. The "retracted", still fully docked vesicle is immediately re-acidified and refilled with transmitter within 1 second after closing of the fusion pore and is thereafter able to refuse again (Zhang et al. 2009). Alternatively, after "full-collapse fusion", vesicles flatten completely into the plasma membrane and must be replaced by newly generated vesicles. The vesicular membrane with its proteinaceous components of completely fused vesicles is taken up through endocytosis in the periphery of the active zone, removing all vesicular residues from the synaptic membrane (Bonanomi et al. 2006, Santos et al. 2009). It still remains unclear if or when the identity of each vesicle including most of their individual outfit of proteins and lipids is retained during endocytosis, or if several vesicles are taken up together in bulk and lose their individual composition. Individual endocytosed vesicles are assumed to perform several cycles of direct refill and fusion, but all synaptic vesicles are finally recycled through an endosomal intermediate, that provides a mechanism for intermixing and resorting of synaptic vesicle membrane proteins (Santos et al. 2009).

1.2 Architecture of the Active Zone

To guarantee the high speed and temporal precision of synaptic transmission, primed vesicles have to be located in close proximity to voltage-gated Ca^{2+}-channels at the active zone, and an adequate supply of synaptic vesicles has to be provided even under conditions of high synaptic activity. In addition, the active zone has to be able to adapt the effectiveness of synaptic transmission by dynamically changing its composition, organization and function in response to changes of synaptic activity. An understanding of the ultra-structure and composition of the active zone is therefore of great importance and has been analyzed in detail by electron microscopy since its discovery in the 1950's (Estable et al. 1954, Robertson 1953) (Figure 1.3). These studies revealed highly organized structures at both the neuromuscular junction as well as central nervous synapses (Figure 1.3B, C).

In an elegant study by Harlow et al (Harlow et al. 2001) examining the frog neuromuscular junction using electron tomography, the active zone appeared as a regular arrangement, with synaptic vesicles connected to voltage-gated Ca^{2+}-channels by so called pegs, ribs and beams (Figure 1.3B). Electron microscope analyses on aldehyde-fixed vertebrate tissue have also shown the presynaptic active zone to be regularly organized (Figure 1.3C), with an arrangement of electron-dense cone-shaped particles extending approximately 50 nm into the cytoplasm and filamentous strands reaching out far into the presynaptic cytoplasm (Zhai & Bellen 2004). A network of cytoskeletal filaments interconnects the cones, with synaptic vesicles residing in the vicinity of the conical thickenings. To reduce artifacts due to fixation of the tissue, in recent studies high pressure freezing was used instead of chemical fixatives (Weimer et al. 2006). With this method, the above-described conical regular arrangement of particles could not be confirmed in synapses of the CA1 region of the rat hippocampus. The electron-dense thickenings are rather irregularly distributed over the surface area of the active zone (Siksou et al. 2007). However, even with this method docked synaptic vesicles were found in the immediate vicinity of electron dense areas at the active zone (Figure 1.3D).
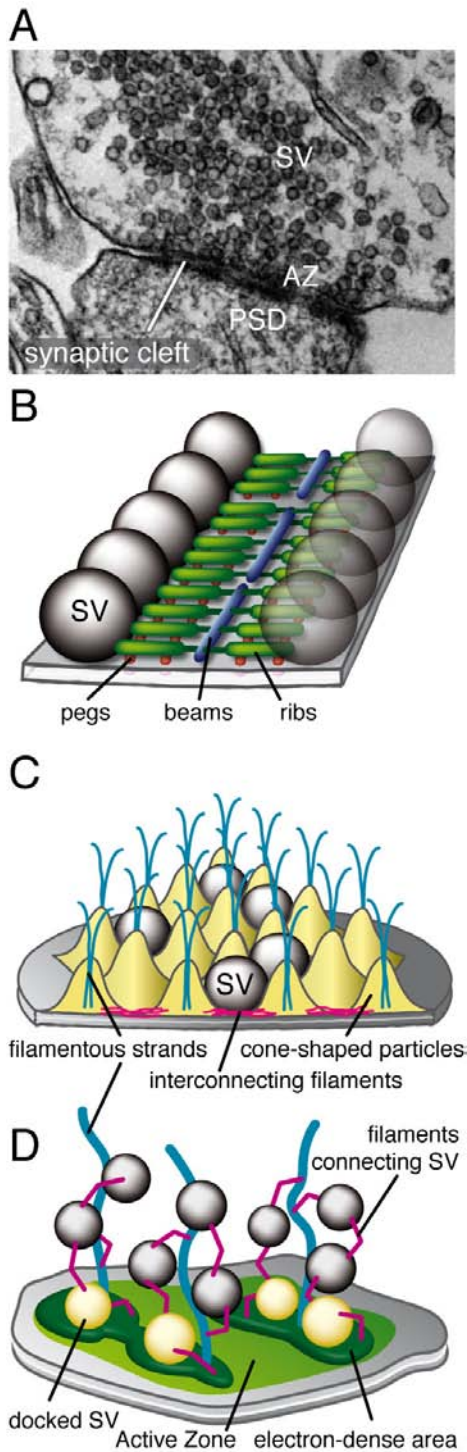
Figure 1.3: Evolving models of the active zone ultra-structure.

(**A**) Electron micrograph picture of a synapse. Synaptic vesicles (SV) are docked to the active zone (AZ). Opposing the AZ, the electron dense band of the postsynaptic density (PSD) on the other side of the synaptic cleft is visible. (B-D) Schemes of different models representing the three dimensional architecture of the presynaptic cytomatrix. (**B**) Reconstruction of the AZ at the frog neuromuscular junction after electron tomography (Harlow et al. 2001). Synaptic vesicles dock to a row of „ribs" (green) at the motor endplate of skeletal muscle innervating nerves. These ribs are interconnected by a different central structure, the „beams" (blue), and are anchored into the presynaptic membrane via short „ribs" (red). (**C**) At central nervous synapses, aldehyde fixated tissue revealed a different kind of organized structure (Zhai & Bellen 2004). Here, a hexagonal pattern of cone-like particles with interconnecting filaments was observed. Docked vesicles are located between the cones and filamentous strands reach out into the presynaptic cytoplasm, presumably leading SVs to their release sites. (**D**) Three dimensional reconstruction of AZ ultra-structure after electron tomography of presynaptic terminals contacting spines in the rat hippocampal CA1 area. To avoid fixation artifacts, hippocampal slices were preserved using high-pressure freezing, followed by cryo-substitution and embedding. Using this fixation method, a dense network of filaments interconnects the SVs. At the AZ, SVs are docked to presynaptic densities. Filaments with adjacent SVs emerge from these densities.

1.3   Active zone enriched and associated protein families

In addition to the proteins involved in membrane fusion, membrane conductance or other functional or structural components that are also present in other parts of the neuron, five protein families have been identified in the presynapse whose members are highly enriched at active zones: RIM (Rab3-interacting molecule), UNC13/Munc13, Bassoon and Piccolo/Akzonin, ELKS/Bruchpilot and Liprin-α. Through direct and indirect protein interactions, all active zone-enriched proteins are coupled and linked to the core fusion machinery (Figure 1.4). In recent years, studies using genetic, biochemical, structural and electrophysiological approaches have begun to elucidate how these proteins are involved in the regulation of synaptic vesicle exocytosis, in mediating use-dependent changes during different forms of plasticity and in the structural organization of the active zone (Schoch & Gundelfinger 2006).
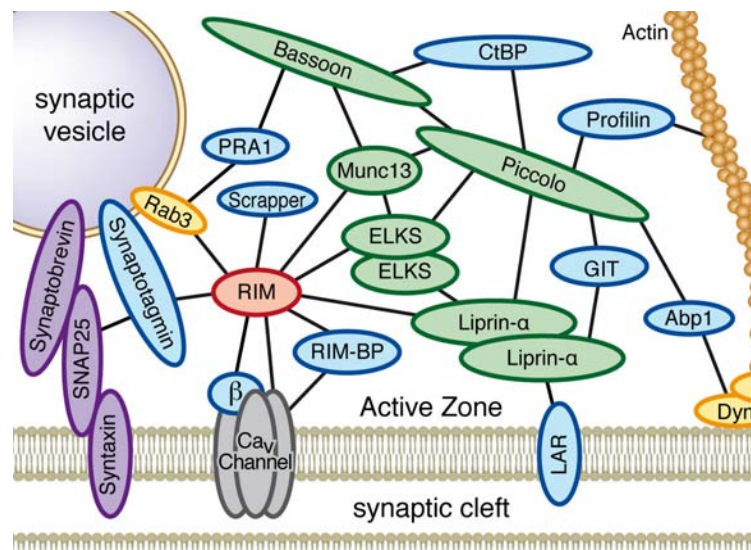
Figure 1.4: The protein network at the active zone

Active zone enriched protein families are depicted in green, interacting proteins in blue, SNARE-complex components in purple and GTPases in yellow. Abp1, Amiloride-binding protein; CtBP, C-terminal binding protein; Dyn, Dynamin; GIT, G protein-coupled receptor kinase-interactor; LAR, LCA Related protein tyrosine phosphatase; PRA, prenylated Rab acceptor.

1.3.1 α-RIMs – central components of the CAZ

The active zone is composed of a network of proteins that includes RIMs (Wang et al. 1997, Wang et al. 2000) as central components (Figure 1.4)(Castillo et al. 2002, Koushika et al. 2001, Schoch et al. 2002). RIMs are multidomain proteins that are expressed in variable forms. The two α-RIMs (RIM1α and 2α) include a

full complement of RIM domains: an N-terminal region that comprises a Rab3-binding sequence and a Munc13-binding zinc finger, a central PDZ-domain, and two C-terminal C2-domains that do not bind Ca^{2+} (Figure 1.5). The two β-RIMs (RIM1β and -2β) contain all of the domains of α-RIMs except for the N-terminal Rab3-binding sequence in RIM1β and both the Rab3-and the Munc13-binding sequence in RIM2β, and the three γ-RIMs (RIM2γ, -3γ, and -4γ) are composed of only of the C-terminal C2-domain preceded by a short N-terminal flanking sequence (Figure 1.5)(Kaeser et al. 2008a, Wang et al. 2000).
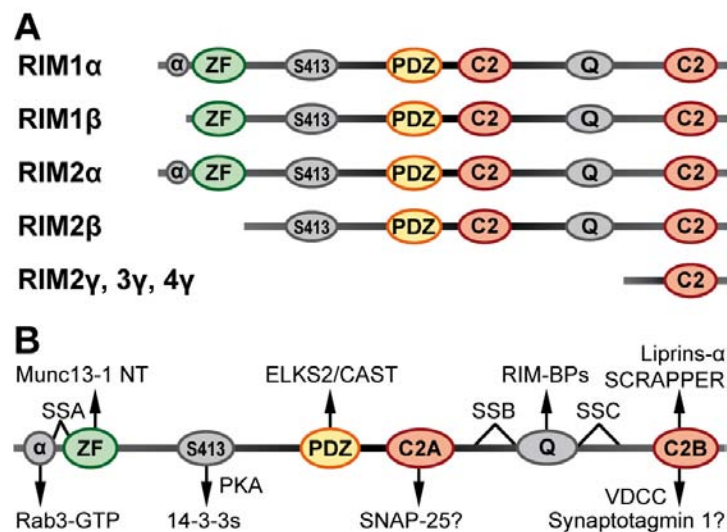
Figure 1.5: RIM family organization and protein interaction domains.

Colored areas mark conserved and functional domains. **A** Domain composition of the RIM iso-forms generated from the four RIM genes. **B** RIM protein interactions mediated by the different domains. (α) Helix α1; (C2) C2-domain / PKC conserved region 2; (PDZ) PDZ-domain / PSD-95, Dlg, and ZO-1/2 - like domain; (Q) Prolin rich sequence; (S413) Serine 413, phosphorylation site for PKA; (SSA, SSB, SSC) Splice sites in the RIM1 and RIM2 gene; (VDCC) β4 subunit of voltage dependent Ca2+-channel; (ZF) Zinc finger domain.

RIMs are encoded by four genes, of which the RIM3 and RIM4 genes generate only a single isoform (RIM3γ and RIM4γ, respectively), whereas the RIM1 gene expresses two (RIM1α and RIM1β), and the RIM2 gene expresses three iso-forms (RIM2α, 2β, and 2γ) (Kaeser et al. 2008a, Wang & Sudhof 2003). Further variation is introduced into α- and β-RIMs (but not γ-RIMs) by extensive alterna-tive splicing (Johnson et al. 2003, Wang et al. 2000, Wang & Sudhof 2003). In addition to interacting with Munc13 and Rab3, α -RIMs bind to multiple other synaptic proteins: ELKS via the central PDZ-domain (Ohtsuka et al. 2002, Wang et al. 2002), RIM-BPs via an SH3-domain binding sequence between the two C2-domains (Wang et al. 2000), and, via the C-terminal C2-domain, to α-

Liprins, Synaptotagmin 1, the synapse associated E3 ubiquitin ligase SCRAP-PER as well as the β-subunit of voltage gated Ca^{2+}-channels (Figure 1.5B and Figure 1.6) (Coppola et al. 2001, Kiyonaka et al. 2007, Schoch et al. 2002, Yao et al. 2007). The direct functional interaction of the RIM1 C-terminus and the β-subunit of voltage gated Ca^{2+}-channels (VDCCs) was shown to suppress voltage-dependent inactivation among different neuronal VDCCs and to anchor neurotransmitter containing vesicles in the vicinity of VDCCs (Kiyonaka et al. 2007). The ubiquitination of RIM by SCRAPPER has been shown to modulate synaptic plasticity (Yao et al. 2007). Furthermore, in vitro interactions with several proteins have been described, including cAMP-GEFII (guanine nucleotide-exchange factor II) (Ozaki et al. 2000), SNAP-25 (Coppola et al. 2001) and 14-3-3 adaptor proteins (Kaeser et al. 2008b, Simsek-Duran et al. 2004, Sun et al. 2003) and are connected indirectly with the active zone proteins Piccolo and
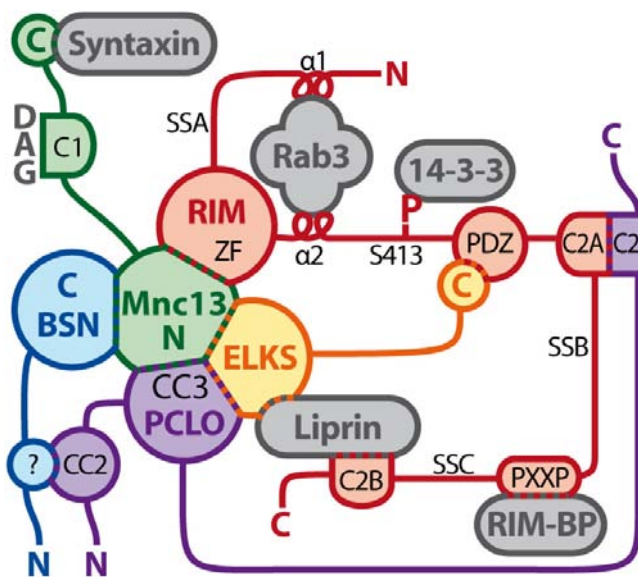
Figure 1.6: Schematic overview of the domain specific interactions of RIM with its interaction partners.

Besides the integral CAZ proteins Piccolo (PCLO), Bassoon (BSN), ELKS and Munc13-1 (Mnc13), additional connections of the different RIM interaction domains are included. (C) C-terminus; (C1) C1-domain; (C2) C2-domain; (CC) coiled-coil-domain; (DAG) Diacylglycerol; (α) α-helix; (N) N-terminus; (PDZ) PDZ-domain; (PxxP) proline rich SH3 interaction motif; (S413) Serine 413, phosphorylation site for PKA; (SSA, SSB, SSC) Splice sites in the RIM1 and RIM2 gene; (ZF) Zinc finger domain

Bassoon via ELKS (Takao-Rikitsu et al. 2004) and with receptor tyrosine phosphatases via Liprins (Serra-Pages et al. 1998). Of these interactions, the C2-domain of γ-RIMs binds to α-Liprins, Syt-1, SCRAPPER and Ca^{2+}-channels. The binding of the N-terminal region of α-RIMs contains two nested sub-domains, an α-helical region that binds to Rab3 (Wang et al. 2001b) and a zinc-finger that binds to Munc13 (Betz et al. 2001, Dulubova et al. 2005). This binding is mutually compatible with each other, resulting in a trimeric complex in which the α-RIM/Munc13 dimer on the active zone is coupled to the synaptic vesicle protein

Rab3 (Figure 1.6) (Dulubova et al. 2005). Finally, RIMs are substrates for cAMP-dependent protein kinase (PKA) that phosphorylates RIM1 and RIM2αβ at two sites (Lonart et al. 2003).

Analysis of RIM1α knockout (KO) mice showed that RIM1α plays a key regulatory role in synaptic vesicle exocytosis at the active zone, from vesicle priming to short- and long-term synaptic plasticity (Calakos et al. 2004, Castillo et al. 2002, Schoch et al. 2002). The interaction with Rab3A is essential for RIM function in presynaptic LTP, which has been shown to be dependent on RIM1α in the mossy fiber to CA3 pyramidal cell synapse (Castillo et al. 2002), the parallel fiber to Purkinje cell synapse (Castillo et al. 2002, Lonart et al. 2003), and the late phase of plasticity at the Schaffer collateral to CA1 pyramidal synapse (Huang et al. 2005). In synapses that show classic presynaptic PKA-dependent LTP (mossy fiber – CA3; parallel fiber – Purkinje cell), the basic properties of synaptic transmission are unaffected by the RIM1α KO. In synapses not capable of the classical presynaptic LTP, such as the CA3 to CA1 Schaffer collateral synapses in the hippocampus, impairments in basic release properties and in short-term plasticity can be observed in the RIM1α KO, resulting in a more severe phenotype than in Rab3 KO mice even when all four Rab3 isoforms are deleted (Schluter 2004). This implies additional functions of RIM1α beyond acting as a downstream effector for Rab3. The late NMDA receptor dependent LTP in Schaffer collateral synapses that is affected by the RIM1α KO is maintained beyond 2h after induction and depends on PKA activation, similar to presynaptic PKA dependent LTP (Huang et al. 2005). Although the late LTP is initialized independently of RIM1α phosphorylation, and requires postsynaptic NMDA receptor activation, its maintenance was shown to involve presynaptic PKA activation and RIM1α. RIM proteins are therefore potentially involved in more general changes of the presynaptic release machinery, like other forms of long-term plasticity requiring postsynaptic induction and presynaptic feedback mechanisms. Despite the severe LTP and STP phenotype, RIM1α deficient synapses do not exhibit major changes in ultra-structure, and RIM1α KO mice have a normal life expectancy (Schoch et al. 2002). The importance of RIM1α function nevertheless is apparent from the severe behavioral abnormalities observed in these mice that include impairments in spatial learning and in fear conditioning as well as an increase in locomotor responses to novelty (Powell et al. 2004).

1.3.2 Munc 13 – essential vesicle priming proteins specifically enriched at the active zone

The UNC13/Munc13- protein family is one of the components of the CAZ that has been characterized in most detail. UNC13 was identified in a study selecting nematodes of the type *Caenorhabditis elegans* for UNCoordinated movements (Maruyama & Brenner 1991). In mammals, four Munc13 genes (Munc13-1 to -4) can be found. The domain structure of Munc13 proteins differs only in the N-terminus from each other (Figure 1.7). In contrast to the other variants, Munc13-1 and ubMunc13-2, a ubiquitously expressed Munc13-2-variant of this otherwise brain-specific protein family, contain a binding-site for Ca^{2+} / Calmodulin and for the CAZ-enriched α-RIM proteins at their N-terminus (Figure 1.6). All Munc13 proteins contain a C1-domain, interacting with the secondary messenger diacylglycerol (DAG), and two C2-domains, as well as an area of high homology between all Munc13 proteins, the MUN domain (Koch et al. 2000), in their central and C-terminal region (Figure 1.7).
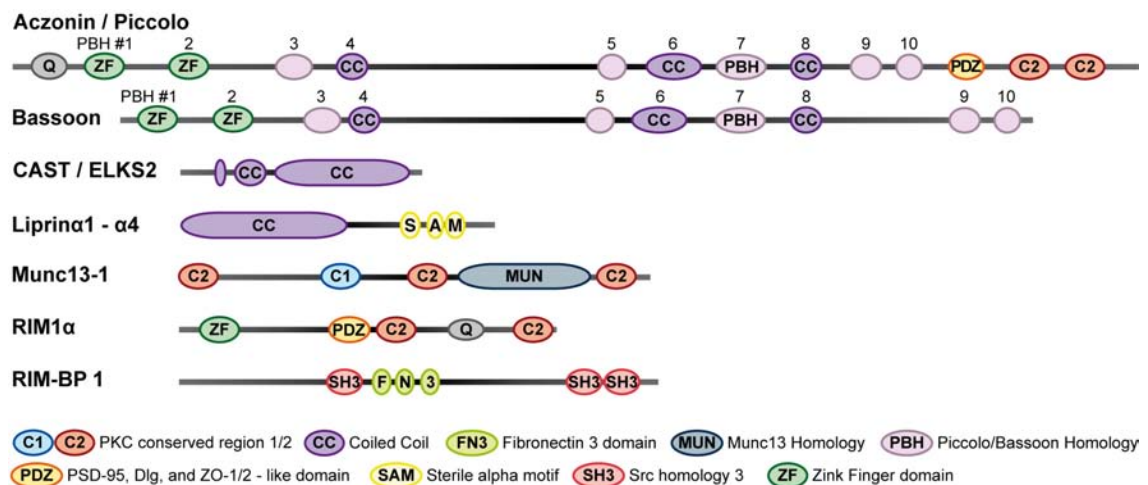
Figure 1.7: Protein domain structure and relative sizes of active zone enriched protein families.
Colored areas mark conserved and functional domains. All protein structures are depicted in N- to C-terminal direction. (C1) C1-domain / PKC conserved region 1; (C2) C2-domain / PKC conserved region 2; (CC) coiled-coil-domain; (MUN) Munc13 homology domain; (PBH) Piccolo/Bassoon homology domain; (PDZ) PDZ-domain / PSD-95, Dlg, and ZO-1/2 - like domain; (Q) Prolin rich sequence; (SAM) SAM domain / Sterile alpha motive domain; (SH3) SH3 interaction motif / Src homology 3 domain; (ZF) Zinc finger domain.

Munc13 is essential for the maturation process of synaptic vesicles to a fusion-ready state, called priming. This was illustrated by the total abrogation of spontaneous and evoked release observed upon deletion of Munc13-1 and the

closely related Munc13-2 in mice, or of the homologs in *C. elegans* and *Drosophila melanogaster* (Brose et al. 2000, Rosenmund et al. 2003). The priming activity of Munc13 is mediated by the C-terminus of the protein, including the MUN and a C2 domain (Stevens et al. 2005), whereas the MUN-domain alone is sufficient to rescue release in Munc13-1/2 double knockout mice (Basu et al. 2005). Also, a constitutively open mutant of the Munc13 binding partner Syntaxin partially rescues release in unc13 null mutants in C. elegans, suggesting a role for unc13 and Munc13s in the conformational transition of Syntaxin-1 during priming (Dulubova et al. 1999, Richmond et al. 2001). Since the MUN domain binds to membrane anchored SNARE complexes and to Syntaxin-1 – SNAP-25 heterodimers (Guan et al. 2008, Weninger et al. 2008), Munc13s could function in opening syntaxin-1, acting in concert with the SNARE binding protein Munc18-1 to form a syntaxin-1–SNAP-25 heterodimer and promote vesicle priming (see Figure 1.2). Electron microscopy studies on Munc13-null mutants of the nematode *C. elegans* showed that in the absence of Munc13 fewer synaptic vesicles are attached directly to the active zone (Weimer et al. 2006), also indicating that the synaptic vesicles contacting the membrane represent the morphological correlate of fusion ready primed vesicles.

The Munc13 isoforms also play a role in the regulation of short-term presynaptic plasticity. Interestingly, Munc13-1 and ub-Munc13-2 differ in this respect: while synapses only containing Munc13-1 show short-term depression upon high frequency stimulation, synapses expressing only ubMunc13-2 develop short term potentiation (Rosenmund et al. 2002). Binding of the C1 domain to diacylglycerol/phorbol ester (Figure 1.6) modifies Munc13 function, and the interaction with Ca^{2+} / Calmodulin that is essential for the function of Munc13 in the expression of short-term synaptic plasticity (Basu et al. 2007, Junge et al. 2004).

Since the phenotype of the *C. elegans* RIM homolog unc10 null mutants resembles the unc13 knockout (Weimer et al. 2006), and this phenotype can also be partially rescued by the open Syntaxin mutant (Koushika et al. 2001), unc10 and RIMs seem to play a role in vesicle priming that is functionally linked to unc13 and Munc13s. Such a link has been provided by the reduction in Munc13-1 levels observed in RIM1α knockout mice (Schoch et al. 2002), by the observation of a direct interaction between the N-terminal regions of RIM1α and Munc13-1 (Betz et al. 2001), and by the impairment of vesicle priming

(Dulubova et al. 2005) and presynaptic recruitment of Munc13 caused by interference with this interaction (Andrews-Zwilling et al. 2006).

Due to the fact that the Munc13 MUN domain directly controls the vesicular release probability (Basu et al. 2005), the various factors involved in distinct presynaptic plasticity processes may regulate release efficiency by altering intramolecular interactions of their receptor domains with the MUN domain and, as a consequence, its priming activity.

The generation of transgenic knock-in mice expressing a fusion protein of Munc13-1 and the enhanced yellow fluorescent protein (EYFP) enabled for the first time investigations concerning the dynamics of a CAZ-enriched protein (Kalla et al. 2006). Measurements at individual synapses showed that, even at the active zone, bound Munc13-1-EYFP rapidly and continuously disappears and reinserts from/into the CAZ. These observations indicate that the presynaptic active zone constitutes a highly dynamic structure.

1.3.3 The Proteins of the ELKS – Family

The 120 kDa proteins of the ELKS – family were identified both as a component of the fraction of insoluble pre- and postsynaptic complexes as well as binding partners for RIM proteins (Ohtsuka et al. 2002, Wang et al. 2002). In the first description of the gene, they were named after their high content of the amino acids glutamate (E) leucine (L), lysine (K) and serine (S) (Yokota et al. 2000) (synonyms: CAZ associated structural protein CAST; Rab6-interacting protein; ELKS/Rab6-interacting protein/CAST ERC). While there is only one ELKS gene in invertebrates, two very homologous genes have been discovered in the vertebrate genome. Interestingly, alternative splicing of the C-terminus of ELKS1 generates two different variants: ELKS1A (ERC1a), which occurs only outside the brain, and ELKS1B, which is exclusively expressed in neurons (Wang et al. 2002)(Figure 1.7). Recent studies have revealed that the ELKS2 gene encodes several proteins and splice variants as well: ELKS2α, previously named ELKS2/CAST, is a brain specific insoluble protein, which becomes detectable only after other synaptic proteins are synthesized (around embryonic day 14.5) (Schoch & Gundelfinger 2006). ELKS2β, produced by an internal promoter in the ELKS2 gene, is weakly expressed during postnatal development and becomes undetectable at day 20. In addition, ELKS2 can be alternatively spliced,

leading to two different variants, the full-length protein ELKS2B and a protein lacking the C-terminal RIM binding sequence, ELKS2A (Kaeser et al. 2009). Taken together, the ELKS2 gene encodes four main proteins ELKS2αA, ELKS2αB, ELKS2βA and ELKS2βB, of which ELKS2αB is the main one.

Apart from several consecutive double helix coiled-coil-domains, allowing ELKS to interact with α-Liprins and either Piccolo or Bassoon, the two neuronally expressed proteins include a specific C-terminal PDZ interacting motif (IWA) which binds to RIMs and the synaptic protein Syntenin-1 (Figure 1.6)(Schoch & Gundelfinger 2006). Through their direct interactions with the other CAZ enriched proteins as well as RIM, ELKS proteins constitute a central component of the protein network at the active zone. Interestingly, the ELKS homologue in *Drosophila*, Bruchpilot, differs from the structure of the vertebrate ELKS proteins: The N-terminal 480 amino acids show up to 67% homology to mouse and *C. elegans* ELKS. By contrast, no sequence homologies to the remaining 1260 amino acids, that show low similarity to cytoskeletal proteins, can be found in these organisms (Figure 1.7).

Fruit flies with a reduced amount of Bruchpilot due to RNA interference have morphological and functional defects, which result in a phenotype with severely restricted flight-ability. Deletion of a large part of the Bruchpilot gene causes the development of the animals to cease after the passage of the larval stage, and to not start pupation. In an elegant analysis using stimulated emission depletion fluorescence microscopy (STED), BRP was shown to be localized in donut shaped structures centered at active zones of neuromuscular synapses (Wagh et al. 2006). Suppression of Bruchpilot leads to a lack of expression of the characteristic electron-dense thickenings (T-bars), and hence to a reduction in the density of calcium channels. Furthermore, a reduction of action potential induced neurotransmitter release and short-term changes in synaptic plasticity can be observed (Kittel et al. 2006). These results suggested that Bruchpilot is crucial to the molecular processes involved in the coupling between synaptic vesicles and Ca^{2+} channels, and thus plays an important role for the organization and function of the active zone. In contrast, ELKS deficient *C. elegans* do not show functional disturbances (Deken et al. 2005).

In mammals, ELKS2 had been found to be enriched in the insoluble postsynaptic density fraction and to be exclusively localized at the presynaptic active zone

(Ohtsuka et al. 2002). ELKS1B is generally enriched in the synaptic plasma membrane, but can also be detected in the soluble cytoplasmic fraction, and ELKS1A is largely cytosolic (Wang et al. 2002). Immuno-electron microscopy in ribbon synapses of the retina revealed that ELKS2 is localized at the base of ribbons, whereas ELKS1B was detected around the ribbons (Deguchi-Tawarada et al. 2006). Recent studies analyzing the function of ELKS in mutant mice have shown that deletion of ELKS1 is lethal, whereas ELKS2 ablation does not impair survival (Kaeser et al. 2009). Electrophysiological analyses of the ELKS2 KO revealed that ELKS2 affects synaptic transmission in inhibitory but not in excitatory neurons. Deletion of ELKS2 induces an enlargement of the RRP in inhibitory synapses, thereby increasing synaptic strength without causing detectable impairments in other synaptic parameters, except for a small decrease in synaptic vesicle numbers. Additionally, no significant ultrastructure changes were detected in neurons lacking ELKS2, indicating that ELKS are not essential for a correct formation of the active zone in mammals (Kaeser et al. 2009).

1.3.4 Bassoon and Piccolo - presynaptic cytomatrix scaffolding proteins

In contrast to the rest of CAZ enriched proteins, Bassoon and Piccolo / Akzonin are not evolutionary conserved and can only be found in vertebrates. The two very large proteins (420 and 530 kDa) consist of a variety of protein-protein interaction domains (Schoch & Gundelfinger 2006), among these are ten regions of high sequence homology, called Piccolo Bassoon homology domains (PBH, Figure 1.7). Furthermore, there are two N-terminal zinc finger and several double-helix domains (coiled coil). Piccolo additionally possesses a PDZ and two C2-domains with a certain homology to the C2-domains of RIM in its C-terminus (Figure 1.7). In recent years, interaction partners for a number of the structural domains have been identified, such as the also CAZ enriched ELKS, PRA1 (prenylated Rab acceptor), GIT1 (G-protein coupled receptor kinase interacting protein, a GTPases activating protein for ARF-GTPases), proteins of the CtBP family (C-terminal Binding Protein / Connected to Bassoon and Piccolo), including the in the retina and cochlear hair cells expressed protein Ribeye, as well as components of the Actin cytoskeleton (Figure 1.4).

Piccolo binds to Abp1, which in turn interacts with Dynamin and Actin. A disruption of this interaction affects the Clathrin mediated endocytosis of synaptic vesicle recycling (**Fehler! Verweisquelle konnte nicht gefunden werden.**). Via these protein interactions, Piccolo could constitute a functional link of the CAZ with the dynamic Actin cytoskeleton and the recycling of synaptic vesicles in the peripheral zone of the active zone (Fenster et al. 2003). The Piccolo C2A domain acts as a low affinity Ca^{2+}-sensor that leads to a conformational change and dimerization of piccolo in the presence of high Ca^{2+} concentration (Garcia et al. 2004). In a study using RNAi to knockdown piccolo in cultured hippocampal neurons, it was found to negatively regulate the translocation of SVs from the reserve to the RRP through a CaMKII dependent modulation of Synapsin dynamics, resulting in an enhanced rate of SV exocytosis in the knockdown. This functional role of Piccolo has not been shown to be shared by Bassoon, which seems to have a more structural importance at the presynapse. In mice expressing a shortened version of Bassoon, a significant proportion of glutamatergic synapses is inactive, while in the remaining synapses no functional differences from control synapses can be found (Altrock et al. 2003). Despite this mild phenotype the mutant animals develop an epileptic phenotype, accompanied by an enlargement of the hippocampus and cerebral cortex and a reduction in neuronal density in layer V of the cortex (Angenstein et al. 2008). Interestingly, the ribbon structure in the CAZ of retinal photoreceptors and cochlear inner hair cells are disconnected from the active zone in Bassoon defective mouse mutants. They rather move freely in the cytoplasm of the presynapses that show strongly disrupted transmitter release. Thus Bassoon seems to play an essential role in anchoring the ribbons to the active zone (Dick et al. 2003, Khimich et al. 2005).

1.3.5 The Liprin-α protein family

α-Liprins, first described as cytoplasmic binding partners for the "leukocyte common antigen related" (LAR) receptor protein tyrosine phosphatase (RPTPase), are not exclusively localized at the presynaptic active zone (Serra-Pages et al. 1998). Nevertheless, studies in *C. elegans* and *Drosophila* suggest that the protein family is crucially involved in its assembly and structural organization (Kaufmann et al. 2002, Stryker & Johnson 2007, Zhen & Jin 1999). The

four Liprin-α variants in mammals, Liprin-α1-4, and the homologous proteins syd-2 in *C. elegans* and Dliprin in *Drosophila* are characterized by an unusually strong evolutionary conservation. All Liprin-α proteins consist of a N-terminal double-helical structure (coiled coil domain) and three C-terminal SAM domains (sterile-α motif) as well as a PDZ-domain binding motif binding to the adaptor protein GRIP1 (Figure 1.7)(Wyszynski et al. 2002). Alternative splicing at the C-terminus of Liprin-α1 and Liprin-α4 results in two shorter isoforms not able to bind GRIP (glutamate receptor interacting protein) anymore (Zurner & Schoch 2009). All α-Liprins interact with a variety of proteins through the SAM domains, such as the LAR receptor protein tyrosine phosphatases (LAR-RPTPs), the MAGUK protein CASK, the Ca^{2+} / Calmodulin dependent protein kinase II (CaMKII) and β-Liprins (Spangler & Hoogenraad 2007, Stryker & Johnson 2007). Additionally, the SAM domains of Liprin-α were shown to interact with ATP (Serra-Pages et al. 2005), and SAM domains in general are known to bind to RNA (Green et al. 2003) and lipid membranes (Barrera et al. 2003). The diverse range of SAM domain interactions alone makes Liprin proteins attractive candidates for linking a multitude of cellular components into large protein complexes. The N-terminal coiled coil domain allows Liprin-α the formation of dimers and binds to the C-terminal C2B-domain of RIM (Figure 1.6)(Schoch et al. 2002), the N-terminal coiled-coil domain of ELKS, the GTPase activating protein GIT1 (Ko et al. 2003) and the motor protein KIF1A (Shin et al. 2003), a neuron specific kinesin-3 capable of transporting synaptic vesicle proteins such as Synaptophysin, Synaptotagmin and Rab3 (Okada et al. 1995) (Figure 1.4). Through their binding partners, α-Liprins are directly linked to essential components of the active zone and the postsynaptic density as well as the machinery for vesicular transport. Liprin-α/syd-2 deficient mutants in *C. elegans* show a diffuse distribution of synaptic vesicles, severe disturbances in the morphology of the active zone and disruption of synaptic transmission (Zhen & Jin 1999). The *Drosophila* Liprin-α homologue Dliprin-α is also necessary for the correct assembly and the maintenance of the active zone and plays a role in the formation of new synaptic connections at the neuromuscular contact sites (Kaufmann et al. 2002). The KIF1A interaction was also confirmed in *Drosophila*, where defective synaptic vesicle movement as well as impaired synaptic transmission was observed in vivo in Liprin-α mutant flies, suggesting a presynaptic defect

(Kaufmann et al. 2002, Miller et al. 2005). In general, Liprin-α colocalizes in vertebrate neurons at the active zone with ELKS and RIM, but is present at the postsynaptic density as well, and appears to be of importance for the morphogenesis and function of synapses (Dunah et al. 2005).

1.3.6 RIM Binding Proteins at the active zone

As mentioned above, a close proximity between voltage gated Ca^{2+}-channels and the presynaptic release machinery is vital for the fast and accurate action potential triggered transmitter release at the active zone. An interesting candidate to constitute a functional and structural link between Ca^{2+}-channels and the synaptic vesicle tethering apparatus is the RIM-BP ("RIM-binding protein") family (Hibino et al. 2002, Wang et al. 2000). RIM-BPs were shown to interact simultaneously with L- or N-type Ca^{2+}-channels and the active zone proteins RIM1 and RIM2 (Figure 1.6)(Hibino et al. 2002, Wang et al. 2000). RIM-BPs are large multidomain proteins and constitute a novel class of proteins. All RIM-BPs contain three SH3-domains, two to three contiguous Fibronectin type III-domains, and isoform specific regions at the N-terminus and between the clustered domains (Figure 4.22). The RIM-BP SH3-domains bind to PXXP-motifs present in RIM1 and RIM2 (RQLPQL/VP) as well as Ca^{2+}-channel $\alpha_{1D/F}$ and $\alpha_{1B/A}$ subunits (RLLPPTP, RQOPQTP, respectively). Further α_1 subunits ($\alpha_{1C/E/G}$) contain potential interaction motifs. Therefore, RIM-BPs are therefore ideal candidates to act as a bifunctional linker between different types of Ca^{2+}-channels and the synaptic vesicle release machinery. In addition, their domain structure suggests that they provide a scaffold for further regulatory proteins. However, RIM-BPs have not yet been studied in detail, and not much is known about this protein family.

1.4   The Synaptotagmin gene family

Accumulating evidence in the recent years point to the synaptic vesicle protein Synaptotagmin-1 (Syt-1) as the main Ca^{2+}-sensor for fast evoked neurotransmitter release at the synapse (Chapman 2008, Fernandez-Chacon et al. 2001, Geppert et al. 1994, Shin et al. 2009, Sun et al. 2007). Syt-1 is the most extensively studied member of a large protein family of 15 Synaptotagmin isoforms in the mammalian genome, that are all composed of a short intravesicular amino

terminus, a transmembrane domain, a variable linker region, and two conserved C-terminal C2-domains that potentially bind Ca^{2+} and/or phospholipids. Synaptotagmins can be classified according to their biochemical properties and by sequence homology (Craxton 2001, Craxton 2004, Sudhof 2002). The individual Synaptotagmins exhibit diverging affinities for Ca^{2+} and phospholipids. Besides Syt-1, most other Synaptotagmin isoforms bind Ca^{2+} via C2-domains (Figure 1.8). Only Syt-4, -8 and -11 to -15 do not bind Ca^{2+} (Bhalla et al. 2005, Bhalla et al. 2008, Li et al. 1995a, Li et al. 1995b, Sugita et al. 2002). Furthermore, several Synaptotagmins have been localized to distinct subcellular compartments. Whereas Syt-1, -2, -9, and -12 are found on synaptic vesicles (Sudhof 2002, Takamori et al. 2006), Syt-3, -6 and -7 are predominantly localized at the synaptic plasma membrane (Butz et al. 1999, Han et al. 2004, Sugita et al. 2001, Virmani et al. 2003).
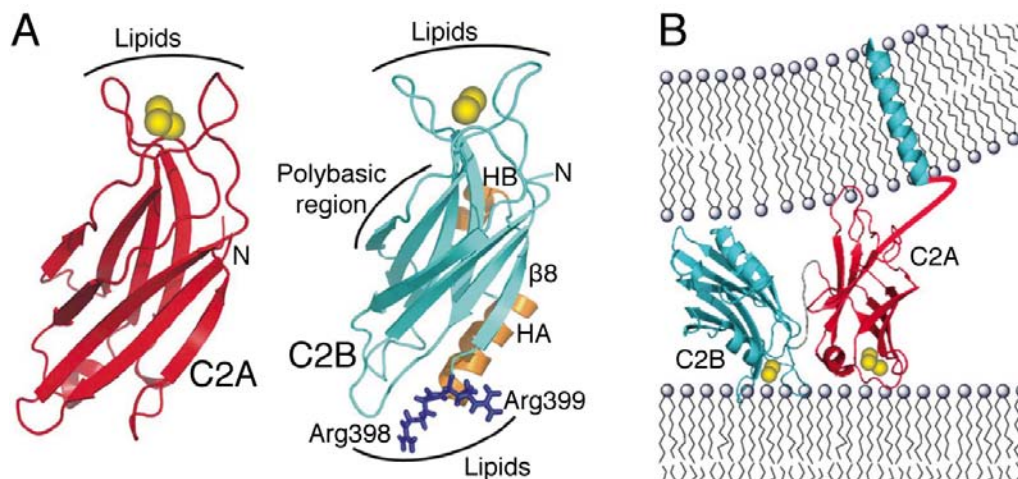
Figure 1.8: Model depicting the domain structure and lipid interaction of Synaptotagmin 1 (modified from Herrick et al. 2009, Xue et al. 2008).
(A) Crystal structure of the cytoplasmic domain of Syt-1. Ca^{2+}-ions are depicted as yellow spheres, helices HA and HB of the C2B domain are colored orange, and Arg398 and Arg399 are shown in blue stick model. Strand β8 of the C2B domain is labeled. The lipid binding sites of both C2 domains are indicated. The binding site for the SNARE complex is assumed to be in the polybasic region on the side of the C2B domain β-sandwich (Xue et al. 2008). (B) Typical Synaptotagmin structure with N-terminal transmembrane domain and C-terminal C2A and C2B domain here shown for Syt-1, that has bound five Ca^{2+}-ions in its C2 domains, increasing the binding affinity to the presynaptic membrane (from Herrick et al. 2009).

The subcellular localization of several Synaptotagmins remains still unknown or controversial. For example, Syt-7 was described to be present on large dense core vesicles (Fukuda et al. 2004, Gauthier et al. 2008, Wang et al. 2005), and at the plasma membrane of neurons or lysosomes (Martinez et al. 2000, Sugita

et al. 2001). Syt-4 was found to be predominantly expressed in astrocytes and to be absent from nerve terminals (Zhang et al. 2004), whereas in other reports it was detected on vesicular structures in neurons and PC12 cells (Fukuda & Yamamoto 2004, Ting et al. 2006, Wang et al. 2001a, Wang et al. 2003), and in *Drosophila* it localizes to the postsynaptic compartment (Adolfsen et al. 2004). Interestingly, the vesicular localization of Syt-4 in PC12-cells was recently shown to be phosphorylation dependent (Mori et al. 2008). The expression of individual Synaptotagmins in the central nervous system (CNS) has been shown by Northern and Western blot analyses, and the regional distribution of some Synaptotagmin isoforms (Syt-1, -2, -3, -4, -9) in the rat or mouse brain has been determined at the transcript and/or protein level (Berton et al. 1997, Fox & Sanes 2007, Marqueze et al. 1995, Maximov et al. 2007, Xu et al. 2007). However, the precise spatial localization of other Synaptotagmin genes, e.g. Syt-5, -6, -7, -10, -12 and -13, is still unresolved. Syt-14 and Syt-15 have been shown to lack expression in the brain (Fukuda 2003a, Fukuda 2003b).

Synaptotagmins (Syts) are evolutionary conserved, besides 15 isoforms in humans and rodents, seven isoforms have been identified in *Drosophila* (Adolfsen & Littleton 2001) which share the common structural organization of N-terminal transmembrane domain (TMD) and two C-terminal C2 domains (http://smart.embl.de, Figure 1.8). The C2 domains of Syt-1, the major Ca^{2+}-sensor for fast synchronous neurotransmitter release (Chapman 2008, Geppert et al. 1994), are able to attach to the presynaptic membrane and change the protein conformation and membrane interaction properties in response to Ca^{2+}-binding at five Ca^{2+}-binding sites (Kuo et al. 2009, Xu et al. 2009). The function of Syt-1 is thought to be conserved in invertebrates (Jorgensen et al. 1995, Mackler et al. 2002, Yoshihara & Littleton 2002). Several studies in vertebrates showed that Syt-2 and -9 also mediate fast Ca^{2+}-triggering of release in neurons. However, release induced by each isoform differs in its kinetics and apparent Ca^{2+} sensitivity (Nagy et al. 2006, Pang et al. 2006a, Pang et al. 2006b, Xu et al. 2007). In contrast, Syt-12 was found to be a modulator of spontaneous synaptic vesicle fusion (Maximov et al. 2007). In chromaffin cells and pancreatic alpha- and beta-cells, Syt-7 is the major Ca^{2+} sensor for exocytosis and accounts, in concert with Syt-1, for most of the Ca^{2+} triggered exocytosis in these cells (Gustavsson et al. 2009, Schonn et al. 2008). The release properties of a

neuron therefore seem to be defined by the subset of Synaptotagmins, which it expresses.

1.5   Synaptic Plasticity

Synapses are highly complex and dynamic structures that are required to continuously remodeled during learning and memory formation. Remodeling of synaptic properties is also evoked through neural insults, neurodegenerative diseases and other disorders affecting neuronal activity patterns. However, each synapse is part of a complex network of excitation and inhibition, and the activity dependent scaling of individual synapses has to stay within the boundaries to ensure a functional network. Resulting long-lasting changes in the excitability of individual neuronal circuits are thought to be the correlate to an adaptive behavior or strengthening of a memory (Kandel 2001).

Already more than 50 years ago, a plastic synapse, that can be modified in strength and efficiency to favor some neuronal pathways within a circuit and weaken others was proposed to be related to these changes (Hebb 1949). Later electrophysiological studies by Katz and colleagues (reviewed in Katz 1969) established that the strength of a connection is fundamentally dependent on three main factors: (1) the number of synaptic contacts; (2) the size of the postsynaptic depolarization caused by the neurotransmitter release from a single synaptic vesicle (the so-called quantal size); and (3) the probability of neurotransmitter release from the active zone of each synapse (p_r).

However, since the first experimentally observed forms of synaptic plasticity in mammals (Bliss & Lomo 1973), it was argued if these changes occur on the presynaptic or postsynaptic side (Nicoll et al. 1988, Regehr & Tank 1991). Within the single synapse, postsynaptic plasticity can occur by changing the number, types, or properties of neurotransmitter receptors. In recent years, regulated trafficking of ionotropic glutamate receptors of the AMPA-type (AMPARs) was identified as a common mechanism underlying activity induced changes in excitatory synaptic transmission (Collingridge & Singer 1990, Malinow & Malenka 2002, Newpher & Ehlers 2008). AMPARs form the main class of ion channels in excitatory synapses that transmit signals in response to binding of the neurotransmitter glutamate, while channels of the NMDA-type are essential for most postsynaptic types of second messenger mediated long-term

changes in synaptic transmission: long-term potentiation to strengthen the connection (LTP), and long-term depression to reduce transmission efficiency (LTD). Many different pathways for the regulation of onset or magnitude of LTP and LTD have been described, including additional or alternative activation of metabotropic glutamate and GABA receptors (mGluRs and GABA$_B$Rs) (Kamikubo et al. 2007, Kelly et al. 2009), but the addition and removal of post-synaptic AMPA-receptors or -subunits appears to be the main common mechanism to control the strength of the excitatory postsynapse (Bredt & Nicoll 2003, Collingridge & Singer 1990). The incorporation of additional ionotropic receptors into the postsynaptic density, placing them directly opposite to the presynaptic active zone, can be divided into an early phase (E-LTP) lasting only one to two hours, and a late phase (L-LTP), that requires stronger stimulation and persists for many hours. The induction of early LTP depends on protein modifications, for instance subunit phosphorylation, and leads to the recruitment of preexisting receptors from perisynaptic membrane or internal compartments to the post-synaptic density (Yudowski et al. 2007). Late LTP, on the other hand, requires synthesis of new proteins from preexisting mRNAs at the synapse, or even new gene transcription (Costa-Mattioli et al. 2007, Kandel 2001, Sutton & Schuman 2006). This can even initiate the formation of new synapses, in addition to the strengthening of preexistent ones (Knott & Holtmaat 2008).

The postsynaptic NMDA dependent form of LTP commonly depends on coincident presynaptic and postsynaptic activity, being only induced if synaptic release occurs during postsynaptic depolarization (Bliss & Collingridge 1993). In contrast to this NMDAR dependent LTP, also solely or predominantly presynaptic forms of LTP can be found in various regions of the brain. The first presynaptic LTP has been described in the hippocampus at synapses between axons of the dentate gyrus granule cells (mossy fibers) and the proximal apical dendrites of CA3 pyramidal cells (Nicoll & Malenka 1995, Nicoll & Schmitz 2005). Since then, several other mechanistically similar forms resembling mossy fiber LTP have been found in other brain regions: in the thalamus at cortico-thalamic synapses (Castro-Alamancos & Calcagnotto 1999), in the cerebellum at parallel fiber – Purkinje cell synapses (Linden 1997, Salin et al. 1996), and potentially in the striatum at cortico-striatal synapses (Spencer & Murphy 2002). This presyn-

aptically triggered and expressed form of LTP may therefore play multiple functional roles in the brain.

In most experiments demonstrating presynaptic LTP, it is triggered by high frequency tetanic stimulation, causing a large, activity dependent increase in Ca^{2+} concentration within the presynaptic axon terminal (Nicoll & Malenka 1995, Nicoll & Schmitz 2005). Voltage gated Ca^{2+}-channels account for the main source of the presynaptic Ca^{2+} increase, although the triggering of LTP at mossy fiber synapses can be facilitated by the activation of presynaptic kainate receptors, particularly by GluR6 (Lauri et al. 2001, Schmitz et al. 2003). Pharmacological manipulations and the analysis of knockout mice led to the hypothesis that the increase in presynaptic Ca^{2+} concentration activates a Ca^{2+}/Calmodulin dependent adenylyl cyclase, leading to an increase in presynaptic cAMP. This results in an activation of phospho-kinase A (PKA), which phosphorylates critical presynaptic substrates, thereby causing a long lasting enhancement in transmitter release (Huang & Kandel 1994, Nicoll & Malenka 1995, Nicoll & Schmitz 2005). Besides this course of action, that is consistent with most of the results from synapses that have been reported to express presynaptic LTP, a very different trans-synaptic signaling mechanism has been proposed for mossy fiber synapses. It implicates interactions between postsynaptic EphB receptor tyrosine kinases and presynaptic B-Ephrin ligands, leading to a long lasting enhancement of transmitter release (Armstrong 2006, Contractor et al. 2002). Additionally, also a heterosynaptic type of plasticity can be found in specific synapses. It is NMDAR dependent, but is completely independent of postsynaptic activity and requires the simultaneous activity of two synapses converging from two different brain regions, i.e. cortical and thalamic inputs into the lateral amygdala. This heterosynaptic LTP is specifically induced at the cortical synapse, while the thalamic synapse show common postsynaptic LRP, and can be inhibited by presynaptic $GABA_{B(1a)}$ receptor activation (Humeau et al. 2003, Shaban et al. 2006).

Consistent with del Castillo's and Katzs' theory of synaptic transmission, an increase in P_r is generally agreed to be the correlate for presynaptic LTP. One mechanism to mediate a long lasting increase in transmitter release is to enlarge the Ca^{2+} influx into the presynaptic terminal in response to an action potential via a long lasting modulation of presynaptic Ca^{2+}-channel subunits. How-

ever, direct measurements of the action potential dependent increase in pre-synaptic Ca^{2+} concentration imaged with Ca^{2+}-sensitive dyes in mossy fiber boutons indicated that no change occurs following the triggering of presynaptic LTP (Kamiya et al. 2002, Regehr & Tank 1991). Therefore, other changes have to account for the increase in P_r. Interestingly, it has been shown that in addition to an increase in P_r, new release sites and previously silent synapses are activated by mossy fiber LTP induction (Enoki et al. 2009, Reid et al. 2004).

Another putative mechanism to enhance P_r is a modulation of the synaptic vesicle release machinery. Therefore, knockout mice have been studied that lack specific presynaptic proteins known to be substrates for PKA, the second messenger kinase strongly linked to LTP. Mice lacking Synapsins-I or –II exhibited normal mossy-LTP, indicating that these PKA substrates were not necessary (Rosahl et al. 1995). In contrast, knockout animals lacking the small GTPase Rab3A, that is located on synaptic vesicles (Castillo et al. 1997), or its binding partner and PKA substrate, the active zone protein Rim1α lack mossy-LTP as well as presynaptic LTP in the cerebellum (Castillo et al. 2002, Powell et al. 2004). These findings have been complemented by a study showing that heterosynaptic plasticity from cortical synapses in the lateral amygdala completely depends on a persistent increase in P_r, and that both cAMP/PKA as well as RIM1α are required for presynaptic LTP (Fourcaudot et al. 2008). Very recently, a similar PKA/RIM1α dependent mechanism for the potentiation of inhibitory GABAergic synapses was postulated, requiring the activation of presynaptic NMDA channels to increase Ca^{2+} concentration in the synaptic terminal (Lachamp et al. 2009).

Furthermore, the discovery of a switch in glutamatergic synapses, that transforms an active presynapse into a silent synapse revealed an additional presynaptic mode of plasticity (Moulder et al. 2003, Moulder et al. 2004). This activity dependent homeostatic mechanism, that is not present in GABAergic synapses, is activated through acute and long-term rises of extracellular [K+], that can be observed during epileptic seizures, ischemia or brain trauma (Moulder et al. 2004). Already at normal levels of activity, a proportion of hippocampal synapses remains silent and can be activated through block of electrical activity, while modest depolarization decreases the percentage of active synapses (Moulder et al. 2006a, Moulder et al. 2006b). Recently, an activation of the

cAMP pathway was identified to activate silent synapses. While the major Ca^{2+} sensitive adenylyl cyclases AC1 and AC8 are not essential to maintain the balance between presynaptically silent and active synapses, AC8 is of crucial importance for rapidly resetting the balance after adaptation to strong activity (Moulder et al. 2008).

1.5.1 An experimental animal model of Temporal Lobe Epilepsy:

A model to study proteins involved in synaptic plasticity in vivo

A transient insult such as a single episode of status epilepticus (SE) can induce multiple structural and functional alterations (collectively referred to as epileptogenesis) that, after a latent period of several weeks, ultimately lead to chronic epilepsy (Scharfman 2007). During the process of epileptogenesis neurons experience pathophysiological electric activity, associated with an imbalance between excitation and inhibition. The resulting chronic epileptic condition is characterized by changes in synaptic plasticity, including alterations in synaptic efficacy, ultimately rendering the brain in a state that generates spontaneous epileptic seizures. In hippocampal primary neurons brief pathophysiological depolarization causes a persistent depression that is mediated by the presynaptic release machinery (Moulder et al. 2004). The physiological processes underlying these changes have been shown to reflect intrinsic properties of the presynapse (Moulder et al. 2006b). An animal model of epilepsy could therefore be used to examine the consequences of strong pathophysiological synaptic activity on the composition of the presynapse.
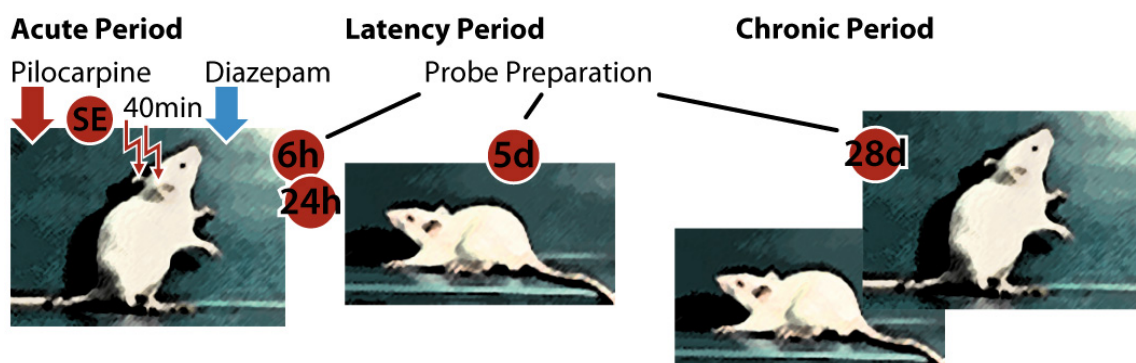
Figure 1.9: The Pilocarpine model of Temporal Lobe Epilepsy (TLE)
A *status epilepticus* (SE) is evoked through pilocarpine injection and leads to acquired cellular plasticity and neurodegeneration accompanied by cellular reorganization during a latency period, culminating in the development of chronic epileptic seizures.

A commonly used model of epilepsy imitates the so-called mesial temporal lobe epilepsy (TLE), a focal epilepsy located in the hippocampus affecting 75-80% of human patients suffering from complex partial seizures. It can be reproduced in animals using *status epilepticus* (SE) animal models (Dam 1992, Morimoto et al. 2004, Wieser & Hane 2004). The method used in this study, the pilocarpine model, belongs to the SE models. It appears to be highly isomorphic with the human disease, and therefore has been used in many laboratories since its first description 25 years ago (Turski et al. 1983). One important feature of the pilocarpine model are the sequential behavioral and physiological changes that can be divided into 3 distinct periods: (1) an acute period that builds up progressively into a limbic status epilepticus terminated after 40min., (2) a latent period with a progressive normalization of EEG and behavior of around 14 to 21 days, followed by (3) a chronic period with spontaneous recurrent seizures (Figure 1.9). This process is associated with neuronal network reorganization in hippocampal and parahippocampal regions: mossy fiber sprouting, interneuron loss and ectopic dentate granule cell proliferation are phenomena shared by TLE patients and pilocarpine treated animals (Blumcke et al. 2002).

The ability of pilocarpine to induce SE likely depends on synergistic activation of metabotropic glutamate receptors (mGluRs) and muscarinic acetylcholine receptors (mAChR) (Moore et al. 2009). Experiments in cultured hippocampal neurons had previously demonstrated that pilocarpine, acting through muscarinic receptors, causes an imbalance between excitatory and inhibitory transmission resulting in the generation of SE-like discharge patterns in the cultured neuronal network (Priel & Albuquerque 2002).

2   Aims

RIM1α, a central active zone protein that has been shown to be essential for evoked vesicle release and synaptic plasticity, is integrated into the CAZ network through various interactions. However, so far little is known about the neuronal distribution and function of the various members of the RIM family and RIM interacting proteins. The goals of this study were:

1. To examine the functional interplay of the two highly homologous α -RIMS, RIM1α and RIM2α.

2. To determine the regional distribution of RIMs and RIM interacting proteins, in particular α-Liprins and RIM-BPs, as well as the Synaptotagmin family.

3. To analyze the influence of pathophysiological synaptic activity on the composition of the active zone.

2.1   The function of α-RIMs

It has been shown that various RIM isoforms are coexpressed in the brain, but their relative expression patterns are unknown, and the potential redundancy between the various RIM isoforms is unresolved. Such redundancy could exist, for example, between RIM1α and RIM2α because both of these RIM isoforms bind to Munc13 and to Rab3 (Dulubova et al. 2005). Therefore, major questions remain unanswered: (1) In which cell types are the various RIM isoforms expressed? (2) Are RIM1α and RIM2α functionally redundant? (3) How do the two α -RIMs relate to each other? (4) Does the deletion of both α-RIMs lead to ultrastructural changes? To examine the role of the α-RIMs in synaptic transmission, single and double KO mice (DKO) lacking either RIM2α or both α-RIMs were biochemically and immuno-histochemically characterized.

2.2   Localization of RIMs and RIM binding proteins

2.2.1   α-Liprins

Several studies about the potential pre- and postsynaptic functions of α-Liprins have already been carried out, supporting their role in trafficking of synapse components as well as in Active Zone and PSD organization (Spangler & Hoogenraad 2007). Nevertheless, to date the regional and subcellular distribution of the Liprin-α family has not been published yet. Therefore in situ hybridizations were performed on sagittal and horizontal rat brain slices of adult (p28) and newborn (p0) rats with radioactive probes detecting Liprin1α – 4α.

2.2.2 Synaptotagmins

Only the functions of Syt-1, -2, -9, and -7 have been studied in detail so far. To gain further insight into the functional roles of the other Synaptotagmins it will be crucial to answer the following questions: (1) How many Synaptotagmins are universally expressed in all neurons as opposed to those that are specifically enriched in specialized areas of the brain? (2) How many and which Synaptotagmin isoforms are coexpressed by individual neurons? As it has been suggested that the complement of Synaptotagmins present within an individual cell determines its functional properties this is of particular importance. In the present study, these questions have been addressed by employing a systematic analysis of expression using radioactive *in situ* hybridization and quantitative real time RT-PCR.

2.2.3 The Rim-BP Protein family

So far RIM-BPs have only been studied in vertebrates, where products of only two genes have been described (Hibino et al. 2002, Wang et al. 2000). In view of the potential importance of the RIM-BP gene family for the structural organization of the presynaptic active zone, comparative and phylogenetic analyses with RIM-BPs were carried out, leading to the discovery of the new family member RIM-BP3. The gene organization including exon/intron structure and sites of alternative splicing was determined to allow further biochemical studies of the three RIM-BP genes. Finally, expression profiles of all three RIM-BPs during development and in different mouse tissues, as well as their regional distribution in the brain was evaluated.

2.3 Effect of pathophysiological synaptic activity on the composition of the presynaptic release machinery

The expression of several presynaptic proteins has been shown to be influenced by pathologically increased synaptic activity. The present work was delineated to study if individual members of the Synaptotagmin family as well as other gene families of the presynaptic release machinery show similar differential regulation in response to increased synaptic activity. Therefore, the progressive changes in the mRNA expression levels of these genes in the hippocampus of rats submitted to the pilocarpine model of epilepsy were evaluated. In addition to studying the time course of expression during the acute, the silent and the chronic phase after SE in the hippocampal subfields, CA1, CA3, and dentate gyrus (DG) by quantitative real-time RT-PCR, the most significant findings on the protein level were verified by quantitative immunoblotting.

3 Materials and Methods

3.1 Animal experiments

Animal studies were carried out on the brains of male Wistar rats (Charles River, Sulzfeld, Germany) and RIM1α and RIM2α knockout mice in a B6 x SV129G background. Animals were considered to be adult at the age of 28 days. Rats and knockout mice were anesthetized by Isofluorane (Baxter, Deerfield, IL, USA) inhalation prior to decapitation.

3.1.1 Genotyping

Genotyping was performed by PCR on DNA extracted from tail tissue with the Sigma GenElute kit according to the included protocol (G1N 350 1KT, Sigma-Aldrich, Germany). 1 μl of the purified DNA solution was used as template in the following PCR reaction (Table 3.1).

Table 3.1: Sequences of primers used for the RIM1α and RIM2α genotyping PCR reactions

Gene	Oligo	Reaction	Sequence	Annealing Temp.	Amplicon length
RIM1α	74	wt FW	GGTCCCCCTGTCCACTCAG	57°C	
RIM1α	78	wt RV	GCAGTGATGGACCGGCAG		350bp
RIM1α	169	KO FW	TTCGGGTTGCTGGATGTGT	57°C	
neomycin	172	KO RV	GTGACGCCCTTTATAGATTCGC		450bp
RIM2α	93	wt FW	AGAAAGGCCGAGCTCATGG	55-57°C	
RIM2α	94	wt RV	TGCACAAGTCTGATGACCCAA		203bp
RIM2α	27	KO FW	TTAAACCAGCCATACCTCAAATCC	55°C	
RIM2α	28	KO RV	AGGGATTTTATGACTGATTTCTAT		600bp

3.1.2 Whole body staining

For the whole body staining embryos at the age of E18,5 (one day before birth) were prepared from the mother's uteri and eviscerated. Afterwards they were immersion fixated in absolute ethanol for four days and acetone for three days, followed by several washes in water. The embryos were stained in a solution containing 0.015% alcian blue and 0.005% alizarin red, 5% acetic acid and 93% ethanol for 10 days, rinsed in water, and were then kept in a solution of 20% glycerol and 1% KOH for 16 h at 37°C. Afterwards, pictures of water submerged

embryos were taken with a digital camera and samples were stored in 20% glycerol at 4°C.

3.1.3 The pilocarpine model of Temporal Lobe Epilepsy

Experiments assessing the regulatory alterations of synaptic proteins after strong pathological synaptic activity were performed on male laboratory Wistar Rats (Charles River). The rats where acquired with a weight of approximately 140-160 g corresponding to ~30 d of age and kept in the animal facility for at least 48 h before the treatment. At the day of the experiment each animal was marked with a number, weighed, and then injected intraperitoneally with 1 mg/kg body weight scopolamine methylnitrate diluted in Ringer. Scopolamine methylnitrate acts as a cholinergic antagonist that primarily attenuates peripheral actions of pilocarpine. 30 min after the injection the rats were subcutaneously injected with 340 mg/kg body weight pilocarpine-hydrochloride (pilocarpine) diluted in aqua ad injectabilia to induce epileptic seizures. During the following hour the rats were monitored for the occurrence of tonic clonic seizures that mostly appear 15-30 min after the pilocarpine injection. When seizures persisted for 5-10 min the rats were considered to have fallen into self sustained Status Epilepticus (SE) starting from the onset of the seizure. These rats were then placed into a separate cage where observation was continued to ensure the rats did not recover from the Status. Rats that did not enter SE one hour after the first injections were injected for a second time with the initial dose of pilocarpine. After 40 min in self sustained Status Epilepticus the animals were injected subcutaneously with 0.8 ml Diazepam and 1 ml 5% glucose. Rats that did not enter Status Epilepticus two hours after the first injection were killed. The pilocarpine treated rats were then housed in single cages until they were used for the experiments. In all experiments pilocarpine treated or epileptic rats were compared to sham control rats. These control animals were also weighed and injected with appropriate doses of scopolamine methylnitrate and 1-2 h later with Diazepam and 5% Glucose.

3.2   DNA methods

3.2.1 cDNA preparation

Total RNA was extracted from whole brain of different developmental stages, various tissues or microdissected brain regions after homogenization in TRI reagent (Sigma-Aldrich, Germany) using the SV Total RNA isolation system (Promega, Madison, WI). Due to the small amount of recovered tissue, the RNA extraction from microdissected hippocampal subregions of pilocarpinized rats was performed using the Dynabeads Oligo(dT)$_{25}$ kit (Invitrogen, Carlsbad, CA). RNA samples were stored at -80°C. Reverse transcription was carried out using 5 µg of total RNA and the Superscript RT III kit (Invitrogen, Carlsbad, CA) with random hexamer primers or 1 µl of Dynabeads derived mRNA solution with oligo(dT) primers.

3.2.2 cDNA cloning

To clone the RIM-BP3 gene, cDNA was prepared from adult mouse testis total RNA using the Superscript RT III kit (Invitrogen, Carlsbad, CA, USA). PCR primers were designed based on UTR sequences for primary amplification (5' – 3':   FW   `TCTCTCTGGCTTCTTGCCGGGCTGCG`,   RV `TGTTGGGCCACCGGATGCCATACCC`). The PCR product was cloned into the pcDNA 3.1-TOPO vector (Invitrogen, Carlsbad, CA, USA) and sequence veri-fied.

3.2.3 Sequence analysis

The National Center for Biotechnology Information (NCBI) (http://www.nlm.nih.gov/), the ENSEMBL (http://www.ensembl.org/), and the TIGR gene indices (http://www.tig.org/) databases were searched using homol-ogy BLAST with standard settings. Searches for splice variants were conducted using EST databases. Multiple alignments were performed using T-coffee (http://tcoffee.vital-it.ch/cgi-bin/Tcoffee/tcoffee_cgi/index.cgi), ClustalW (http://www.ebi.ac.uk.clustalw/index.html) and Dialign (http://bibiserv.techfak.uni-bielefeld.de/dialign/) (Morgenstern 2004). Phyloge-netic analyses were conducted with Phyml Online (http://atgc.lirmm.fr/phyml/) using standard settings with 100 bootstraps and the WAG substitution model for sequence evolution (Whelan & Goldman 2001).

3.2.4 Real time RT-PCR

The relative expression levels of the various genes were assessed by quantita-
tive real time RT-PCR on the ABI Prism 9700HT sequence detection system
(PE Applied Biosystems, Foster City, CA, USA) using either SYBR Green
(Qiagen, Hilden, Germany) or fluorescently labeled sequence specific probes
(biomers.net, Ulm, Germany) as detection method. PCR oligonucleotide primers
and probes were selected using Primer Express (PE Applied Biosystems, Fos-
ter City, CA, USA) and typically flanked a segment of approximately 100-150
bases. Primer assays used for SYBR Green detection were purchased from
Qiagen. The sequences or catalogue numbers of all primer pairs and probes
are given in Table 3.3. Each SYBR Green reaction consisted of 6.25 µl 2x
SYBR Green PCR Master Mix, 0.375 µl forward primer (10 pM), 0.375 µl re-
verse primer (10 pM), and up to 5.5 µl template cDNA. The amount of template
cDNA was calculated after a test run with freshly prepared samples to deter-
mine the concentration required for equal Synaptophysin CTs of 18 to 20.
Primer/Probe reactions were run as follows: TaqGold activation at 95°C for 10
min, followed by 50 cycles of 20s at 95°C, 30s at 59°C and 40s at 72°C. After
extensive testing of the three housekeepers Actin, Synaptophysin and Hy-
poxanthine phosphoribosyltransferase 1 (Hprt1), Synaptophysin was chosen as
a normalization control for all reactions (if not stated otherwise). The expression
level of the genes was calculated using the formula $z = (ProbeCT) - (Synapto-
physinCT)$; relative Probe expression $= 2^{\wedge}(-z)$.

Table 3.2: Sequences of the alternative Synaptotagmin primer pairs and probes used for real time RT-PCR

Gene	Position	Orientation	Sequence (5' – 3')
Syt-1	729	FW	TGGGAAAGCTCCAATATTCA
Syt-1	730	RV	GACTTTGACGTATGGATCGG
Syt-1	731	Probe	TCCAGGCTGCTGAACTGCCC
Syt-2	654	FW	CCGCTTCTCTAAGCATGACA
Syt-2	655	RV	CGCCTTGTAGGTCTCTCCAT
Syt-2	675	Probe	ACCTTGGCCAGCCCATCGAG
Syt-3	656	FW	CAGAGATGCTGGCTAACCCT
Syt-3	657	RV	GCCTAGACCAGACCCTCACT
Syt-3	676	Probe	CAATCCTTTGCCGCCCTTGG
Syt-4	475	FW	CATGGCTCCTATCACCACCAG
Syt-4	476	RV	GAAGACGAGGCCAAAAGCACT
Syt-4	477	Probe	CGCGTGGAATTCGATGAAATTCCCA
Syt-5	658	FW	CAGGTATTGGACAAGCACCA
Syt-5	659	RV	AAGATGCCTACCAGGAGCTG
Syt-5	677	Probe	TCCAGTGAATACTGCAGTCGGCCT
Syt-6	660	FW	TACTATGTGATGGGCGGAGA
Syt-6	661	RV	TCCATAACGGAGATGAGCAG
Syt-6	678	Probe	TCAACCCTGTCTACAACGAGGCCA
Syt-7	662	FW	CACCGTGAAAGTCATGAAGG
Syt-7	663	RV	ATTCTTCCGTTTCACCTTGG
Syt-7	679	Probe	AGCTGCCGGCCAAGGACTTC
Syt-8	664	FW	CTGTGCTGGTGGTGTGTGT
Syt-8	665	RV	CCAATAGCTGCACCTTCAGA
Syt-8	680	Probe	CCACCAGCAGAGCTGCCCAA
Syt-9	666	FW	AGCCTGCTAACTCTCGTGGT
Syt-9	667	RV	AGCACAGTTTCCAAGACACG
Syt-9	681	Probe	ACCGCCTGTGGTCTTGCCCT
Syt-10	750	FW	GCACGGAACCTGTCTTACAA
Syt-10	751	RV	CCCTCGGAGTCAACTGATTT
Syt-10	752	Probe	TCCTCCCGATGCTGGTTCTGG
Syt-11	668	FW	CTGTGCTGGTGGTGTGTGT
Syt-11	669	RV	GGGTCTTGTGCTTCTTCTCC
Syt-11	682	Probe	ACATGCTGCCACCAGCAGGC
Syt-12	732	FW	ATGGGAGGAAGATGAGCAAG
Syt-12	733	RV	GGAGAGACAGGTCCTGAAGC
Syt-12	734	Probe	TCATCCCTCTTCACCGCCGTC
Syt-13	735	FW	AGGTGACCTTGAAACACCAG
Syt-13	736	RV	TGATCATCTCATTCCACACG
Syt-13	737	Probe	CGGGCCAAGCACAAGATCAA
Synaptophysin	472	FW	TCCTGCAGAACAAGTACCGAGA
Synaptophysin	473	RV	GCGAACACTGCTGTGGCC
Synaptophysin	474	Probe	AACAACAAAGGGCCAATGATGGACTTCC

Table 3.3: Qiagen catalogue numbers of the primer pairs and probes used for real time RT-PCR

Gene	Catalogue Nr.
Bassoon	QT00392350
GIT1	QT01084783
LCBP1	QT00410060
Liprin1α	QT01594712
Liprin2α	QT01616839
Liprin3α	QT01577415
Liprin4α	QT01596756
Munc13-1	QT01082438
Munc13-2ub	QT01082431
Piccolo	QT00194418
PTP	QT00195048
RIM-BP1	QT00413707
RIM-BP2	QT00441532
RIM1α	QT00179067
RIM2α	QT01082165
RIM2γ	QT00190701
RIM3γ	QT00191079
RIM4γ	QT00194971
Synaptotagmin 1	QT01573019
Synaptotagmin 2	QT00193151
Synaptotagmin 3	QT00191989
Synaptotagmin 4	QT00195664
Synaptotagmin 5	QT00184065
Synaptotagmin 6	QT00410480
Synaptotagmin 7	QT00195601
Synaptotagmin 8	QT00400841
Synaptotagmin 9	QT00184884
Synaptotagmin 10	QT01569043
Synaptotagmin 11	QT00178185
Synaptotagmin 12	QT00179816
Actin	QT00442029
GapDH	QT00199633
Synaptophysin	QT00179879

Table 3.4: Sequences of the primer pairs used for real time RT-PCR SYBR Green essays

Gene	Primer-#	Position	Sequence (5' – 3')
RIM-BP1	482	4784 FW	CCAGATCCTCAAGGTGTTT
RIM-BP1	483	4913 RV	TGTCTCCCTGTTGGAGTGTC
RIM-BP1	574	1662 FW	GTGAGGGTCTTTGTGGCTCT
RIM-BP1	575	1772 RV	AAACACCTTGAGGAGTTGGC
RIM-BP2	484	310 FW	GGCTCAGGTTGAAGCTAAGAA
RIM-BP2	485	435 RV	TTAAACTGCTCGCTTTGCAC
RIM-BP2	486	2443 FW	CTTCCTGAAAGGGTCAGAGC
RIM-BP2	487	2559 RV	TCCTCCTCATCTTCCTCCAT
RIM-BP3	488	881 FW	AGGCTTCTGAATCCGAGGTA
RIM-BP3	489	1018 RV	GCTTGTTCTCGGAGCTTTCT
RIM-BP3	490	2077 FW	ACCACCCAAGCTTCAGAGTC
RIM-BP3	491	2177 RV	TGTATGTCCCTGGTAGGCAA
RIM-BP3	566	881 FW	AGGCTTCTGAATCCGAGGTA
RIM-BP3	567	1018 RV	GCTTGTTCTCGGAGCTTTCT
RIM-BP3	568	2270 FW	AGTCTCTGGACTCCAAACCG
RIM-BP3	569	2398 RV	CCACTTCACTTGCTGTGTCC
Liprin-α1	421	1783 FW	TGTCGATGTGTCTGATGGTG
Liprin-α1	422	1928 RV	TCAGCCTGATCTCTTTGTTGA
Liprin-α2	423	2596 FW	GCCGTCAGAATGACTCACACC
Liprin-α2	424	2689 RV	TGGCACTGCCAAGCCC
Liprin-α3	431	3023 FW	TCCACAGGGTTAGTCTGCAC
Liprin-α3	432	3135 RV	CATCACGTCTCTGATTTGGG
Liprin-α4	433	2339 FW	GCCATGTTCTGCTCACAGAC
Liprin-α4	434	2453 RV	TCAAGCAGCTGGTGTTTCTT

3.2.5 In situ Hybridization

Male Wistar rats (4 weeks old) were anaesthetized and decapitated. The brains were removed and quickly frozen in TissueTek (Sakura Finetek) over isopentane/liquid nitrogen. Sections were cut at 12 mm on a cryostat, thaw-mounted on silane coated slides, fixed with 4% (w/v) paraformaldehyde in PBS, dehydrated, and stored under ethanol until hybridization. Each section was hybridized for 15-20 h in 150µl hybridization buffer (50 % deionized formamide / 10% (v/v) dextrane sulphate / 0.3 M NaCl / 30 mM Tris/HCl (pH 8) / 4 mM EDTA / 1x Denhardt's / 0.4 mg/ml polyadenylic acid / 0.5 mg/ml denatured salmon sperm DNA) containing the amount of radiolabeled probe equating to 400,000 counts. The oligonucleotide probes were generated with terminal transferase (Fermentas) using [35S]dATP (Amersham Biosciences, Freiburg, Germany), probes were only used if the activity measured with a scintillation counter exceeded 250,000 counts per µl. See Table 3.5 for antisense oligonucleotide sequences. Optimal oligonucleotide sequences (45-mers, 50-60% GC, low hairpin and dimer forma-

tion probability) were selected by using Oligo 6.7 (Cascade, CO, USA). In control experiments, hybridizations were performed with a 1000-fold excess of the respective unlabelled oligonucleotide. After hybridization sections were washed twice with 1x SSC / 0.1% (v/v) 2-mercaptoethanol at room temperature for 20 min, once with 1x SSC / 0.1% (v/v) 2-mercaptoethanol at 57 °C for 45 min, once with 1x SSC at room temperature for 5 min, and once with 0.1x SSC at room temperature for 2 min. Sections were then dehydrated, airdried and exposed to Kodak BioMax film (Eastman Kodak, New Haven, CT, USA) for 2 weeks at room temperature. For analysis with brightfield optics, slides were then dipped in photographic emulsion (LM1; Amersham Biosciences/ NBT2, Kodak), incubated for 8-10 weeks and developed in Kodak D-19 developer for 3.5 min. and to confirm cytoarchitecture, sections were counterstained with H&E.

Table 3.5: Oligonicleotides used for *in situ* hybridization

Gene	Position	Sequence
Liprin1α	1805R	TCCCAGTCCTGTTCATTGAGGGTCTGCACCTTGGAGGGCTCGTCC
Liprin1α	2419R	TTGCTCACGGGACCATCCTGGGAGCCTGTGGAGTTCCTCAGATCC
Liprin2α	2584R	GGGTGTGAGTCATTCTGATGGCTCTGGGTGTTGGGGGAGGAGAAG
Liprin2α	53R	CGTTGGCTCATTGGGGTGTCCTCATTAATCGTGGGCATCACTTCG
Liprin3α	2350R	TGTCTCCTGGAATGGCTGGACCCTCCCCTCGTGGAACACCGGCTT
Liprin3α	869R	CCATCCCCATCCTTGCCCGGCTCCTCCAGTCCTGACCGCCTTCTA
Liprin4α	1095R	ACAGCTCCTGCAGATGCCGGGCTTTCTCCTCACACTGGCGGTGCA
Liprin4α	1922R	ATGGAGCCACGCTTGCGCAGCTGGGTCAGGTTGAGGGCCTCCATG
RIM1α	902R	TTTGTCCTCATTGTTCGATCGCAGAGACACACGGCCTCCGCAGCG
RIM1α	1381R	CGGGTTGCACCACAGACTTGGGGACACGTTTGCGCTCGCTCTTCT
RIM2α	536R	GCTGCTGCGGTGTATTAGACCCACTATTGTAAAACCACGCGCCCG
RIM2α	745R	CTGAAGGCATGTCACTGGCGATCTGGTGCTTCATTCCTGAGCCAT
RIM2β	111R	AAACCCCATGGAAATGAGATAAAACAGAATTGCAGACCTGGCGCA
RIM2β	194R	GGACACTGACGGACTTCTTTTTCTTGCATTGTTCAGCGTTTGTCC
RIM2γ	311R	CCAGGGAGTTCATACAAGGAAAATAGCCAGCTAGAGCCTCAAAGG
RIM2γ	337R	ACCTCCTCCTTCTCCTTCATCTTCTTCCAGGGAGTTCATACAAGG
RIM-BP1	405R	ACAGCGCTGTTGCAGCTCTCCTAGGGCCCTCAGCAGCTCCAGATT
RIM-BP1	3064R	GCCCATCAGCATAGACTGCGTAGCCTGTAACCCGGACACCATTGG
RIM-BP2	327R	TCCGGTGGGGCCCTCGTGACCTTTGTGGATGGAAGTGGCTAGTCC
RIM-BP2	2545R	AGCGGGTCATAGTCAAACAGAGCAACGAAGATGCGGGCCGGGAGC
Syt-1	639R	ACTGGCTGGCTCAGTGGCATTGTGTGGGACAAGGGTCGCAACAGT
Syt-1	955R	GAATGACAACAGTCAGTTTGCCGGCAGTAGGGACGTAGCGGAGGG
Syt-2	517R	AGCCTGCAGGACGCCCACGGTGAGCTGGTTGGCTTGGAAATCATA
Syt-2	2374R	CTACTCCGGCTACCATCACTGAGGGTCAAAGGGTCCAGAGGGTCA
Syt-3	823R	TCAGCAAATGGTGGATGGTGGGCTGGGTGTGCATGATGGTGCGGA

Syt-3	1689R	TGAGCTCCCCAAGATCTGCCTTTTCCGAGCCACCCTCCAGGATGT
Syt-4	989R	CAGGACGGTGAAGTGCAGGGACAGCTCTTGGATGTGGGGATAAGG
Syt-4	1551R	GGTGGCCAGGAAGCTAACCATCACAGAGCATATGCCACTTAGCAA
Syt-5	703R	AGTGTGGATTCAGGGTCTGCCGATGCACCTTGGTCTCATGTCGCC
Syt-5	1139R	TGGTCACAGGGCACCTCAAAGCTGAAGGCCTCGTTGTAATAGGGG
Syt-6	589R	CATCTGCACCTCGGCTGGGATATCTGGGGAAGTATGGCTGATCTT
Syt-6	1123R	GCGGGAGAAGCGGTCAAAGTCAAAGACACTGAGATGCAGCTTGCG
Syt-7	1395R	GCAGCTCCTGGGCCTTCATGACTTTCACGGTGAGTGTGGACTCCT
Syt-7	1962R	TGATGGTGGTCTCCCTCAGCTTCTCCGTGGGTATGTCAAAGGCGA
Syt-8	463R	CCAAAATCATACTCCAGGGAGAGCAGCAGTTGCCCCCACGGTTGG
Syt-8	698R	ACCGCTTGAAGTCCAATAGCTGCACCTTCAGAGTGGCTTTGGGCA
Syt-9	344R	TCTGGCACGGTCCCGCAGGTGGTAGATGAAATCTTGGCAGCTGTC
Syt-9	962R	GTCCCAGAGAAGTCCTTGGCGGGCAGATTGACGGCTTTGTGGATC
Syt-10	308R	CACTTGAGATGCTCTGCGGAAGGGTACTGACATTGGGGGCCACGA
Syt-10	705R	AGTTTCCCACAGGTTTTGACGTCGTCTTTTCTGTTGCCCTCGGAG
Syt-11	538R	CCCTCGTCCACTTTCCCTATGAGAACCATCTTTGTCCCTCCGAAC
Syt-11	1200R	TTGAGGACCACGACTGTCATTCTCTGTGCGACGGGCTGGTATGAC
Syt-12	372R	CCGACGTCCAGAGCTTCCACAGACTCACAGCTGCAATGCCAAGCA
Syt-12	1825R	GCCAGTGCTGAAGCCCACATCCCTCTGCAGGCCAATGGACATACT
Syt-13	300R	GGGCTGGACAGGCTCTGTGGACTTTTTAACGTTGAACTGTTGGGC
Syt-13	388R	CCAGGGTGTAGTCTGCGTAGTTGATGACTTCTGGGGCCGTCACAG

3.2.6 Image acquisition and processing after in situ hybridization

X-Ray films were scanned with a transmission light scanner (Quatographic X-finity ultra XFU 1600, Braunschweig, Germany) for wholebrain overview pictures. Slides were analyzed with a Zeiss Axioscope 40 light microscope equipped with Nomarski optics and collected by means of a high resolution digital camera (Zeiss AxioCam HRm) and Zeiss Axiovision 4.6 software (Carl Zeiss, Jena, Germany). Images were adjusted for brightness and contrast and assembled as plates using Adobe Photoshop CS2 (v. 9.0.2) and Adobe Illustrator CS2 (v. 12.0.1; Adobe Systems, San Jose, CA). Rat brain structures were named according to Paxinos and Watson (Paxinos 1988).

3.2.7 Quantification of expression strength

The range of observed expression strengths of each Synaptotagmin isoform was classified based on six categories: very strong expressing cells (++++), strongly expressing cells (+++), moderately expressing cells (++), weakly expressing cells (+), a punctate staining signifying single cell expression pattern (o) and cells with no detectable signal (-) (Table 1). Only isoforms with strong overall expression and low exposure time were classified as very strong to

weak (Syt-1 – 5, Syt-7 and Syt-11). If gene expression was low and required longer exposure, cells with an exceptionally strong signal were categorized as moderately expressing. Nevertheless, since labeling affectivity and affinity of the oligonucleotides can vary a comparative analysis between the different isoforms remains qualitative. On the other hand, this methodology allows the reliable comparison of expression strength of individual isoforms in different brain regions. The judgments were made relative to the intensity of the background signal (Suppl. Fig. 1).

3.3   Protein methods

3.3.1   Preparation of rodent brain

After removal of the skin, the skull of decapitated animals was opened with a cut through the occipital bone, the sagittal suture and the frontal bone using fine scissors. This allows to break away the skull the two halves of the skull, and to carefully take out the whole brain. Specimens predetermined for sectioning were frozen in TissueTek embedding medium (Sakura Finetek Europe B.V., Zoeterwoude, The Netherlands) as previously described (Schoch et al. 2006). Sections of 12 μm thickness were cut using a Microm HM 560 Microtom (Microm, Walldorf, Germany). Specimens for western blot analysis were separated into brain areas and frozen at -80°C.

3.3.2   Hippocampal subfield microdissection
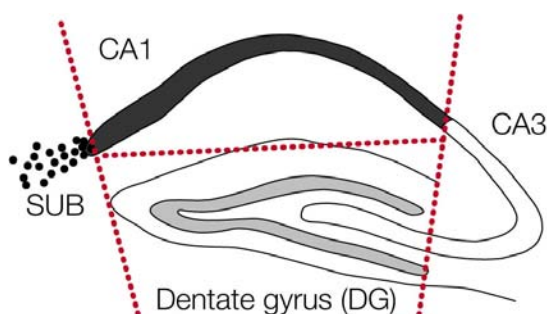
Figure 3.1: Illustration depicting the cuts (red dotted lines) placed to collect hippocampal microdissects
700 μm thick horizontal slices were used to determine mRNA and protein expression levels. CA1, CA3 Cornu ammonis subregions; SUB subiculum.

Rat brains from pilocarpinized and control animals were submerged in ice cold PBS and freshly cut into 700 μm thick horizontal slices using a Leica 1000S Vibratome (Leica, Nussloch, Germany) with Integraslice blades (Campden Instruments, UK). The slices were then transferred to a Petri dish to cut out the hippocampus under visual control using a illuminated 5 fold magnifying loupe

LTS120 (Conelek, Germany). Each hippocampal slice was then microdissected into CA3, CA1, and DG and frozen in liquid nitrogen prior storage at -80°C. In detail, the CA3 microdissects were acquired by cutting along the two ends of the granule cell layer. Then a cut parallel to the first one along the tip of the DG was placed to remove the Subiculum. Finally CA1 and DG where separated by cutting along the hippocampal fissure (Figure 3.1). The tissue was afterwards used for mRNA extraction followed by TaqMan or protein extraction with SDS-PAGE and western blot analysis.

3.3.3 Morphometric analysis of motoneurons

E18.5 embryonic brains and cervical spinal cords (C3-C5) were fixed in 4% PFA over night and embedded in paraffin. 4μm serial sections were prepared. Moto-neurons were identified by incubating the sections with NeuN antibody (Chemicon, 1:1000) and subsequent DAB detection (Vector Labs, Burlingame, CA, USA) and HE staining. NeuN positive motoneurons were counted independently on right and left hemiventral columns in a defined area. Motoneuron density per 100 mm^2 was calculated and analyzed by Student's t test (double mutants (3 animals), n=19; controls (3 animals), n=18).

3.3.4 Fluoro-Jade B essay

For the Fluoro-Jade B essay 4μm serial sections of E18.5 embryonic cervical spinal cords were processed according to the protocol of the Fluoru-Jade B kit from Histo-Chem, Jefferson, AR, USA.

3.3.5 Protein quantifications of the RIM knockout mice

The quantifications were performed on brain homogenates from four two months old RIM2α KO, and four E18.5 RIM1/2α double KO mice using litter-mate controls. Brains were sonicated on ice in protein extraction buffer (10mM EDTA, 2% SDS, Complete Protease Inhibitor and Pefabloc SC (Roche Applied Science, Mannheim) in PBS) with a weight ratio of ten : one (tissue : buffer). Aliquots were boiled in SDS sample buffer (Laemmli 1970) and stored at 80°C until further use. The lysates (10-80 μg; determined using the BCA protein assay; Pierce, Rockford, IL) were analyzed by SDS-PAGE and immunoblotting on Immobilon-P membranes (Millipore, Bedford, MA) using the Mini Protean System (Bio-Rad, Munich, Germany). Membranes were incubated with the primary

antibodies as described (Towbin et al. 1979) with 5% dry milk instead of BSA as a blocking agent. Signals were detected with ^{125}I-labeled secondary goat anti-rabbit antibodies and measured in a Fujix BAS5000 (Ray Test, Straubenhardt, Germany). VCP and α-Tubulin antibodies were used as internal standards depending on the size of the protein of interest. Signals analyzed with AIDA quantification software (Ray Test) were normalized to internal standards and plotted as percentage of wild type ± SEM.

3.3.6 Protein fractionation

Whole brains of embryonic E18.5 mice were homogenized in PBS/10mM EDTA/Complete proteinase inhibitor (Roche) (10µl Buffer/mg tissue) with a Heidolph DIAX900 homogenizer. Two of three fractions of each homogenate were further extracted with either 1% TritonX-100 or 1% SDS. All probes were centrifuged for 1 hour at 100,000xg/4°C. After removal of the supernatant, the remaining pellets were washed and resuspendet in extraction buffer containing 2% SDS.

3.3.7 Quantitative western blot of microdissected hippocampi

Protein sample preparation and SDS PAGE western blotting was carried out as described in chapter 3.3.4. IR Dye labeled secondary antibodies and the LI-COR Odyssey detection system (LI-COR, Lincoln, NE) were used for blot quantification. Data is presented as means ± SEM. Statistical analysis was done using one sample t-test (Microsoft Excel or GraphPad Prism) to determine the significance of the difference between mean and control level (normalized to 100% for each blot). Differences were considered significant at $p < 0.05$. EM: Statistical analysis was performed with Student's t-tests (two-sided, unpaired data with unequal variances).

3.3.8 Antibodies

Table 3.6: Antibodies and dilutions used in western blot experiments.

Protein	Antibody	Dilution
14-3-3	14-3-3e	1:500
CASK	C63120	1:500
Complexin	L668	1:250
Complexin	L669	1:250
ERC1a	4791	1:1000
ERC1b/2	4790	1:1000
ERC2	5004	1:1000
GRIP	P225	1:1000
Liprin	4396	1:1000
Liprin2	L2	1:100
Liprin4	L4	1:100
Munc13	M	1:200
Munc13-1	41	1:500
ubMunc13-2	52	1:500
BMunc13-2	50	1:500
Munc18	I370	1:500
PSD95	L667	1:2000
Rab3A	42.2	1:2500
Rab3A	42.1	1:2500
Rab3C	42.2	1:2500
Rab5A	621.1	1:1000
Rababtin	Q699	1:500
Rabphilin	I734	1:4000
RIM-BP1	U1615	1:250
RIM-BP1	RB1-16T3	1:100
RIM-BP2	4193	1:500
RIM-BP2	RB2-11T3	1:100
RIM1α	R809	1:2000
RIM1M	R1M	1:1000
RIM2α	U1565	1:5000
RIM3γ	R3	1:100
RIM4γ	R4	1:100
SNAP25	SNAP25	1:10000
Synapsin	E028	1:1000
Synaptobrevin	69.1	1:10000
Synaptophysin	P611	1:2000
Synaptophysin	SySy101011	1:20000
Synaptoporin	α-P37	1:1000
Synaptotagmin 1	41.1	1:10000
Synaptotagmin 3	754N	1:500
Synaptotagmin 4	SIV	1:250
Synaptotagmin 6	756	1:500
Synaptotagmin 7	R3996	1:500
Synaptotagmin 10	U5009	1:500
Synaptotagmin 12	U5400	1:500
Syntaxin	HPC-1	1:10000

3.4   Miscellaneous

All chemicals were of the highest available purity and were purchased from standard sources. All animal experiments were conducted in accordance with the guidelines of the Animal Care and Use Committee of the University of Bonn and the European Community Council Directive of 24 November 1986 (86/609/EEC).

4   Results

4.1   Localization and function of α-RIMs

RIMs constitute a gene family with four members, of which RIM1α and RIM2α contain the full set of domains. Due to internal promoters, RIM1 and RIM2 generate multiple transcripts. Even though the functional role of RIM1α has been addressed in several studies, so far its localization as well as the distribution of the RIM2 transcripts has not been investigated yet.

4.1.1   Differential expression of RIM1 and RIM2 isoforms

To examine whether RIM1α, RIM2α, RIM2β and RIM2γ are differentially expressed in the brain, *in situ* hybridizations were performed on brain sections from adult rats (Figure 4.1, left panels). To control for specificity, two oligonucleotides were used for each RIM-isoform (data not shown). The labeling was abolished when excess unlabeled oligonucleotides were added to the hybridization mix (Figure 4.1, right panels).

Autoradiographs of hybridized rat brain sections revealed differential but overlapping expression patterns of RIM mRNAs. In each case, regions rich in glial cells (e.g. white matter of cerebral cortex and cerebellum) were unlabelled, indicating a neuron specific expression of RIM isoforms (Figure 4.1, left panel). RIM1α mRNA was present throughout the brain with highest levels in the cortex, cerebellum, hippocampus and thalamus. RIM2α mRNA is concentrated in the cerebellum, the olfactory bulb and the dentate gyrus of the hippocampus. However, comparison of the signals obtained with the negative control indicates that RIM2α is also ubiquitously expressed in brain, albeit at low levels. RIM2β and RIM2γ mRNAs are present in a pattern similar to RIM1α, but based on the intensity of the hybridization signal both seem to be expressed at lower levels and exhibit regional differences (e.g., RIM2β is expressed more in the thalamus, and RIM2γ more in the brainstem; Figure 4.1). These results show that the various RIM1 and RIM2 isoforms exhibit a differential, but highly overlapping expression pattern in rat brain.
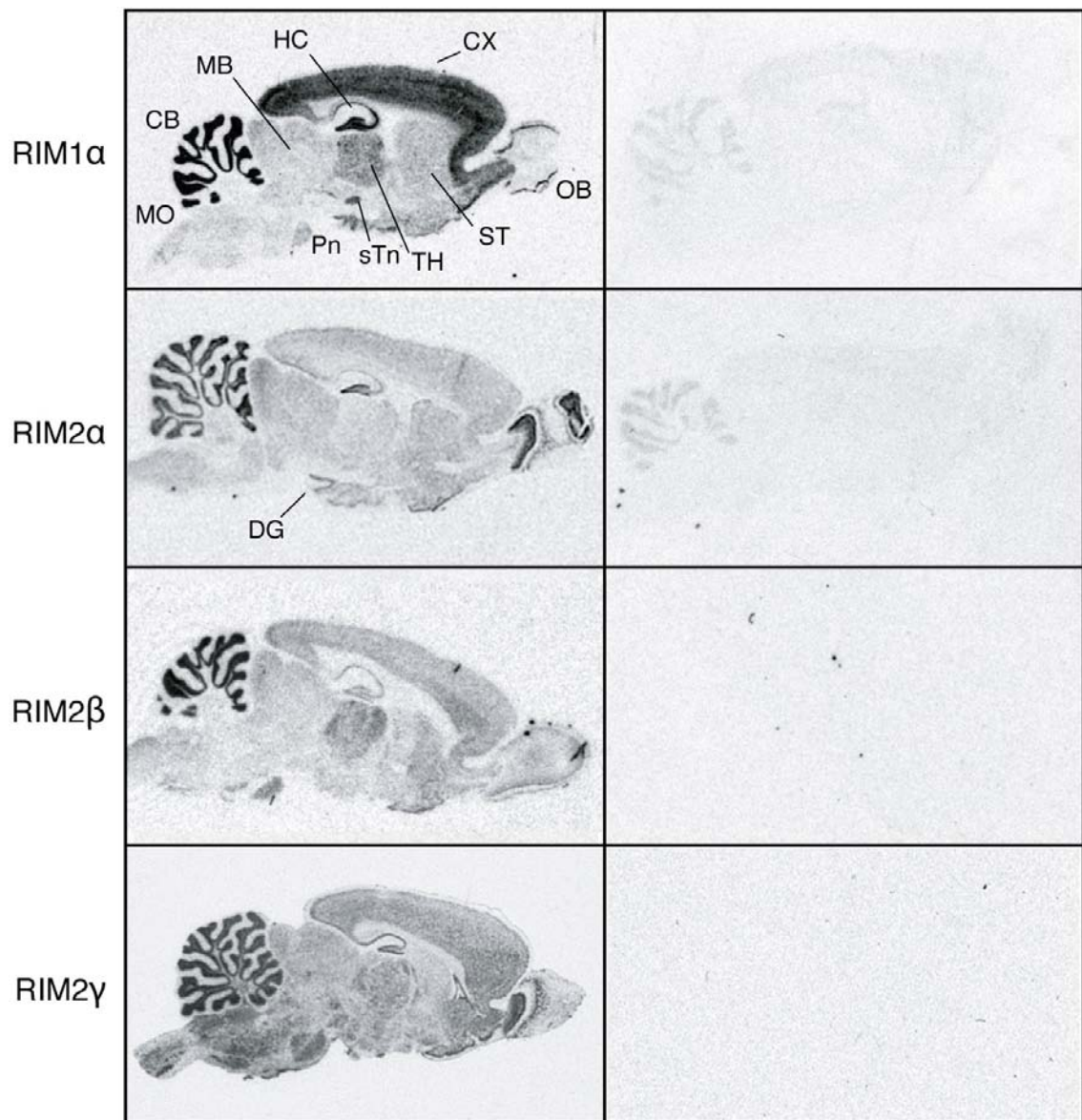
Figure 4.1: *In situ* hybridization of RIM mRNAs in rat brain.
Film images showing the distribution of RIM mRNAs in adult rat brain (CB, cerebellum; CX, cerebral cortex; DG, dentate gyrus; HC, hippocampus; MB, midbrain; OB, olfactory bulb; Pn, pontine nucleus; sTn, subthalamic nucleus; ST, Striatum; TH, thalamus; MO medulla oblongata).
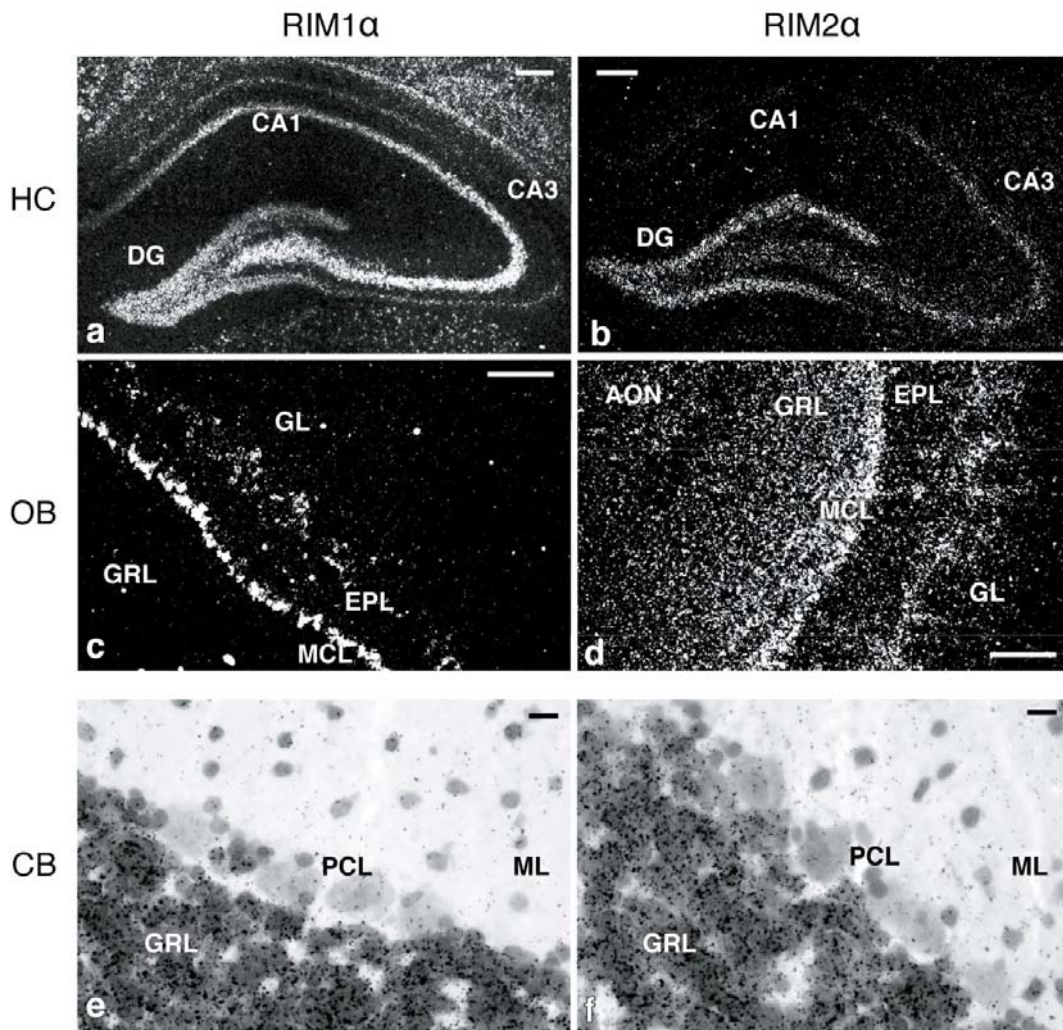
Figure 4.2: Micrograph pictures of α-RIM *in situ* hybridization
Dark field images of emulsion dipped sections from rat hippocampus, olfactory bulb and cerebellum (AON, anterior olfactory nucleus; DG, dentate gyrus; EPL, external plexiform layer; GL, glomerular layer; GRL, granule cell layer; MCL, mitral cell layer; ML, molecular layer; PCL, Purkinje cell layer; scale bar = 100 µm Ba-d, 20 µm Be,f).

To determine the cellular distribution of α-RIM mRNA species, emulsion dipped sections were analyzed. In the hippocampus, RIM1α could be detected at high levels in the dentate gyrus and the CA3 region, and at lower levels in the CA1 region (Figure 4.2 HC). In contrast, strong labeling for RIM2α was largely restricted to the dentate gyrus, with lower levels observed in the CA3 region. In the olfactory bulb, significant RIM1α expression was detected in the mitral cell layer (MCL) and in some cells of the external plexiform layer (EPL), whereas the cells of the granule cell layer (GRL) and the glomerular layer (GL) were devoid of a RIM1α signal (Figure 4.2 OB). In contrast, RIM2α showed strong expression in the glomerular layer, the mitral cell layer and the granule cell layer.

Within the cerebellum, RIM1α and RIM2α expression was highly concentrated in the granule cell layer (Figure 4.2 CB). Therefore, most neurons express multiple isoforms of RIMs with distinct relative expression levels.

4.1.2 Characterization of RIM2α knockout mice.

As shown in chapter 4.1.1, RIM1α and RIM2α are expressed in overlapping but distinct patterns throughout the brain. RIM1α plays an important role in the regulation of synaptic transmission. However, the function of RIM2α had not been studied so far.
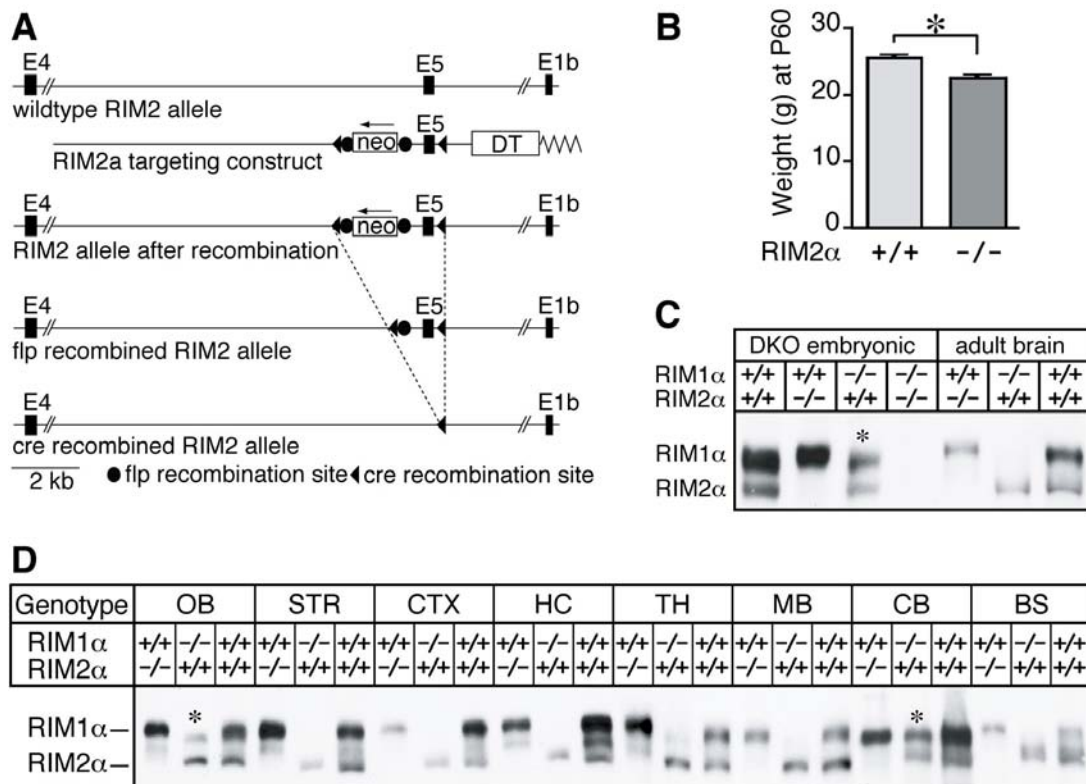
Figure 4.3: Generation and characterization of RIM2α KO mice.
(**A**) Structures of the *RIM2* wildtype gene (wildtype allele), of the targeting vector used for homologous recombination (targeting construct), and of the RIM2 transgene alleles after homologous recombination before and after further recombination through Flp and Cre recombinases. In the targeting vector, exon 5 is flanked by loxP sites (black triangles) and the neomycin resistance gene cassette (neo) that is flanked by flp recombination sites (black circles). A diphtheria toxin gene (DT) is included for negative selection. (**B**) Weights of male RIM2α KO and littermate control mice (N=36, asterisk = p < 0.001). (**C**) Immunoblots of E18.5 embryonic and adult wildtype, RIM1α KO, RIM2α KO and embryonic double KO whole brain homogenates. (**D**) α-RIM immunoblots of proteins from different brain regions from adult RIM1α KO, RIM2α KO, and wildtype control mice; blots were probed with an antibody that recognizes both RIM1α and RIM2α (abbreviations of brain areas: OB, olfactory bulb; STR, striatum; CTX, cortex; HC, hippocampus; TH, thalamus; MB, midbrain, BS, brain stem; CB, cerebellum; * asterisks mark bands of alternatively spliced RIM2α isoforms of higher molecular weight).

Therefore, to examine and compare their functions, mice deficient for RIM2α were generated. They were derived from mutant mice in which the fifth exon of the RIM2α gene (which encodes part of the zinc finger; Wang & Sudhof 2003) is flanked by loxP sites. These mice were crossed to transgenic mice that express cre recombinase in the male germ line to produce KO mice in which the floxed exon was deleted (Figure 4.3A) (O'Gorman et al. 1997). Homozygous RIM2α KO mice were viable and fertile. However, systematic analysis of the offspring from heterozygous matings revealed that homozygous KO mice were slightly smaller than littermate wildtype controls (males, N=36) (Figure 4.3B), and less frequent than would be expected based on mendelian inheritance (24.1% wildtype, 56.3% heterozygous and 19.6% homozygous mutant mice in offspring at >1 month of age; N=591; p<0.01). Immunoblotting confirmed that the KO mice lacked RIM2α (Figure 4.3C, D and Figure 4.4).
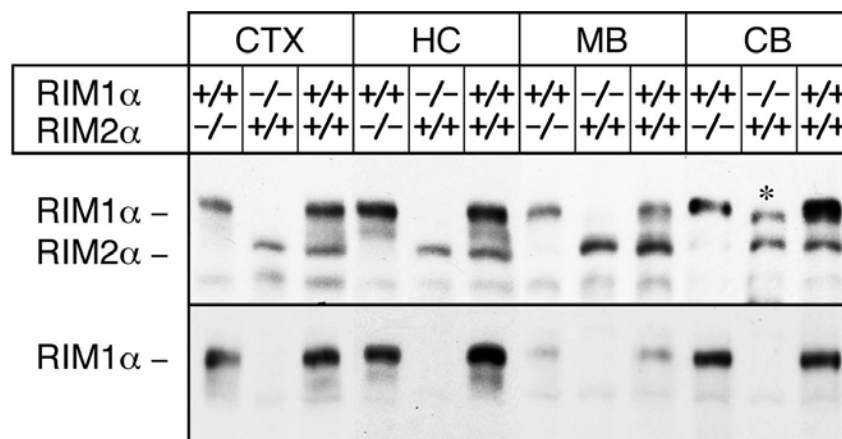
Figure 4.4: Immunoblot analysis of RIM1α KO, RIM2α KO and wildtype mice
Proteins from cortex (CTX), hippocampus (HC), Midbrain (MB) and cerebellum (CB) from adult RIM1α KO, RIM2α KO and wildtype control mice. Blots were probed with antibodies that recognize the PDZ-domain of RIM1 and RIM2 (upper panel) and RIM1α (lower panel). The asterisk marks the band of an alternatively spliced high molecular weight isoform of RIM2α.

Similar to the RIM1α KO mice (Schoch et al. 2002), RIM2α mutant mice exhibited a deficit in maternal behavior, as they did not take care for their litters even after multiple pregnancies. To examine if RIM2α deficiency results in changes in overall brain morphology, paraffin slides from brains of adult wildtype and KO littermates were analyzed by H&E staining and NeuN immunohistochemistry (Figure 4.5). The brains of RIM2α KO mice showed a normal morphology, cell density, cytoarchitecture and connectivity as compared to wildtype controls.
In order to check if ultrastructural parameters were altered, brains of adult mice were additionally analyzed by electron microscopy (Schoch et al. 2006). No

changes in active zone length, synapse structure, vesicle density or distribution were found in the RIM2α KO. Additionally, quantitative immunoblotting of multiple pre- and postsynaptic proteins were performed to check for compensatory changes in synapse protein composition (Table 4.1). No change in the amounts of any of the tested proteins was found. Taken together, these data demonstrate that although RIM2α KO mice are viable and exhibit no apparent developmental abnormalities, behavior and survival of these mice are slightly impaired.
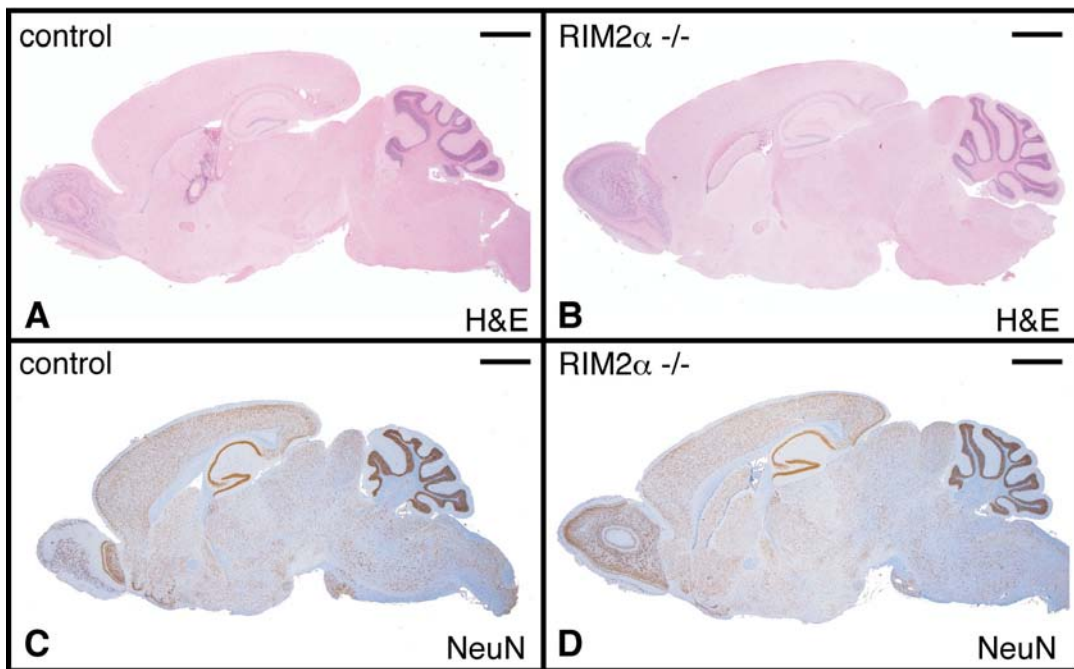
Figure 4.5: RIM2α knockout histological analysis
(A and B) Comparison of H&E- and **(C and D)** NeuN-stained sections from RIM2α knockout and wildtype mice. Deletion of RIM2α did not change the distribution, number or size of neurons in the brain; scale bars: 5 mm

To search for compensatory changes in the expression of RIM1α as the only other α-RIM isoform in RIM2α KO mice, immunoblotting analyses of the relative expression of RIM1α and RIM2α in protein homogenates of various brain regions in wildtype, RIM1α KO, and RIM2α KO mice was performed (Figure 4.3D and Figure 4.4). Antibodies to the zinc-finger region of RIM1α and RIM2α often crossreact because of their structural similarities (Schoch et al. 2002). Moreover, these antibodies detect multiple bands even when one of the two α-RIM isoforms is deleted because of the extensive alternative splicing of RIMs (Wang & Sudhof 2003). Consistent with the *in situ* hybridization data, immunoblotting of different brain regions in single RIM1α and RIM2α KO mice showed that RIM1α

is the more abundant isoform, whereas RIM2α was found at low levels in most rostral brain regions examined, but at high levels in the cerebellum and olfactory bulb (Figure 4.3D). However, no region specific compensatory changes in RIM1α protein levels in RIM2α KO mice, or conversely of RIM2α protein levels in RIM1α KO mice were detected (Figure 4.3D and Figure 4.4). Interestingly, alternative splicing of RIM2α seems to be regulated in a region specific manner. While in most brain regions a smaller isoform was detected, in cerebellum and olfactory bulb an additional larger protein could be observed (asterisks in Figure 4.3D, Figure 4.4).

Table 4.1: Expression levels of neuronal proteins in wildtype and RIM2α KO mice

Protein	WT	SEM	HET	SEM	KO	SEM	Antibod.
RIM2α	100	± 11,6	31,8	± 4,0	11,1	± 1,1	115-2
RIM2α	100	± 6,7	46,3	± 13,7	9,2	± 0,6	U1565
RIM1α	100	± 6,1	102,7	± 5,4	109,7	± 7,3	R809
CASK	100	± 0,9	101,8	± 4,8	98,2	± 8,6	C63120
ERC1a	100	± 4,4	98,4	± 9,2	87,8	± 3,7	4791
ERC1b/2	100	± 6,0	108,1	± 7,8	91,6	± 2,8	4790
ERC2	100	± 14,1	106,3	± 9,3	101,4	± 11,6	5004
Liprin	100	± 4,5	92,4	± 6,4	95,3	± 5,2	4396
Munc13-1	**100**	**± 6,1**	**97,1**	**± 6,5**	**104.4**	**± 7,6**	**13-1**
Munc13-2	**100**	**± 3,9**	**116,6**	**± 7,3**	**102,7**	**± 13,7**	**13-2**
Munc13-3	**100**	**± 3,6**	**106,9**	**± 7,0**	**118,6**	**± 11,1**	**13-3**
Rab3	100	± 4,2	107,8	± 5,5	109,8	± 6,5	42.2
Rabphilin	100	± 3,3	104,4	± 4,9	105,7	± 5,7	I734
RimBP2	100	± 5,3	105,8	± 8,6	95,6	± 8,7	4193
SNAP25	100	± 8,5	117,4	± 14,6	113,3	± 19,5	I733
Synapsin	100	± 1,6	91,2	± 3,0	87,5	± 4,0	E028
Synaptotagmin	100	± 7,9	113,2	± 4,1	112,9	± 6,1	41.1
Syntaxin	100	± 6,1	112,0	± 5,6	105,8	± 7,3	HPC-1

The levels of the indicated proteins were quantified in brain homogenates from adult wildtype and KO littermates obtained in heterozygous crossings, using immunoblots probed with I^{125}-labeled secondary antibodies and analyzed with a phosphoimager. All analyses were performed for a given protein on a single gel, with signals quantified by normalization to an internal standard (β-Tubulin, annexin6, or VCP) that was visualized in parallel with the protein of interest on the same blot. This procedure minimizes artifacts caused by differences in transfer or probing efficiency. Data are expressed in percent normalized to the wildtype levels ± SEM. Antibodies used are indicated on the right. Variations between the results for the same protein obtained with different antibodies reflect differences in crossreactivities and specificities of different antibodies. Note that the remaining levels of RIM2α observed in the RIM2α KO with various RIM2α antibodies are most likely due to background activity of the antibodies.

4.1.2.1 Impaired survival of RIM1α/2α double KO mice.

To assess the redundant or divergent functions of the two α-RIMs, RIM1α/2α double KO (DKO) mice were generated. Analysis of the offspring from systematic breeding of double heterozygous RIM1α/2α KO mice revealed that the survival of RIM1α or RIM2α homozygous mutant mice exhibited no significant decrease as long as two RIM1α or RIM2α wildtype alleles were present (Figure 4.6A). However, in >100 crossings, no surviving mouse that was homozygous mutant for both RIM1α and RIM2α was observed, demonstrating that RIM1α and RIM2α are redundant in terms of survival. Moreover, even single homozygous RIM1α or RIM2α KO mice exhibited significantly impaired survival when one of the other two α-RIM alleles was also deleted (i.e., in the RIM1α-/-2α+/- or RIM1α+/-2α-/- genotypes, p<0.001; see Figure 4.6A).
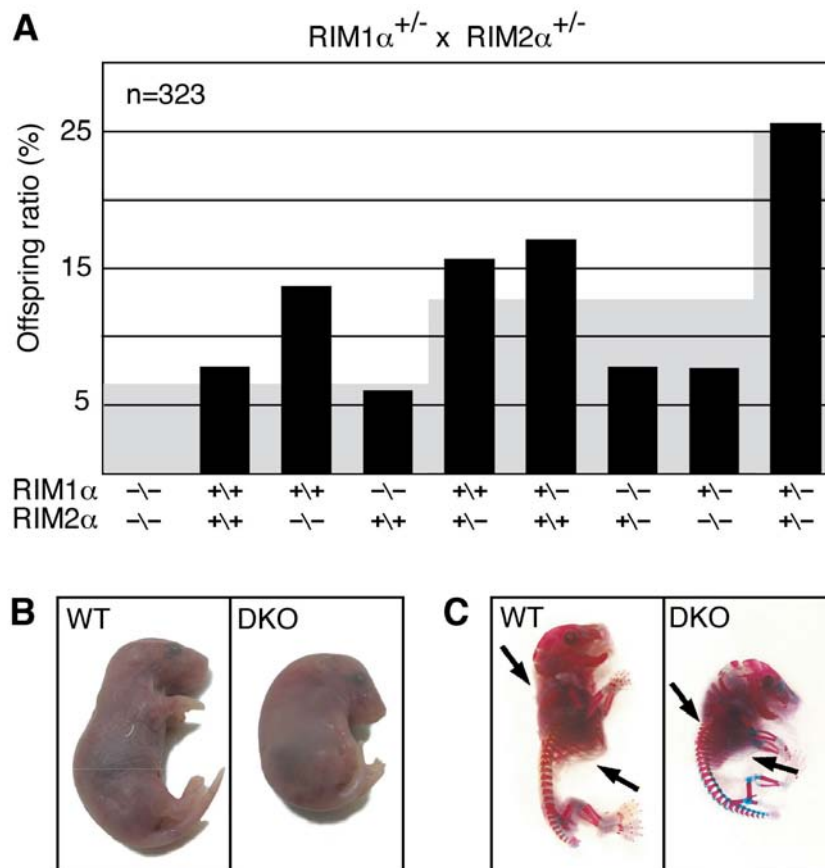
Figure 4.6: RIM1α/2α offspring analysis

(A) Survival analysis of the offspring from matings of double heterozygous RIM1α/2α mutant mice. The black bars plot the observed frequency of the indicated genotypes as percentage of the total, while the gray background indicates the expected frequency based on mendelian inheritance (N=323). (B and C) Images of E18.5 RIM1α/2α double KO mutant and control littermate mice overall morphology (B) and skeleton (C, bones are stained in blue and cartilage in pink; black arrows point to ribcage and cervical vertebrae).

RIM1α/2α DKO mice died immediately after birth because they could not breathe. The mutant mice did not respond to tactile stimuli, and exhibited an abnormal body posture similar to Synaptobrevin 2 KO mice (Figure 4.6B, Schoch et al. 2001), suggesting that they were paralyzed. However, DKO mice could be recovered alive at E18.5 as embryos by hysterectomy; at this age, DKO mice were present in a normal mendelian ratio, suggesting that the deletion of both α-RIMs does not impair survival in utero (data not shown). Thus for all subsequent studies on DKO mice, embryos at E18.5 were analyzed. Although whole body staining for bone and cartilage revealed no major developmental defects in DKO mice, their vertebrae in the KO skeleton seemed more compact at the cervical level, and the ribcage appeared enlarged (Figure 4.6C), possibly because of permanent paralysis of the embryo during development.

4.1.2.2 Brain morphology and synapse structure of RIM1α/2α DKO mice.

Histochemistry and immunocytochemistry of brain sections revealed that RIM1α/2α double KO mice displayed no obvious impairments in central nervous system development (Figure 4.8). However, H&E- and NeuN-stained vibratome sections of paraffin embedded spinal cords showed an increased number of ventral horn motoneurons at all cervical levels in RIM1α/2α DKO mice as compared to control littermates (Figure 4.6B). A morphometric analysis of NeuN immunopositive motoneurons revealed a significant increase (** $p < 0.005$) in motoneuron density in E18.5 DKO spinal chords (Figure 4.6C).
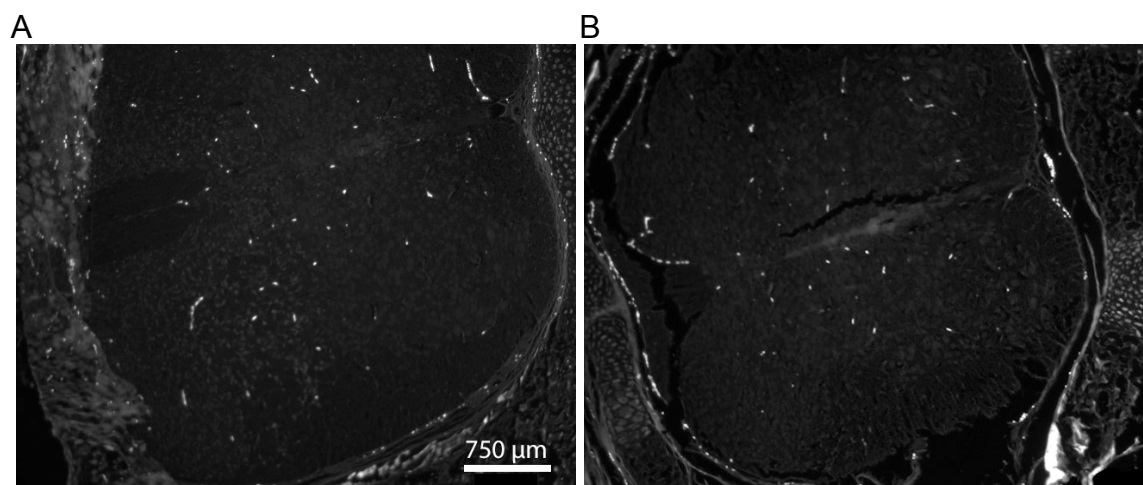
Figure 4.7: Fluoro Jade B staining of horizontal sections of spinal cord from wildtype (A) and RIM1α/2α DKO (B) mice (E18.5)
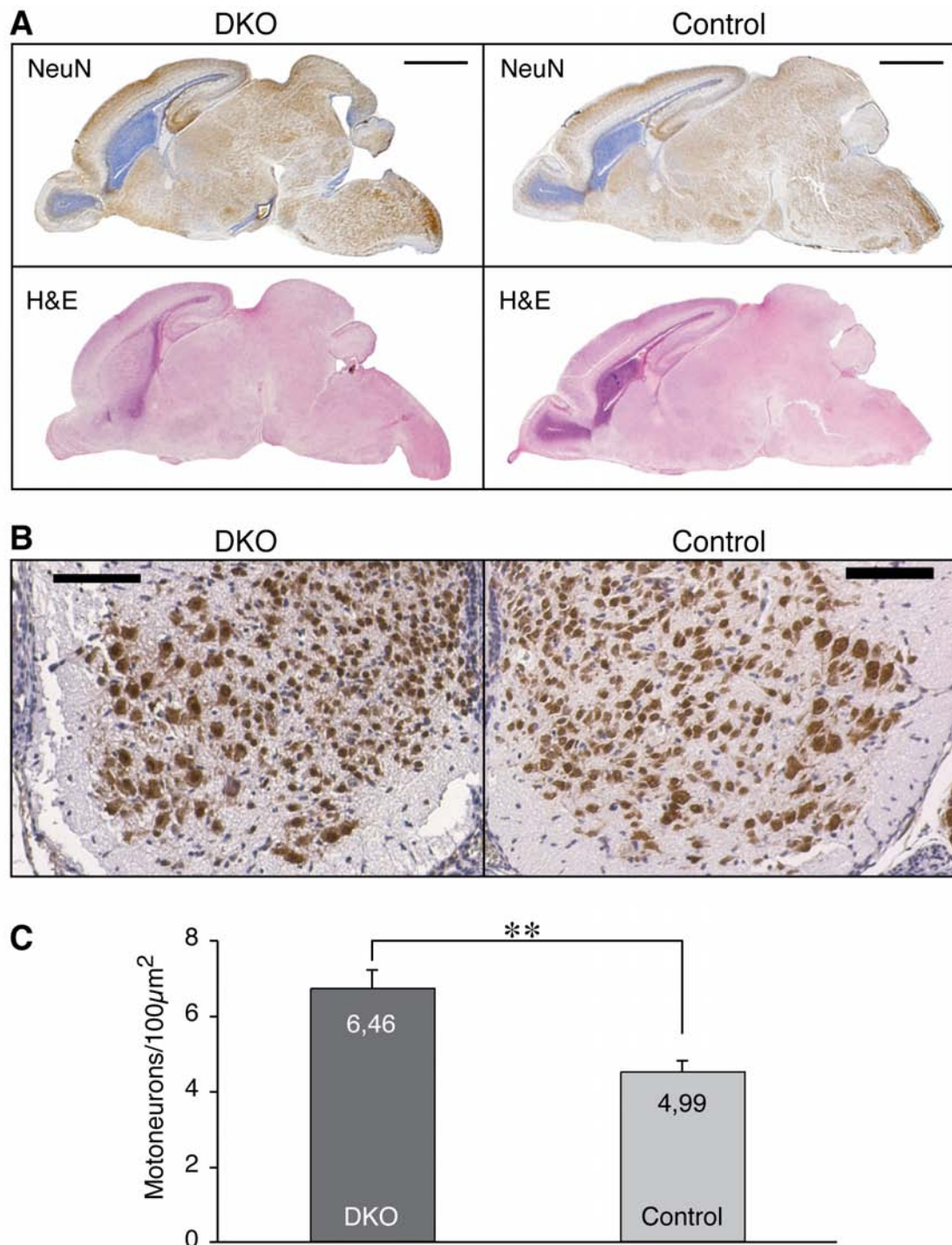
Figure 4.8: Morphology of RIM1α/2α DKO brains and spinal cord.

(**A**) H & E- and NeuN-stained sagittal section of brains from E18.5 mice of the indicated geno-type (Scale bar = 2 mm). (**B**) NeuN stained coronal sections of spinal cord from E18.5 mice of the indicated genotype (scale bar = 100 µm). (**C**) Morphometric analysis of NeuN-immunopositive spinal motoneurons (**p<0.005).

No sign of neurodegeneration was detectable in the spinal cord by TUNEL (data not shown) or Fluoro JadeB staining (Figure 4.7). The increase in motoneurons may be due to decreased synaptic transmission at the neuromuscular junction (NMJ) (see below) (Harris & McCaig 1984, Oppenheim 1991).To test whether
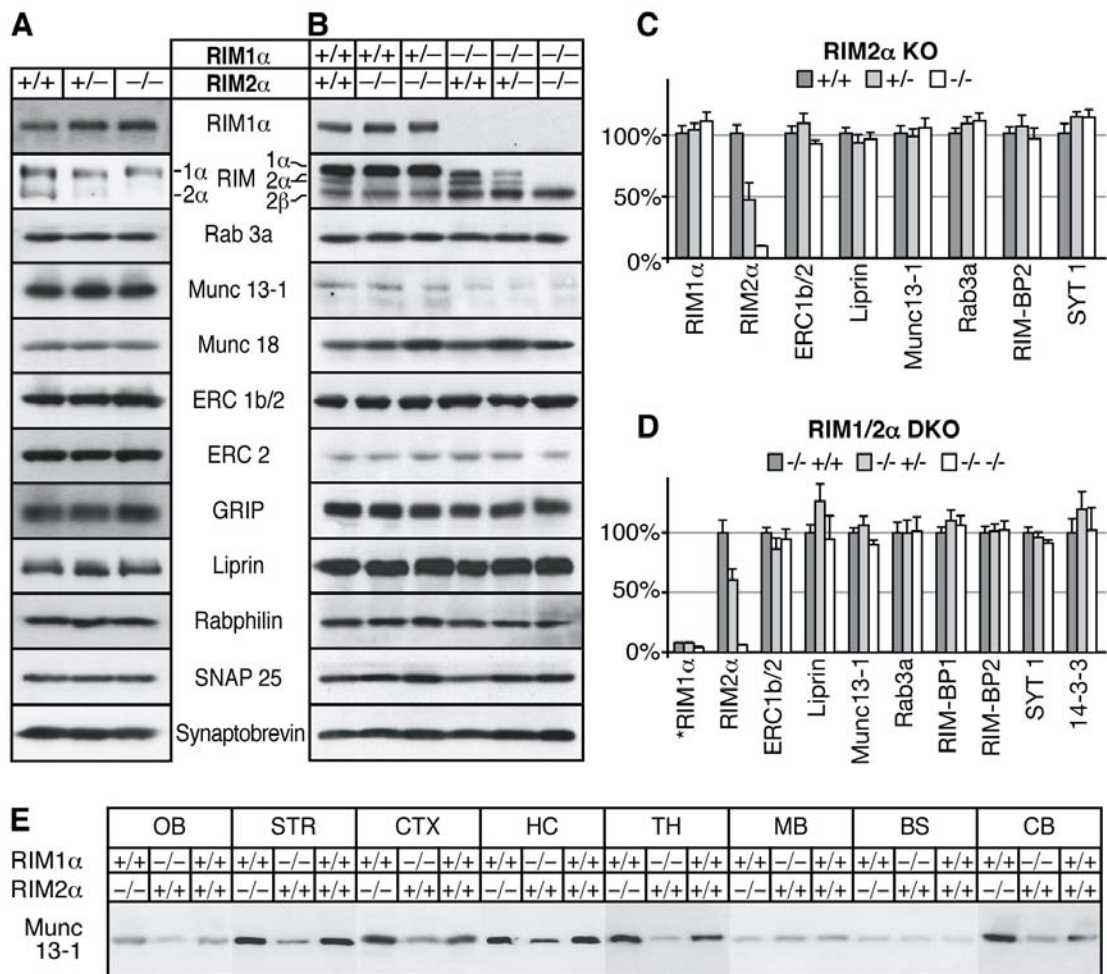
Figure 4.9: Analysis of synaptic protein levels in brains from RIM2α KO mice and RIM1α/2α DKO embryos.

Brain homogenates of the indicated genotypes were analyzed by immunoblotting using antibodies to the indicated proteins (A, B), the blots were quantified and all data normalized to control level (C, D, *RIM1α level in D normalized to wildtype). (A, C) RIM2α KO (adult), (B, D) RIM1α/RIM2α DKO (E18.5). (E) Proteins from different brain areas of adult RIM1α KO, RIM2α KO and wildtype mice were analyzed with an antibody against Munc13-1 (abbreviations of brain areas: OB, olfactory bulb; STR, striatum; CTX, cortex; HC, hippocampus; TH, thalamus; MB, midbrain, BS, brain stem; CB, cerebellum;).

deletion of α-RIMs causes a major change in the protein composition of the brain, the levels of neuronal proteins in adult littermate wildtype, heterozygous, and homozygous mutant RIM2α KO mice were quantified (Figure 4.9A, C and Table 4.1), and in E18.5 embryos that were homozygous for the RIM1α KO allele and wildtype, heterozygous, or homozygous mutant for the RIM2α KO allele (Figure 4.9B, D and Table 4.2).

Table 4.2: Levels of neuronal proteins in RIM1α/2α KO mice compared to RIM1α KO mice

Protein	-/- +/+	SEM	-/- +/-	SEM	-/- -/-	SEM	Antibod.
RIM2α	100	± 10.5	60.7	± 9.0	6.6	± 0.3	U1565
RIM2α	100	± 6.7	56.9	± 3.9	11.51	± 2.3	115-2
14-3-3	100	± 11.6	119.2	± 14.8	102.0	± 18.7	14-3-3e
CASK	100	± 5.7	117.7	± 3.8	111.8	± 8.6	C63120
Complexin	100	± 8.6	109.9	± 10.4	104.3	± 3.2	L668
Complexin	100	± 14.1	107.1	± 34.5	98.6	± 14.3	L669
ERC1b/2	100	± 3.9	86.4	± 8.9	94.4	± 8.2	4790
GRIP	100	± 10.7	89.7	± 5.4	97.8	± 6.8	P225
Liprin	100	± 3.7	106.0	± 7.4	89.7	± 3.8	4396
Munc13	**100**	**± 1.0**	**109.3**	**± 4.0**	**90.5**	**± 7.8**	**M**
Munc13-1	**100**	**± 6.4**	**126.1**	**± 14.4**	**94.6**	**± 19.4**	**13-1**
Munc13-2	100	± 5.9	81.7	± 4.8	110.4	± 6.7	13-2
Munc13-3	100	± 7.0	108.2	± 15.4	100.4	± 7.6	13-3
Munc18	100	± 5.4	98.9	± 7.6	107.3	± 8.0	I370
PSD95	100	± 7.6	88.0	± 18.0	101.6	± 13.1	L667
Rab3A	100	± 10.7	112.0	± 14.8	91.06	± 7.8	42.2
Rab3A	100	± 8.5	99.7	± 10.6	101.2	± 11.9	42.1
Rab3C	100	± 8.1	101.4	± 5.5	102.4	± 2.4	42.2
Rab5A	100	± 9.5	101.9	± 8.0	114.9	± 9.3	621.1
Rababtin	100	± 4.9	87.1	± 10.4	90.1	± 6.8	Q699
Rabphilin	100	± 5.1	99.0	± 9.4	91.9	± 8.7	I734
RIM-BP1	100	± 4.4	109.9	± 8.5	106.0	± 8.1	U1615
RIM-BP2	100	± 5.0	101.1	± 6.0	102.1	± 7.7	4193
SNAP25	100	± 6.1	124.4	± 24.7	115.7	± 5.7	SNAP25
Synapsin	100	± 4.4	109.7	± 12.4	92.31	± 7.2	E028
Synaptobrevin	100	± 7.2	105.1	± 18.1	102.3	± 11.5	69.1
Synaptophysin	100	± 3.5	94.82	± 9.6	98.1	± 3.4	P611
Synaptoporin	100	± 6.9	83.42	± 2.8	97.3	± 7.2	α-P37
Synaptotagmin	100	± 4.3	96.01	± 4.4	90.8	± 3.0	41.1
Syntaxin	100	17.8	98.37	± 1.8	101.5	± 7.1	HPC-1
	+/+ -/-		-/- -/-				
RIM1α	100	10.1	4.2	1.1			
Munc13-1	**100**	**2.8**	**45.8**	**6.5**			

Experiments were carried out as described for Table 4.1, except that brain homogenates from littermate mice that are homozygous mutants for RIM1α but are wildtype, heterozygous mutant, or homozygous mutant for RIM2α were used, and that mice were analyzed at E18.5 instead of adult mice.

No significant changes in any protein in adult RIM2α KO mice compared to controls, and in particular, no significant decrease in Munc13-1 in RIM1α/2α double KO embryos compared to RIM1α KO embryos was observed. To rule out region specific changes in Munc13-1 level, different brain areas were investigated, but no obvious alterations were detected (Figure 4.9E). These results were unexpected because previous studies showed that Munc13-1 is decreased ~50% in RIM1α KO mice (Schoch et al. 2002), which prompted the hypothesis that the remaining Munc13-1 is stabilized by RIM2α. As shown here, however, additional deletion of RIM2α does not cause a major further decrease in Munc13-1 levels beyond that observed in RIM1α KO mice. A recent report described a role for RIM1α in the regulation of presynaptic recruitment of Munc13-1 and ubMunc13-2 (Andrews-Zwilling et al. 2006). It was therefore checked if the deletion of both α-RIMs results in a redistribution of Munc13-1 from the membrane bound to the soluble fraction (Figure 4.10).

Buffer				Triton-X 100				SDS			
DKO		Control		DKO		Control		DKO		Control	
P	S	P	S	P	S	P	S	P	S	P	S
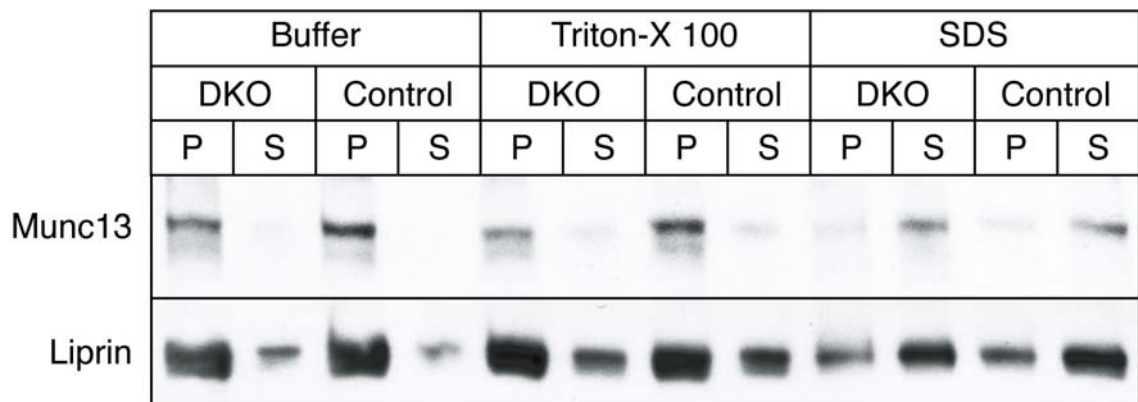
Figure 4.10: Analysis of Munc13 and Liprin solubility
Soluble (S, supernatant) and insoluble (P, pellet) fractions of control and double KO brain homogenates were analyzed in buffer containing either no or the indicated detergent. Blots were probed with antibodies against Munc13-1 and Liprin3α.

Soluble and membrane bound protein fractions from wildtype and RIM1α/2α DKO embryonic brains were separated by ultra thorax homogenization in buffer or in the presence of detergents of different strength and high speed centrifugation. In agreement with Andrews-Zwilling an increase of Munc13-1 in the soluble fraction in brains of DKO mice was detected. However, the majority of Munc13 was still found in the insoluble fraction with buffer or non denaturing detergents but was solubilized with SDS. To investigate whether the deletion of both α-RIMs alters synapse assembly, the ultrastructure of RIM1α/2α DKO synapses in the spinal cord was analyzed in collaboration with Dr. Frank

DKO   Control
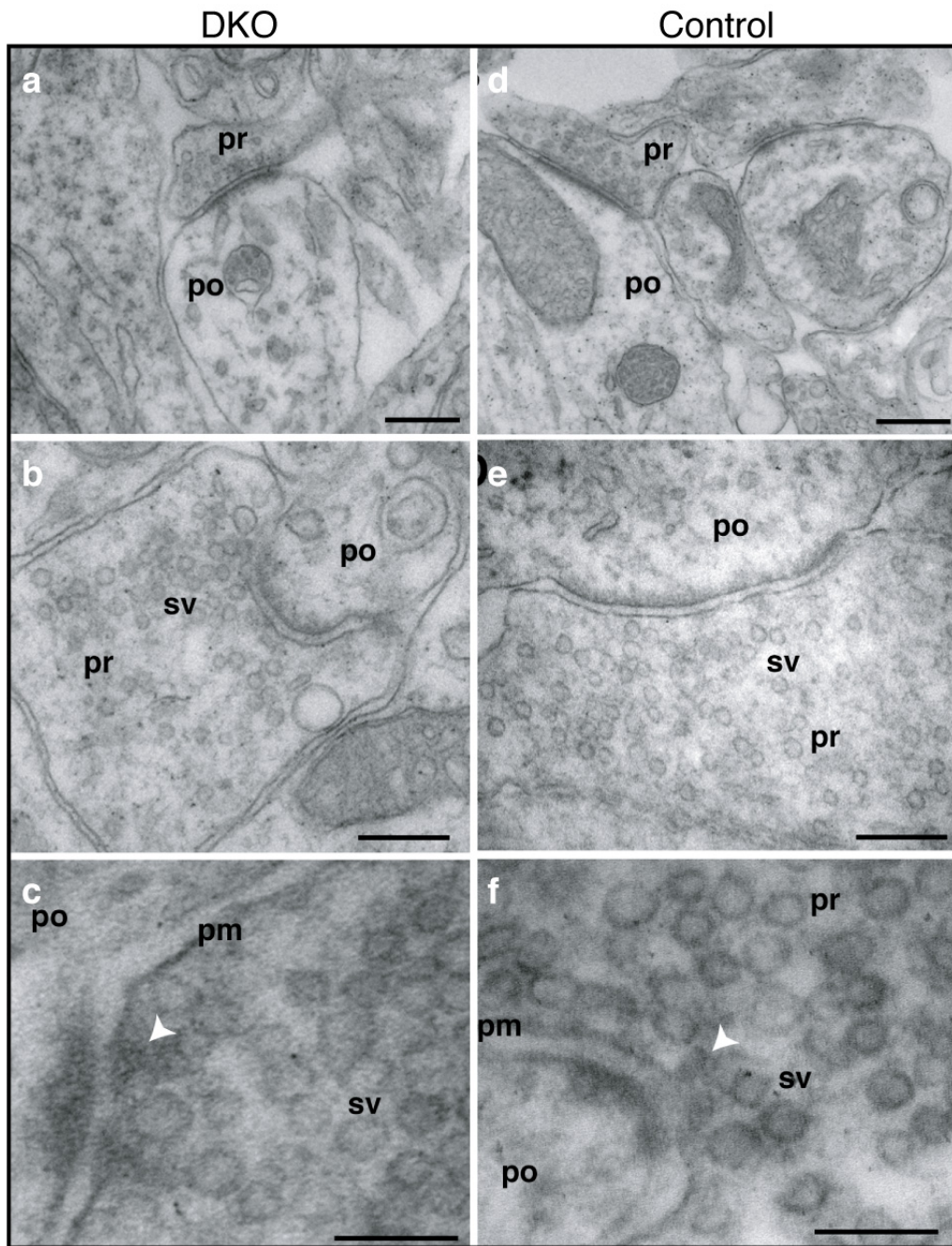
Figure 4.11: Electron micrographs of synapses in the spinal cord.
The arrows in (c, f) point to presynaptic dense projections in active zones. Abbreviations: pr, presynaptic; po, postsynaptic; sv, synaptic vesicles; pm, presynaptic plasma membrane. Scale bars, a = 300 nm, d = 370 nm, b = 300 nm, e = 240 nm, c = 100 nm, f = 130 nm.

Schmitz by electron microscopy. Typical synaptic structures were observed in RIM1α/2α double KO neurons (Figure 4.11), and no significant changes in synapse density (double KO = 35.7 ± 24.1 per 103 µm2; control [RIM1α DKO, RIM1α control] = 25.1 ± 21.3 per 103 µm^2; N=3 for both genotypes; 50 synapses for both genotypes), presynaptic bouton area (DKO = 0.290 ± 0.087 µm2; control = 0.228 ± 0.100 µm^2; N=3 and 50 synapses), density of synaptic vesi-

cles (DKO = 196 ± 136 synaptic vesicles per µm^2 bouton area; control = 202 ± 150 synaptic vesicles per µm2 bouton area; N=3 and 50 synapses), active zone length (DKO = 397 ± 177 nm; control = 354 ± 165 nm; N=3 and 50 synapses), or number of docked vesicles (DKO 7.8 ± 4.2 per µm active zone; control = 8.3 ± 5.4 per µm active zone; N=3 and 50 synapses) were detected. Thus deletion of α-RIMs does not cause a major alteration in synapse structure.

4.1.2.3 Structure of the neuromuscular junction in RIM1α/2α double KO mice.

Additionally, the morphology of the NMJ in the phrenic nerve/diaphragm muscle preparation was examined in collaboration with the lab of Dr. Weichun Lin (UT Southwestern Medical Center, Dallas, TX, USA). Therefore, immunostainings of whole mount muscles at E18.5 were incubated with antibodies to presynaptic proteins (Synaptotagmin 2, SV2B, Synaptophysin, Rab3A, Liprin-α and ELKS1) and with Texas Red conjugated α-bungarotoxin that labels postsynaptic acetylcholine receptors (data not shown). Strikingly, in RIM1α/2α double KO mice synapses visualized by Synaptotagmin 2 or other presynaptic markers colabeled with Acetylcholine receptor staining were only poorly aligned along the midline of the hemidiaphragm and more randomly distributed across a broader region of the muscle. Nevertheless, all axon terminals were always juxtaposed to acetylcholine receptors clusters.

To test if the observed pattern of synaptic contacts in the mutant NMJs is based on an increase in innervation, or an expansion of innervation, whole mount diaphragm muscles were stained with antibodies to the neurofilament protein or to Syntaxin 1, both of which label axons. Costaining with Texas Red conjugated α-bungarotoxin showed that in control mice, synapses were distributed regularly. In RIM1α/2α double KO mice, however, phrenic nerves exhibited abnormally extensive branching, and their terminal arborizations covered a much broader surface of the muscle. In conclusion, these immunolabeling data demonstrate an increased branching of presynaptic motor nerves and an increased formation of synapses on muscle fibers that are additionally more irregularly distributed than in the control situation. These phenomena, together with the observed increase in the number of α-motoneurons, are common features when synaptic transmission at the neuromuscular junction is impaired (Brandon et al., 2003; Misgeld et al., 2002).

4.2   Localization of RIM interacting proteins

Through their multiple protein domains RIMs have been shown in vitro to inter-act with multiple presynaptic proteins. However, for many of these binding part-ners it is not known to what degree their regional and cellular expression over-lap throughout the brain. Because of their importance for the structural organi-zation of the active zone and the Ca^{2+}-sensing step, distribution of the RIM in-teracting proteins Liprins, RIM-BPs and Synaptotagmins were analyzed.

4.2.1   Differential expression of the Liprin-α protein family

To obtain information on the mRNA distribution of the Liprin-α protein family, *in situ* hybridizations were performed on sagittal and horizontal brain slices of adult (p28) and newborn (p0) rats with radioactive probes detecting Liprin1α, -2α, -3α and -4α (Figure 4.12).

All four family members are expressed throughout the newborn brain in over-lapping patterns that vary in different brain regions between the four isoforms (Figure 4.12 left row). While Liprin4α is equally expressed in most brain regions, with the strongest expression levels in the hippocampus, lower cortical layers and olfactory bulb granule cells, the remaining isoforms show stronger regional differences. Liprin3α mRNA is most abundant in the hind- and midbrain, includ-ing the thalamus, as well as in the hippocampus, while the striatum, sub-thalamic regions and the olfactory bulb show less expression. In the cortex, the outer cortical layers exhibit the strongest signal, showing an inverse staining compared to Liprin4α. Expression of Liprin2α, and to a lower degree of Liprin1α, is enriched in the forebrain, with the most intense labeling in the outer cortical layers, the hippocampus, the olfactory bulb and the striatum, while hind brain and brain stem show less expression.
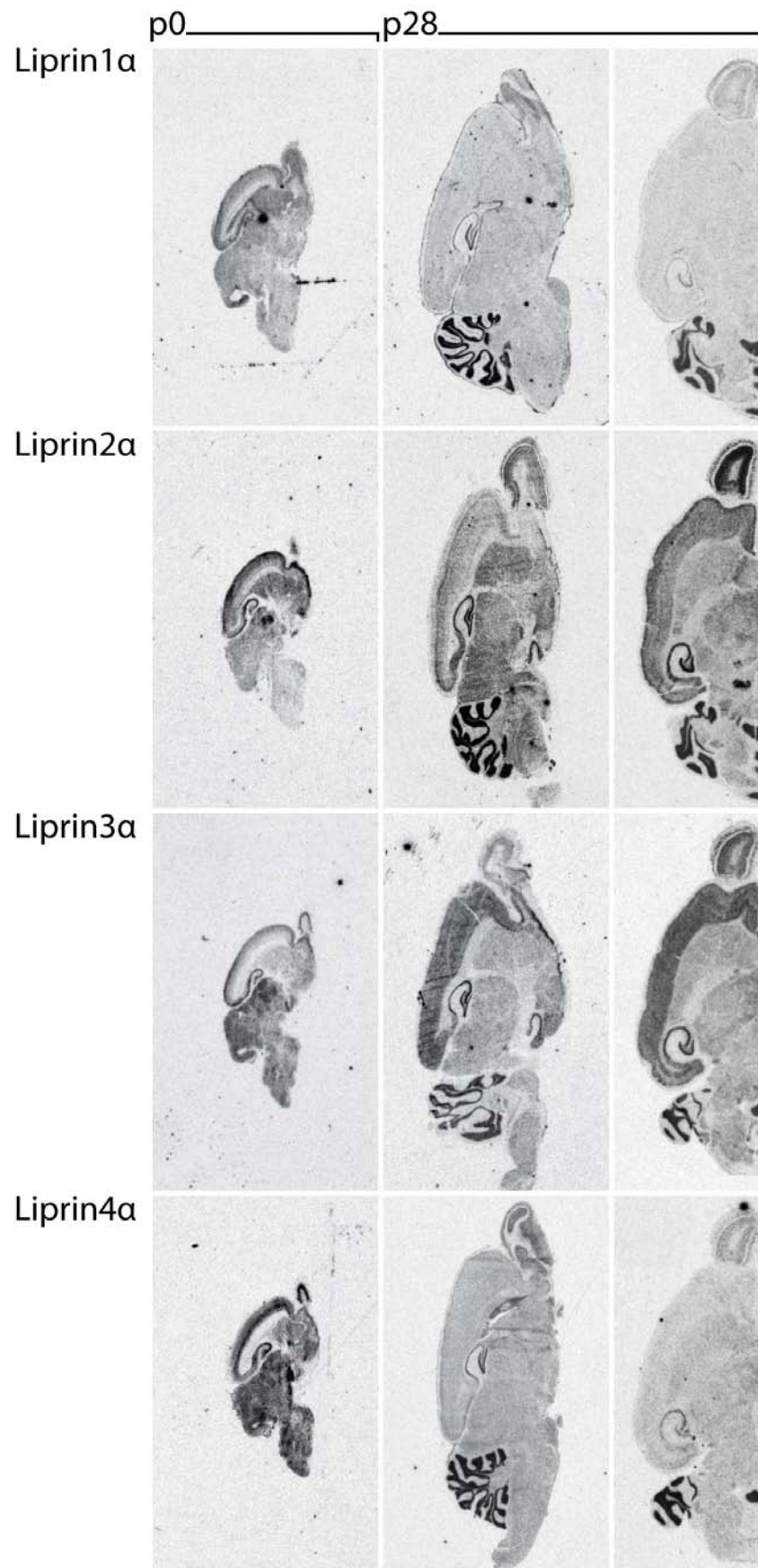
Figure 4.12: Distribution of Liprins-α in the neonatal and adult brain.

X-ray pictures of *in situ* hybridizations of the Liprin protein family on sagittal (p0, p28) and horizontal (p28) rat brains.

In the adult brain, Liprin1α and -4α expression declines, within most brain regions, except the cerebellum, the olfactory bulb and the hippocampus, showing only residual expression (Figure 4.12, middle and right column). In the hippocampus, Liprin1α is most strongly expressed in the gyrus dentatus granule cells, while Liprin4α can be detected in higher levels in the CA3 (ventral HC) and CA1 (dorsal HC) regions. Liprin2α mRNA is found at high levels throughout the adult brain, in particular in the olfactory bulb granule cells and mitral cells, cortical layer 2, the hippocampus and the cerebellum. *In situ* hybridization also revealed strong expression of Liprin3α, however the mRNA distribution varies between the different brain regions. The strongest signals were observed in the olfactory bulb, the cortex and the hippocampus. Compared to Liprin2α, the distribution of Liprin3α throughout the cortical layers is more uniform. Only weak signals were detected in striatum, thalamus, hindbrain and brainstem.

4.2.2 Synaptotagmin gene expression in the rat brain

Synaptotagmins are a large family of membrane trafficking proteins. They are evolutionary conserved and have 15 members in rodents and humans. The regional distribution of some of the Synaptotagmin isoforms has been published already (Berton et al. 1997, Ullrich & Sudhof 1995), but a comparative study of all Synaptotagmins is still missing. Therefore a systematic analysis of expression using radioactive *in situ* hybridization and quantitative real time RT-PCR as well as multiplex RT-PCR on a single cell level was performed.

4.2.2.1 Expression patterns of Synaptotagmin genes

The spatial expression pattern of Synaptotagmins-1 to -13 was analyzed in brains of rats (P28) by radioactive ISH and quantitative real time RT-PCR. To compare the expression of the different genes in different regions of the brain the ISH analysis was performed on horizontal, sagittal, and coronal sections. The ISH analysis allowed the reliable comparison of expression strength of individual isoforms between different brain regions (Table 4.3). However, due to variations in the sensitivity between different probes, a comparative analysis between the different isoforms can only be qualitative. Therefore, the relative expression levels of the different Synaptotagmins in the olfactory bulb, basal ganglia, cerebral cortex, hippocampus, diencephalon and cerebellum was additionally determined by quantitative real time RT-PCR (q-rtPCR) (Figure 4.13). For the individual Synaptotagmin isoforms the expression strength in the analyzed brain regions determined by q-rtPCR reflected the results obtained by ISH (Figure 4.13 and Figure 4.15, Table 4.3). The q-rtPCR revealed that Syt-1 is the most abundant Synaptotagmin isoform in all brain regions tested, whereas most of the other isoforms are only present at significantly lower levels. However, in some areas like the cerebellum other isoforms, i.e. Syt-2 and -12, were also expressed strongly. Expression levels for Syt-8 were below the detection limits of the ISH (data not shown) and barely detectable by q-rtPCR (Figure 4.14).

Table 4.3: Expression of Synaptotagmin-1 to -13 in various brain regions

X-ray films exposed for 1-2 weeks (grey background) and 4-6 weeks (white) due to general differences in the expression levels. Brain regions and abbreviations depicted on the left, mRNA labeling intensity on the right ranging from no labeling (-) to very strong labeling (++++) or strong punctuate labeling (o). amygd. amygdaloidal; ant. anterior; BS brainstem; c. cells; cereb. cerebellar; colic. colliculus; nu. nucleus/nuclei; thal. thalamus/thalamic.

	Synaptotagmin	Syt	1	2	3	4	5	6	7	9	10	11	12	13
Olf. bulb	glomerular layer	Glo	+++	-	++	++	++	+	+++	+	+	+++	++	++
	mitral layer	Mi	++++	-	++	+++	+++	+++	++++	++	+++	++++	++	++
	granular layer	Gr	+++	-	++	+++	+++	+++	++	-	++	+++	++	+
Neocortex	Lamina I	I	-	-	-	-	-	-	-	-	-	++	-	-
	Lamina II	II	++++	-	++	+++	+++	-	++	-	+	++++	+	+
	Lamina III	III	++++	o	++	++	++	-	+	-	-	++++	+	+
	Lamina IV	IV	++++	++	++	+++	++	-	++	-	+	+++	+	+
	Lamina V	V	++++	o	+	++	+++	+++	+++	-	+	+++	+	+
	Lamina VI	VI	++++	-	+	+	+++	-	+++	-	-	+++	-	+
	white matter	WM	-	-	-	-	-	-	-	-	-	++	-	-
Hippocampus	dentate gyrus	DG	+++	-	+++	+++	++	++	++++	+	++	++++	+	+
	CA3 pyramidal c.	CA3	++++	o	+++	++++	++	o	+++	-	+	++++	++	++
	CA1 pyramidal c.	CA1	++++	o	+++	+++	++	o	++	+	+	++++	+++	+
	subiculum	Si	++++	o	+++	+++	++	-	+	-	-	+++	+	+
	entorhinal cortex	Ent	++++	-	++	+++	++	-	+++	-	-	++++	++	-
	hilus	HI	o	-	o	o	o	-	o	-	-	++	o	o
Striatum	putamen	CPu	+++	+	++	++	+++	+++	++	+	-	+++	++	-
	nu. accumbens	Acb	+++	+	++	++	+++	+++	++	-	-	++++	++	-
	ventral pallidum	VP	++++	++++	++	++	++	-	-	-	+	++++	+	+
	Islands of Calleja	ICj	+++	++++	-	+	++	+++	+			++++	++	-
Midbrain	posterior thal.	PT	++++	-	++	++	++	-	+++	+	-	++++	+	+
	anterior thalamus	AT	++++	++	++	++	+	-	++	++	-	++++	+	++
	ventral thalamus	VT	++++	+++	++	++	+	-	+++	++	-	++++	+	+
	dorsal thalamus	DT	++++	-	++	++	+	-	+++	++	-	++++	+	++
	reticular thal. nu.	Rt	++++	+++	++	++	+	++	+	-	-	++++	+	+
	hypothalamic nu.	HY	+++	-	++	++	++	-	+	-	+	++++	++	++
	medial amygd. nu.	MeA	++++	-	+	+++	++++	-	-	-	-	++++	++	+
	zona incerta	ZI	+++	++++	++	++	+	+	+	-	+	++++	++	+
	substantia nigra	SN	+	+++	++	+	-	-	-	-	-	++++	+	++
	ant. pretectal nu.	APT	+++	+++	++	++	+	++	+	-	-	++++	++	++
	superior collic.	SC	++++	++	++	++	+	+	++	+	-	++++	++	+
	inferior colliculus	IC	+++	++++	++	++	++	++	++	+	-	++++	++	+
Cerebellum	Purkinje cell layer	PC	-	++++	-	+++	-	-	++++	-	-	-	-	-
	granular layer	GL	++++	++++	++	+++	++	+	+++	+++	-	++++	+++	++
	molecular layer	ML	-	+	-	-	-	+	-	-	-	++	-	-
	deep cereb. nu.	DCn	+++	+++	+++	+++	+++	++	++	-	-	+++	+	++
BS	medulla oblongata	MO	+	+++	+	++	+	++	+	-	-	++++	+	+
	pontine nuclei	Pn	++	++++	++	++	++	++	++	-	+	++++	+	++
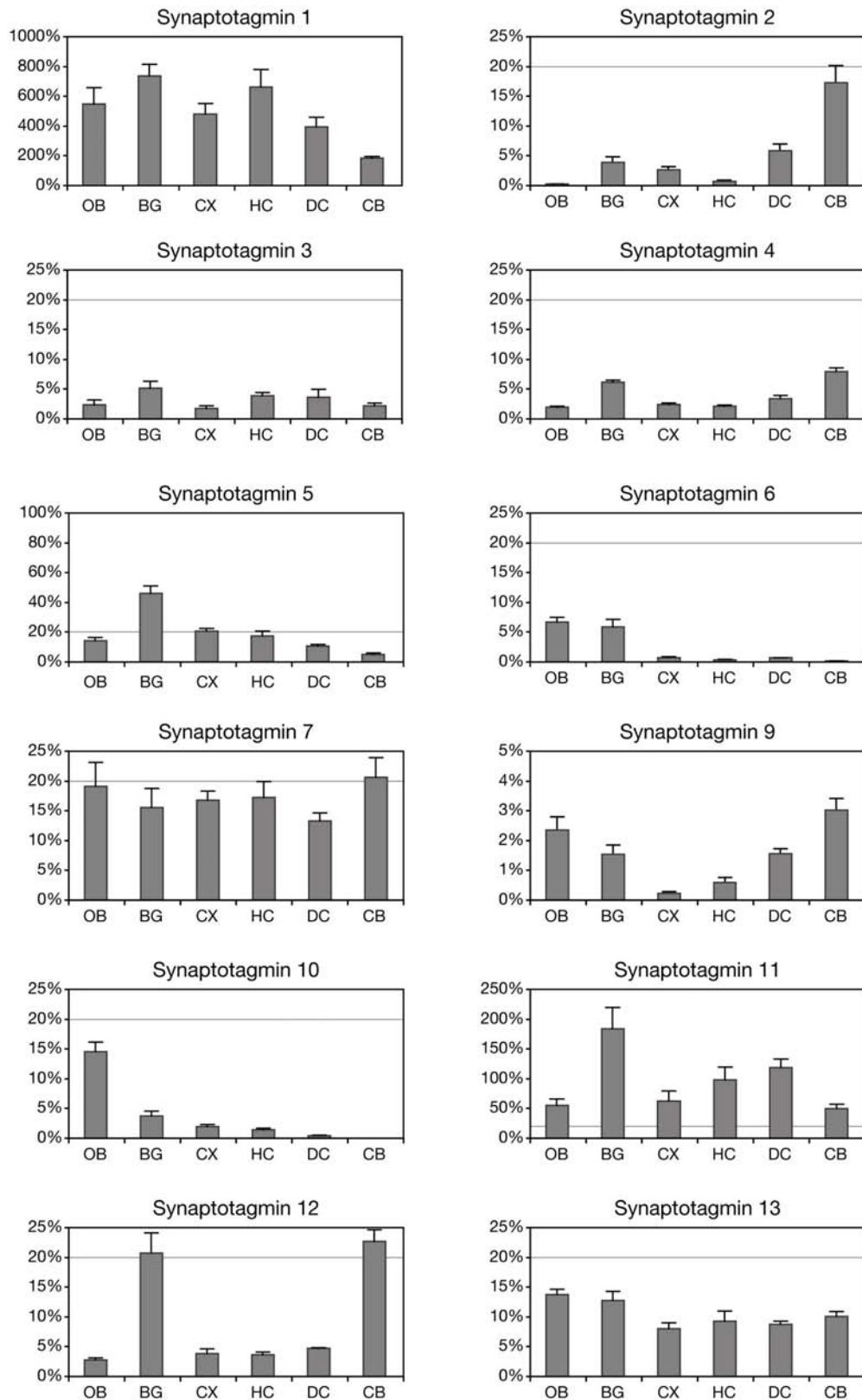
Figure 4.13: Synaptotagmin mRNA expression in various brain regions.

Quantitative real-time RT PCR Data of Synaptotagmin 1 - 13 from six different rat brain regions. Expression levels are normalized to internal Synaptophysin control. The 20% line is accentuated to ease comparison of different-scaled graphs.

N = four adult male rats; OB olfactory bulb; BG basal ganglia; CX cortex; HC hippocampus; DC diencephalon; CB cerebellum.
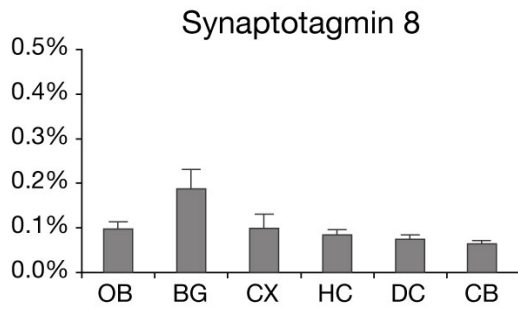
Figure 4.14: Quantitative real-time RT PCR Data of Synaptotagmin 8.

Data from six different rat brain regions, generated with fluorescent probes. Expression levels are normalized to internal Synaptophysin control. N = four adult male rats; OB olfactory bulb; BG basal ganglia; CX cortex; HC hippocampus; DC diencephalon; CB cerebellum.
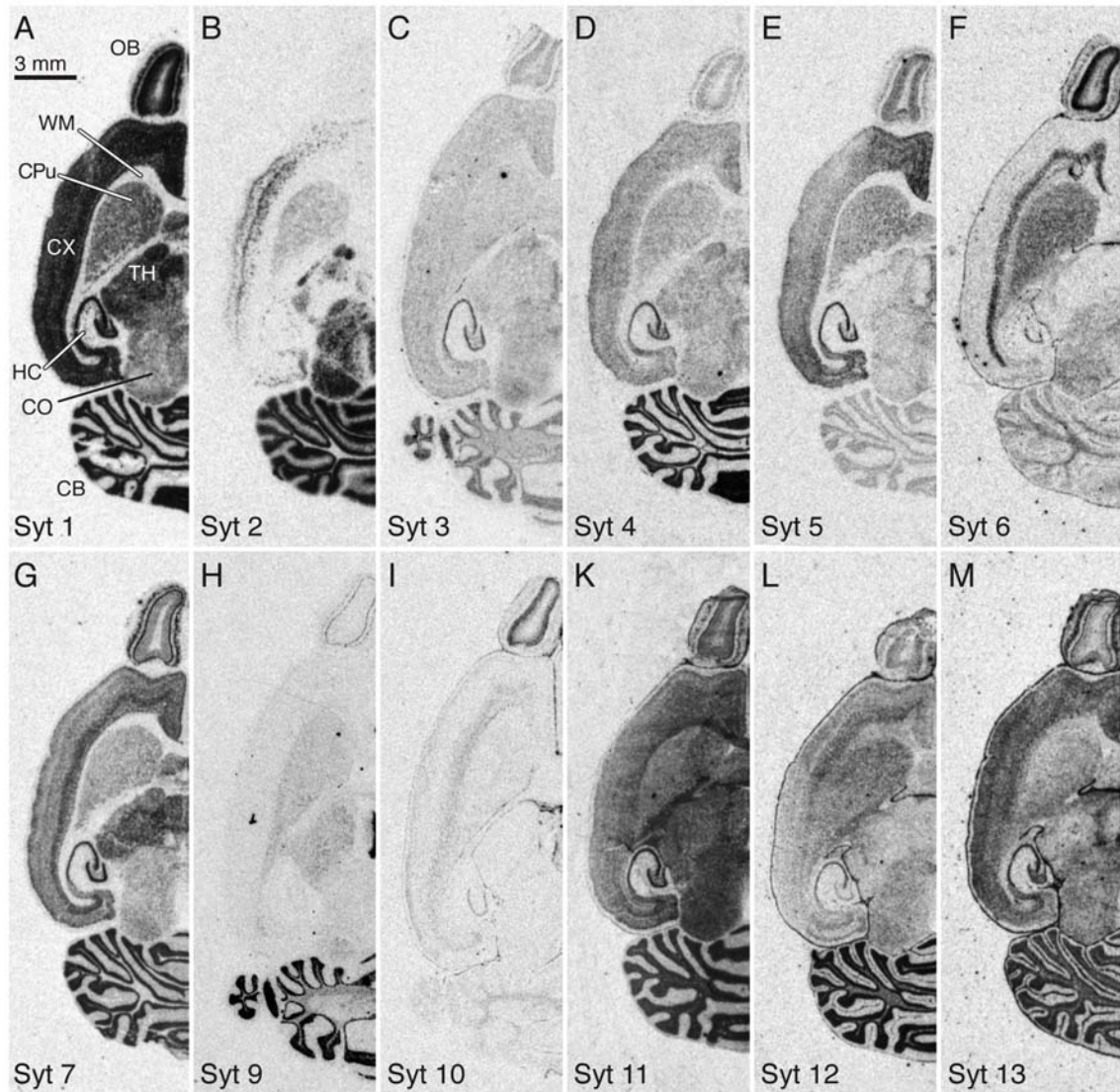
Figure 4.15: Distribution of Synaptotagmin genes in P28 rat brain.

X-ray film images showing the localization of all members of the Synaptotagmin gene family on horizontal sections of rat brain detected with radioactive *in situ* hybridization (ISH) using 35S labeled oligonucleotides specific for Synaptotagmins (Syts) -1 to -13 (Syt-8 was not detectable in P28 rat brain). Negative controls with excess unlabeled oligonucleotides were devoid of signal (Figure 4.16). BG basal ganglia; CB cerebellum; CO colliculus; CX cortex; HC hippocampus; MHb medial habenular nucleus; OB olfactory bulb; TH thalamus; WM white matter regions, i.e. corpus callosum, capsule, fimbria of the hippocampus.
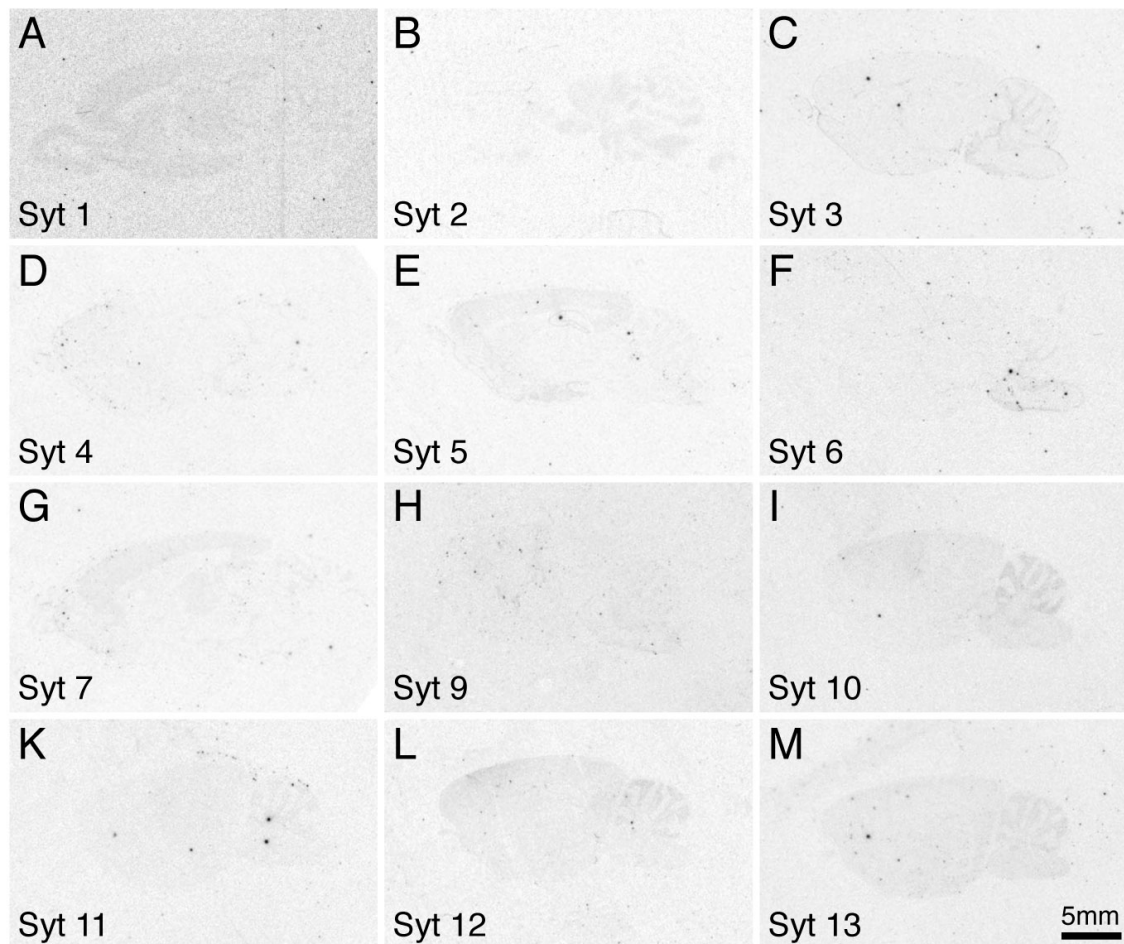
Figure 4.16: X-ray film images showing the background controls of the different Synaptotagmin probes performed with 1000-fold excess of the respective unlabeled oligonucleotide.

4.2.2.2 Olfactory bulb

In juvenile rats, expression of eleven Synaptotagmins (Syt-1, Syt-3 – Syt-7, Syt-9 – Syt-13) was detected in the olfactory bulb in variable patterns; only transcripts for Syt-2 and Syt-8 were absent (Figure 4.13, Figure 4.15, Figure 4.17 and Table 4.3). Whereas Syt-9 mRNA was only found in the glomerular (Gl) layer and in mitral cells (Mi), transcripts for the remaining Synaptotagmin genes were also present in the granular layer (GrO). The most abundant Synaptotagmin isoform in the olfactory bulb is Syt-1, which showed its strongest expression in the mitral cell layer, and was equally expressed at high levels in the glomerular layer and the olfactory bulb granular layer. Labeling for Syt-3 and Syt-12 was detected in the three layers at equal intensity; however, their level of hybridization was overall low. Syt-6 and -10, and to a lower degree Syt-4 and -5 were predominantly expressed in the olfactory bulb granule cells and mitral cells. Syt-10 is only expressed at very low levels throughout the brain, but transcript levels

in the granule cells are very high, thereby representing the only cell type with significant Syt-10 expression under native conditions. Syt-6 exhibited a similar pattern of expression in the olfactory bulb, even though Syt-6 transcript levels in most remaining parts of the brain are higher than the ones observed for Syt-10. Syt-7 and Syt-13 are most prominently expressed in the glomerular layer and the mitral cell layer, but at weaker levels also in the granular layer.
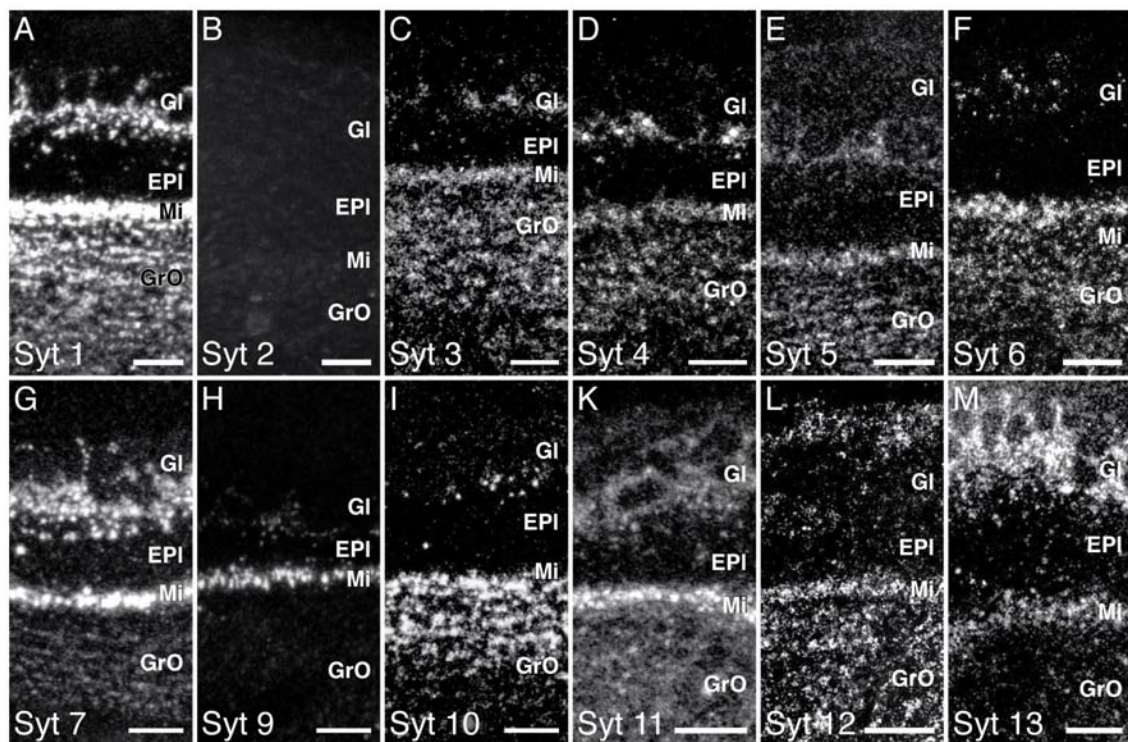
Figure 4.17: Synaptotagmin gene expression in the olfactory bulb of rat brain.
Dark field images of emulsion-dipped tissue sections reveal the expression of Syts within the different cell layers of the olfactory bulb. EPI external plexiform layer; Gl glomerular layer; GrO granule cell layer of the olfactory bulb; Mi mitral cell layer.

4.2.2.3 Cerebral cortex

In the cerebral cortex, ISH experiments revealed the expression of the mRNAs encoding 11 of the 13 Synaptotagmin genes examined in this study (Table 4.3, Figure 4.13, Figure 4.15 and Figure 4.18). Syt-8 and Syt-9 were not detectable in cortical cells by ISH and only very low Syt-9 mRNA levels were measured by quantitative real time RT-PCR. Whereas Syt-1, -3, -4, -5, -11, -12, and -13 were expressed in cortical layers II to VI of the frontal cortex as well as the motor cortex, Syt-2, -6, -7, and -10 exhibit a more layer-specific expression pattern. Syt-1 was very strongly and uniformly expressed throughout the cortex besides layer I. Syt-3, -5, -11 and -13 exhibited a similar more less uniform pattern of expression in the cortex, however, with the exception of Syt-11, their transcripts were

present at a lower level in all laminas examined. In particular, signals for Syt-3 and -13 were very weak. Syt-2 showed a distinct punctate labeling most likely reflecting expression in the big pyramidal neurons in lamina III and V. Expression of Syt-6 was strictly confined to layer V resulting in a low overall expression level as determined by quantitative real time RT-PCR. Syt-7 was predominantly found in neurons of layers V and VI, and at weaker levels in the upper laminas. Transcript levels of Syt-10 in the cortex were very low and were mainly restricted to layer II, V and VI. Syt-11, the one Synaptotagmin with a distinct expression in nonneuronal parts of the brain, was also detected in layer I and the cortical white matter regions like the corpus callosum, the external capsule and the fimbria of the hippocampus (white matter, WM).

Figure 4.18: Synaptotagmin gene expression in the cortex of rat brain.
Dark field images of emulsion-dipped tissue sections reveal the expression of Syts within the different cortical layers.

4.2.2.4 Hippocampus

In the hippocampal formation, weak to strong expression or punctate labeling, indicating single cell expression in a small subset of cells was found in at least one of the two parts of the cornu ammonis pyramidal cell layers (CA1, CA3) and the dentate gyrus (DG) for most of the Synaptotagmin genes. The only exceptions were Syt-2, Syt-8 and Syt-9, for which almost no labeling could be de-

tected (Table 4.3, Figure 4.13, Figure 4.15 and Figure 4.19). However, analysis of dark field images of emulsion dipped tissue sections revealed that Syt-2 is exclusively found in a subpopulation of cells scattered mainly in the CA1 and CA3 subfields. Syt-1 mRNA was present at very high levels in the pyramidal cell layer of the CA subfields and the granular cell layer of the dentate gyrus. In addition, a strong punctuate labeling was found in the Hilus and to a lesser extent in the stratum radiatum and the stratum oriens, indicating that Syt-1 is expressed by the interneurons and/or glial cells located in these areas as well.
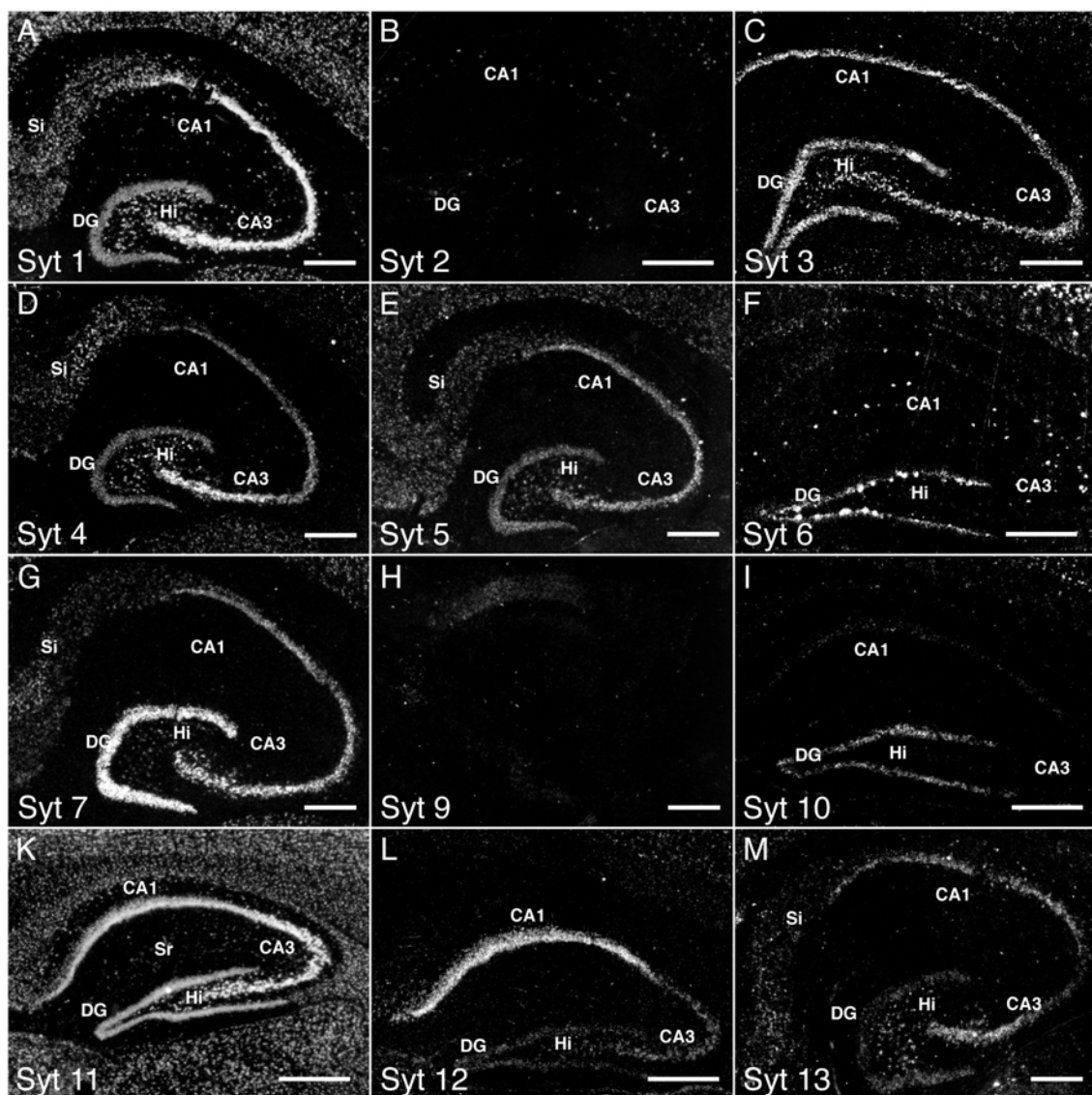
Figure 4.19: Synaptotagmin gene expression in the hippocampus.
Dark field images of emulsion-dipped tissue sections reveal the expression of Syts within the different hippocampal subregions. CA cornu ammonis region; DG dentate gyrus; HI hilus region; Sr stratum radiatum; scale bars = 500µm.

Syt-3, -4, -5, and -11 exhibited a similar more less uniform expression pattern with punctate single cell labeling in the hilar region. Their overall level of ex-

pression was weaker though, with the exception of Syt-11, which showed equally stronger expression in all subfields. Syt-7 was very prominently expressed in the DG, with lower, but still strong expression in the CA3 region and moderate levels in CA1. Several other Synaptotagmin isoforms showed even stronger subregion-specific variations in their expression patterns. Syt-10 transcripts were mostly present in the DG, even though the overall level of Syt-10 mRNA in the hippocampus was very low. Syt-6 exhibited a similar pattern of distribution, but furthermore showed intense labeling in a distinct subset of cells within the dentate gyrus and the CA subfields. In contrast, strong expression of Syt-12 was only observed in the CA1 region. Syt-13 mRNA was moderately expressed in the CA3 layer, whereas its expression in the other parts of the hippocampus was relatively weak.

4.2.2.5 Basal ganglia

Within the main structures of the basal ganglia, such as caudate putamen (CPu), ventral pallidum (VP), and nucleus accumbens (Acb), radioactive ISH revealed the presence of all Synaptotagmin isoforms, albeit with diverging distributions (Table 4.3, Figure 4.13, Figure 4.15 and Figure 4.20). Transcripts for Syt-1, Syt-3 – Syt-7, Syt-11 and Syt-13 were detected in the putamen and nucleus accumbens in an abundance that was similar or lower than the one observed in the cortex. Syt-2 showed a strong punctate labeling in the ventral pallidum (VP) and the islands of calleja (ICj), whereas the hybridization pattern in the putamen was weaker and more uniform. In contrast, expression of Syt-6 was confined to the putamen, nucleus accumbens and the islands of calleja as the ventral pallidum and the lateral septal nucleus were void of a hybridization signal. Interestingly, in the ISH Syt-9 and Syt-12 were the only Synaptotagmin isoforms with a higher abundance in the putamen than in the cortex (Table 4.3 and Figure 4.13), even though the overall level of expression was low to moderate in the basal ganglia. Labeling for Syt-10 can only be detected in the ventral pallidum.

4.2.2.6 Midbrain and Diencephalon

In the midbrain and the diencephalon, the level of expression of the individual Synaptotagmin genes varied from very strong, as observed for Syt-1 and Syt-11, to not detectable in Syt-10 (Table 4.3, Figure 4.13, Figure 4.15 and Figure

4.20). Syt-1 was expressed in all parts of the diencephalon, most prominently in the thalamus (TH), the medial amygdaloidal nuclei (MeA) and the superficial layers of the superior colliculi (SC). Strong expression of Syt-1 mRNA was also detected in the inferior colliculi (IC), the anterior pretectal nucleus (APT), the hypothalamic nuclei (HY) and zona incerta (ZI). Interestingly, the substantia nigra (SN) only showed weak Syt-1 expression.
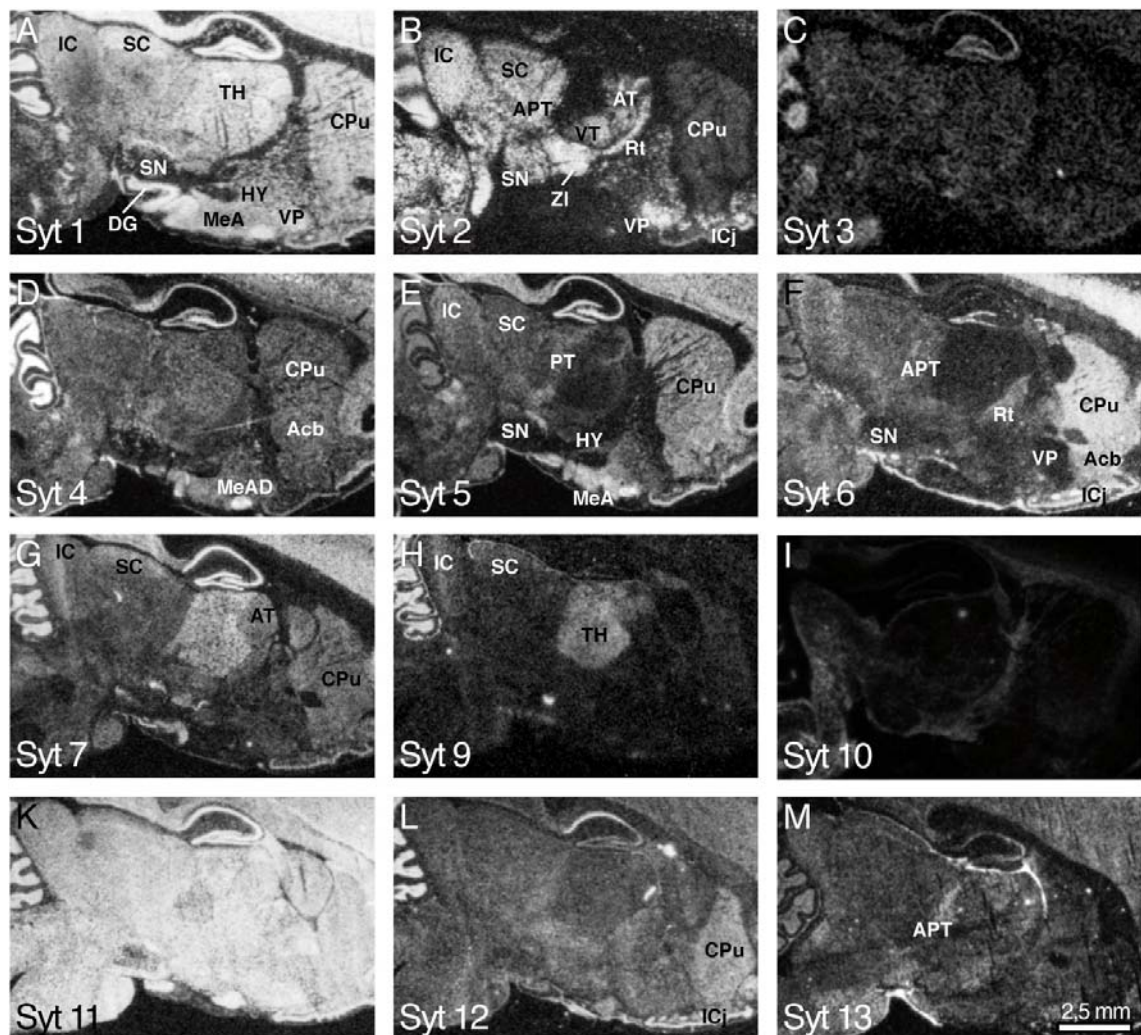
Figure 4.20: Sagittal view of Synaptotagmin gene expression in rat brain.
Inverted scans of films exposed to labeled tissue sections reveal the expression of Syts within the basal ganglia, midbrain, diencephalon and brainstem. Acb nucleus accumbens; APT anterior pretectal nucleus; AT anterior thalamus; CPu caudate putamen; DG dentate gyrus; DT dorsal thalamus; HY hypothalamic nuclei; IC inferior colliculus; ICj Islands of Calleja; MeA medial amygdaloidal nucleus; MeAD medial amygdaloidal nucleus, anterio-dorsal part; Pn pontine nuclei; PT posterior thalamus; Rt reticular thalamic nucleus; SC superior colliculus; SN substantia nigra; TH thalamus; VP ventral Pallidum; VT ventral thalamus; ZI zona incerta.

Syt-2 exhibited a more restricted pattern of expression. Highest levels of expression were found in the inferior colliculus and zona incerta. Distinct parts of the anterior and ventral thalamus as well as the reticular thalamic nucleus (Rt),

the substantia nigra, the anterior pretectal nucleus and the superior colliculi showed moderate to strong labeling, too. Interestingly, the dorsal and posterior parts of the thalamus were void of any signal, while the anterior, ventral and ventro-lateral nuclei were strongly labeled. Syt-3 and -4 were found throughout the diencephalon in a more less uniform distribution, at an overall moderate level of expression. However, Syt-4 showed stronger expression in the medial amygdala, especially the anterior-dorsal amygdaloidal nucleus (MeAD). Syt-5 expression was lower in most parts of the midbrain, only the posterior thalamus (PT), hypothalamic nuclei (HY) and the inferior colliculus showed moderate signals. Interestingly, labeling in the medial amygdaloidal nuclei was very strong, while the substantia nigra did not show Syt-5 expression. Moderate Syt-6 signals were confined to the reticular thalamic nucleus (Rt), the APT, the inferior colliculus (IC) and, to a lesser extent, the superior colliculus (SC), while the thalamus and substantia nigra (SN) show no Syt-6 expression. In contrast, the thalamus was the midbrain region with the highest level of expression for Syt-7 and Syt-9. However, whereas Syt-7 was one of the most abundant Synaptotagmin isoforms in the thalamus besides Syt-1 and Syt-11, the overall expression level of Syt-9 was low. Moderate Syt-7 mRNA labeling was found in the dorsal collicular layers, where also weak labeling for Syt-9 was detected. Strong Syt-9 expression was only found in the medial habenular nucleus (MHb, Figure 4.15). Syt-11 was very strongly expressed throughout all parts of the diencephalon and mesencephalon. Syt-12 labeling was uniformly low, with strongest levels in the APT, the reticular thalamic nucleus (Rt) and subthalamic regions, for example the amygdala and zona incerta. The thalamus only showed a weak expression, and also the substantia nigra expressed low levels of Syt-12. Syt-13 mRNA was found in the anterior pretectal nuclei and the anterior-dorsal thalamus, while the posterior thalamus exhibited weaker expression.

4.2.2.7 Brainstem

In the brainstem, transcripts of all Synaptotagmin isoforms, except Syt-9, could be detected (Table 4.3 and Figure 4.20). However, the overall level of expression was quite low, only Syt-2 and Syt-11 showed a strong labeling. Syt-1, the isoform with the highest abundance in the brain besides Syt-11, was less abundant in the brainstem than in all other brain regions. Only in the pontine nuclei a

moderate hybridization signal could be detected. On the other hand, Syt-2 is most strongly expressed in the hindbrain, in particular in the brain stem, where a strong punctate distinct labeling for Syt-2 was observed. Syt-11 is the most abundant Synaptotagmin isoform in the brain stem as its mRNA is uniformly expressed and supposedly present in spinal neurons and glial cells.

4.2.2.8 Cerebellum
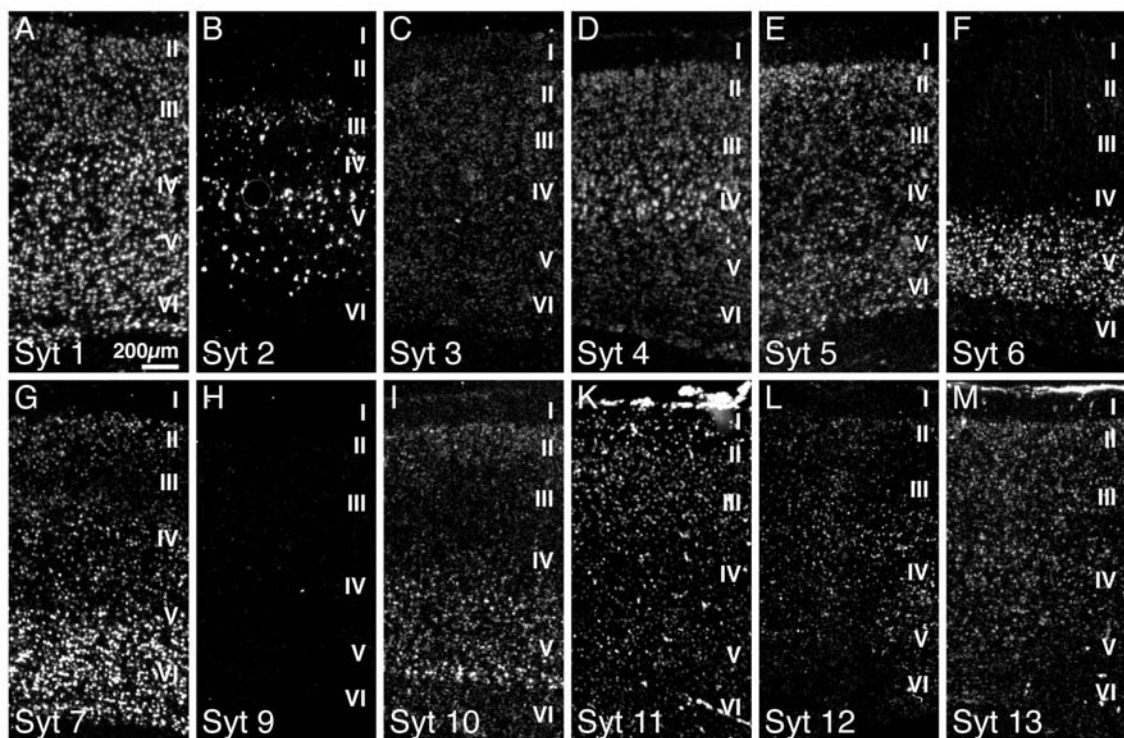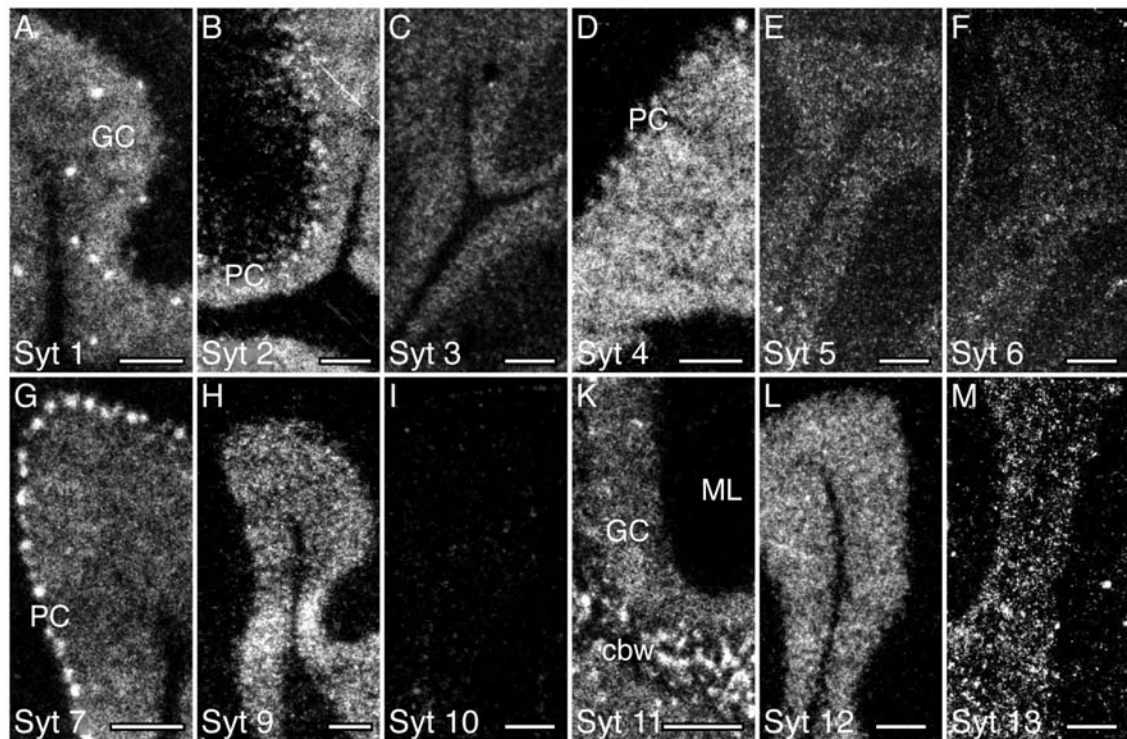

Figure 4.21: Synaptotagmin gene expression in the rat cerebellum.
Dark field images of emulsion-dipped tissue sections reveal the expression of Syts within the different hippocampal subregions. cbw cerebellar white matter; GC cerebellar granule cells; ML molecular layer; PC purkinje cells; scale bars = 100µm.

In the cerebellar granule cell layer (GC), medium to strong expression of most Synaptotagmin genes was observed (Table 4.3, Figure 4.13, Figure 4.15 and Figure 4.21). The only exceptions were Syt10, for which no specific labeling could be detected, and Syt-6, which was only expressed at very low levels. Interestingly, within the granular cell layer individual cells showed a very strong labeling for Syt-1, potentially representing Golgi cells (GC). Syt-7 was most prominently expressed in the Purkinje cells (PC), however also Syt-2 and Syt-4 transcripts were clearly labeled in these cells. The molecular layer of the cerebellum (ML) is mainly devoid of Synaptotagmin transcripts, only hybridization with probes against Syt-2, Syt-6 and Syt-11 resulted in a weak labeling. In the

deep cerebellar nuclei, expression of all Synaptotagmin genes, except Syt-9, was observed.

4.2.2.9 Glial cells

Based on the ISH signals, in some cases, expression patterns of Synaptotagmins could be distinguished from neuronal expression already on a macroscopic level. Whereas no labeling was observed for neuron-specific genes in areas of high axonal density like the white matter regions or layer I of the cortex, hybridization of a probe to mRNA present in glial cells resulted in a strong signal in these regions. Syt-11 was the only Synaptotagmin isoform for which a marked ISH signal in putative glial cells was observed, e.g. a strong labeling was detected in the capsule, the corpus callosum and the fimbria of the hippocampus (Figure 4.15 and Figure 4.20).

4.2.3 Expression of RIM-BP genes
- identification of a new RIM-BP family member

RIM-binding proteins (RIM-BPs) were identified as binding partners of the presynaptic active zone proteins RIMs as well as for voltage gated Ca^{2+}-channels (Hibino et al. 2002, Wang et al. 2000). They were suggested to form a functional link between the synaptic-vesicle fusion apparatus and Ca^{2+}-channels. However, so far nothing is known about RIM-BP expression, regional distribution or genomic organization.

4.2.3.1 Identification of a third member of the RIM-BP gene family

While designing primers and probes for the RIM-BP genes, we identified a novel RIM-BP-related gene in addition to the previously described RIM-BP1 and RIM-BP2 genes (Hibino et al. 2002, Wang et al. 2000), referred to as RIM-BP3. This gene was related to existing ESTs and its existence was verified by cloning the full length sequence of this novel gene from mouse testes cDNA (Figure 4.23). The RIM-BP3 gene expresses a single transcript with a domain organization similar to RIM-BP1 and RIM-BP2 (Figure 4.22A). The primary structure of human and mouse RIM-BP3 consists of 1639 and 1606 amino acid residues, respectively, with a calculated molecular mass of around 180 kDa. The RIM-BP3 N-terminus exhibits only a low degree of homology with the N-terminal region of RIM-BP1. The amino acid composition of this region is characterized by

its high content of arginine, glutamic acid, aspartic acid, and serine (Figure 4.22B). Furthermore, sequence analysis revealed a mixed charge cluster within the first 120 AA and a proline rich region (Figure 4.22B). All RIM-BP proteins contain a central SH3-domain and a cluster of Fibronectin III (FNIII) repeats. However, whereas in RIM-BP1 and RIM-BP2 three FNIII repeats are found, only the second and third FNIII repeats are present in RIM-BP3. In their C-terminus all RIM-BP proteins are composed of two SH3-domains followed by sequences that diverge in length and composition between the three isoforms. Within the RIM-BP family RIM-BP3 is most closely related to RIM-BP1, both in size and in amino acid composition. Even though the overall identity for the full-length proteins is only about 21%, the SH3- and FNIII-domains exhibit a significant conservation with identities ranging from 41% to 75% (Figure 4.22C, Table 4.4).
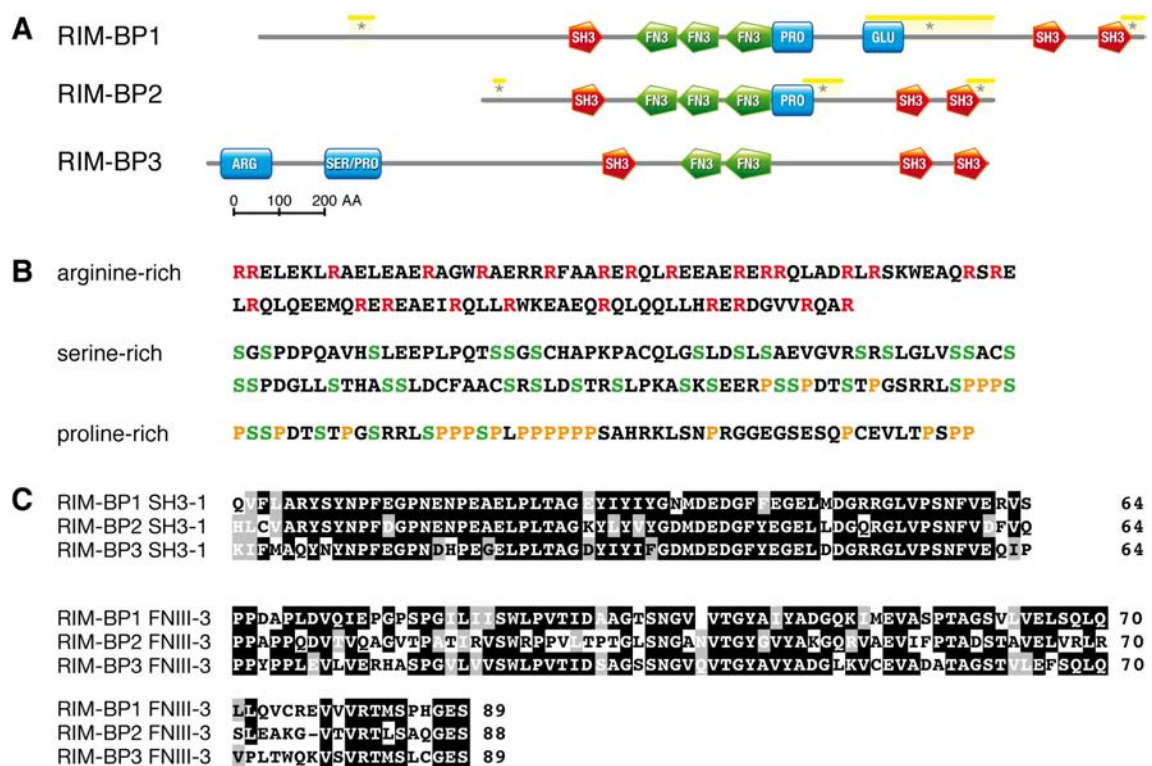
Figure 4.22: Structure of the RIM-BP protein family.
(A) Diagram of the domain composition of RIM-BPs. RIM-BPs share a similar domain organization with a SH3-domain and a cluster of Fibronectin type III (FNIII) repeats in the center of the protein and a doublet of SH3-domain in the C-terminus. Asterisks mark the three sites of alternative splicing in RIM-BP1 and -2. **(B)** The RIM-BP3 N-terminus contains an arginine-rich (AA 30-137), serine-rich (AA 214-330) and proline-rich (AA 312-366) region. **(C)** The RIM-BP SH3- and FNIII-domains are highly homologous, as shown here for SH3-1 and FNIII-3. Filled black boxes mark amino acids identical in all three human RIM-BP proteins and grey boxes indicate conserved residues.

Table 4.4: Identity and similarity of RIM-BP proteins

	RIM-BP1 : RIM-BP2	RIM-BP1 : RIM-BP3	RIM-BP2 : RIM-BP3
SH3-1	77% / 89%	75% / 88%	69% / 84%
SH3-2	76% / 90%	48% / 60%	49% / 61%
SH3-3	72% / 83%	48% / 66%	39% / 63 %
SH3-2+3	47% / 55%	35% / 47%	32% / 44%
FNIII-1	44% / 65%	NA	NA
FNIII-2	38% / 53%	41% /57%	27% / 53%
FNIII-3	46% / 64%	61% / 75%	45% / 63%
FNIII-2+3	44% / 62%	48% / 61%	35% / 54%
ORF	24% / 33%	21% / 29%	14% / 24%

Amino acid identities and similarities of protein sequences were determined the sequence ma-
nipulation suite (accessible at http://www.ualberta.ca/~stothard/javascript/ident_sim.html) after
their pair-wise alignment using ClustalW (Gonnet protein weight matrix and settings of a gap
open penalty of 10, a gap extension penalty of 0.05, and no gap separation penalty) . Amino
acids were counted as similar within the following groups (1) GAVLI, (2) FYW, (3) CM, (4) ST,
(5) KRH, (6) DENQ, and (7) P.

4.2.3.2 Expression of the RIM-BP genes

Quantitative realtime PCR analyses of mouse tissues was performed with prim-
ers specific to RIM-BP1, -2 and -3 to elucidate their expression as compared to
Actin, that was used as normalization control. RIM-BP1 and -2 were synthe-
sized at high levels exclusively in brain of all tissues analyzed. RIM-BP3 mRNA
in contrast was detected ubiquitously, with the highest level of expression in
testes (Figure 4.23 A, B). To examine the regional expression of RIM-BPs
within the brain, cDNA from different brain regions was prepared and RIM-BP
mRNA levels were measured by RT-PCR. While RIM-BP1 exhibits a strong
ubiquitous expression throughout the brain, high levels of RIM-BP2 mRNA can
be detected in all brain regions with exception of the cerebellum. RIM-BP3
showed a low uniform expression throughout all brain regions (Figure 4.23C).
During early brain development, starting at embryonic day 12.5 till birth (E12.5 -
P0), all RIM-BP genes were expressed at an equally low level. However,
whereas RIM-BP1 and -2 exhibited the strong increase in expression between
P0 and P15 typically observed for synaptic proteins, RIM-BP3 expression levels
remained unchanged (Figure 4.23D).
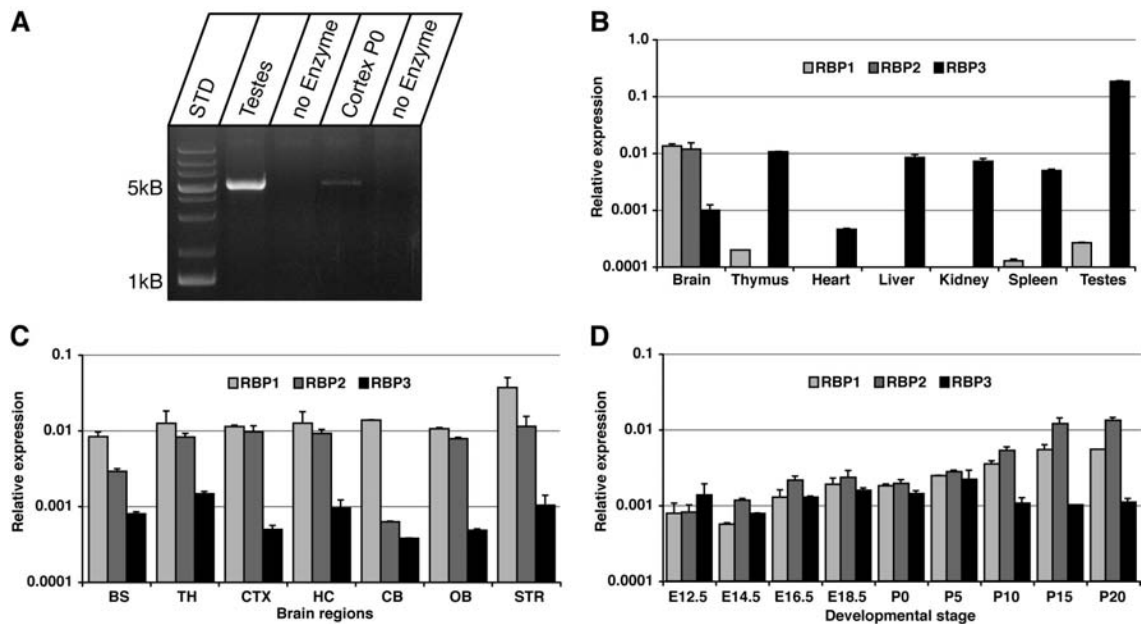
Figure 4.23: Expression of RIM-BP genes

(A) Amplification of full-length RIM-BP3 from mouse testes and p0 cortex cDNA. Control experiments were performed with template RNA that had not been reverse transcribed to rule out genomic contamination. **(B, C, D)** Quantitative real-time PCR expression profiles of mouse cDNA from different tissues (B), brain regions (C) and whole brain of different developmental stages (D). The expression level is depicted as the average of three independent reactions normalized to Actin, the error bar indicates the standard error of the mean (SEM).

To further investigate the neuronal distribution of RIM-BPs, radioactive *in situ* hybridizations on brain sections from adult and newborn rats was performed (Figure 4.24). Two oligonucleotide probes were used for each RIM-BP isoform to ensure that identical labeling patterns were obtained (data not shown). The labeling was abolished when excess unlabelled oligonucleotide probe was added to the hybridization mix (Figure 4.24 C, F). Due to the low abundance of RIM-BP3 mRNA in the adult rat brain (Figure 4.23 A to D) Even though four independent ISH probes against RIM-BP3 were tested, no specific signal could be detected (data not shown). Autoradiographs of hybridized rat brain sections revealed differential but overlapping expression patterns of RIM-BP1 and -2 mRNAs. Regions rich in glial cells (e.g. white matter of cerebral cortex and cerebellum) were unlabelled, indicating a neuron-specific expression of these two RIM-BP isoforms (Figure 4.24 A, D). RIM-BP1 mRNA was present throughout the brain with highest levels in the cerebellum, cortical layers II/III and V/VI, hippocampus and olfactory bulb. Striatum, thalamus and the pontine nuclei also show a strong RIM-BP1 expression (Figure 4.24A). RIM-BP2 mRNA was highly concentrated in the telencephalon, consisting of hippocampus, olfactory bulb,

and cortex, while it is expressed at lower levels in all other brain regions. Consistent with the RT-PCR data, it was barely detectable in the adult cerebellum (Figure 4.24D). The regional distribution of both RIM-BP1 and -2 detected in the adult brain already emerges at the day of birth (p0). RIM-BP1 could be detected ubiquitously in the p0 brain, with less abundance in white mater of cortex and brain stem (Figure 4.24B), while RIM-BP2 shows a more distinct expression pattern with a strong signal in the telencephalon (Figure 4.24E). However, whereas RIM-BP2 was barely detectable in the midbrain and brain stem at p28, expression levels were low in these areas at p0.
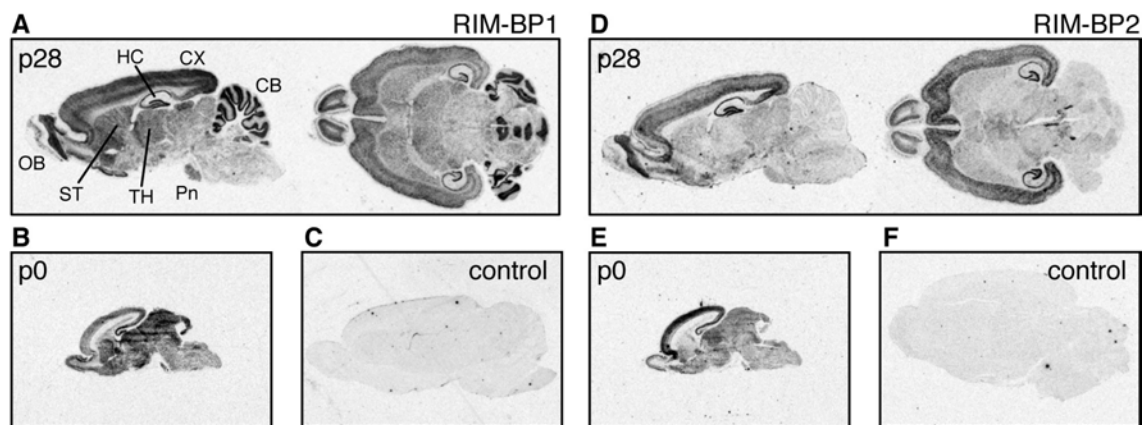
Figure 4.24: Localization of RIM-BP expression in rat brain.

(A, B, D, E) *In situ* hybridizations were performed on horizontal and sagittal sections of adult (p28) and new born (p0) rat brain using ^{35}S labeled oligonucleotide probes. (A, D) Autoradiograph pictures of horizontal and sagittal sections of p28 rat brain show distinct expression patterns of RIM-BP1 (A) and RIM-BP2 (D) expression. (B, D) Film images of sagittal sections showing the distributions of RIM-BP1 (B) and RIM-BP2 (E) at p0. (C, F) Control experiments with 1000-fold excess of unlabeled oligonucleotide did not result in any labeling. BS: brain stem; TH: thalamus; CX: cortex; HC: hippocampus; CB: cerebellum; OB: olfactory bulb; STR: striatum; Pn: pontine nuclei.

4.2.3.3 Structure of the RIM-BP genes

The three RIM-BP genes are dispersed in the human and mouse genome. However, the genes are highly conserved between human and mouse, with a very similar arrangement of exons and introns, whereby the mouse genes are more condensed (Figure 4.25). The properties of the human and mouse RIM-BP genes are summarized in Table 4.5, the structures of the genes are depicted schematically in Figure 4.25, and the sizes of the exons and the sequences of the exon-intron junctions are presented in G7Table 4.6 – Table 4.9.
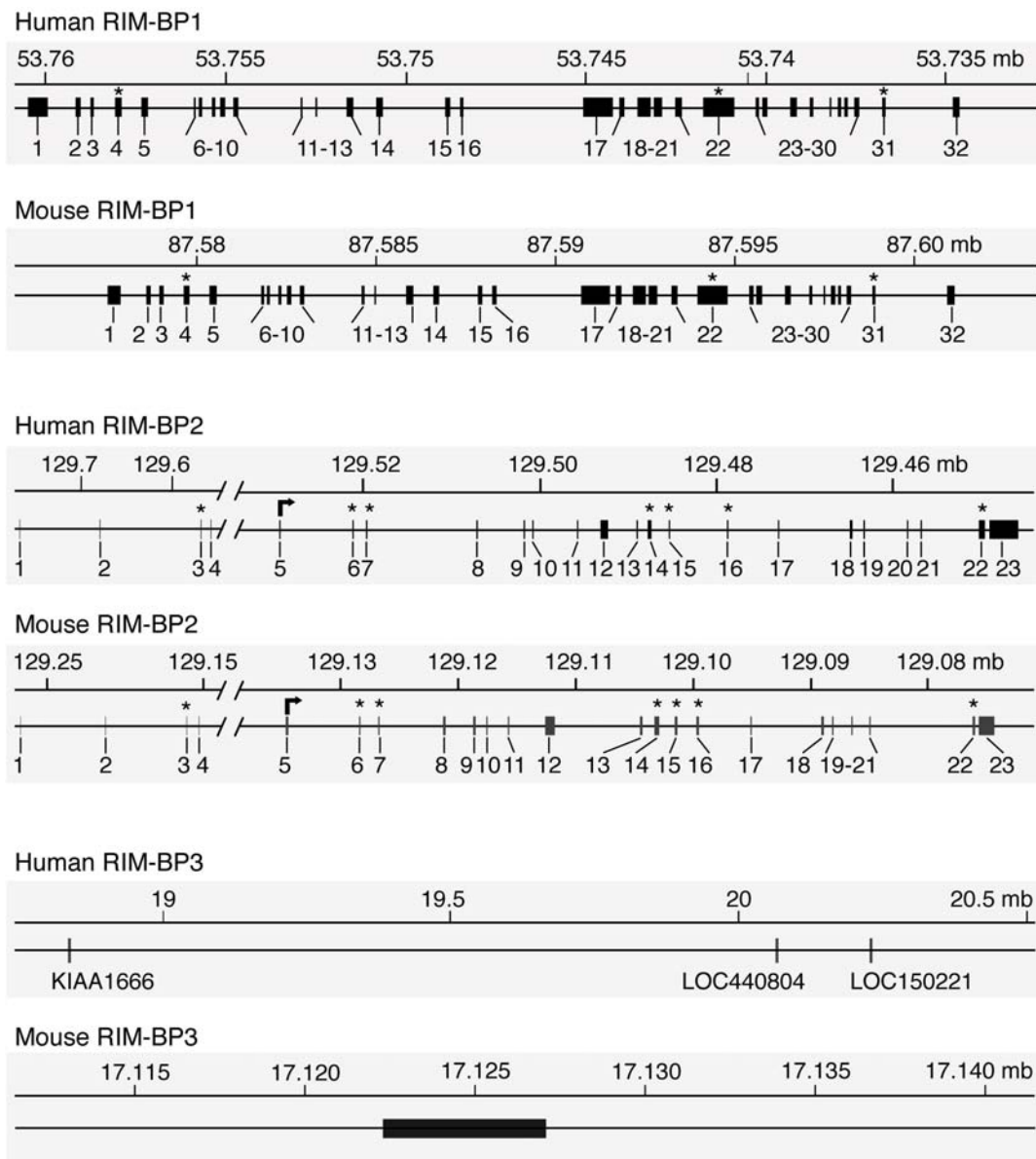
Figure 4.25: Structures of the human and mouse RIM-BP genes.
Diagrams depict the positions of the exons and introns in the RIM-BP genes (G7Table 4.6 – Table 4.9). Exons are identified by numbers; the first translated exon is marked by an arrow in RIM-BP2, asterisks mark exons subject to alternative splicing. The rulers above each gene diagram show the positions in the USCD database genome sequences.

Even though the RIM-BP1 gene codes for a large protein of 1907aa and 1895aa for the human and mouse protein, the human and mouse RIM-BP1 gene loci are relatively small with 27.5 and 24.5 kb, while the human and mouse RIM-BP2 genes measure 316.6 and 320.1 kb. This results in an inverse correlation between the size of the gene loci and the size of the corresponding protein, as the RIM-BP2 gene, encoding for the smaller RIM-BP2 protein with 1076aa (human) and 1079aa (mouse) is more than ten times the size of the RIM-BP1 gene. In contrast to the RIM-BP1 gene the human and mouse RIM-BP2 genes contain several non-coding exons in its 5'-UTR. The RIM-BP2 protein is mainly composed of a short N-terminal RIM-BP1 homology region and the SH3- and FNIII-domains that characterize the RIM-BP protein family. The homology domains are connected to each other by short linker sequences that diverge significantly between the three RIM-BPs. Therefore, positions of exon-intron junctions are only conserved within the functional domains between the RIM-BP1 and -2 genes. The RIM-BP3 gene, even though it encodes for a large protein, is contained within one exon of ~ 5,5 kb. In the human, in contrast to all other genomes analyzed, three copies of the RIM-BP3 gene can be found on chromosome 22 within 1.4 mb (Table 4.5).

Table 4.5: Chromosomal locations and sizes of RIM-BP genes and proteins

Gene	Human				Mouse			
	Location	[kb]	Protein names	[AA]	Location	[kb]	Protein names	[AA]
RIM-BP1	17q23.2	27.5	RIM-BP1, RBP1, PRAX-1, KIAA0612, PBR-IP	1907	11C	24.5	RIM-BP1, Bzrap1, mKIAA0612	1895
RIM-BP2	12q24.33	320.2	RIM-BP2, RBP2, KIAA0318	1076	5F	193.3	RIM-BP2, A930033C01Rik mKIAA0318	1079
RIM-BP3.1	22q11.21	6.1	KIAA1666 XM_371429	1639	16qA3	4.9	Gm603, LOC239731	1606
RIM-BP3.2	22q11.21	5.5	LOC440804 OTTHUMT00000075415	1639				
RIM-BP3.3	22q11.21	5.5	LOC150221 OTTHUMT00000075691	1639				

The sequence homology between these three duplicates is very high, at 99% for the overall sequences, whereas the phylogenetic distance between the second and third RIM-BP3 (LOC440804 and LOC150221, respectively) is even lower than the distance of these both to RIM-BP3.1 (KIAA1666). This indicates that they did not replicate at once, but a second duplication event occurred to generate the third RIM-BP3.3 gene.

4.2.3.4 Alternative splicing of RIM-BPs

Analysis of EST and cDNA sequences in public databases revealed that the RIM-BP1 and RIM-BP2 transcripts each contain three sites of alternative splicing (Table 4.10; marked by asterisks in Figure 4.22A), that are conserved in human and mouse: The first in the N-terminal region, the second between the FNIII domain and the C-terminal SH3-domains and the third at the C-terminus.

Splicing at the N-terminal first splice site results in the inclusion or exclusion of exon 4 in the RIM-BP1 transcript, whereas in RIM-BP2 the alternatively spliced sequence is encoded by two very short exons (6 and 7) that are in frame and therefore can be independently spliced (G7Table 4.6 and Table 4.7, Figure 4.25). Interestingly, the second splice site is located between the FNIII-domains and the C-terminal SH3-domains. In RIM-BP1 the alternatively spliced cassette exon 22 is very large (840 bp) and comprises the majority of the linker region between the functional domains. Furthermore, this sequence contains one negative charge cluster consisting of a string of 11 consecutive glutamic acid residues and is rich in proline, serine, arginine and glycine. In the RIM-BP2 gene alternative splicing at the second splice sites results in the exclusion of exon 15 and the usage of alternative splice donor and acceptor sites in exon 14 and 16, respectively, leading to the deletion or insertion of two short 18- and 8-residue sequences (Table 4.8 and Table 4.9, Figure 4.25). Therefore, the second splice site impacts the distance between the FNIII- and SH3-domains in the RIM-BP2 gene as well. At the third splice site inclusion or exclusion of exon 31 of RIM-BP1 and intron retention between exon 22 and 23 in RIM-BP2 leads to the generation of two proteins with diverging C-terminal sequences.

No evidence for alternative splicing of the *C. elegans* RIM-BP transcript was detected. The *Drosophila* RIM-BP appears to be alternatively spliced at the N-terminus as ESTs encompassing three different transcript variants can be found in the databases.

G7Table 4.6: Exon-intron structure of the human RIM-BP1 (bzrap1) gene

Exon	Nucleotide number			Size	Flanking seq.	Sequence start	Sequence end	Flanking seq.
1	53,760,280	–	53,759,948	330		ATG GAG CAA	TTC CTG AAG	gtaagggat
2	53,759,150	–	53,759,043	108	cccatgccag	GCC AAG CTG	CAG ATG CTG	gtgaggc
3	53,758,781	–	53,758,653	129	cccttgtcag	AGG AAG AGC	CTG AGG GTG	gtgaggaaa
4*	53,758,073	–	53,757,894	180	ctctggctag	GTG AGT GCC	GTG GGC AAG	gtgcgagga
5	53,757,362	–	53,757,171	192	ccaacctcag	GAG GGT CCC	CCG GGA GAG	gtgagcgcc
6	53,755,905	–	53,755,828	78	gcatttccag	GCC ACG CCC	CAG CAG CTG	gtaagtcct
7	53,755,741	–	53,755,658	84	gacccctcag	GAA TCG GAG	GAG GAG CTG	gtgagctct
8	53,755,399	–	53,755,310	90	gcccgctcag	GAA CTG CAG	AAG GAG CAG	gtaccactt
9	53,755,136	–	53,755,014	123	ccctcgccag	GTG GAG TGG	GTG CTG AAG	gtgaggaga
10	53,754,772	–	53,754,668	105	tgtgtttcag	CAC ATG CGG	CTG CAG CAG	gtggggcgg
11	53,752,941	–	53,752,891	51	ccacctgtag	GCC CAG GCT	CTG CTG GAG	gtagggcgc
12	53,752,489	–	53,752,469	21	cctgcaacag	TCT ACC TTG	TCC ATG CAG	gtagcgcct
13	53,751,657	–	53,751,451	205	cttggcccag	GCC CGG GTT	GGC CCC AAA G	gtaaggtgg
14	53,750,812	–	53,750,640	173	ttctctttag	AC CTT GAC CTC	ACA CCT GAG	gtaattgct
15	53,748,900	–	53,748,787	116	ttgcccccag	GTG GAC ACA	GCA CGT TAT AG	gtgggtccc
16	53,748,492	–	53,748,384	110	cccctaacag	C TAC AAC CCC	TTT TTT GAA G	gtaggaatg
17	53,745,082	–	53,744,252	831	ctcctgccag	GA GAG CTC ATG	CTC CCA GCA G	gtatgtggg
18	53,744,082	–	53,743,931	152	ctgcccccag	GC CCA CCT GAT	GGG CAG AAG	gtatagccc
19	53,743,573	–	53,743,196	378	caccctgcag	ATC ATG GAG	TGC TCC CAG	gtaccctgt
20	53,743,111	–	53,742,872	240	tctgttccag	GAG GAG GCT	AGG GCT GAG	gtaggggtt
21	53,742,518	–	53,742,327	192	cttcttgcag	AAG GAG GAC	GGG GCC AAG	gtaacgggg
22*	53,741,740	–	53,740,901	840	cctccaccag	TCC CAG CCC	CTC TCC CGG	gtccgtgct
23	53,740,301	–	53,740,202	100	ctttttgcag	GCA ACA GAG	GCA GAG CTA G	gtgagcacc
24	53,740,122	–	53,739,971	152	gtctccacag	TC CCT GCG AGG	ATC CTG AAG	gtgactgat
25	53,739,328	–	53,739,160	169	ttgcctccag	GTG TTT GGG	GAG GGC TCA G	gtatgacct
26	53,738,773	–	53,738,702	72	tctggatcag	GG AAT GGT CCG	TCC AAG AAA G	gtgggtaag
27	53,738,225	–	53,738,193	33	ctttccacag	CT GAG TCG GAA	CCC TGT CCA G	gtgaaggaa
28	53,738,003	–	53,737,900	104	cccccctgcag	GC CCC CCT AAG	GAC GTG GAG	gtgaggacc
29	53,737,818	–	53,737,747	72	ttttccacag	GCA GAG CTG	TTC TAC TAT	gtgagaaca
30	53,737,531	–	53,737,421	111	ttctctccag	GGG GAA TTA	GAG AGT CAG	gtcagtgag
31*	53,736,759	–	53,736,698	62	ctgtcctcag	AGA ACG AGG	CAG TGC TAG	
32	53,734,807	–	53,734,627	180	cacatttcag	GAC TGG GGC	AAG GAG TGA	

Data are based on the analysis of human genome sequences in the NCBI, Ensembl and USCD databases. Nucleotide numbers corre-
spond to those of the assembled USCD genome.
*Exons that are subject to alternative splicing.

Table 4.7: Exon-intron structure of the mouse RIM-BP1 (bzrap1) gene

Exon	Nucleotide number	Size	Flanking seq.	Sequence start	Sequence end	Flanking seq.
1	87,577,594 – 87,577,923	327		ATG GAG CAA	GCT TAT AAG	gtaagagagg
2	87,578,632 – 87,578,739	108	cctatgccag	GCC AAG TTC	CAG ATG CTG	gtgaggcctg
3	87,578,976 – 87,579,104	129	tccttgtcag	AGA AAA AGC	ATG AGG GTG	gtgaggacag
4*	87,579,655 – 87,579,834	180	ctctggctag	GTG AGT GCC	GTG GGC AAG	gtgcgaaggg
5	87,580,393 – 87,580,578	186	cccaccccag	GAA GGT CCC	CCG GGA GAG	gtgagcgcct
6	87,581,823 – 87,581,900	78	ctatttgcag	GCC GTA CTT	CAG CAG CTG	gtaagttcga
7	87,581,988 – 87,582,071	84	gaccccacag	GAG TCT GAG	GAG GAG CTG	gtaagttcct
8	87,582,308 – 87,582,397	90	caccccacag	GAG CTA CAG	AAG GAG CAG	gttcggtttc
9	87,582,561 – 87,582,683	123	ccctctccag	GTG GAA TGG	GTG CTG AAG	gtgagagact
10	87,582,912 – 87,583,016	105	tgtgtttcag	CAT ATG CGG	CTG CAG CAG	gtgggatcag
11	87,584,625 – 87,584,675	51	ctgtttgtag	GCC CAG GCA	CTG CTG GAG	gtagggcct
12	87,584,996 – 87,585,016	21	tcctcaccag	TCT ACC TTG	TCC ATG CAG	gtacagtcta
13	87,585,873 – 87,586,077	205	ttgttttcag	GCC CGG GTT	GGC CCC AAA G	gtgaggagtc
14	87,586,606 – 87,586,778	173	ttctctttag	AT CTT GAC CTC	ACA CCA GAG	gttagtgctg
15	87,587,854 – 87,587,969	116	cccgccccag	GTG GAC ACA	GCA CGC TAT AG	gtgggtccct
16	87,588,252 – 87,588,361	110	accccaacag	C TAC AAC CCC	TTT TTT GAA G	gtaggacgat
17	87,590,719 – 87,591,549	831	cctctgtcag	GG GAG CTC ATG	CTT CCA GCA G	gtatgtatgt
18	87,591,697 – 87,591,848	152	cctcttccag	GT CTG CCT GAT	GGG CAG AAG	gtatggcttg
19	87,592,168 – 87,592,533	366	ttccctatag	ATT ATG GAG	TGC TCT CAG	gtacttgtct
20	87,592,620 – 87,592,859	240	tccattgcag	GAA GAG GCT	AGA TCT GAG	gtagagctgg
21	87,593,242 – 87,593,430	189	cctttcacag	AAA GAA GAT	GGA GCC AAG	gtaatggggt
22*	87,593,962 – 87,594,801	840	ccactcccag	CCC CAG CCA	CCC TCC CGG	gtctgtgccc
23	87,595,424 – 87,595,523	100	ctctttgcag	GCA ACA GAA	ACT GAG CTG G	gtgagcatct
24	87,595,620 – 87,595,771	152	ctctccacag	CC CCT CCA AGG	CTC CTC AAG	gtgactgact
25	87,596,398 – 87,596,566	169	ctgcttccag	GTG TTT GGA	GAG GCC TCA G	gtatgaccct
26	87,597,077 – 87,597,148	72	tctcactcag	GA AAT GGT CCC	TCC AAG AAA G	gtaaagaccc
27	87,597,497 – 87,597,529	33	ctctccacag	TG GAG CTG GAA	CTC TGT CCA G	gtgagaagcc
28	87,597,685 – 87,597,788	104	tccctgatag	GT CCT CCT AAG	GAT GTG GAG	gtgagggccc
29	87,597,877 – 87,597,948	72	ctcatcacag	GCA GAG CTG	TTC TAC TAT	gtaagatcct
30	87,598,140 – 87,598,244	105	tcctcctcag	GGG GAG CTG	GAG AGT CAG	gtcagtgaag
31*	87,598,855 – 87,598,905	30	ctgttctcag	AGA ACG AGG	CAG TGC TAG	gtaagtgggg
32	87,600,931 – 87,601,108	177	tacatttcag	GAC CCC AGA	GAC TGA TAG	

Data are based on the analysis of human genome sequences in the NCBI, Ensembl and USCD databases. Nucleotide numbers correspond to those of the assembled USCD genome.
*Exons that are subject to alternative splicing.

Table 4.8: Exon-intron structure of the human RIM-BP2 gene

Exon	Nucleotide number			Size	Flanking seq.	Sequence start	Sequence end	Flanking seq.
1	129,766,765	–	129,766,720	76	tcgcccccag	*TTTGTAATC*	*CTTCTAAAG*	gtaggctgag
2	129,678,954	–	129,678,820	135	cttcccgcag	*CTTGGAAAT*	*AACTTTGTG*	gtaagtcgtc
3*	129,568,415	–	129,568,326	90	tttgtcctag	*GAAAATGAA*	*CATGACAAG*	gtagctgata
4	129,557,268	–	129,557,146	123	ccgcttgcag	*GTGAAGGCA*	*GTCCTGAAG*	gtaagctggc
5	129,529,514	–	129,529,410	105	gtccccacag	*CAT* **ATG** *CGA*	CTG CAG AAG	gtaagcggcg
6*	129,521,241	–	129,521,191	51	cataaaaaag	GCT CAG GTT	AGC ATG CAG	gtaaggagcg
7*	129,519,667	–	129,519,647	21	cttcgcgcag	AAC ACC TTG	AGC ATG CAG	gtattctaga
8	129,507,198	–	129,506,994	205	tgccgtgcag	TCC AAG GTT	CTC GGC AAA G	gtaagcgcct
9	129,501,838	–	129,501,693	146	tcgtggccag	GT CAG GAG AGC	GAG TCA GAC	gtgagtcccg
10	129,500,774	–	129,500,698	77	tttttcacag	ATG GAG AAT	GCC CGC TAT AG	gtaagtgcgg
11	129,495,767	–	129,495,658	110	ttctctgcag	T TAC AAC CCC	TTC TAT GAA G	gtctctgttg
12	129,493,158	–	129,492,346	813	tacccaacag	GA GAG CTC CTC	TTG CCT GCA G	gtgagccctg
13	129,489,014	–	129,488,863	152	cccctcccag	GA CCC CCA GCA	GGG CAG AGG	gtgagttttc
14a	129,487,789	–	129,487,296	396	ttgtccacag	GTG GCT GAA	TCC ACC ACC	gtcgccaagg
14b	129,487,789	–	129,487,340	450	ttgtccacag	GTG GCT GAA	AGC AGC AGG	gtaaggctgg
15*	129,485,378	–	129,485,232	147	tctttccaag	TTA GAG AAA	GGC AAG CAG	gtgagagcgg
16a	129,478,821	–	129,478,677	135	tggagacgag	TAC CAC ACA	GCC CTC AAG	gtgagtggct
16b	129,478,835	–	129,478,677	159	tggcccccag	CCG CAC TGT	GCC CTC AAG	gtgagtggct
17	129,473,059	–	129,472,951	109	ttgtctttag	ATT TTA GGG	CCA TCC ATC G	gttagtggcc
18	129,464,804	–	129,464,623	182	ttgctcgcag	AC GAT TAC GGG	ATC ATC AAG	gtgcgggatg
19	129,463,285	–	129,463,117	169	ttggctctag	GTT TAT GGT	GAG AAA ATA G	gtaagcgcaa
20	129,458,327	–	129,458,224	104	atctgaacag	AG AGA AGC AGG	GAT GTC GAG	gtaccagcca
21	129,456,741	–	129,456,670	72	atctccacag	GCC GAA CTT	TTT TAT TAT	gtaagttttt
22a	129,450,311	–	129,450,176	135	ggtgttttag	GGG GAG CTG	GCA AAA AGG	gtaagcaaac
22c*	129,450,175	–	129,450156	19	aggcaaaaag	GGT AAG CAA	CCT ATT **TAG**	
23	129,450,155	–	129,450,128	27	ttggaaacag	AAG AAG AGT	ACA CCT **TAA**	

Data are based on the analysis of human genome sequences in the NCBI, Ensembl and USCD databases. Nucleotide numbers corre-
spond to those of the assembled USCD genome. Exons with „a" and „b" forms contain alternative splice donor or acceptor se-
quences and „c" marks an intron retention.
*Exons that are subject to alternative splicing.

Table 4.9: Exon-intron structure of the mouse RIM-BP2 gene

Exon	Nucleotide number			Size	Flanking seq.	Sequence start	Sequence end	Flanking seq.
1	129,267,766	–	129,267,675	92	ctggccccag	*TTTGTAATC*	*ACATCCAAG*	gtaggctgcg
2	129,212,430	–	129,212,319	112	tgctctttag	*AAATGACCC*	*AGATTGGTG*	gtaagtggcc
3*	129,160,379	–	129,160,292	88	tcgtttccag	*GATGATGAA*	*CATGACCAG*	gtaataacac
4	129,152,485	–	129,152,371	115	ctgcttacag	*GTGAAGGCT*	*GTCCTGAAG*	gtaggccctt
5	129,134,579	–	129,134,451	102	gtccctacag	*CAT* **ATG** CGA	CTG CAG CAG	gtgagcccag
6*	129,128,320	–	129,128,270	51	ccaccaccag	GCT CAG GTT	CTG TTA GAG	gtgagcacag
7*	129,126,711	–	129,126,691	21	cgccacccag	AAC ACC CTG	TGC ATG CAG	gtattcagtg
8	129,121,269	–	129,121,065	205	tgctgtgcag	TCC AAG GTC	ATC CAC AAA G	gtaagtgatg
9	129,118,671	–	129,118,535	137	tcccatccag	GT CAC GAG GGC	GAG TCC GAG	gtgagtccta
10	129,117,569	–	129,117,493	77	tgctccacag	ATG GAC AAT	GCC CGC TAC AG	gtaggaatgt
11	129,115,735	–	129,115,626	110	ctccctgcag	T TAC AAC CCC	TTC TAT GAA G	gtctgtggat
12	129,112,551	–	129,111,739	813	tacccaacag	GA GAG CTT CTG	CTG CCT GCA G	gtgagccatg
13	129,104,466	–	129,104,315	152	ctccttccag	GA CCT CCA GCC	GGG CAG AGG	gtgagacgtg
14a	129,103,322	–	129,102,900	402	ttgtgtgtag	GTG GCT GAG	TCT ACC ACT	gtcgccggcc
14b	129,103,322	–	129,102,867	456	ttgtgtgtag	GTG GCT GAG	AGC AAC AGG	gtaagttgta
15*	129,101,506	–	129,101,360	147	tctttccaag	TTA GAG AAA	GGC AAG CAG	gtgagagtgt
16a	129,099,633	–	129,099,499	135	tggagatgag	TAC CAC ACA	GCC CTC AAG	gtgagcactg
16b	129,099,657	–	129,099,499	159	ttgactatag	CCC CAC TGT	GCC CTC AAG	gtgagcactg
17	129,095,084	–	129,094,967	118	ctgggtctag	ATT TTA GGA	CCA TCC ATT G	gtgagtggtc
18	129,089,061	–	129,088,877	185	cccgctccag	AT GAA TAC ACC	ATC ATC AAG	gtactgatgg
19	129,088,213	–	129,088,045	169	gtgactccag	GTA TAT GGA	GAG AAA ATA G	gtgagtgtgg
20	129,086,511	–	129,086,408	104	ggttttgcag	AG AGA AGT AGA	GAT GTT GAG	gtaccagcct
21	129,085,008	–	129,084,937	72	gtctttgcag	GCT GAA CTT	TTT TAT TAT	gtaagtttt
22a	129,076,182	–	129,076,048	135	gtgattacag	GGA GAG CTG	GCC AAA AGG	gtaagccagc
22c*	129,076,047	–	129,076,029	18		GTA AGC CAG	CCC CCT **TAG**	
23	129,075,557	–	129,075,530	27	ttggacatag	AAG AAG AGT	ACA CCC **TAA**	

Data are based on the analysis of mouse genome sequences in the NCBI, Ensembl and USCD databases. Nucleotide numbers correspond to those of the assembled USCD genome. Exons with „a" and „b" forms contain alternative splice donor or acceptor sequences and „c" marks an intron retention.
*Exons that are subject to alternative splicing.

Table 4.10: Supporting transcripts for alternatively spliced exons in RIM-BP1 and -BP2

Exon	Ensembl transcript ID	Tigr Gene Indices	GenBank entry numbers
Human RIM-BP1			
Δ4	ENST00000268893	THC2615957	AB014512
4	ENST00000343736	THC2474753	DA12059; NM_004758; AF039571
Δ22	N/A		CD580515; CD580263; CD580374
22	ENST00000268893 ENST00000343736 ENST00000335562	THC2474753 THC2615957	CN285807; AB014512; NM_004758; AF039571; CR597762
Δ31	ENST00000335562	THC2606548	BI753129; BQ639257; BC031401
31	ENST00000268893	THC2474753 THC2615957	BX452091;BX433153; AB014512; NM_004758; AF039571; CR597762
Mouse RIM-BP1			
Δ4	ENSMUST00000100644	NP1398349	CAI35956
4	ENSMUST00000039627	THC1599479	BB266895 AK043747
Δ22	ENSMUST00000039599	TC1603709 TC1599243	BQ769688; BC083181; BC055691; BU705894
22	ENSMUST00000039627 ENSMUST00000100644	THC1599479 NP1398349 TC1583777	CN525117; CF170433; BQ956844; BC066146; BI732955; NM_172449; AK051895
Δ31	ENSMUST00000039599	TC1583777 TC1603709	BY596029; BY593048; BY593156; BC083181; BC066146 NM_172449; AK051895
31	ENSMUST00000039627	THC1599479 TC1644068	CX42315; BU705976; BU058159; CO426309; CD804484; CD804634; CX731341; BG342667; BI729560; BU55691; AK122329
Human RIM-BP2			
2+3	ENST00000261655	THC2479580 THC2632166	AL519755; DR000170
Δ3			BC007632; BE261199; BE262639; BF313475; BQ883029
Δ2+3			NM_015347; AB002316
18abc			BX641152
18ac			AY699979; BF433304; BM810381; CK818024; CK818025; AB002316
Mouse RIM-BP2			
2+3			BB632555; AK038814; NM_001073313; NM_001081388
Δ3	ENMUST00000031370		AK044685; AK147417; CJ12868; CJ12561; CJ12468
Δ2+3		THC1604770 THC1597580	XM_973293; XM_895913; XM001002174
Δ11		THC1604770	AK038814
18abc			AK147417
18ac			BB177134; CF745262; BB281703; BG295992; NM_001081388

4.2.3.5 Evolution of RIM-BP genes

In the ENSEMBL Databank various members of the RIM-BP gene family were identified in the whole set of genomes presently available. Genomic alignments were used to select the species where the sequenced genome covered all potential RIM-BP genes (Table 4.11).
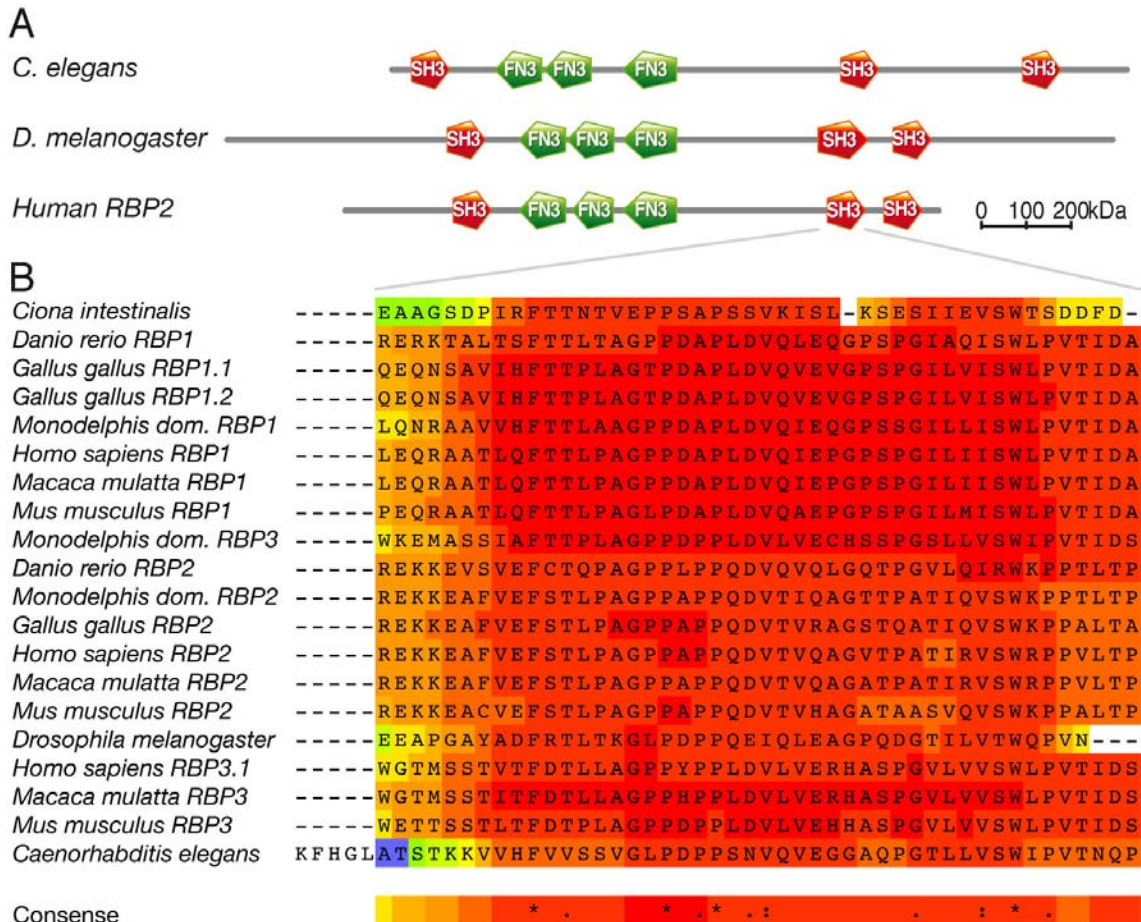
Figure 4.26: Conservation of RIM-BP domain structure and sequence during evolution.
(A) Domain structure of vertebrate and invertebrate RIM-BP proteins. **(B)** High sequence homology within the conserved domains exemplified by a ClustalW alignment of the second SH3 domain of vertebrate and invertebrate RIM-BP sequences. Darker boxes represent higher degrees of homology.

A single RIM-BP gene was identified in *C. elegans* as the product of the *tag-168* gene and in *Drosophila* as the product of the *CG31302* gene (Figure 4.26, Figure 4.27). Furthermore, the genomes of *anopheles gambiae*, *aedes aegypti* and *ciona intestinalis* contain one single RIM-BP gene, while all vertebrate genomes analyzed contain at least two and up to five RIM-BP genes. The transcripts were aligned with T-Coffee [http://tcoffee.vital-it.ch/cgi-

bin/Tcoffee/tcoffee_cgi/index.cgi] (Notredame et al. 2000), using the longest predicted transcript variants in case of possible alternative gene assembly.

The RIM-BP genes can be classified as members of the RIM-BP gene family based on their domain composition of three SH3- and three contiguous FNIII-domains and the structural organization of these domains that is identical in vertebrate and invertebrate RIM-BPs (Figure 4.26A). These signature domains are highly conserved in all species analyzed, exemplified by the alignment of the second SH3 domain of various vertebrate and invertebrate RIM-BP sequences (Figure 4.26B). In contrast to these highly homologous regions, the linker sequences connecting these domains exhibit almost no similarity between invertebrates and vertebrates or even between various invertebrates. The *C. elegans* and *Drosophila* RIM-BP genes are complex and rather large genes (~17,5 kb with 20 exons for *C. elegans*, and ~16,8 kb with 14 exons for *Drosophila*, Figure 4.27). However, the gene structures differ greatly between the different invertebrates and the vertebrates. In the human and mouse genome, introns in the two vertebrate multi-exon RIM-BP genes are located at identical positions and the exons have the same length. The *C. elegans* and *Drosophila* gene structures are neither similar to the vertebrate RIM-BP1 nor the RIM-BP2 genes (Figure 4.27).

The single exon RIM-BP3 gene can only be found in therian mammals. In the prototherian platyplus *Ornithorhynchus anatinus*, only one RIM-BP1 and -2 homolog was discovered. RIM-BP3 is present in one copy in the genomes of the marsupial *monodelphis domestica* and the eutherians *bos taurus, canis familiaris, mus musculus, rattus norvegicus, macaca mulatta,* and *pan troglodytes.* Interestingly, three copies of the RIM-BP3 gene are located in close proximity on chromosome 22 in *homo sapiens*. All three transcripts were identified by the SEGE intronless Genes in Eukaryotes database as functional intronless genes [http://sege.ntu.edu.sg/wester/intronless/search.htm] (Sakharkar & Kangueane 2004). In some of the lower vertebrates that lack RIM-BP3, the alignments also resulted in three or even four RIM-BP genes. The phylogenetic analysis with PHYML, a tool to estimate maximum likelihood phylogenies of DNA and protein sequences [http://atgc.lirmm.fr/phyml] (Guindon & Gascuel 2003, Guindon et al. 2005), confirmed in these cases that RIM-BP1 or both RIM-BP1 and -2 had been replicated (Figure 4.28). In the only bird genome available, the genome of
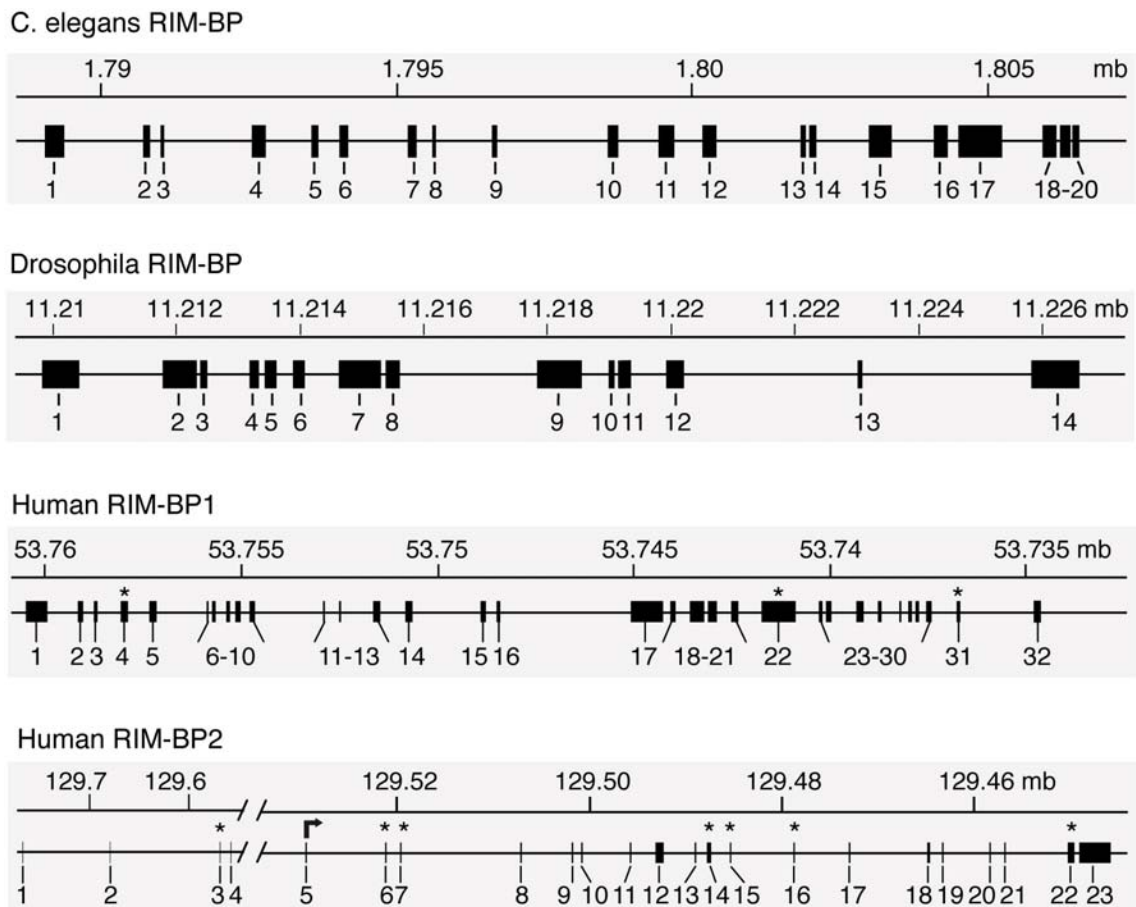
Figure 4.27: Comparison of the *C. elegans* and *Drosophila* gene structures with the Human RIM-BP1 and RIM-BP2 genes.

Asterisks mark exons that are subject to alternative splicing.

the chick (*Gallus gallus*), two RIM-BP1 genes were found. A second copy of both RIM-BP1 and -2 is present in the genomes of all *Teleostei* of the suborder *Acanthopterygii* that were available at the time (Table 4.11). However, in the zebra fish, *Danio rerio,* representing the suborder *Ostariophysi*, only one RIM-BP gene of each kind is present in the genome. The resulting phylogenetic tree (Figure 4.28) shows the great distances in homology between nematodes (*C. elegans*), arthropods (*Anopheles*, *Drosophila*) and Chordates (*Ciona*). The analysis also revealed that the vertebrate RIM-BP2 genes seem to be most closely related to the other phyla, with RIM-BP1 and RIM-BP3 diverging thereafter.
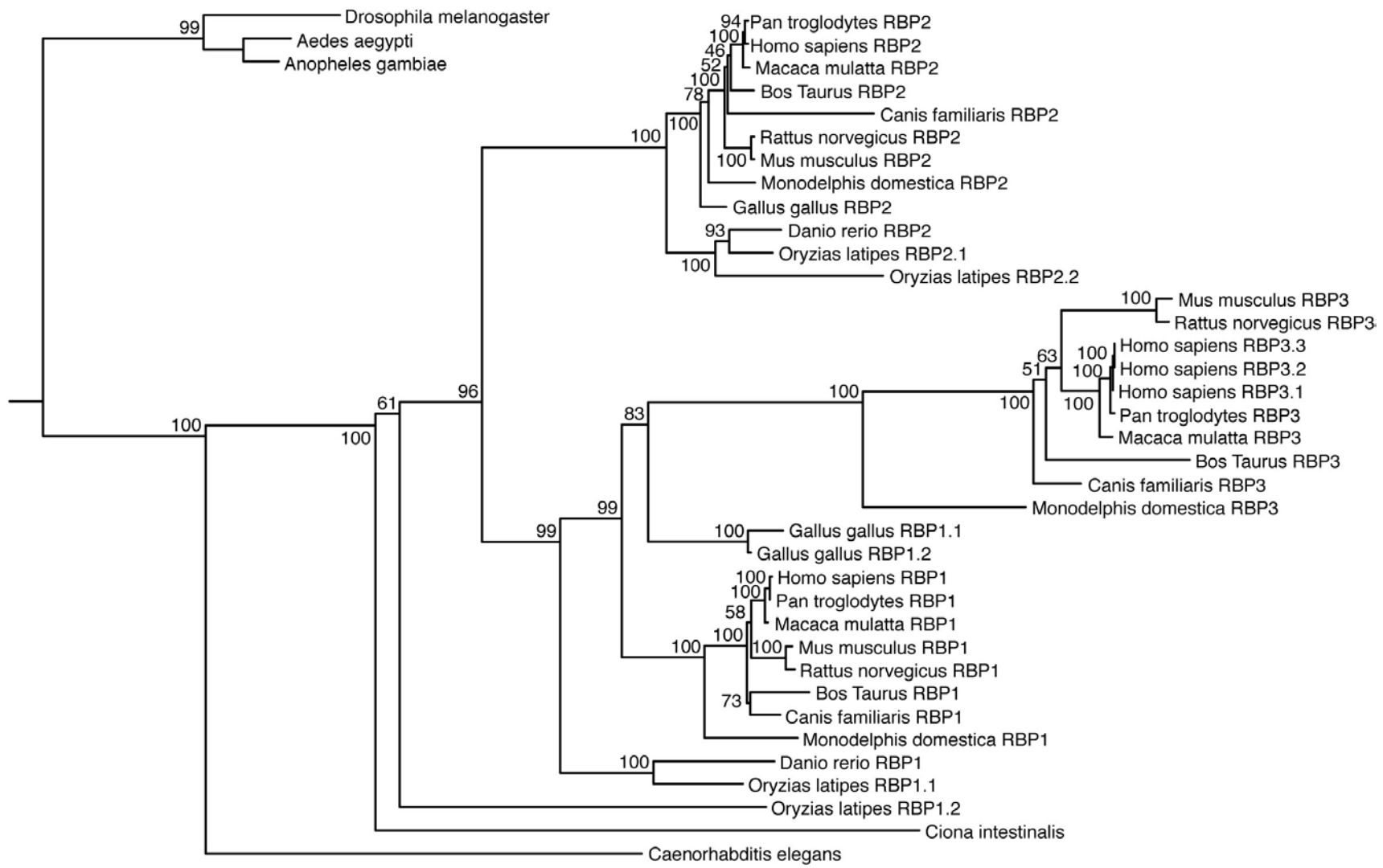
Figure 4.28: Phylogenetic tree of RIM-BP*s* from various organisms including nematodes, arthropods, chordates and higher vertebrates

Phylogenetic distances between the organisms were calculated with PHYML [http://atgc.lirmm.fr/phyml]. Numbers at the branches are confidence values based on the bootstrap method. B = 100 bootstrap replications (Felsenstein 1985)

Table 4.11: ENSEMBL gene annotations of the RIM-BP family genes

			Species	RIM-BP1	RIM-BP2	RIM-BP3
		Invertebrata	*Caenorhabditis elegans*	Y39A3CL.2		
			Aedes aegypti	AAEL010952-PA		
			Anopheles gambiae	ENSANGG00000004249		
			Drosophila melanogaster	CG31302		
			Ciona intestinalis	ENSCING00000009211		
Vertebrata		*Aves*	*Gallus gallus*	ENSGALG00000001023 ENSGALG00000022277	ENSGALG00000002579	
	Teleostia		*Danio rerio*	ENSDARG00000056675	ENSDARG00000001154	
			Gasterosteus aculeatus	ENSGACG00000020236 ENSGACG00000011249	ENSGACG00000012233 ENSGACG00000017586	
			Oryzias latipes	ENSORLG00000011077 ENSORLG00000004343	ENSORLG00000013723 ENSORLG00000010821	
			Takifugu rubripes	SINFRUG00000135305 SINFRUG00000129219	SINFRUG00000134423 SINFRUG00000126025	
			Tetraodon nigroviridis	GSTENG00016264001 GSTENG00030122001	GSTENG00007842001 GSTENG00005329001	
	Mammalia	*PT*	*Ornithorhynchus anatinus*	ENSOANG00000004747	ENSOANG00000000603 + ENSOANG00000008919*	
		Theria	*Monodelphis domestica*	ENSMODG00000014734	ENSMODG00000015603	ENSMODG00000017663
			Echinops telfairi	ENSETEG00000001281	ENSETEG00000006232	ENSETEG00000003692
			Loxodonta africana	ENSLAFG00000003026	ENSLAFG00000013819	ENSLAFG00000017924
			Felis catus	ENSFCAG00000012264	ENSFCAG00000014310	ENSFCAG00000008005
			Canis familiaris	ENSCAFG00000017493	ENSCAFG00000006721	ENSCAFG00000015276
			Bos Taurus	ENSBTAG00000011616	ENSBTAG00000009797	ENSBTAG00000001047
			Mus musculus	ENSMUSG00000034156	ENSMUSG00000029420	ENSMUSG00000071636
			Rattus norvegicus	ENSRNOG00000007957	ENSRNOG00000022893	ENSRNOG00000030452
			Macaca mulatta	ENSMMUG00000018087	ENSMMUG00000009048	ENSMMUG00000016353
			Pan troglodytes	ENSPTRG00000009450	ENSPTRG00000005634	ENSPTRG00000029501

PT: Prototheria; *The *O. anatinus* gene is encompassed in two independent contigs in ENSEMBL, each part represented by one annotation.

4.3 Functional analysis of active zone associated proteins – changes in gene expression of presynaptic proteins after pathologically increased synaptic activity

To investigate possible modulations of presynaptic protein expression following changes in the intensity of synaptic activity, the mRNA expression levels of several active zone enriched proteins and of the Synaptotagmin family were studied at three time points after pilocarpine induced status epilepticus (SE) in three subregions of the hippocampus (HC): the dentate gyrus (DG), the CA1 and the CA3 region. The three time points, six hours, five days and 28 days after SE, reflect the different phases of epileptogenesis within the hippocampus. The first time point corresponds to the acute phase after SE, the second time point to the silent phase with no epileptiform activity, when pathological alterations, like changes in cellular plasticity, as well as neurodegeneration accompanied by structural reorganization lead to an epileptic lesion that is apparent in the third time point reflecting the chronic period. Here, in the model as well as in human patients, the hippocampus has developed into an epileptic focus, showing segmental cell loss and a hyperexcitable network. The second time point five days after SE lies within the latent or silent period during which the reorganizations on cellular and network level occur that ultimately lead to an epileptic hippocampus generating spontaneous seizures. The last time point 28 days after SE is well within the chronic phase where all animals are suffering from such spontaneous occurring epileptic seizures.

4.3.1 The Synaptotagmin gene family

Synaptotagmins (Syts) constitute a family of proteins known to play a role in the regulation of membrane trafficking and of the fusion of vesicles with the plasma membrane in neurons and endocrine cells (Hay 2007, Sudhof 2002, Yoshihara & Montana 2004). However, mainly Syt-1 and Syt-2 function has been studied in detail. Interestingly, two members of the Synaptotagmin gene family, Syt-4 and Syt-10, were identified in screens for genes induced by synaptic activity (Babity et al. 1997b, Vician et al. 1995). Therefore, the Synaptotagmins represent interesting candidates to be involved in the molecular mechanisms underlying the functional and structural alterations in the hippocampus during epileptogenesis.
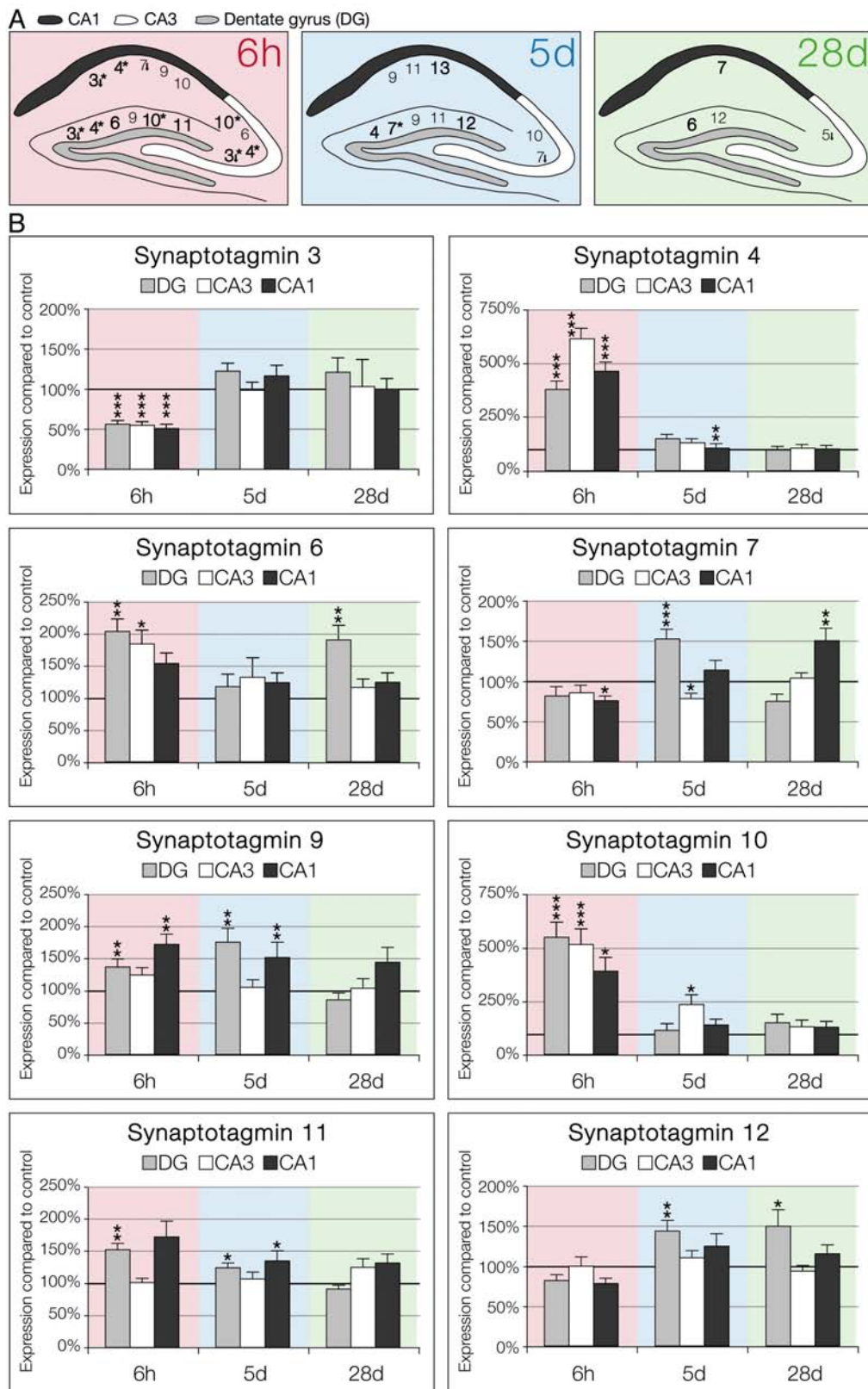
Figure 4.29: Differential expression of the Synaptotagmin gene family after pilo-carpine-induced SE

Synaptotagmins depicted by numbers in (**A**) were significantly regulated up or down (down ar-row) at the indicated time points after SE. Statistical significance as compared to no status con-trol using TTest: regular numbers p<0,05 (*); bold numbers p<0,01 (**); bold numbers with as-terisks p<0,001 (***). (**B**) Graphs showing the time course of regulation in the acute (6h), the latent (day five) and the chronic (day 28) phase of epileptogenesis. For data, see Table 4.12.

To quantify mRNA expression levels at different time points after SE, the hippo-campi of pilocarpine injected and control rats were microdissected into the three subfields CA1, CA3 and DG six hours, five days and 28 days after the end of the status. Real time RT-PCR of extracted mRNA from these probes revealed that several members of the Synaptotagmin gene family showed significant changes in mRNA expression after pilocarpine-induced Status epilepticus (SE). The results are schematically summarized in Figure 4.29, which depicts the genes showing the strongest effects. Table 4.12 summarizes the data obtained for the whole Synaptotagmin gene family collected at the three time points for the three hippocampal subregions. Surprisingly, only Syt-3 exhibited a strong significant downregulation at the earliest time-point and returned to control level in the later time points. In contrast, Syt-4, -6, -9 and -10 showed an upregulation at the early phase of epileptogenesis, that in most cases persisted at day five after SE, at least in some hippocampal subregions. Interestingly, the expression of Syt-7, -12 and -13 was increased after the early phase at day five, and con-tinued to stay elevated into the chronic phase at day 28 in the case of Syt-7 and -12. Syt-6 expression, on the other hand was strongly elevated in the acute phase in DG and CA3, as well as in the DG of chronic epileptic animals, while in the latent period no changes in Syt-6 expression where detected.

Table 4.12: Differential expression of the Synaptotagmin gene family.

Percentage of expression and Student's T-test were calculated in comparison to control tissue from the same hippocampal area for each group. N ≥ 5.

Gene	HC-Region		6h	5d	28d
Syt-1	**CA1**	**Mean**	**97%**	**124%**	**96%**
		SEM	0,055	0,087	0,054
		TTest	0,755	0,036	0,553
	CA3	**Mean**	**95%**	**96%**	**88%**
		SEM	0,064	0,068	0,052
		TTest	0,668	0,651	0,066
	DG	**Mean**	**118%**	**120%**	**86%**
		SEM	0,119	0,115	0,063
		TTest	0,392	0,120	0,381
Syt-3	**CA1**	**Mean**	**51%**	**116%**	**100%**
		SEM	0,056	0,129	0,131
		TTest	*0,000*	0,205	0,980
	CA3	**Mean**	**55%**	**98%**	**103%**
		SEM	0,048	0,098	0,330
		TTest	*0,000*	0,880	0,931
	DG	**Mean**	**56%**	**122%**	**120%**
		SEM	0,045	0,096	0,179
		TTest	*0,000*	0,067	0,090
Syt-4	**CA1**	**Mean**	**464%**	**105%**	**102%**
		SEM	0,393	0,174	0,117
		TTest	*0,000*	0,789	0,909
Syt-4	**CA3**	**Mean**	**614%**	**130%**	**106%**
		SEM	0,470	0,142	0,118
		TTest	*0,000*	0,113	0,650
	DG	**Mean**	**380%**	**150%**	**98%**
		SEM	0,348	0,155	0,116
		TTest	*0,000*	**0,005**	0,893
Syt-5	**CA1**	**Mean**	**108%**	**108%**	**101%**
		SEM	0,106	0,123	0,130
		TTest	0,661	0,561	0,954
	CA3	**Mean**	**101%**	**87%**	**70%**
		SEM	0,083	0,111	0,098
		TTest	0,964	0,405	0,018
	DG	**Mean**	**98%**	**104%**	**94%**
		SEM	0,119	0,085	0,143
		TTest	0,938	0,735	0,697
Syt-6	**CA1**	**Mean**	**153%**	**123%**	**124%**
		SEM	0,164	0,148	0,148
		TTest	0,086	0,237	0,133
	CA3	**Mean**	**184%**	**131%**	**115%**
		SEM	0,212	0,309	0,132
		TTest	0,027	0,377	0,382
	DG	**Mean**	**203%**	**117%**	**190%**
		SEM	0,191	0,190	0,230
		TTest	**0,003**	0,453	**0,001**
Syt-7	**CA1**	**Mean**	**76%**	**114%**	**151%**
		SEM	0,052	0,106	0,144
		TTest	0,040	0,282	**0,003**
	CA3	**Mean**	**86%**	**79%**	**104%**
		SEM	0,082	0,055	0,056
		TTest	0,392	0,035	0,579
	DG	**Mean**	**82%**	**153%**	**75%**
		SEM	0,106	0,110	0,078
		TTest	0,324	*0,001*	0,245

Gene	HC-Region		6h	5d	28d
Syt-9	**CA1**	**Mean**	**171%**	**150%**	**143%**
		SEM	0,154	0,240	0,223
		TTest	0,016	0,044	0,084
	CA3	**Mean**	**124%**	**104%**	**102%**
		SEM	0,108	0,120	0,152
		TTest	0,217	0,843	0,885
	DG	**Mean**	**136%**	**174%**	**85%**
		SEM	0,124	0,214	0,101
		TTest	0,015	0,012	0,323
Syt-10	**CA1**	**Mean**	**388%**	**138%**	**127%**
		SEM	0,636	0,261	0,271
		TTest	0,020	0,196	0,438
	CA3	**Mean**	**513%**	**233%**	**129%**
		SEM	0,729	0,448	0,311
		TTest	**0,004**	0,030	0,534
	DG	**Mean**	**546%**	**112%**	**148%**
		SEM	0,711	0,314	0,388
		TTest	***0,000***	0,697	0,287
Syt-11	**CA1**	**Mean**	**171%**	**134%**	**131%**
		SEM	0,248	0,155	0,141
		TTest	0,118	0,045	0,065
	CA3	**Mean**	**101%**	**106%**	**124%**
		SEM	0,060	0,107	0,130
		TTest	0,957	0,600	0,095
	DG	**Mean**	**152%**	**123%**	**90%**
		SEM	0,098	0,070	0,064
		TTest	**0,003**	0,011	0,492
Syt-12	**CA1**	**Mean**	**78%**	**124%**	**114%**
		SEM	0,062	0,155	0,115
		TTest	0,210	0,190	0,235
	CA3	**Mean**	**99%**	**110%**	**93%**
		SEM	0,116	0,089	0,074
		TTest	0,967	0,475	0,514
	DG	**Mean**	**82%**	**143%**	**149%**
		SEM	0,069	0,131	0,206
		TTest	0,166	**0,006**	0,030
Syt-13	**CA1**	**Mean**	**96%**	**135%**	**111%**
		SEM	0,072	0,082	0,129
		TTest	0,775	**0,001**	0,424
	CA3	**Mean**	**100%**	**116%**	**95%**
		SEM	0,075	0,078	0,062
		TTest	0,981	0,127	0,551
	DG	**Mean**	**89%**	**125%**	**79%**
		SEM	0,064	0,141	0,087
		TTest	0,439	0,108	0,119

Due to the faster timescale of transcription and possible posttranscriptional modifications, changes on the mRNA level do not always correspond to the physiologically more relevant changes in the amount of translated protein. A quantitative immunoblotting analysis was performed to examine the most interesting mRNA results on the protein level (Table 4.13). Such an analysis is limited by the availability of specific antibodies. The protein extracts used were prepared from probes of the same time point and hippocampal subregion as the

corresponding mRNA. Overall, the observed expressional mRNA changes were stronger than at the protein level.
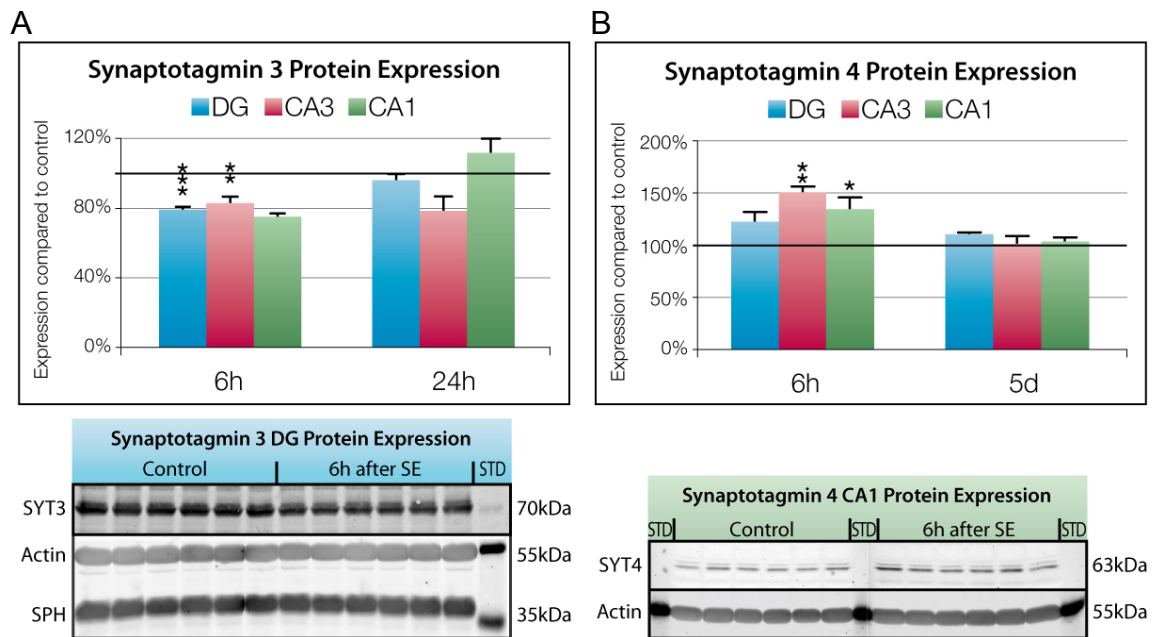
Figure 4.30: Syt-3 and Syt-4 protein levels at two early time points.
A Downregulation of Synaptotagmin 3 six hours after SE was detected in the DG and CA3 on the protein level (see example of blot from DG protein extracts from six controls and six animals after SE). **B** Synaptotagmin 4 upregulation could be confirmed in the two regions with the strongest transcriptional change, CA3 and CA1. Immunoblots were quantified using fluorescent secondary antibodies, normalized to Actin and Synaptophysin. Below the graphs summarizing the results two representative blots are shown. (*) p<0,05; (**) p<0,01

Consistent with the mRNA expression data, a significant downregulation of Syt-3 in the DG and CA3 region was confirmed on the protein level in the acute phase, while the effect was not significant in CA1 at this early time point (Figure 4.30A). Even though the Syt-4 protein expression was increased to a lesser degree than the mRNA levels, a significant increase in CA3 and CA1 was detected by immunoblot as well (Figure 4.30A). The analysis of Syt-6 protein expression was difficult due to very weak antibody signal that was highly variable. However, an upregulation in the acute phase consistent with the mRNA results was detected in the DG (Table 4.13). In accordance with the results of the mRNA analysis, a strong upregulation of Syt-7 in the DG as well as a downregulation in CA3 was observed five days after SE. 28 days after SE Syt-7 protein levels were still strongly increased in DG and CA1, whereas the mRNA expression was back to baseline at that time (Figure 4.31 A). As there were no specific antibodies against Syt-9 and Syt-11 available, it was not possible to further investigate the expressional changes of these two proteins.
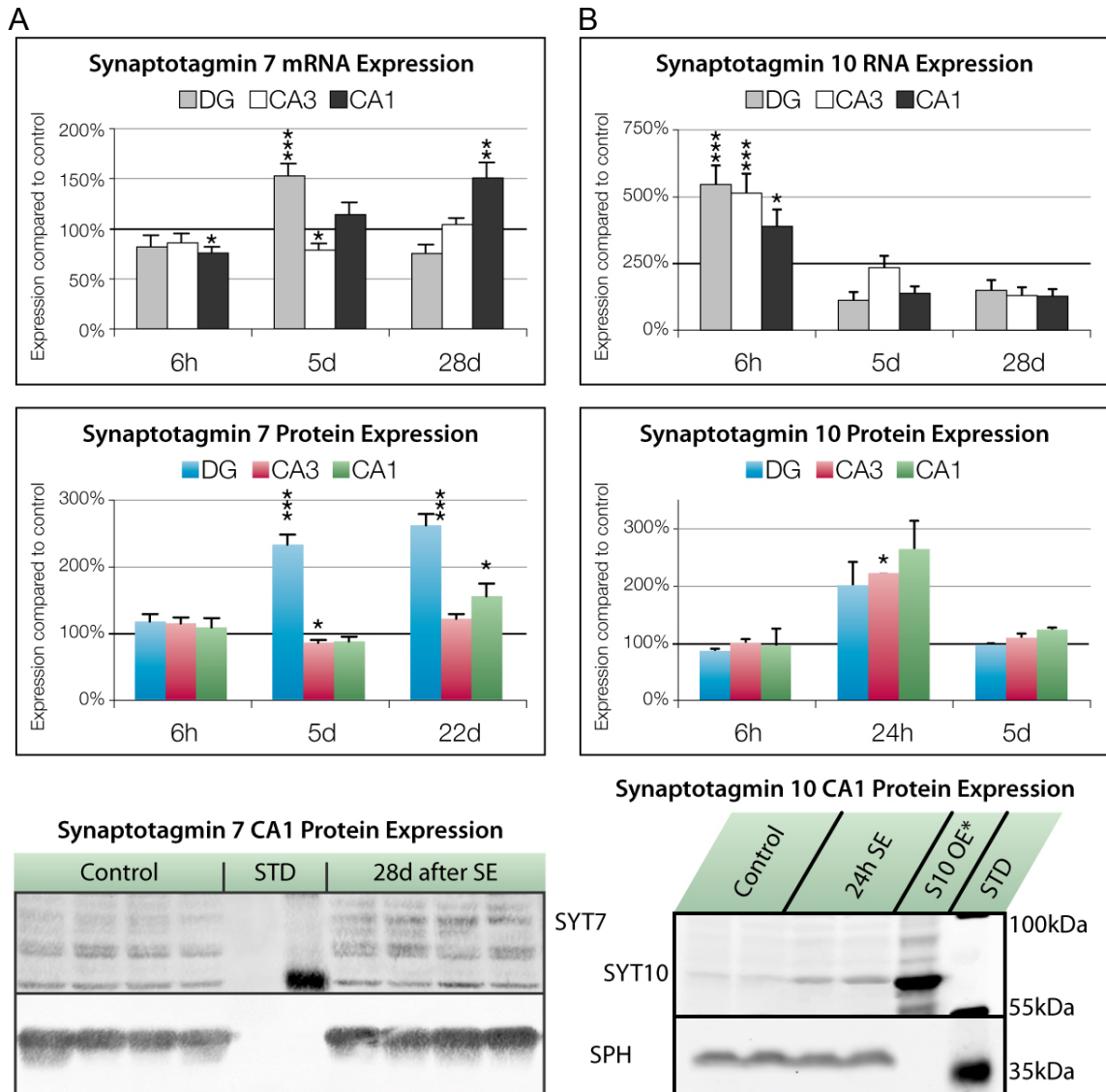
Figure 4.31: Expressional changes of Syt-7 and Syt-10 on the mRNA and the protein level.

A Syt-7 expression on the mRNA as well as the protein level in the acute, latent and chronic phase. **B** Syt-10 mRNA expression during epileptogenesis and protein expression levels six hours, 24 hours and five days after SE, showing the delayed protein upregulation in the acute phase. Immunoblots were quantified using fluorescent secondary antibodies, normalized to Synaptophysin. Beneath the graphs summarizing the results two representative blots are shown. (*) p<0,05; (**) p<0,01; (***) p<0,001

Interestingly, no changes in protein expression could be detected for Syt-10 6h after SE, even though the mRNA levels exhibited a dramatic increase in all subregions of the hippocampus. However, 24 hours after SE, Syt-10 protein levels showed a significant increase in the CA3 (Figure 4.31B). Although being increased in the DG and CA1 as well, we were not yet able to show a significant raise due to high variability in the protein expression levels. In addition, the expressional upregulation of Syt-12 in the DG five days after SE could be verified on the protein level (Table 4.13).

Table 4.13: Quantification of Synaptotagmin protein expression at various time points after SE.

Protein	Time after SE	Data	DG Control	DG Pilo	CA3 Control	CA3 Pilo	CA1 Control	CA1 Pilo
Syt3	6h	Mean	100,0%	79,1%	100,0%	82,9%	100,0%	74,2%
		SEM	1,6%	1,5%	2,8%	3,5%	14,1%	2,2%
		TTest		**0,0000**		**0,0064**		0,0782
	24h	Mean	100,0%	96,1%	100,0%	78,4%	100,0%	111,6%
		SEM	2,5%	3,4%	0,2%	8,1%	6,1%	8,3%
		TTest		0,7534		0,1154		0,3757
Syt4	6h	Mean	100,0%	121,6%	100,0%	149,0%	100,0%	133,1%
		SEM	7,2%	8,8%	9,4%	5,9%	6,3%	11,6%
		TTest		0,0682		**0,0013**		**0,0365**
	5d	Mean	100,0%	109,2%	100,0%	100,3%	100,0%	102,4%
		SEM	8,6%	1,4%	11,2%	7,3%	6,5%	3,5%
		TTest		0,3295		0,9824		0,7545
Syt6	6h	Mean	100,0%	153,7%	100,0%	205,3%	100,0%	115,0%
		SEM	31,6%	17,6%	8,5%	43,0%	6,5%	9,1%
		TTest		0,1687		**0,0372**		0,2096
	5d	Mean	100,0%	123,1%	100,0%	88,5%	100,0%	86,0%
		SEM	17,5%	8,7%	3,6%	4,7%	2,4%	4,7%
		TTest		0,2705		0,3206		**0,0116**
Syt7	6h	Mean	100,0%	117,2%	100,0%	114,2%	100,0%	107,8%
		SEM	4,1%	10,3%	1,8%	8,1%	10,6%	13,8%
		TTest		0,1533		0,1180		0,6635
	5d	Mean	100,0%	232,0%	100,0%	85,0%	100,0%	87,5%
		SEM	6,4%	14,7%	3,3%	4,2%	2,9%	6,1%
		TTest		**0,0000**		**0,0229**		0,0605
	22d	Mean	100,0%	260,1%	100,0%	120,9%	100,0%	154,4%
		SEM	16,4%	16,9%	16,0%	6,9%	8,8%	18,4%
		TTest		**0,0005**		0,2743		**0,0374**
Syt10	6h	Mean	100,0%	85,6%	100,0%	93,5%	100,0%	117,5%
		SEM	3,2%	6,1%	10,3%	5,7%	5,1%	9,0%
		TTest		0,0632		0,5943		0,1277
	24h	Mean	100,0%	199,6%	100,0%	220,9%	100,0%	262,6%
		SEM	1,7%	42,8%	5,4%	0,6%	10,0%	51,3%
		TTest		0,1501		**0,0025**		0,1019
	5d	Mean	100,0%	98,7%	100,0%	120,1%	100,0%	91,3%
		SEM	3,1%	3,6%	15,1%	7,2%	2,4%	8,2%
		TTest		0,7868		0,2628		0,2487
Syt12	5d	Mean	100,0%	190,0%	100,0%	172,5%	100,0%	84,6%
		SEM	3,4%	10,5%	3,3%	13,6%	2,4%	4,4%
		TTest		**0,0000**		**0,0038**		**0,0052**

Data normalized to Synaptophysin is shown as relative expression compared to control. Significant up- (green) or downregulation (red) in the corresponding mRNA expression measurements is represented by shaded boxes, significant regulation on the protein level is signified by colored text.

4.3.2 Active zone enriched proteins

Components of the presynaptic active zone are involved in the regulation of short- and long-term synaptic plasticity. To examine if pathophysiological synaptic activity results in changes in the composition of active zone components, the expression of genes and proteins specifically enriched in the presynapse or functionally linked to the fusion apparatus were analyzed during epileptogenesis as described in the previous chapter.

The genes and proteins checked were the RIM family, RIM1, RIM2, RIM2γ, RIM3γ and RIM4γ, the brain specific RIM binding proteins RIM-BP1 and RIM-BP2, the RIM associated proteins Munc13-1, Munc13-2, the synaptic scaffolding proteins Bassoon and Liprin1α - 4α as well as the Liprin interacting protein GIT1 (G protein-coupled receptor kinase interactor 1) (Table 4.14).

Table 4.14: Differential expression of various active zone enriched proteins.

Percentage of expression and Student's T-tests of each group were calculated in comparison to tissue from the same hippocampal area of control animals. N ≥ 5.

Gene	HC Region		6h	5d	28d
Bassoon	**CA1**	**Mean**	**169%**	**143%**	**96%**
		SEM	0,222	0,142	0,071
		TTest	**0,008**	0,028	0,694
	CA3	**Mean**	**123%**	**124%**	**176%**
		SEM	0,154	0,076	0,229
		TTest	0,220	0,016	**0,006**
	DG	**Mean**	**136%**	**125%**	**135%**
		SEM	0,127	0,109	0,142
		TTest	0,100	0,097	0,035
GIT1	**CA1**	**Mean**	**131%**	**117%**	**73%**
		SEM	0,114	0,086	0,042
		TTest	0,046	0,151	*0,000*
	CA3	**Mean**	**132%**	**140%**	**147%**
		SEM	0,071	0,106	0,086
		TTest	**0,003**	**0,006**	*0,000*
	DG	**Mean**	**199%**	**141%**	**121%**
		SEM	0,137	0,166	0,103
		TTest	*0,000*	0,056	0,074
Liprin1α	**CA1**	**Mean**	**136%**	**129%**	**59%**
		SEM	0,243	0,150	0,103
		TTest	0,203	0,138	**0,004**
	CA3	**Mean**	**49%**	**166%**	**110%**
		SEM	0,052	0,186	0,188
		TTest	**0,001**	0,018	0,701
	DG	**Mean**	**72%**	**145%**	**105%**
		SEM	0,076	0,147	0,148
		TTest	0,012	0,024	0,775
Liprin2α	**CA1**	**Mean**	**215%**	**96%**	**91%**
		SEM	0,212	0,054	0,072
		TTest	*0,000*	0,628	0,321

Gene	HC Region		6h	5d	28d
Liprin2α	**CA3**	**Mean**	**168%**	**109%**	**113%**
		SEM	0,162	0,096	0,073
		TTest	*0,001*	0,468	0,188
	DG	**Mean**	**373%**	**113%**	**93%**
		SEM	0,244	0,084	0,103
		TTest	*0,000*	0,296	0,618
Liprin3α	**CA1**	**Mean**	**102%**	**73%**	**85%**
		SEM	0,052	0,107	0,130
		TTest	0,785	0,034	0,283
	CA3	**Mean**	**100%**	**133%**	**121%**
		SEM	0,072	0,094	0,090
		TTest	0,991	0,013	0,063
	DG	**Mean**	**136%**	**94%**	**111%**
		SEM	0,110	0,024	0,067
		TTest	0,014	0,578	0,202
Liprin4α	**CA1**	**Mean**	**47%**	**72%**	**45%**
		SEM	0,032	0,067	0,061
		TTest	*0,000*	0,026	*0,000*
	CA3	**Mean**	**45%**	**74%**	**55%**
		SEM	0,040	0,034	0,040
		TTest	*0,000*	**0,008**	*0,000*
	DG	**Mean**	**46%**	**75%**	**48%**
		SEM	0,076	0,109	0,087
		TTest	**0,005**	0,106	*0,001*
Munc13-1	**CA1**	**Mean**	**39%**	**83%**	**85%**
		SEM	0,054	0,062	0,076
		TTest	*0,000*	0,016	0,130
	CA3	**Mean**	**44%**	**110%**	**90%**
		SEM	0,055	0,153	0,083
		TTest	*0,000*	0,579	0,465
	DG	**Mean**	**67%**	**113%**	**93%**
		SEM	0,109	0,178	0,109
		TTest	0,119	0,522	0,635
Munc13-2	**CA1**	**Mean**	**213%**	**93%**	**103%**
		SEM	0,267	0,056	0,163
		TTest	*0,000*	0,917	0,897
	CA3	**Mean**	**236%**	**66%**	**120%**
		SEM	0,402	0,082	0,128
		TTest	**0,002**	0,013	0,269
	DG	**Mean**	**1014%**	**147%**	**119%**
		SEM	0,671	0,162	0,197
		TTest	*0,000*	0,023	0,367
RIM1	**CA1**	**Mean**	**143%**	**90%**	**109%**
		SEM	0,147	0,067	0,141
		TTest	0,014	0,238	0,556
	CA3	**Mean**	**146%**	**91%**	**83%**
		SEM	0,125	0,100	0,060
		TTest	**0,005**	0,438	0,135
	DG	**Mean**	**205%**	**87%**	**96%**
		SEM	0,204	0,146	0,063
		TTest	*0,000*	0,448	0,572
RIM2	**CA1**	**Mean**	**298%**	**86%**	**57%**
		SEM	0,546	0,121	0,081
		TTest	**0,002**	0,373	**0,002**
	CA3	**Mean**	**290%**	**60%**	**115%**
		SEM	0,554	0,095	0,130
		TTest	**0,003**	0,024	0,451

Gene	HC Region			6h	5d	28d
RIM2	**DG**	**Mean**		**430%**	**75%**	**62%**
		SEM		0,533	0,097	0,102
		TTest		*0,000*	0,188	**0,004**
RIM2γ	**CA1**	**Mean**		**145%**	**104%**	**100%**
		SEM		0,138	0,107	0,083
		TTest		**0,006**	0,822	0,981
	CA3	**Mean**		**149%**	**101%**	**93%**
		SEM		0,104	0,133	0,110
		TTest		**0,004**	0,931	0,586
	DG	**Mean**		**238%**	**103%**	**99%**
		SEM		0,238	0,129	0,079
		TTest		*0,000*	0,889	0,958
RIM3γ	**CA1**	**Mean**		**104%**	**121%**	**82%**
		SEM		0,135	0,065	0,092
		TTest		0,801	0,033	0,087
	CA3	**Mean**		**60%**	**100%**	**90%**
		SEM		0,078	0,110	0,075
		TTest		**0,002**	0,980	0,428
	DG	**Mean**		**224%**	**105%**	**85%**
		SEM		0,340	0,082	0,109
		TTest		**0,002**	0,803	0,232
RIM4γ	**CA1**	**Mean**		**144%**	**138%**	**75%**
		SEM		0,071	0,062	0,059
		TTest		*0,000*	*0,001*	**0,006**
	CA3	**Mean**		**178%**	**128%**	**79%**
		SEM		0,228	0,106	0,122
		TTest		**0,007**	0,042	0,164
	DG	**Mean**		**505%**	**113%**	**116%**
		SEM		0,381	0,094	0,208
		TTest		*0,000*	0,300	0,451
RIM-BP1	**CA1**	**Mean**		**68%**	**103%**	**115%**
		SEM		0,035	0,058	0,177
		TTest		*0,000*	0,623	0,406
	CA3	**Mean**		**82%**	**123%**	**97%**
		SEM		0,051	0,056	0,127
		TTest		0,060	**0,002**	0,876
	DG	**Mean**		**65%**	**165%**	**113%**
		SEM		0,050	0,225	0,035
		TTest		**0,005**	0,020	0,083
RIM-BP2	**CA1**	**Mean**		**108%**	**130%**	**203%**
		SEM		0,301	0,125	0,308
		TTest		0,797	0,101	**0,002**
	CA3	**Mean**		**81%**	**160%**	**152%**
		SEM		0,083	0,146	0,172
		TTest		0,125	**0,003**	0,012
	DG	**Mean**		**107%**	**158%**	**288%**
		SEM		0,129	0,164	0,458
		TTest		0,667	**0,009**	*0,000*

To examine whether the observed modulations on the mRNA level were translated into a change on the protein level, quantitative western blot analyses were performed for the genes that were most strongly regulated after SE.

Table 4.15: Quantification of protein expression at various time points after SE.

Gene	Time	Data	DG Control	DG Pilo	CA3 Control	CA3 Pilo	CA1 Control	CA1 Pilo
Liprin2	6h	Mean	100,0%	85,2%	100,0%	190,9%	100,0%	126,1%
		SEM	8,4%	8,7%	10,5%	16,3%	9,9%	10,4%
		TTest		0,2502		**0,0016**		0,1070
	5d	Mean	100,0%	102,9%	100,0%	80,1%	100,0%	136,8%
		SEM	10,7%	6,3%	5,4%	5,9%	13,0%	3,5%
		TTest		0,8253		**0,0464**		**0,0337**
Liprin4	6h	Mean	100,0%	59,6%	100,0%	100,1%	100,0%	70,8%
		SEM	12,0%	3,9%	8,8%	9,6%	4,9%	5,1%
		TTest		**0,0095**		0,9919		**0,0034**
	5d	Mean	100,0%	60,7%	100,0%	35,4%	100,0%	58,2%
		SEM	3,9%	1,2%	9,7%	2,1%	14,3%	3,6%
		TTest		**0,0004**		**0,0007**		**0,0394**
	22d	Mean	100,0%	11,3%	100,0%	33,8%	100,0%	23,4%
		SEM	46,4%	3,2%	41,4%	11,6%	38,2%	5,3%
		TTest		0,0670		0,1746		0,0946
Munc13-1	6h	Mean	100,0%	92,3%	100,0%	49,7%	100,0%	53,7%
		SEM	6,9%	1,9%	4,7%	1,3%	15,5%	6,1%
		TTest		0,3060		**0,0000**		**0,0239**
	24h	Mean	100,0%	106,2%	100,0%	62,6%	100,0%	92,4%
		SEM	1,3%	13,1%	0,6%	7,9%	10,1%	4,1%
		TTest		0,6238		**0,0406**		0,5591
Munc13-2	6h	Mean	100,0%	142,5%	100,0%	120,7%	100,0%	119,1%
		SEM	8,9%	9,9%	4,3%	20,6%	14,4%	13,9%
		TTest		**0,0111**		0,3503		0,2721
	24h	Mean	100,0%	665,4%	100,0%	140,1%	100,0%	273,1%
		SEM	25,1%	140,7%	%	%	29,9%	24,8%
		TTest		0,0584				**0,0468**
RIM1	6h	Mean	100,0%	103,4%	100,0%	114,9%	100,0%	110,7%
		SEM	11,4%	11,0%	2,6%	7,6%	4,2%	5,2%
		TTest		0,8322		0,1378		0,1490
RIM2	6h	Mean	100,0%	95,8%	100,0%	80,9%	100,0%	121,0%
		SEM	3,4%	4,7%	15,6%	8,5%	5,3%	7,6%
		TTest		0,4834		0,3084		0,0529
RIM3	6h	Mean	100,0%	115,4%	100,0%	109,3%	100,0%	103,1%
		SEM	6,1%	6,2%	12,7%	16,2%	4,0%	3,8%
		TTest		0,1085		0,6614		0,5903
	5d	Mean	100,0%	114,0%	100,0%	116,7%	100,0%	85,9%
		SEM	2,6%	13,2%	9,8%	10,4%	8,6%	9,5%
		TTest		0,3286		0,2776		0,2999
RIM4	6h	Mean	100,0%	83,7%	100,0%	68,7%	100,0%	84,6%
		SEM	18,7%	9,0%	7,0%	2,3%	14,5%	7,7%
		TTest		0,4511		**0,0017**		0,3741
	5d	Mean	100,0%	120,8%	100,0%	161,2%	100,0%	82,3%
		SEM	2,5%	7,9%	5,3%	10,0%	6,2%	5,6%
		TTest		**0,0371**		**0,0007**		0,0637

Data normalized to Synaptophysin is shown as relative expression compared to control. Significant up- (green) or downregulation (red) on the mRNA level (Table 4.14) is represented by shaded boxes, significant regulation on the protein level is signified by colored text. N ≥ 5.

4.3.2.1 Bassoon

The large scaffolding protein Bassoon, together with it's highly homologous in-
teraction partner Piccolo, is a core component of the CAZ (cytomatrix at the ac-
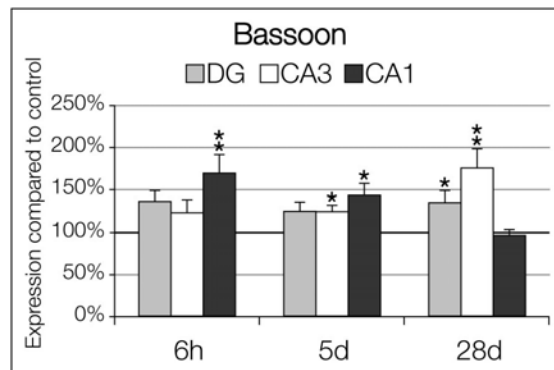tive zone) (Fenster et al. 2000, tom Dieck et al. 1998).

Figure 4.32: Differential mRNA expression of the active zone scaffolding protein
Bassoon in the three hippocampal subregions at different time points after SE
(N ≥ 5).

Bassoon was significantly upregulated during all three phases of epileptogene-
sis, albeit in different hippocampal subregions: in the acute phase, Bassoon
mRNA expression in the CA1 region was strongly increased, an effect that was
less apparent in the latency period and back to baseline in the chronic phase. In
CA3, Bassoon expression was weakly upregulated at in the latency period and
more strongly enhanced in the chronic phase. mRNA levels in the DG were
slightly elevated throughout epileptogenesis, showing a significant increase in
the chronic phase.

4.3.2.2 GIT1

GIT1 mRNA exhibited an upregulation in the acute phase after SE, with the
strongest increase in mRNA expression in the DG, but significant increases in
CA3 and CA1 as well. In the latency period, GIT1 levels stayed elevated in the
CA3 region, and even showed an increase in the chronic phase. In contrast,
mRNA expression in the CA1 region declined during epileptogenesis, showing
no significant change in the latent period and a highly significant reduction at
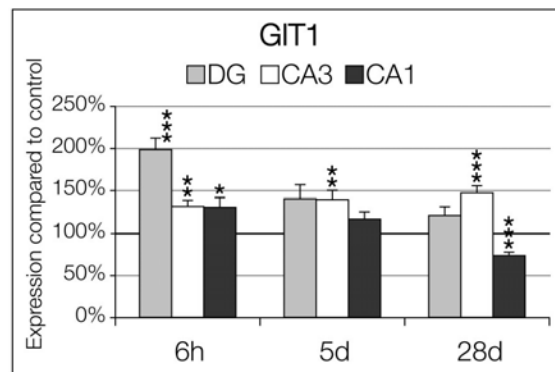28d after SE.

Figure 4.33: Differential mRNA expression of the Liprin binding protein GIT1 in the three hippocampal subregions at different time points after SE (N ≥ 5).

4.3.2.3 α-Liprins

The four different Liprin family members show a diverse regulation during epileptogenesis (Figure 4.34). Liprin3α did not show any modulation of expression throughout epileptogenesis, while the other isoforms showed changes in expression in at least single hippocampal subregions and time points. In the acute phase, only Liprin2α mRNA exhibited a significant upregulation in all hippocampal subregions. On the protein level, an increase was only detected in the CA3 region at this time point. In contrast, Liprin4α mRNA was significantly downregulated in all subregions, as well as Liprin1α in the CA3 region. The protein levels of Liprin4α were significantly reduced in the DG as well as CA1 region at this time point. In the latency period, only Liprin4α mRNA showed a significant reduction in the CA3 region, while the other Liprin isoforms were not significantly regulated. In contrast, the protein expression of Liprin4α was significantly reduced at this time point, and also Liprin2α protein levels were reduced in the CA3 region, while they were increased in CA1. mRNA quantification in the chronic phase again revealed a strong Liprin4α downregulation in the whole hippocampus, while Liprin1α was downregulated only in the CA1 region. Due to a high variability in the signals of the controls the downregulation of Liprin4α could not be unequivocally demonstrated at the protein level (Table 4.15), albeit a strong reduction of the Liprin4α signal was observed.
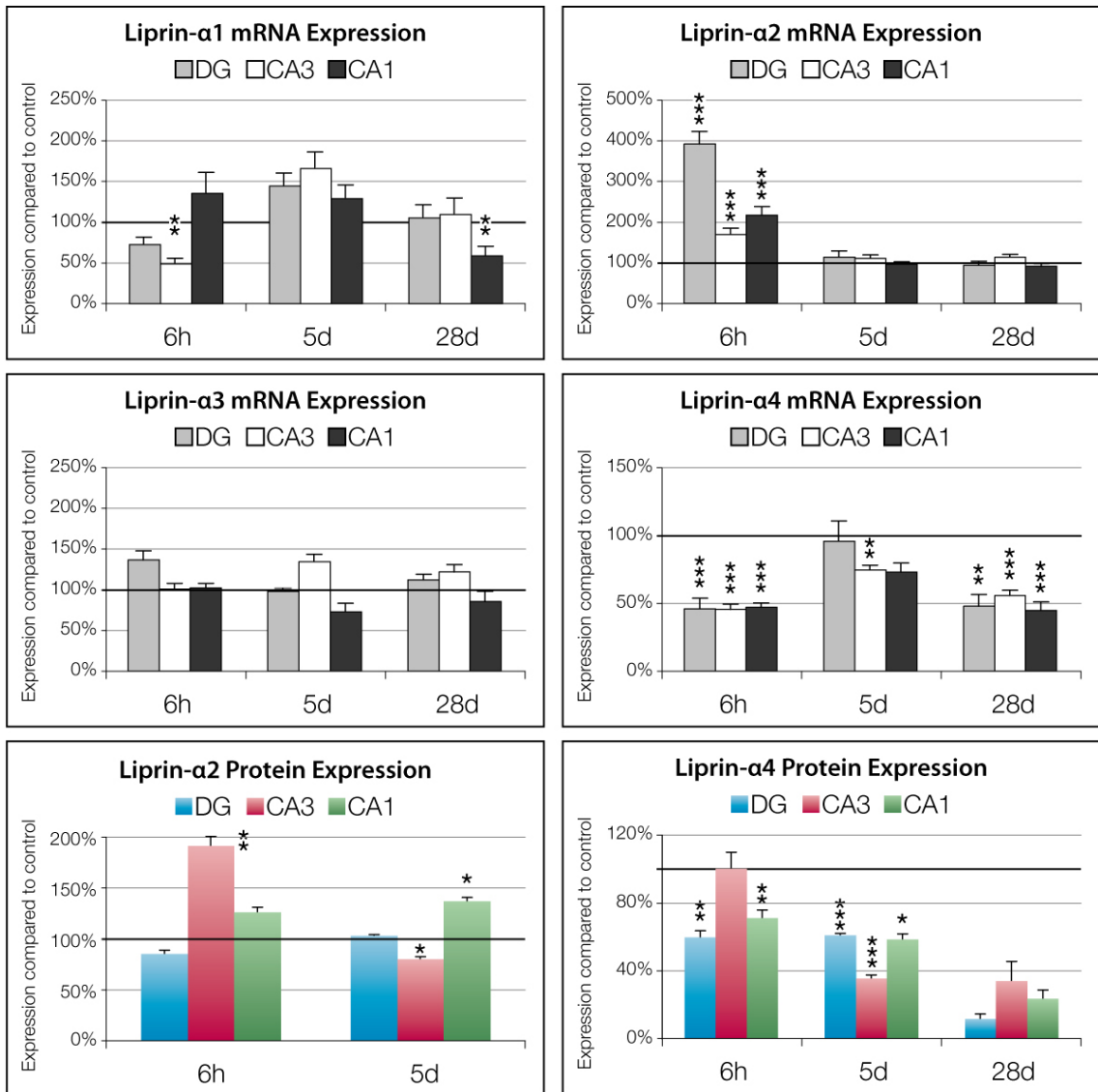
Figure 4.34: Differential mRNA Expression of the Liprin protein family as well as protein expression of Liprin2α and -4α at different time points after SE (N ≥ 5).
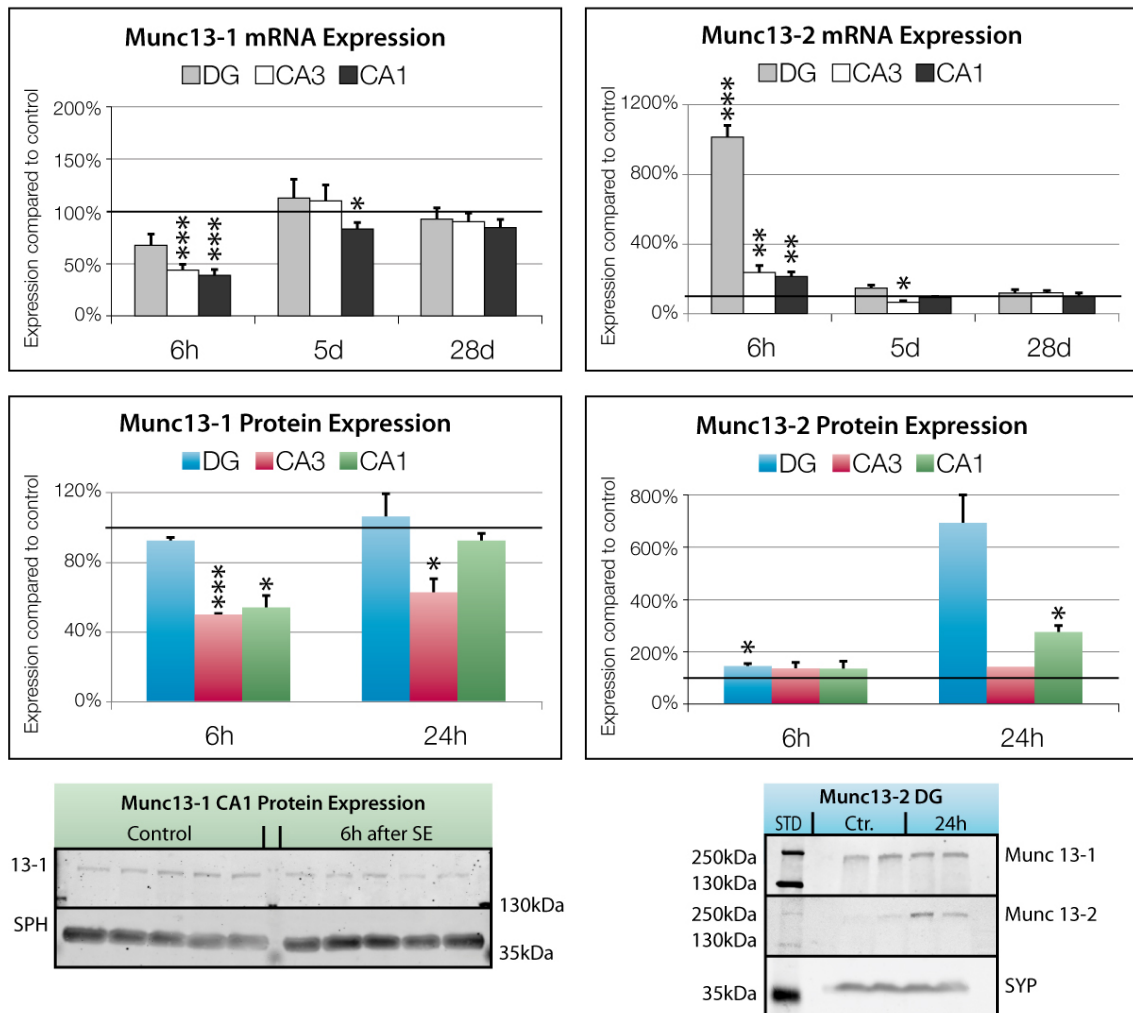
4.3.2.4 Munc13

Figure 4.35: Differential mRNA and protein expression of Munc13-1 and Munc13-2 at various time points after Status epilepticus (N ≥ 5).

Interestingly, Munc13s exhibited opposing alterations in expression in the acute phase. Munc13-2 mRNA expression was strongly increased, whereas Munc13-1 levels declined by more than 50% in CA3 and CA1. The decrease of Munc13-1 in the CA region was supported by a significant reduction of the protein level to 75%. The strongest Munc13-2 mRNA upregulation was observed in the DG, accompanied by a significant increase to 250% in the CA region. Quantitative immunoblotting did not reveal a significant increase in the protein levels of Munc13-2 6h after SE. However, 24h after SE, at the end of the acute phase, protein levels in the DG as well as in the CA1 region showed a strong increase compared to control.

4.3.2.5 RIM

All five transcripts of the RIM family that were examined, RIM1α, RIM2α, RIM2γ, RIM3γ and RIM4γ, were highly and significantly upregulated in the acute phase in most areas of the hippocampus (Figure 4.36). They showed the strongest effect in the dentate gyrus with at least 250-300% expression as compared to control for the RIM2γ and RIM3γ mRNAs, and increasing up to 900% for RIM1. Only one gene was downregulated in the acute phase in one distinct area of the HC on both mRNA and protein level: RIM3γ expression declines in the CA3 region by 30-40% (Figure 4.36, Table 4.15). Despite the robust early effect on the mRNA level, changes on the protein level were not significantly detectable with our antibodies. This may be due to a delayed response on the protein level as shown for the Munc13-2 regulation and will have to be evaluated further. In the latency period of epileptogenesis, RIM mRNA levels almost returned to baseline, with a slight enhancement in expression of RIM3γ in the CA1 region and RIM4γ in CA3 and CA1, while elevated protein levels were only detected for RIM4γ in the DG and CA3. In the chronic phase, RIM3γ mRNA expression was back to control level, while RIM4γ levels were reduced in the CA1 region and RIM2 expression rose up again to 200% in the CA3 region (Figure 4.36).

4.3.2.6 RIM-BP

Unlike the RIM genes, RIM-BP1 mRNA was significantly down regulated in the DG and CA1 in the acute phase. In the latency period, expression in the DG was still reduced, while mRNA levels in the CA1 region returned to basal expression levels, and levels in CA3 even increased. Interestingly, RIM-BP2 showed an opposing course of expression, the two genes only share a significant upregulation in CA3 in the latent phase. But in the acute phase, when RIM-BP1 expression was reduced in the DG and CA1, RIM-BP2 was not changed at all. However, in the chronic phase, expression in the CA1 was significantly increased, and also in the DG a strong bias towards upregulation was observed.
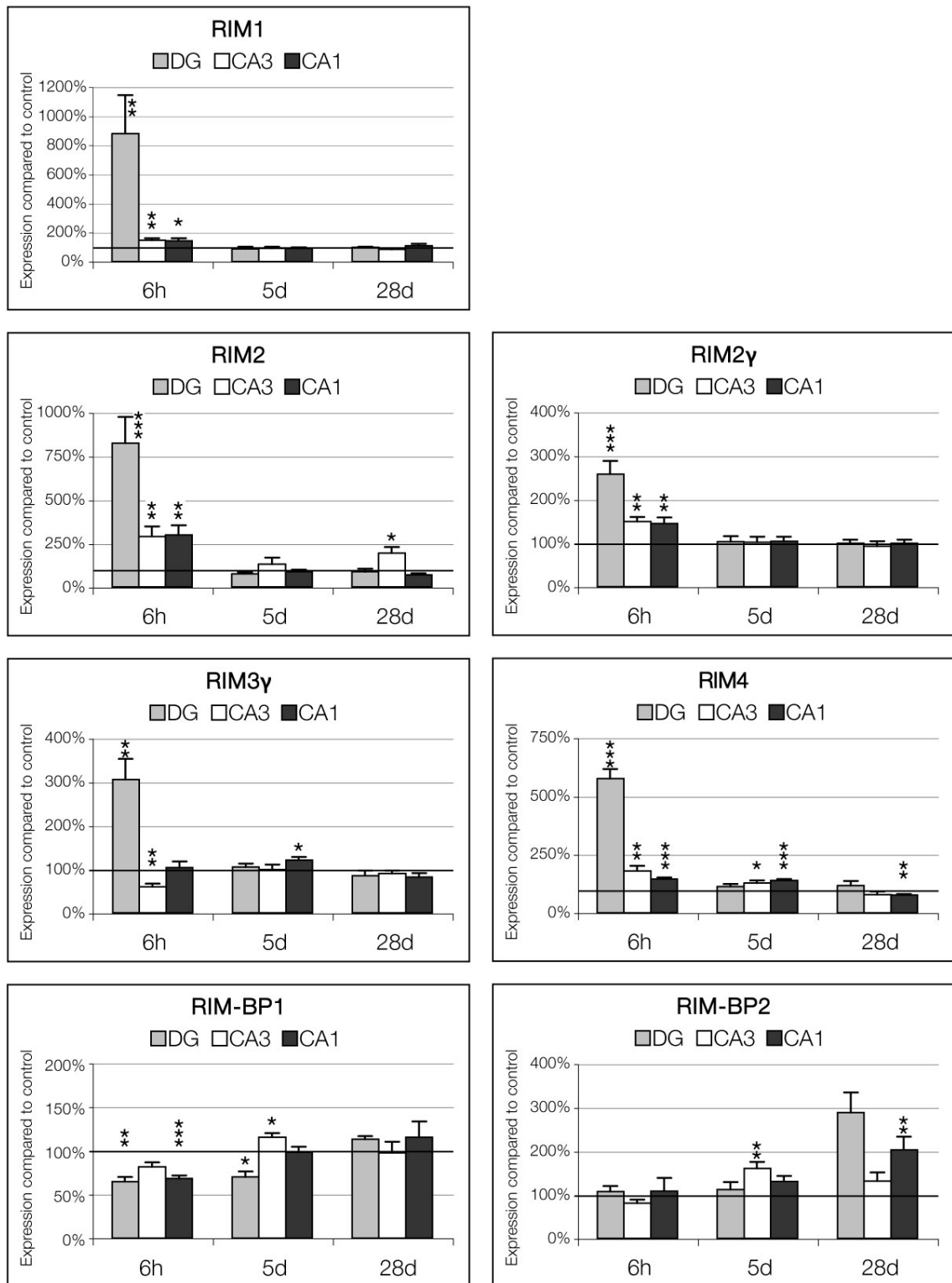
Figure 4.36: Differential mRNA Expression of the RIM and RIM-BP family at different time points after Status epilepticus (N ≥ 5).

5   Discussion

5.1   Expression of active zone associated gene families in the rat brain

The first part of this study concentrated on the distribution of the various members of the RIM family in the brain, and if they are coexpressed within one neuron. Furthermore, the distribution of RIM interacting proteins as well as Synaptotagmins was assessed to determine the complement of active zone proteins coexpressed within each brain region.

5.1.1 Distribution of RIMs.

RIMs comprise a family of active zone proteins, with two full length α-isoforms (RIM1α and RIM2α) that interact with a host of other active zone proteins in addition to synaptic vesicle proteins, and β- and γ-isoforms that exhibit more restricted interaction patterns. The currently available data demonstrate that RIM1α performs a central role in regulating neurotransmitter release, but suggest that other RIM isoforms may also be involved in the regulation of synaptic vesicle exocytosis (Calakos et al. 2004, Castillo et al. 2002, Lonart et al. 2003, Powell et al. 2004, Schoch et al. 2002). Although the various RIM isoforms are coexpressed in the brain, their relative expression patterns were unknown, and it was unclear whether potential redundancy among RIM isoforms exists. Such redundancy could be present, for example, between RIM1α and RIM2α because these two RIM isoforms are the only RIMs that bind to Munc13 and to Rab3 (Dulubova et al. 2005).

To analyze if RIM isoforms are coexpressed and could thus be redundant, *in situ* hybridizations and immunoblotting was performed. Results showed that RIM1α, 2α, 2β, and 2γ are ubiquitously present throughout the brain in overlapping, but non identical expression patterns (Figure 4.1). RIM1α is the most abundant isoform that appears to be expressed uniformly. RIM2α is also present in all brain areas, but at lower levels; high levels of RIM2α were observed in a small subset of neurons, such as olfactory bulb granule cells, hippocampal dentate gyrus granule cells, and cerebellar granule cells. As we were able to

show in the analysis of the RIM1/2 DKO (see chapter 5.2), the two highly ho-mologous α-RIM isoforms show significant functional differences. While RIM1α is viable for mossy-fiber LTP and synaptic short term plasticity, RIM2α is only able to rescue functional evoked transmitter release. A higher expression of RIM2α in some brain areas could therefore account for reduced synaptic long- and short-term plasticity in the affected synapses.

RIM2β and RIM2γ are also expressed ubiquitously in brain, again with high lev-els in a subset of neurons, for example the thalamus for RIM2β and the medulla oblongata for RIM2γ. Immunoblotting of protein homogenates from single RIM1α and RIM2α KO mice verified the differential distribution and divergent expression levels of RIM1α and RIM2α in brain (Figure 4.3D). These findings suggest that in some neurons, all RIM isoforms appear to be present, most conspicuously cerebellar granule cells, whereas in other neurons, one isoform predominates, for example hippocampal CA1 neurons that primarily express RIM1α, or olfactory bulb granule cells that primarily express RIM2α (Figure 4.1B).

5.1.2 The Synaptotagmin gene family

This study is the first comprehensive expression analysis of Synaptotagmins in the rodent brain. Information about the regional distribution of members of the Synaptotagmin gene family occurring in the CNS has until now only been re-ported for a subset of genes (Berton et al. 1997, Fox & Sanes 2007, Marqueze et al. 1995, Maximov et al. 2007, Xu et al. 2007). Detailed information about the regional expression patterns of all Synaptotagmins will be required as a first step towards an understanding of their functional roles. Only the functions of Syt-1, -2, and -9 that act as essential calcium sensors for fast synaptic vesicle release (Fernandez-Chacon et al. 2001, Geppert et al. 1994, Pang et al. 2006a, Pang et al. 2006b, Xu et al. 2007) and of Syt-7 that is a major sensor for exocy-tosis in chromaffin cells (Schonn et al. 2008) are well described. Another critical issue is the question which complement of Synaptotagmins is or could be pre-sent in an individual cell, as recent studies have provided evidence for the hy-pothesis that certain functional properties of a cell in the brain are defined by the subset of expressed Synaptotagmin isoforms (Xu et al. 2007).

5.1.2.1 Distribution of Synaptotagmin Gene Expression

The expression analyses revealed that with respect to their expression the Synaptotagmin gene family can be divided into two groups: firstly, isoforms universally expressed in most brain areas, and secondly, isoforms that are specifically enriched in individual cells or confined to distinct parts of the brain. Eight of the 13 Synaptotagmins analyzed here, Syt-1, -3, -4, -5, -7, -11, -12, and -13, belong to the first group. However, the overall level of expression as well as the distribution throughout the different brain regions varied strongly between the different isoforms. As a result each Synaptotagmin gene exhibited a distinct pattern of expression. The Synaptotagmins of the second group, Syt-2, -6, -9, and -10, showed a highly restricted regional distribution.

Of the Synaptotagmins analyzed in this study, eight exhibit Ca^{2+}-dependent phospholipid binding (Syt-1, -2, -3, -5, -6, -7, -9, and -10), and five do not (Syt-4, -8, -11, -12, and -13) (Bhalla et al. 2005, Dai et al. 2004, Li et al. 1995b, Sugita et al. 2002, von Poser et al. 1997, von Poser & Sudhof 2001). Synaptotagmins that bind phospholipids in a Ca^{2+}-dependent manner have been further classified into three distinct groups based on the disassembly kinetics of Ca^{2+}-Syt-liposome complexes: fast (Syt-1, -2, and -3), medium (Syt-5, -6, -9, and -10), and slow (Syt-7) (Hui et al. 2005). In addition, Synaptotagmins differ in their subcellular localization: four Synaptotagmins are localized to synaptic vesicles, Syt-1, -2, -9, and -12 (Takamori et al. 2006), whereas the remaining Syts are thought to be present on the plasma membrane and/or other types of secretory vesicles (Tucker & Chapman 2002).

The three Synaptotagmin isoforms that exhibit Ca^{2+}-dependent phospholipid binding and are present on synaptic vesicles, Syt-1, -2, and -9, are the only Synaptotagmin proteins that function as Ca^{2+} sensors for fast synchronous release in the mammalian brain (Maximov & Sudhof 2005, Pang et al. 2006a, Pang et al. 2006b, Xu et al. 2007). Our data, in accordance with previous studies (Marqueze et al. 1995, Pang et al. 2006b, Ullrich et al. 1994, Xu et al. 2007), shows that all brain regions express at least one member of this functional class of Synaptotagmins. Syt-1 is the most abundant isoform and is expressed throughout most parts of the brain at high levels, in particular in the forebrain, and only shows low expression in the brainstem. In contrast, Syt-2 and -9 mRNA is strongly expressed only in specific subregions. As Syt-2 is most

prominently found in the hindbrain and brainstem, the expression patterns of Syt-1 and Syt-2 seem to be partly complementary. It has been reported that Syt-1 and -2 are also found in distinct subsets of central synapses (Fox & Sanes 2007). Syt-9 transcripts were only detected at very low levels in the cerebellar granule cells, the mitral cell layer of the olfactory bulb, the thalamus and the putamen. This distribution differs from the observation in knock-in mice expressing an N-terminal GFP-Syt-9 fusion protein, where protein expression in the limbic system, the basal ganglia and the hippocampus was observed (Xu et al. 2007). There can be several reasons for this discrepancy. As the overall level of Syt-9 transcripts is very low, it could have been impossible to detect expression in the hippocampus, whereas immunohistochemistry with GFP anti-bodies resulted in the detection of low levels of the fusion protein. Also the ge-netic background of knock-in mice can result in differences in the exact pattern of expression (Hebert & McConnell 2000). However, our results reflect the automated non radioactive ISH findings in the Allan Brain Atlas for the mouse brain (www.Brain-map.org), where the strongest signals are also located in the thalamus and the olfactory bulb. Syt-1, -2, and -9 form a hierarchy of Ca^{2+} sen-sors with distinct properties with regard to release kinetics and apparent Ca^{2+} sensitivities, Syt-2 being the fastest and Syt-9 the slowest isoform with a much lower apparent Ca^{2+} sensitivity (Hui et al. 2005, Xu et al. 2007). The observed differential distribution patterns support the hypothesis that Syt-1 is the Ca^{2+} sensors for fast synchronous release in most neurons throughout the brain, however, the properties of individual neurons or even distinct synapses, e.g. in the thalamus (Syt-9) or the hindbrain (Syt-2), are determined by the coexpres-sion of the two additional members of this class.

Syt-12, a Ca^{2+} independent Synaptotagmin isoform that can be phosphorylated by PKA, is also found on synaptic vesicles. In cultured neurons it has no effect on evoked release but selectively modulates spontaneous synaptic vesicle exo-cytosis (Maximov et al. 2007). Syt-12 transcripts are found at low levels ubiqui-tously throughout the brain and at high levels only in the cerebellum and stria-tum. The distribution patterns within specific subregions are quite distinct, i.e. in the hippocampus and cortex. Syt-12 expression can be induced by external stimuli like thyroid hormone (Dong et al. 2005, Thompson 1996). Even though the expression patterns of Syt-12 and Syt-1 are largely overlapping, Syt-12

does not seem to modulate Syt-1 function but rather acts independently in the regulation of spontaneous synaptic vesicles fusion and potentially participates in mediating plasticity in response to external stimuli.

Among the Synaptotagmin isoforms that bind phospholipids in a Ca^{2+}-dependent manner and that are absent from synaptic vesicles Syt-3, -5, -6, and -10 were found to form a distinct phylogenetic branch. This group of Synapto-tagmin proteins is characterized by their lack of binding activity for inositol 1,3,4,5-tetrakisphosphate and the presence of a conserved N-terminal cysteine motif that mediates homo- and heterodimer formation (Fukuda et al. 1999, Ibata et al. 1998). While Syt-3 and Syt-6 were shown to be localized to the plasma membrane (Butz et al. 1999), the precise subcellular localization of Syt-5 and Syt-10 in neurons is not known so far. Syt-3 exhibited a moderate, relatively uniform distribution throughout all brain regions, as reported previously (Berton et al. 1997, Ullrich et al. 1994). In contrast, Syt-5, Syt-6, and Syt-10 showed more region specific expression patterns and are the only Synaptotagmin iso-forms with very low expression levels in the cerebellum. Intriguingly, Syt-6 and -10 are specifically enriched only in a very limited subset of cells, i.e. in the olfac-tory bulb, the cortex and the hippocampus, however, Syt-10 levels in the hippo-campus can be upregulated in response to strong synaptic activity (Babity et al. 1997b). So far the function of this class of Synaptotagmins has been mainly studied outside of the nervous system. Here, Syt-3 has been reported to regu-late the recycling of the chemokine receptor CXCR4 in T-cells (Masztalerz et al. 2007), the Ca^{2+}-induced insulin exocytosis in pancreatic cells (Gao et al. 2000) and the formation and delivery of internalized cargo from early endosomes to the perinuclear recycling compartment in mast cells (Grimberg et al. 2003). Syt-6 plays a role in the regulation of acrosomal exocytosis (Michaut et al. 2001, Roggero et al. 2007). Even though Syt-3, -5, -6, and -10 cannot substitute for Syt-1, -2, or -9 as Ca^{2+} sensors for fast synchronous release it is very likely that they are involved in the regulation of exocytotic or endocytotic fusion processes in neurons. While Syt-3 is expressed ubiquitously, the other isoforms are only found in distinct subregions. If this class of Synaptotagmins performs a uniform function, as is the case for the synaptic vesicle Synaptotagmins that bind Ca^{2+} and phospholipids, they could act either alone or in combination, thereby con-ferring distinct properties onto the neurons in which they reside. The overall low

abundance of these Synaptotagmins and the induction of Syt-10 gene expression by synaptic activity (Babity et al. 1997b) support the hypothesis that neurons can dynamically modulate their complement of this class of Synaptotagmins.

Syt-7 does not belong to any of the above described subclasses of Synaptotagmins even though it exhibits Ca^{2+}-dependent phospholipid binding. It is enriched in synapses but excluded from synaptic vesicles (Sugita et al. 2001, Virmani et al. 2003). Syt-7 is one of the more abundant Synaptotagmin isoforms and its distribution throughout the brain is very similar to the one observed for Syt-1. Because of its biochemical properties it was therefore proposed to be the candidate for the slow asynchronous Ca^{2+} sensor. In a recent study using mice deficient for Syt-7 or Syt-1 and -7 this hypothesis could not be verified (Maximov et al. 2008). However, Syt-7 was shown to be a major Ca^{2+} sensor for the exocytosis in adrenal chromaffin cells (Schonn et al. 2008). In neurons Syt-7 might additionally be involved in the regulation of synaptic neuropeptide release or some other form of Ca^{2+}- induced exocytosis.

With the exception of Syt-8 that is not detected at significant levels in the brain, all non Ca^{2+}-binding Synaptotagmin isoforms, Syt-4, -11, -12, and -13, are found throughout the brain in overlapping patterns. A recent report showed that Syt-4, -11, and -12 inhibit SNARE catalyzed fusion of liposomes, and that Syt-4 and -11 also antagonized the ability of Syt-1 to catalyze these fusion events (Bhalla et al. 2008). Whereas Syt-11 was abundantly expressed in all brain areas Syt-4 was detected at much lower levels. This data is in accordance with previously published reports, in which Syt-4 expression was found in all areas of the brain and slightly decreased during postnatal development (Berton et al. 1997, Ullrich et al. 1994), while a recent study failed to detect significant Syt-4 expression in neurons (Zhang et al. 2004). Syt-4 was reported to play a negative regulatory role during dense core vesicle exocytosis (Wang et al. 2001a, Wang et al. 2003). In contrast over expression of Syt-4 in primary hippocampal neurons did not alter excitatory fast synaptic transmission or fusion pore kinetics (Ting et al. 2006) but analysis of Syt-4 deficient mice led to the hypothesis that Syt-4 is a regulator of short-term synaptic plasticity (Ferguson et al. 2004). To unequivocally understand Syt-4 function in neurons further studies will be required. Based on the similarity of their sequence and their biochemical proper-

ties Syt-4 and Syt-11 could perform redundant functions but so far no data regarding Syt-11 function has been reported.

Syt-4, as Syt-10, is upregulated in response to synaptic activity and seems to be turned over rapidly (Babity et al. 1997b, Tocco et al. 1996, Vician et al. 1995). However, these two isoforms have opposing properties with regard to Ca^{2+}-dependent phospholipid binding and to the in vitro liposome fusion assay (Bhalla et al. 2008, Sugita et al. 2002). The expression patterns of Syt-4 and Syt-10 are also diverging, as in the native brain Syt-10 is only strongly expressed in the olfactory bulb, whereas Syt-4 is present at low levels throughout the brain. In the hippocampus Syt-10 transcripts are mainly detected in the dentate gyrus and Syt-4 mRNA is found in all hippocampal subregions. It will be necessary to gain insight into the subcellular localization of Syt-10 and its neuronal functions in order to see if Syt-4 and Syt-10 are involved in regulating the same processes albeit in opposite directions.

Based on emerging evidence that astrocytes may release 'gliotransmitters' and modulate synaptic activity and that gliotransmitter release depends on increase in intracellular Ca^{2+} (Parpura et al. 1994, Volterra & Meldolesi 2005) it was suggested that Synaptotagmins expressed by astrocytes might act as Ca^{2+} sensing molecules for regulated vesicle fusion. In accordance with this assumption, a previous study reported expression of Syt-4, -5 and -11 in astrocytes (Zhang et al. 2004).

5.1.2.2 Coexpression of Synaptotagmin isoforms in CA1 pyramidal neurons and Astrocytes

The results of the ISH analyses revealed that the various Synaptotagmin isoforms exhibit distinct but overlapping expression patterns. In order to examine which Synaptotagmin isoforms are expressed in one type of neuron, and if individual cells coexpress diverging sets of Synaptotagmin genes mRNA from single CA1 pyramidal neurons of transgenic mice expressing EGFP under control of the human GFAP (glial fibrillary acidic protein) promoter isolated was isolated (Mittelstaedt et al. 2009). Morphological and electrophysiological criteria were used for cell type identification prior to RNA extraction. After recording, RT-PCR analyses with primers recognizing the respective Synaptotagmin isoforms as well as the marker genes Synaptophysin and GFAP were performed. All CA1

neurons tested were GFAP mRNA negative and all contained transcripts encoding Synaptophysin, confirming specificity of the cell selection and RT-PCR protocol (Table 5.1). Syt-1, -4, -5 and -11 were expressed abundantly and were found in almost all cells analyzed (Table 2). In contrast, Syt-2, -3, -12 and -13 were only rarely detected, and Syt-10 and Syt-6 were never found in the CA1 neurons (Table 5.1).

Table 5.1: Post recording detection of Synaptotagmin isoforms in individual cells of the mouse hippocampus

A CA1 Pyramidal Neurons

Syt	1	2	3	4	5	6	10	11	12	13	GFAP	Synapto-physin
Total cell number	14	5	5	16	5	5	16	9	13	13	14	32
Positive cells	14	1	1	16	5	0	0	8	1	3	0	32

B CA1 Stratum Radiatum Astrocytes

Syt	1	2	3	4	5	6	7	10	11	GFAP	Synapto-physin
Total cell number	22	5	3	22	18	18	9	2	21	24	24
Positive cells	7	0	0	6	4	0	7	0	19	24	0

C Coexpression of Syts in individual CA1 pyramidal neurons

Syt	1	2	3	4	5	6	11	12	13
6 cells	+			+			+		
3 cells	+	-	-	+	+	-			
1 cell	+	-	+	+	+	-			
1 cell	+	+	-	+	+	-			
1 cell								+	+
2 cells								-	+
11 cells								-	-

D Coexpression of Syts in individual hippocampal astrocytes

Syt	1	4	5	6	7	11
2 cells	-	+	-/+	-	+	+
4 cells	+	+	-/-/-	-/-/-	-/-	+
3 cells	+	-	-/-	-/-	+	+/+/-
3 cells	-	-	+/-/-	-	+	+/+/-

mRNA from electrophysiologically identified CA1 pyramidal neurons (A) and astrocytes (B) was isolated after electrophysiological identification and analyzed by multiplex RT-PCR to detect co-expression of Syt mRNAs (C, D). In (A, B), Synaptophysin and GFAP were used as positive and negative controls, respectively. '+' indicates positive, '–' negative PCR results. In case of multiple signs (D), each sign represents the result from one individual cell. Gray areas in A and B indicate very high up to complete expression.

The use of different sets of primer pairs for multiple Synaptotagmins in single cell Multiplex RT-PCR revealed different subsets of Synaptotagmins in individual CA1 pyramidal neurons. In all cases probed, Syt-1, -4 (n = 9) and -11 (n = 6) were detected together in one cell. Furthermore, Syt-1, -4 and -5 were coexpressed in all cells tested (n = 5). These findings demonstrate that CA1 pyramidal neurons coexpress several Synaptotagmin isoforms and can differ in the respective combination of these genes. To look for the expression of Synaptotagmin isoforms in astrocytes transgenic hGFAP/EGFP mice were used. Green fluorescent astrocytes were identified morphologically and by their predominating 'passive' whole cell current patterns (Fig. 7D; Matthias et al. 2003, Steinhauser et al. 1994). All cells selected for post recording analysis were GFAP mRNA-positive and Synaptophysin mRNA-negative (n = 24; Table 5.1). Recently, Syt-4 and Syt-11 mRNA have been localized to astrocytes (Zhang et al. 2004). While confirming that astrocytes abundantly express Syt-11 (n = 19 of 21 cells), only a minority of astrocytes was found to express Syt-4 (n = 6 of 22 cells). Among the other Synaptotagmins tested, only Syt-7 was frequently encountered (n = 7 of 9 cells). Syt-1 (n = 7 of 22 cells) and Syt-5 (n = 4 of 18 cells) were rarely found while transcripts encoding Syt-2, Syt-3 or Syt-6 were consistently absent in hippocampal astrocytes (Table 5.1B). Half of the individual cells coexpress both Syt-7 and Syt-11 simultaneously (n = 5 of 9 cells). Additionally, they showed all possible combinations of Syt-1 and Syt-4 expression. Interestingly, the astrocytes lacking Syt-7 were the ones expressing both Syt-1 and -4 (Table 5.1D).

The results of this analysis confirm Syt-11 as an astrocytic Synaptotagmin but disagree about a fundamental role for Syt-4 in astrocytes. In the single-cell RT-PCR measurements, this isoform was encountered only in every fourth glial cell. It is very unlikely that the rare presence of Syt-4 was due to technical artifacts, because it was reliably detected in neurons, a finding that also contradicts the report by Zhang et al. (Zhang et al. 2004). Part of this discrepancy might be due to the use of cultured cells in the latter study. Indeed, robust Syt-4 immunoreactivity has been observed in cultured astrocytes (Crippa et al. 2006, Stenovec et al. 2007). Together, this data support a role for Syt-4 in transmitter release from neurons, but not from astrocytes. Similar to Syt-11, abundant expression of Syt-7 in hippocampal astrocytes could be shown. In contrast to Syt-11 and Syt-4

that both do not bind Ca^{2+} (Dai et al. 2004, von Poser et al. 1997), Syt-7 displays a high Ca^{2+} affinity (Sudhof 2002, Sugita et al. 2001). Syt-7 is the major Ca^{2+} sensor for exocytosis in chromaffin cells even though it does not play a role in neuronal synaptic vesicle exocytosis (Maximov et al. 2008, Schonn et al. 2008). In cultured astrocytes, two discernable forms of vesicular exocytosis have been demonstrated, triggered by different receptors (Bowser & Khakh 2007). Hence, it is conceivable that Synaptotagmin isoforms with variable Ca^{2+} sensitivity, i.e. Syt-7 and Syt-11, could be involved in evoked gliotransmitter release in a receptor-specific manner.

Taken together, the distribution of the various Synaptotagmin isoforms resembles the RIM family expression in the brain, showing different but overlapping expression patterns in different brain regions. The specific subset of Synaptotagmin and RIM isoforms could therefore reflect a possibility to preset the properties and adaptation range of a neuron in a given brain region to a specific genetically determined value.

5.1.3 Liprin expression

Liprin-αs are a family of highly evolutionarily conserved multidomain scaffolding proteins composed of two subfamilies, named Liprins-α and Liprins-β. The mammalian genomes contain four Liprin-α (Liprin-α1, -α2, -α3, and -α4) and two Liprin-β isoforms (Liprin-β1 and -β2). They are all six composed of three C-terminal sterile alpha motif (SAM) domains and several N-terminal coiled-coil domains, with Liprin-β being slightly shorter than Liprin-α. Liprin-αs directly interact with the C2B domain of RIM-αs, the only RIM domain that is included in all RIM family members (Schoch et al. 2002). Interestingly, the two brain specific Liprin-α isoforms, Liprin2α and -3α (Zurner & Schoch 2009), are both strongly expressed in the rat brain, while showing a diverging expression pattern. RIM1α, on the contrary, is much more abundant than its family homologue, RIM2α. Comparing the expression patterns of the two families, it becomes obvious that most areas of highest RIM1α expression nicely overlap with Liprin3α expressing areas, namely cortex, cerebellum and hippocampus. All these areas coexpress Liprin2α, which was additionally found in the thalamus, striatum and olfactory bulb. While Liprin2α expression in the thalamus is complemented by Rim1α and RIM2β, RIM2α is most prominently expressed in the olfactory bulb

granule cells. In summary, RIM and Liprinα family members show a heteroge-neous expression pattern in brain areas coexpressing at least one member of each family, but differing in their combination while apparently all members of both families are coexpressed only in the cerebellar granule cells. However, the ratio of the different Liprin and α-RIM isoforms varies between different brain regions. There is evidence pointing to functional differences between the differ-ent Liprin and RIM isoforms. For example, RIM2α can not rescue mossy-fiber LTP abolished through RIM1α deletion and Liprin1α is the only Liprin-α regu-lated by synaptic activity. Therefore, a change in the composition of the active zone may have an influence on its functional properties. Further studies looking into common and diverse functional properties of the various Liprin-α isoforms is therefore required to understand the synaptic characteristics that are modified through the regulation of Liprin-α expression. In summary, the observed distri-bution pattern supports the hypothesis that the interaction of RIMs and Liprins is physiologically relevant.

5.1.4 RIM-BP expression

The analysis of the expression pattern of the RIM-BP family revealed that RIM-BP1 and -2 are present throughout the brain in overlapping, but non-identical expression patterns (Figure 4.24). RIM-BP1, as the most abundant isoform, is expressed almost ubiquitously in all neuron-rich brain regions. In contrast, RIM-BP2 is concentrated in rostral brain regions, with the strongest expression in the telencephalon, and low abundance in caudal areas. Interestingly, in contrast to most other active zone proteins, it is barely detectable in the cerebellum. Whereas RIM-BP1 and -2 mRNA levels increase during synaptogenesis, RIM-BP3 expression remains low in the brain during development. RIM-BP3 levels are especially high outside the nervous system, where RIM-BP1 and -2 cannot be detected. However, the data suggests that all neurons express at least ex-press RIM-BP1, approving its supposed function as molecular linker of RIM to voltage-gated calcium channels (Hibino et al. 2002). The additional expression of RIM-BP2 in a subset of brain areas could point to a similar role of the ratio between the two proteins in the finetuning of synaptic strength as we propose for RIM1α and RIM2α.

Overall, we were able to show that most brain regions express several isoforms of one family of active zone proteins. In general, one protein is most abundantly expressed in nearly all parts of the brain, while other family members are more regionally restricted to different brain areas. This could point towards a fine-tuning of the synaptic properties within each brain region by a varying subset of proteins with slightly differing kinetics expressed in the cell. Functionally, this difference has been shown in the case of Munc13-2, for example, that is functionally important only in a subset of hippocampal synapses (Breustedt et al. 2009). As mentioned before, Synaptotagmins also show differences in their binding kinetics as well as functional properties (Bhalla et al. 2008, Sudhof 2002). Considering the differential regional distribution of the various members of active zone protein families, it is therefore very likely that this diverse localization reflects differences in the physiological properties of the different family member, and could be used to modify the synaptic properties of the neuron.

5.2   α-RIM protein function at the active zone

From the two α-isoforms of the RIM family present in the mammalian genome, to date only RIM1α had been analyzed functionally. After examining the expression patterns of various RIM isoforms, the RIM2α KO mice were analyzed to test the possibility that RIM1α and RIM2α are functionally redundant.

5.2.1 Essential functions of RIM2α.

Whereas deletion of RIM1α causes large changes in the amount and regulation of neurotransmitter release (Calakos et al. 2004, Schoch et al. 2002), that the single deletion of RIM2α, the only other α-RIM, was found to have milder phenotypic consequences compared to the deletion of RIM1α. RIM2α-deficient mice are impaired, but their release properties in hippocampal synapses appear to be normal. It is puzzling that RIM1α but not RIM2α KO mice exhibit a loss of mossy-fiber LTP in the CA3 region of the hippocampus (Castillo et al., 2002; Schoch et al, 2006), because RIM1α and RIM2α are both highly expressed in the dentate granule cell neurons that supply the mossy fiber synapses, and both are phosphorylated by PKA at a site equivalent to serine413 in RIM1α (Lonart et al., 2003). Furthermore, it has been postulated that α-RIMs play a role in regulating insulin release from pancreatic β-cells (Iezzi et al. 2000, Kashima et al.

2001). However, no changes in body fat content or in blood glucose levels in the RIM1α and 2α KO mice could be shown (Schoch et al, 2006).

5.2.2 Redundant functions of RIM1α and 2α.

Although deletion of either RIM1α or RIM2α does not significantly impair survival of mice, deletion of both α-RIMs causes complete lethality at birth, while the absence of only three of the four α-RIM alleles – in either combination – induces a ~40% lethality (Figure 4.6A). No obvious developmental abnormalities, changes in synapse structure, or alterations in brain composition were detected in the RIM1α/2α double KO mice (Figure 4.8 and Figure 4.9), suggesting that these mice perished because of a functional, and not a developmental defect. Because of the severe loss of motor control in RIM1α /2α double KO mice, the NMJ was studied as a model system to examine the consequences of deleting both α -RIMs. As indirect indicators of defective synaptic transmission at the neuromuscular junction, an increased density of motoneurons in the ventral horn of the spinal cord was found, in addition to increased branching of presynaptic motor nerves and increased numbers of irregularly distributed motor synapses on skeletal muscle fibers. These effects are considered consequences of an impaired function at the neuromuscular junction (Dahm & Landmesser 1991, Harris & McCaig 1984, Oppenheim 1991). Direct measurement of synaptic transmission at the neuromuscular junction by Weichun Lin revealed profound defects. He found that spontaneous release was unchanged in frequency, but evoked synaptic transmission was strongly reduced (Schoch et al, 2006). The miniature frequency could not be enhanced in the double mutants by increasing the Ca^{2+} concentration under depolarizing conditions, while the amplitudes and failure rate of evoked release were massively decreased and increased, respectively (Schoch et al, 2006). This phenotype demonstrates that deletion of α - RIMs does not abolish spontaneous or Ca^{2+}-dependent exocytosis, but severely and specifically impairs Ca^{2+}-triggering of exocytosis. Interestingly, a recent study at the NMJ of *C. elegans* showed that Unc-10/RIM localization is restricted to dense projections and that the number of membrane-contacting vesicles is reduced in unc-10 deficient animals (Weimer et al. 2006). It was therefore hypothesized that the Rab3 – unc10/RIM – unc13/Munc13 tripartite complex localizes primed synaptic vesicles in close proximity of calcium channel

containing dense projections. Consistent with a loss of synaptic transmission, the pattern of synapses in the NMJs of double KO mice exhibited morphological changes that are typically observed upon complete block of synaptic transmission in NMJs (Brandon et al. 2003, Misgeld et al. 2002, Schoch et al. 2006). Munc13-deficient NMJs also display an impairment of evoked transmitter release similar to NMJs lacking α-RIMs. But different from NMJs lacking α-RIMs, Munc13-deficient NMJs exhibit an increased frequency of spontaneous transmitter release (Varoqueaux et al. 2005). Moreover, NMJs deficient for the SNARE protein SNAP-25 also exhibit increased spontaneous transmitter release but lack evoked release (Washbourne et al. 2002). Based on the observation of decreased evoked and increased spontaneous release in Munc13 and SNAP-25 KO mice, it was hypothesized that Munc13-mediated priming via SNARE proteins is essential for the majority of synaptic vesicles at the NMJ, while a small subpopulation of vesicles undergo spontaneous Munc13-independent priming (Varoqueaux et al. 2005). The increase in mini frequency observed in Munc13 and SNAP-25 KO mice was then explained by an increase in the number of synapses in mutant NMJs. However, NMJs lacking α-RIMs exhibit the same morphological changes (increase in number of motoneurons, in branching of presynaptic nerve fibers, and in neuromuscular synapse formation) and the same loss of evoked release as Munc13-deficient synapses, but the mini frequency is not increased. These results thus suggest that the increase in mini frequency in Munc13- and SNAP-25-deficient synapses is not due to an increased number of synaptic contacts in the NMJ, but could be a homeostatic response to the decrease in neurotransmitter release. Thus α-RIMs may act as downstream effectors of Munc13s, presumably via the N-terminal interaction between these two proteins (Betz et al., 2001; Dulubova et al., 2005).

This study indicates that in some synapses as at the NMJ, loss of either RIM1α or RIM2α can be compensated by the respective other, whereas in hippocampal excitatory and inhibitory neurons RIM1α can compensate for RIM2α but not vice versa. A similar result has been obtained in the analysis of Munc13-1/-2 deficient neurons which show a complex pattern of redundancy (Varoqueaux et al. 2002). In GABAergic hippocampal neurons both isoforms are redundant, however, in glutamatergic neurons the presence of Munc13-1 is required. Further-

more, Munc13-1 or -2 equipped synapses exhibit diverging short-term plasticity characteristics in spite of their high structural homology (Breustedt et al. 2009, Rosenmund et al. 2002). Nevertheless, the molecular mechanisms underlying this phenotype are still unclear. As RIM1α and RIM2α are also structurally highly homologous, interact with the same set of proteins and are both PKA-substrates, a detailed gain- and loss-of-function analysis in RIM1α/2α-deficient neurons can now address the molecular basis that determines their individual and redundant functions. However, our study clearly demonstrates a severe defect in synaptic transmission that can at least partially explain the dramatic lethal phenotype observed in the absence of α-RIMs.

5.3   The RIM-BP family

Structural and functional data suggest that a protein complex ensures the tight coupling between the synaptic vesicle release machinery and presynaptic voltage-gated calcium channels (Harlow et al. 2001). The RIM-BP protein family has been proposed to be a part of this molecular linker (Hibino et al. 2002). RIM-BPs display structures typical of adaptor proteins and have been shown to interact with the active zone proteins RIM1 and RIM2 as well as with different α-subunits of voltage-gated calcium channels (Hibino et al. 2002, Wang et al. 2000). Here, the complete DNA sequence, genomic organization, and expression profiles of the mouse and human RIM-BP genes are presented. Furthermore, a novel member of the RIM-BP gene family has been identified and cloned, RIM-BP3, sharing the domain composition and structural organization with RIM-BP1 and RIM-BP2.

The analysis of genomic and transcript databases described here revealed that RIM-BPs are evolutionarily conserved in invertebrates and vertebrates and were diversified during evolution into a family containing three genes (Figure 4.27, Figure 4.28). This finding supports the idea that RIM-BPs are likely to have a fundamental function that is shared between invertebrates and vertebrates.

RIM-BP1 and RIM-BP2 are large multi domain proteins, while the smaller phylogenetically older RIM-BP2 protein is encoded by a much larger gene. The exons encoding the domains that are homologous between the RIM-BP1 and RIM-BP2 proteins are highly conserved in their size and nucleotide sequence

and show a similar exon-intron structure. Furthermore, the RIM-BP orthologs in human and mouse exhibit similarities. First, the lengths of the exons are often identical for the human and mouse RIM-BP orthologs and comparable for their introns resulting in a conserved structural arrangement of human and mouse RIM-BP genes. Second, the splice patterns of RIM-BP transcripts are identical for the human and mouse orthologs. However, only the RIM-BP2 gene contains several non-coding exons in its 5'-UTR which could potentially be involved in translational regulatory processes. Interestingly, RIM-BP3, the most recent member of this gene family, is encoded by a single exon. Even though the human and mouse genomes contain several thousand intronless genes, e.g. many histone and G-protein coupled receptor (GPCR) genes (Sakharkar & Kangueane 2004), it has to be excluded that this intronless gene is a pseudogene. Four lines of evidence support that RIM-BP3 constitutes an actively transcribed gene: (1) cDNA was cloned encoding RIM-BP3 from testis cDNA preparation that did not contain detectable genomic contaminations (Figure 4.23A); (2) high levels of RIM-BP3 were detected by quantitative real-time PCR in cDNA from various organs (Figure 4.23B); (3) RIM-BP3 proteins of all species exhibit a very high degree of sequence conservation (Figure 4.26B, Figure 4.27A); (4) a systematic analysis of intronless genes in which all identifiable processed pseudogenes were eliminated, classified RIM-BP3 as being transcribed. Therefore, RIM-BP3 can be classified as a functional member of the RIM-BP gene family. Recently, RIM-BP3 was indeed shown to play a vital role in spermatogenesis, controlling microtubule organization in the acrosome-acroplaxome-manchette complex through interaction with the microtubule-binding protein Hook1 and potential binding to the microtubule-based molecular motor protein KIF3B (Zhou et al. 2009). This could point to a related function of RIM-BP1 and -2 in the active zone, where they could also contribute to the organization of the CAZ.

The RIM-BP gene family is defined by its domain composition (SH3- and FNIII-domains, regions rich in charged amino acids and proline) and by the structural organization of its modules. The RIM-BP proteins are particularly conserved throughout the SH3- and FNIII domains (Figure 4.22, Figure 4.26A), whereas the sequences adjacent to the functional domains diverge in length and composition. Interestingly, the linker region between the central and the C-terminal

modules in RIM-BP1 and RIM-BP2 is subject to alternative splicing. As a result, the distance between the functional domains would be altered. These structural changes might induce changes in the protein-protein interactions mediated by the FNIII- and SH3-domains.

The RIM-BP SH3- and FNIII-domains are rather atypical and do not exhibit significant homology with similar domains in other proteins. The protein interactions known so far for RIM-BPs, with RIMs and voltage-gated calcium channels, are mediated via their SH3-domains (Hibino et al. 2002, Wang et al. 2000). The RIM-BP SH3-domains bind to class I binding motifs ($+X\phi PX\phi P$; with + = basic, ϕ hydrophobic, and X = any amino acid) (Li 2005). Within this motif the core proline residues are required for the formation of the ligand structure and play an important role in binding. The residues that flank the core determine the selectivity of a ligand. The SH3-binding sequences in RIMs (RQLPQL/VP) and in the α_{1E} (RQLPPVP) subunit of the voltage-gated calcium channel fit the canonical sequence for class I ligands, whereas the motifs in α_{1A}, α_{1B}, α_{1D} and α_{1F} differ by a non hydrophobic threonine residue in the sixth position. α_{1C} and α_{1G} also contain a similar motif with a PXXP core. In addition to the SH3-domains RIM-BP1 and -2 encompass three and RIM-BP3 two contiguous Fibronectin type III domains. FNIII domains are independently folded modules of 100 amino acids and have been shown to mediate specific protein-protein interactions mainly in extracellular but also in intracellular compartments. FNIII domains are contained within hundreds of different proteins including receptor protein kinases and phosphatases, neuronal adhesion molecules and cytoplasmic muscle proteins (Bork & Doolittle 1992). Even though the amino acid composition of FNIII domains is not well conserved between different proteins, the structures of most FNIII modules are very similar, corresponding to a β-sandwich formed by two antiparallel β-sheets (Goll et al. 1998). To date, no binding partners for the RIM-BP FNIII domains have been described. Further analysis of the function of the RIM-BP modules, along with the identification of interacting proteins, will clarify their exact cellular roles.

In summary, the modular domain structure of RIM-BPs and their conservation during evolution supports their potential role as important molecular adaptors. However, the precise biological function of RIM-BP proteins still remains to be defined in future studies. With the characterization of the RIM-BP gene family

and their gene structure described here, this issue can now be addressed in further experiments.

5.4   Changes in expression after pilocarpine-induced SE

Altered expression and distribution of synaptic proteins constitute key aspects in epileptogenesis and impaired hippocampal excitability, as observed, for example, in human patients with Ammonshorn sclerosis (AHS), as well as in animal models of temporal lobe epilepsy (TLE, see Blumcke et al. 2000). Using the pilocarpine model of TLE, it has been shown that interference with the expression level of just one component of the synapse can lead to increased or reduced seizure susceptibility after status epilepticus (Pitsch et al. 2007). Although the mechanisms leading to chronic epilepsy are not entirely understood, the pathologic outcome of the structural and functional cellular reorganization of the hippocampus seems to depend on slight changes in the composition of synaptic components, reacting to the strong, pathogenic synaptic activity induced by the initial epileptic seizures (Majores et al. 2007). Using the pilocarpine model of temporal lobe epilepsy therefore permits to analyze the direct effect of highly increased synaptic activity on synaptic proteins involved in long term synaptic plasticity, and to look for presynaptically expressed genes that change their expression during epileptogenesis and the chronic phase of epilepsy, hinting towards an epileptogenic function of these genes or proteins (Majores et al. 2007).

This study differentiates between the three main regions of the hippocampus, the Dentate gyrus (DG) and the Cornu ammonis regions CA1 and CA3, as they develop very differently during epileptogenesis: the CA1 region can show extensive destruction, and the CA3 pyramidal neurons exhibit intense gliosis in the latent phase, leading to a segmental cell loss in this area, and AHS (Mello et al. 1993). Thereby, the DG granule cell axons („mossy fibers") loose their target pyramidal neurons in the CA3 region and sprout out of the DG, building new connections to other granule cells and surrounding neurons (Mello et al. 1992). Specific changes in the expression of a gene in the DG could therefore be related to the generation of new axonal branches and presynapses, while invisible structural and functional synaptic reorganization processes happen in all three HC areas to some extend.

5.4.1 Altered expression of various Synaptotagmins during epileptogenesis

The Synaptotagmin family of proteins contains at least 13 members that are expressed in the brain. While Syt-1 is widely accepted to be the main Ca^{2+} sensor in fast evoked synaptic vesicle fusion, little is known about the functional role of most of the other family members. Our expression analysis revealed that one neuron expresses various sets of Synaptotagmins, resulting in the question if this complement is regulated by synaptic activity. Therefore, quantitative real-time RT-PCR and quantitative immunoblotting of hippocampal subregions at different time points after SE were used to examine if expressional alterations of the various Synaptotagmin isoforms in response to strong synaptic activity and with it changes in synaptic signaling pathways differs from each other. Indeed, distinct changes were observed for several Synaptotagmin isoforms, but the expression of the Ca^{2+}-sensor for Ca^{2+}-evoked transmitter release, Syt-1, was not altered at any time point examined. In a recently published study, Syt-1 protein expression was reported to be increased in the brain-dissects of epileptic patients refractory to antiepileptic drugs (Xiao et al. 2009). Interestingly, patients with defined local epileptic foci that were not refractory did not show a difference in expression compared to control tissue from patients with head trauma, and without a history of seizures. As the animal model used in this study reflects locally defined temporal lobe epilepsy, that can be repressed by antiepileptic medication (Remy et al. 2003), the study of Xiao et al. confirms the results of this study. In accordance with previous reports an mRNA upregulation of two Synaptotagmins could be shown that had originally been identified as genes induced by synaptic activity, Syt-4 and Syt-10 (Babity et al. 1997b, Thompson 1996, Vician et al. 1995). Additionally, mRNA upregulation was detected in Syt-6, -7, -9, -11 and -12 that were complemented by significant changes on the protein level for Syt-6, -7 and -12, a significant downregulation of Syt-3 in the acute phase, and of Syt-7 during the latency period was shown in the CA3 region of the hippocampus.

Through the use of a different epilepsy model and the study of protein expression in addition to mRNA expression at more timepoints and in different hippocampal subregions, the results of this study complement and further augment

the available data on Syt-4 and Syt-10 from previous studies (Babity et al. 1997a, Glisovic et al. 2007).

Previously, the strongest increase of Syt-10 mRNA had been observed six hours after kainate-induced SE in the DG (Babity et al. 1997a). The results of this analysis additionally showed a markable rise of Syt-10 mRNA levels in the CA3 and CA1 region in the early acute phase, six hours after SE. Interestingly, the upregulation on the protein level was delayed and could only be shown 24h after SE. So far, nothing is known about Syt-10 function, but it is intriguing that it is barely expressed in the native brain (Figure 4.15), but strongly upregulated in the hippocampus following pathological synaptic activity.

Published data showed Syt-4 mRNA upregulation from four to 24h after SE in all hippocampal subregions (Glisovic et al. 2007). The results of this study confirm these findings and additionally show Syt-4 upregulation on the protein level at least in the CA3 and CA1 region six hours after SE. Syt-4, one of the most abundant Synaptotagmins in our CA1 single cell analysis (Mittelstaedt et al. 2009), has recently been shown to regulate BDNF secretion in axons as well as dendrites. Deletion of Syt-4 enhanced LTP and increased vesicle release in this study, while overexpression decreased exocytosis (Dean et al. 2009). These results support the hypothesis that neurons regulate their complement of Synaptotagmins to maintain synaptic activity at a physiological level, since the upregulation of Syt-4 after exposure to epileptiform activity could account for an early reactive decrease in neuronal excitability.

Syt-3, together with Syt-6, has been biochemically shown to be predominantly enriched in synapses and in the synaptic plasma membrane, but not in the vesicular fraction (Butz et al. 1999). Together with Syt-5 and Syt-10 they both belong to a group of Synaptotagmins that share a high homology of ammino acid composition in their C2 domains and bind phospholipids in a Ca^{2+}-dependent manner (Rickman et al. 2004). Additionally, all four proteins contain a conserved N-terminal cysteine motif that mediates homo- and heterodimer formation (Fukuda et al. 1999). Syt-3 has further been implied in endocytotic recycling in mast cells (Grimberg et al. 2003), where it is associated with the transport of internalized receptors to endocytiotc recycling compartments. Syt-3 could therefore also play a role in the structural reorganization during epileptogenesis that might require the internalization of presynaptic membrane and associated pro-

teins. However, to date no functional role for Syt-3 in neurons has been described. Nevertheless, the strong down-regulation of Syt-3 in the acute phase in response to strong pathophysiological synaptic activity points to a role for Syt-3 in the adaptive changes occurring during early epileptogenesis.

Syt-6, that belongs to the same subfamily of Synaptotagmins as Syt-3 and Syt-10, is one of the most strongly upregulated isoforms during the acute phase. The functional role of Syt-6 in neurons is not well established yet. In sperm, Syt-6, together with the nonneuronal Syt-8, is critical for membrane fusion and acrosome exocytosis (Hutt et al. 2005, Roggero et al. 2007). Furthermore, in the hippocampus, expression of Syt-6 is restricted to a subpopulation of interneurons (Mittelstaedt et al. 2009). As epileptogenesis has been linked to an imbalance of excitation and inhibition (Scharfman 2007), the strong upregulation observed for Syt-6 in the acute phase might contribute to changes in the synaptic properties of interneurons. It would therefore be interesting to further investigate the expression of Syt-6 in the various interneuron populations of the hippocampus. In summary, it is intriguing that three out of four members of this subfamily show expressional alterations during epileptogenesis. While two Synaptotagmins (Syt-6 and –10) are up-, and one (Syt-3) is down-regulated, Syt-5 levels remain unchanged.

Another Synaptotagmin exhibiting differential expression during epileptogenesis is Syt-7. It has been described as a major Ca^{2+} sensor in Ca^{2+}-dependent exocytosis in pancreatic β-cells and adrenal chromaffin cells (Gauthier et al. 2008, Schonn et al. 2008). Previous studies in neurons located Syt-7 at the plasma membrane, where it was suggested to be functionally involved in vesicle recycling and clathrin coated endocytosis (Virmani et al. 2003). But more consistent with its role in endocrine cells, Syt-7 has also been shown to play a role in Ca^{2+} evoked exocytotic events of late endosomes/lysosomes in neurons from sympathetic cervical ganglia mediating the addition of new membrane to developing neurite extensions (Arantes & Andrews 2006). The postulated function in neurite outgrowth correlates with the finding that Syt-7 is strongly upregulated in the DG during the latency period, where in the course of the cellular reorganization the so called mossy fibers, axonal projections of the DG granule cells to CA3 pyramidal cells, start building new axonal branches sprouting through the DG, forming autapses and even branching out into the DG molecular layer

(Buckmaster et al. 2002). In the CA3 region, neurite outgrowth however seems to be reduced, fitting to the significant downregulation of Syt-7 at this time point. Later developments in the hippocampus then result in an increase of Syt7 expression in the CA1 region during the chronic phase, where most of the neurons die during epileptogenesis. This upregulation could indicate a stronger outgrowth of neurites through the sclerotic tissue, but is more likely caused by an astrocytic function of Syt-7, as it was the most abundant Synaptotagmin isoform besides Syt-11 in astrocytes in our analysis of cellular distribution of Synaptotagmins in the CA1 region (Mittelstaedt et al. 2009).

Syt-12 has been found to selectively modulate spontaneous synaptic vesicle exocytosis and to be phosphorylated in a cAMP dependent manner (Maximov et al. 2007). It is expressed at low levels throughout most parts of the brain, including the hippocampus, in a developmentally delayed pattern (Maximov et al. 2007, Mittelstaedt et al. 2009). Interestingly, its expression was not altered in the acute phase, but was increased about 50% in the later stages in the dentate gyrus. While nothing is known about the constitutional role of Syt-12, its overexpression in cultured neurons dramatically increased the rate of spontaneous release, but had no effect on synchronous and asynchronous components of release triggered by action potentials (Maximov et al. 2007). An upregulation of this Synaptotagmin isoform during the later phases of epileptogenesis could therefore partly account for the increased excitability of the epileptic brain.

In summary, the data of this study shows that strong synaptic activity results not only in an upregulation of Syt-4 and Syt-10, as previously described, but that the expression of multiple members of the Synaptotagmin gene family is regulated by synaptic activity. Most expressional changes were found in the acute phase, however, a few Synaptotagmins exhibit distinct changes in the latent and chronic phase as well. These results thereby support the hypothesis that the functional properties of a cell are influenced by the set of Synaptotagmin isoforms it expresses, insofar as the isoforms differ in their functional properties and in their response to upstream signaling pathways. But still several open questions remain to be addressed: As the function of most Synaptotagmins besides Syt-1 are not fully understood, the functional consequences of their differential regulation in the hippocampus remain unclear. In addition, the results presented in this study were obtained by measuring expression changes

within one hippocampal subregion, which is composed of multiple cell types, e.g. glutamatergic and GABAergic neurons and interneurons as well as astrocytes. Further studies will have to elucidate in which cell types these changes occur, and if all cells of one type are affected. This would allow for selective manipulations of the Synaptotagmin complement of these cells and the analysis of the resulting consequences on the physiological properties of the cell.

5.4.2 Changes in the composition of active zone proteins after SE

Neurons undergo homeostatic plasticity and synaptic scaling to maintain their overall firing rate while adapting to persistent alterations in input strength. However, since its discovery in 1998, the mechanism underlying these concepts of synaptic plasticity is not understood (Turrigiano et al. 1998). While it was firstly described to be dependent on changes in the mEPSC amplitude by modulations of the levels of AMPARs, and thereby be mostly postsynaptically located (O'Brien et al. 1998, Turrigiano et al. 1998), increasing evidence points towards an additional presynaptic component of these modifications in adult neurons (Tokuoka & Goda 2008, Wierenga et al. 2006). For example, it has been shown that glutamatergic presynaptic terminals are able to binarily adjust the release competence of their synaptic vesicles in response to a block of electrical activity or overall increases of spiking (Moulder et al. 2006b). The present study was therefore outlined to investigate whether and how altered synaptic network activity in vivo, caused by pilocarpine induced SE, influences the molecular composition of the active zone. It could show that in the acute phase, most components of the active zone that were examined showed a significant upregulation at the mRNA level. However, the changes on the protein level seemed to be delayed, as almost no changes were observed six hours after SE, but after 24h. Strikingly, Munc13-1 and -2 showed an opposing regulation. This is of particular interest, as, dependent on the kind of synapse, both Munc13 isoforms can exhibit different physiological characteristics. While most synapses mainly depend on Munc13-1 under normal conditions and function normally without Munc13-2, at mossy fiber (DG to CA3) synapses, the absence of Munc13-2 was shown to lead to a decrease in release probability accompanied by an increase in short-term facilitation, and to a remarkable reduction of asynchronous transmitter release (Breustedt et al. 2009). In hippocampal autaptic cell cultures however,

synapses solely driven by Munc13-2 were found to display synaptic short-term facilitation (Rosenmund et al. 2002). The ratio of Munc13-1 and Munc13-2 thereby seems to play a role in the regulation of the release probability of the synapse. The results of this study revealed that Munc13-1 was downregulated in CA1 and CA3 in the acute phase six hours after SE on both, mRNA and protein level, while Munc13-2 showed a massive 10-fold increase on the mRNA level in the DG, accompanied by a rising protein concentration in DG and CA1 persisting at least for 24h after SE. Under normal physiological conditions, an increase of Munc13-2 would be expected to lead to a decrease in short-term facilitation, and would therefore be a suitable response to the increased synaptic activity induced by the SE. However, this effect could be inverted by mossy fiber sprouting, leading to the formation of autapses within the DG granule cells and a subsequent short-term facilitation. Munc13 could thereby play two diverging roles during the course of epileptogenesis: on the one hand a modulation of the Munc13-1 to Munc13-2 ratio could keep the synaptic activity at a physiologically healthy level. On the other hand, a change in the ratio could, in combination with other epileptogenic components that lead to the structural reorganization of the hippocampus, promote an increased synaptic excitability and thereby the development of a chronic epileptic phenotype.

While Munc13 has been shown to regulate release probability at mossy fiber synapses, the loss of the other presynaptic component implicated in docking and priming at the active zone, RIM1α, causes an increase in paired-pulse facilitation and a reduction of release probability at Schaffer-collateral CA3 to CA1 synapses (Calakos et al. 2004, Schoch et al. 2002). Later studies revealed that RIM1α seems to be important for all presynaptically mediated forms of synaptic plasticity in excitatory (Fourcaudot et al. 2008, Lonart et al. 2003, Lu et al. 2006, Pelkey & McBain 2008) and inhibitory (Chevaleyre et al. 2007, Kaeser et al. 2008a, Lachamp et al. 2009) synapses. Our work revealed a strong increase in RIM mRNA levels in the acute phase of epileptogenesis, but no change in the later time-course of epileptogenesis. Interestingly, in the chronic phase of an animal model of TLE, RIM1 KO mice exhibit a higher frequency of epileptic seizures (personal communication, Julika Pitsch). The underlying physiological cause is not clear yet, but the involvement of RIM1α in the plasticity of excitatory as well as inhibitory neurons could lead to an imbalance within the hippo-

campal neuronal network. For example, it has been shown that RIM1α plays an important role in the restoration of the feed forward inhibitory control of the CA3 network after the mGluR7b dependent weakening of mossy-fiber – interneuron synapses during high frequency stimulation. This so-called de-depression and subsequent potentiation of inhibitory interneurons is absent in the RIM1α KO mice (Pelkey et al. 2008). Additionally, a recent study has shown that the degradation of RIM1α and Munc13-1 by the ubiquitin-proteasome system is part of a homeostatic mechanism to silence single synapses under conditions of increased synaptic activity (Jiang et al. 2010). Although it was not checked in this study if RIM2α is degraded equally to RIM1, it is possible that RIM2α constitutes a less variable and more stable component of the active zone, as it is neither involved in synaptic plasticity. Since RIM2α is the only variant available in the RIM1 KO, and also Munc13-1 is already reduced in these mice, this mechanism of activity-dependent synaptic silencing would be disabled in the knockout mice. The strong early upregulation of RIM in the acute phase of epileptogenesis could have a similar disabling effect on synaptic homeostasis, as it could counteract the increased protein degradation by the ubiquitin-proteasome system.

α-Liprins, with their multitude of potential interaction partners, have been implicated in developmental and structural functions in the pre- as well as postsynaptic densities (Spangler & Hoogenraad 2007). So far, only Liprin1α has been reported to be differentially regulated through posttranslational mechanisms in response to synaptic activity. Both CaMKII-mediated degradation and the ubiquitin-proteasome system have been shown to play a role in the regulation of Liprin1α protein levels, and thereby to regulate dendritic branching and spine density postsynaptically (Hoogenraad et al. 2007). Additionally, Liprin1α was recently reported to regulate cell motility and filopodial outgrowth through its interaction with integrins (Asperti et al. 2009, Asperti et al. 2010). While this study did not reveal a change of Liprin1α expression following epileptiform activity, Liprin2α and Liprin4α were opposingly regulated during epileptogenesis. It is puzzling that the amount of Liprin4α, that is the weakest α-Liprin expressed in the brain (Zurner & Schoch 2009), is further reduced during epileptogenesis, while the already abundant Liprin2α is upregulated.

The altered levels of Liprins could have direct consequences for synaptic function. Liprins have been implicated in the development and maturation of syn-

apses as well as postsynaptic AMPA receptor targeting through their interaction with the multi-PDZ domain protein GRIP (Spangler & Hoogenraad 2007, Stryker & Johnson 2007, Wyszynski et al. 2002). α-Liprins recruit the receptor protein tyrosine phosphatases LAR to GRIP (Dunah et al. 2005), and a block of the interaction between Liprins and GRIP inhibits the muscarinic acetyl cholin receptor dependent LTD in CA1 pyramidal neurons (Dickinson et al. 2009). In drosophila, the complex of the Liprin-α analogue DLiprin-α and LAR is presynaptically required to interact with the cell adhesion molecule N-cadherin for the regulation of photoreceptor axon targeting (Prakash et al. 2009). Besides changing the constitutive functions of α-Liprins in maintaining the composition of the pre- and post synapse, altered levels of Liprins could therefore additionally interfere with α-Liprin function in synaptic plasticity. But nothing is known so far about the diverging functions of the four highly homologous members of the α-Liprin family in vertebrates. The differential localization and regulation after SE suggests distinctive roles in the constitutive and plastic functions of α-Liprins at the synapse. While Liprin2α, shown in our work to be regulated through synaptic activity in the acute phase, could represent a member of the family implicated in immediate forms of synaptic plasticity, the other highly expressed α-Liprin isoform, Liprin3α, is only slightly changed in CA1 (down) and CA3 (up) on the mRNA level during the silent phase, potentially representing a more constitutive function within the Liprin-α family.

The results of this study support the hypothesis that the presynaptic release apparatus plays an important role in adaptive changes induced by strong depolarization or lack of activity. This can be mediated by short term plasticity, for example presynaptic silencing, changes in release probability and facilitation, or in the long term by changes in the protein composition of the pre- and postsynaptic compartment or the addition of newly generated synaptic vesicle release sites. However, alternations could also contribute to progression of an altered hippocampal network.

6   Synopsis

In this study we analyzed the expression and function of the two full-length members of the RIM family. We found that α-RIMs are expressed in differential but largely overlapping expression patterns. Analyzing RIM2α KO mice as well as the double RIM1α and 2α deletion, we could show that they are functionally redundant, and that RIM1α can compensate for the loss of RIM2α at neuromuscular as well as central nervous synapses, while the RIM1α KO had been shown to be deficient for presynaptic plasticity. We further demonstrate that α-RIMs are selectively required to maintain Ca^{2+}-triggered neurotransmitter release, but not synapse structure.

In addition, I analyzed the expression of several RIM interacting protein families that are present at the active zone. Liprins-α are differentially expressed at distinct developmental stages, with Liprin2α and -3α being the main Liprin-α isoforms in the brain, slightly diverging in their expression patterns that in most regions overlap with RIM1α expression. I also performed the first comprehensive expression analysis of all Synaptotagmins in the rodent brain, showing that all but one Synaptotagmin, Syt-8, are expressed in distinct but overlapping patterns, and that individual neurons as well as astrocytes are equipped with diverging sets of multiple Synaptotagmin isoforms. While all hippocampal CA1 neurons tested expressed at least Syt-1, -4 and -5, most Stratum radiatum astrocytes contained Syt-7 and -11 transcripts.

The analysis of RIM-BP expression resulted in the identification of a novel member of the RIM-BP family and prompted a detailed investigation of the complete DNA sequence, genomic organization, and expression profiles of the mouse and human RIM-BP genes, adaptor proteins that have been shown to interact with the active zone proteins RIM1 and RIM2 as well as with different α-subunits of voltage-gated calcium channels. Additionally, I have identified and cloned a novel member of the RIM-BP gene family, RIM-BP3, sharing the domain composition and structural organization with RIM-BP1 and RIM-BP2. My findings support the idea that RIM-BPs are likely to have a fundamental function that is shared between invertebrates and vertebrates. Whereas RIM-BP1 and -2 expression is restricted to neurons, RIM-BP3 is testis specific. Recent findings

show indeed that RIM-BP3 plays a vital role in acrosome-acroplaxome-manchette complex organization during spermatogenesis, suggesting a similar organizational function at the active zone for RIM-BP1 and -2.

In the second part of my work, I focused on the effect of pathophysiological synaptic activity on the expression of active zone proteins. Using an experimental animal model for temporal lobe epilepsy, I could confirm that changes in synaptic activity in the hippocampus are associated with alterations in the composition of the presynaptic release machinery. Several distinct changes were observed at three different time points after Pilocarpine-induced Status epilepticus. The highest number of proteins were differentially regulated in the acute phase (six hours after SE), e.g. RIMs, Munc13-1 and -2, Liprin-1α, -2α and -3α as well as several Synaptotagmins, while the expression of the main Ca^{2+} sensor for evoked exocytosis, Syt-1, remained unchanged. Interestingly, a Synaptotagmin isoform suggested to play a role in Ca^{2+} evoked neurite outgrowth, Syt-7, is upregulated in the dentate gyrus (DG) during the period of reorganization and mossy fiber sprouting in this area, while being significantly reduced in the CA3 region of the hippocampus that looses it's innervation by the DG at this time point. Additionally, I observed a significant inverse regulation of Liprin2α and -4α, as well as Munc13-1 and Munc13-2. While nothing is known about the varying functions of the highly homologous α-Liprins yet, the shift in Munc13-1 to Munc13-2 ratio could lead to a change in synaptic excitability, that on the one hand may counteract the epileptogenic process, but on the other hand increase short-term facilitation and thereby the development of epileptic seizures due to the structural reorganization occurring in this area.

7 Outlook

The results obtained in this study raise several questions that need to be addressed in further experiments.

It is not clear how pathophysiologic synaptic activity affects functional properties of the synapse, for example the organization and dynamic of the active zone. To evaluate the organization of the active zone, high resolution STED or electron microscopic analyses will have to be performed.

The dynamics of active zone proteins can be studied using time lapse imaging of fluorescence recovery after photobleaching (FRAP) and photo activation of fluorescently tagged proteins in cultured neurons and acute hippocampal slices. This is interesting in a very short time frame, regarding the mobility of active zone proteins within seconds and minutes after strong stimulation, as well as in a longer period concerning protein dynamics within the axon during several hours in high activity conditions.

Comparing the stability of individual proteins under physiological and pathophysiological conditions with and without blockers of protein degradation could provide new insight in the regulation of active zone composition through active regulation of protein degradation in addition to protein transport and synthesis, as recently shown for several active zone proteins.

The different methods evaluating the dynamics of individual proteins of the same family, like the abundantly expressed α-Liprins Liprin2α and Liprin3α, as well as the two α-RIMs RIM1α and RIM2α, Munc13-1 and Munc13-2 or Synaptotagmins of the same functional subgroup would allow further insights in the functional differences between these highly homologous family members.

Additionally, the individual effect of the different α-Liprins on cell morphology and synaptic function will have to be further examined in more detail in experiments overexpressing or reducing the expression of one of the family members in culture as well as in vivo experiments.

Bibliography

Adolfsen, B., and Littleton, J.T. (2001). Genetic and molecular analysis of the synaptotagmin family. Cell Mol Life Sci *58*, 393-402

Adolfsen, B., Saraswati, S., Yoshihara, M., and Littleton, J.T. (2004). Synaptotagmins are trafficked to distinct subcellular domains including the postsynaptic compartment. J Cell Biol *166*, 249-260

Altrock, W.D., tom Dieck, S., Sokolov, M., Meyer, A.C., Sigler, A., Brakebusch, C., Fassler, R., Richter, K., Boeckers, T.M., Potschka, H., Brandt, C., Loscher, W., Grimberg, D., Dresbach, T., Hempelmann, A., Hassan, H., Balschun, D., Frey, J.U., Brandstatter, J.H., Garner, C.C., Rosenmund, C., and Gundelfinger, E.D. (2003). Functional inactivation of a fraction of excitatory synapses in mice deficient for the active zone protein bassoon. Neuron *37*, 787-800

Alvarez de Toledo, G., Fernandez-Chacon, R., and Fernandez, J.M. (1993). Release of secretory products during transient vesicle fusion. Nature *363*, 554-558

Andrews-Zwilling, Y.S., Kawabe, H., Reim, K., Varoqueaux, F., and Brose, N. (2006). Binding to Rab3A-interacting molecule RIM regulates the presynaptic recruitment of Munc13-1 and ubMunc13-2. J Biol Chem *281*, 19720-19731

Angenstein, F., Hilfert, L., Zuschratter, W., Altrock, W.D., Niessen, H.G., and Gundelfinger, E.D. (2008). Morphological and Metabolic Changes in the Cortex of Mice Lacking the Functional Presynaptic Active Zone Protein Bassoon: A Combined 1H-NMR Spectroscopy and Histochemical Study. Cereb. Cortex *18*, 890-897

Arantes, R.M., and Andrews, N.W. (2006). A role for synaptotagmin VII-regulated exocytosis of lysosomes in neurite outgrowth from primary sympathetic neurons. J Neurosci *26*, 4630-4637

Armstrong, J.N. (2006). B-Ephrin Reverse Signaling Is Required for NMDA-Independent Long-Term Potentiation of Mossy Fibers in the Hippocampus. Journal of Neuroscience *26*, 3474-3481

Ashery, U., Bielopolski, N., Barak, B., and Yizhar, O. (2009). Friends and foes in synaptic transmission: the role of tomosyn in vesicle priming. Trends Neurosci *32*, 275-282

Asperti, C., Astro, V., Totaro, A., Paris, S., and de Curtis, I. (2009). Liprin-alpha1 promotes cell spreading on the extracellular matrix by affecting the distribution of activated integrins. J Cell Sci *122*, 3225-3232

Asperti, C., Pettinato, E., and de Curtis, I. (2010). Liprin-alpha1 affects the distribution of low-affinity beta1 integrins and stabilizes their permanence at the cell surface. Exp Cell Res *316*, 915-926

Babity, J.M., Armstrong, J.N., Plumier, J.C., Currie, R.W., and Robertson, H.A. (1997a). A novel seizure-induced synaptotagmin gene identified by differential display. Proc Natl Acad Sci USA *94*, 2638-2641

Babity, J.M., Armstrong, J.N., Plumier, J.C., Currie, R.W., and Robertson, H.A. (1997b). A novel seizure-induced synaptotagmin gene identified by differential display. Proc Natl Acad Sci U S A *94*, 2638-2641

Balaji, J., and Ryan, T.A. (2007). Single-vesicle imaging reveals that synaptic vesicle exocytosis and endocytosis are coupled by a single stochastic mode. Proc Natl Acad Sci U S A *104*, 20576-20581

Barrera, F.N., Poveda, J.A., Gonzalez-Ros, J.M., and Neira, J.L. (2003). Binding of the C-terminal sterile alpha motif (SAM) domain of human p73 to lipid membranes. J Biol Chem *278*, 46878-46885

Basu, J., Shen, N., Dulubova, I., Lu, J., Guan, R., Guryev, O., Grishin, N.V., Rosenmund, C., and Rizo, J. (2005). A minimal domain responsible for Munc13 activity. Nat Struct Mol Biol *12*, 1017-1018

Basu, J., Betz, A., Brose, N., and Rosenmund, C. (2007). Munc13-1 C1 domain activation lowers the energy barrier for synaptic vesicle fusion. J Neurosci *27*, 1200-1210

Berton, F., Iborra, C., Boudier, J.A., Seagar, M.J., and Marqueze, B. (1997). Developmental regulation of synaptotagmin I, II, III, and IV mRNAs in the rat CNS. J Neurosci *17*, 1206-1216

Betz, A., Thakur, P., Junge, H.J., Ashery, U., Rhee, J.S., Scheuss, V., Rosenmund, C., Rettig, J., and Brose, N. (2001). Functional interaction of the active zone proteins Munc13-1 and RIM1 in synaptic vesicle priming. Neuron *30*, 183-196

Bhalla, A., Tucker, W.C., and Chapman, E.R. (2005). Synaptotagmin isoforms couple distinct ranges of Ca2+, Ba2+, and Sr2+ concentration to SNARE-mediated membrane fusion. Mol Biol Cell *16*, 4755-4764

Bhalla, A., Chicka, M.C., and Chapman, E.R. (2008). Analysis of the Synaptotagmin Family during Reconstituted Membrane Fusion: UNCOVERING A CLASS OF INHIBITORY ISOFORMS. J Biol Chem *283*, 21799-21807

Bliss, T.V., and Lomo, T. (1973). Long-lasting potentiation of synaptic transmission in the dentate area of the anaesthetized rabbit following stimulation of the perforant path. J Physiol *232*, 331-356

Bliss, T.V., and Collingridge, G.L. (1993). A synaptic model of memory: long-term potentiation in the hippocampus. Nature *361*, 31-39

Blumcke, I., Becker, A.J., Klein, C., Scheiwe, C., Lie, A.A., Beck, H., Waha, A., Friedl, M.G., Kuhn, R., Emson, P., Elger, C., and Wiestler, O.D. (2000). Temporal lobe epilepsy associated up-regulation of metabotropic glutamate receptors: correlated changes in mGluR1 mRNA and protein expression in experimental animals and human patients. J Neuropathol Exp Neurol *59*, 1-10

Blumcke, I., Thom, M., and Wiestler, O.D. (2002). Ammon's horn sclerosis: a maldevelopmental disorder associated with temporal lobe epilepsy. Brain Pathol *12*, 199-211

Bonanomi, D., Benfenati, F., and Valtorta, F. (2006). Protein sorting in the synaptic vesicle life cycle. Prog Neurobiol *80*, 177-217

Bork, P., and Doolittle, R.F. (1992). Proposed acquisition of an animal protein domain by bacteria. Proc Natl Acad Sci U S A *89*, 8990-8994

Borst, J.G., and Sakmann, B. (1996). Calcium influx and transmitter release in a fast CNS synapse. Nature *383*, 431-434

Bowser, D.N., and Khakh, B.S. (2007). Two forms of single-vesicle astrocyte exocytosis imaged with total internal reflection fluorescence microscopy. Proc Natl Acad Sci U S A *104*, 4212-4217

Brandon, E.P., Lin, W., D'Amour, K.A., Pizzo, D.P., Dominguez, B., Sugiura, Y., Thode, S., Ko, C.P., Thal, L.J., Gage, F.H., and Lee, K.F. (2003). Aberrant patterning of neuromuscular synapses in choline acetyltransferase-deficient mice. J Neurosci *23*, 539-549

Bredt, D.S., and Nicoll, R.A. (2003). AMPA receptor trafficking at excitatory synapses. Neuron *40*, 361-379

Breustedt, J., Gundlfinger, A., Varoqueaux, F., Reim, K., Brose, N., and Schmitz, D. (2009). Munc13-2 Differentially Affects Hippocampal Synaptic Transmission and Plasticity. Cereb Cortex

Brose, N., Rosenmund, C., and Rettig, J. (2000). Regulation of transmitter release by Unc-13 and its homologues. Curr Opin Neurobiol *10*, 303-311

Buckmaster, P.S., Zhang, G.F., and Yamawaki, R. (2002). Axon sprouting in a model of temporal lobe epilepsy creates a predominantly excitatory feedback circuit. J Neurosci *22*, 6650-6658

Bucurenciu, I., Kulik, A., Schwaller, B., Frotscher, M., and Jonas, P. (2008). Nanodomain coupling between Ca2+ channels and Ca2+ sensors promotes fast and efficient transmitter release at a cortical GABAergic synapse. Neuron *57*, 536-545

Butz, S., Fernandez-Chacon, R., Schmitz, F., Jahn, R., and Sudhof, T.C. (1999). The subcellular localizations of atypical synaptotagmins III and VI. Synaptotagmin III is enriched in synapses and synaptic plasma membranes but not in synaptic vesicles. J Biol Chem *274*, 18290-18296

Cai, H., Reim, K., Varoqueaux, F., Tapechum, S., Hill, K., Sorensen, J.B., Brose, N., and Chow, R.H. (2008). Complexin II plays a positive role in Ca2+-triggered exocytosis by facilitating vesicle priming. Proc Natl Acad Sci U S A *105*, 19538-19543

Calakos, N., Schoch, S., Sudhof, T.C., and Malenka, R.C. (2004). Multiple roles for the active zone protein RIM1alpha in late stages of neurotransmitter release. Neuron *42*, 889-896

Castillo, P.E., Janz, R., Sudhof, T.C., Tzounopoulos, T., Malenka, R.C., and Nicoll, R.A. (1997). Rab3A is essential for mossy fibre long-term potentiation in the hippocampus. Nature *388*, 590-593

Castillo, P.E., Schoch, S., Schmitz, F., Sudhof, T.C., and Malenka, R.C. (2002). RIM1alpha is required for presynaptic long-term potentiation. Nature *415*, 327-330

Castro-Alamancos, M.A., and Calcagnotto, M.E. (1999). Presynaptic long-term potentiation in corticothalamic synapses. J Neurosci *19*, 9090-9097

Chapman, E.R. (2008). How does synaptotagmin trigger neurotransmitter release? Annu Rev Biochem *77*, 615-641

Chen, X., Tomchick, D.R., Kovrigin, E., Arac, D., Machius, M., Sudhof, T.C., and Rizo, J. (2002). Three-dimensional structure of the complexin/SNARE complex. Neuron *33*, 397-409

Chen, X., Barg, S., and Almers, W. (2008). Release of the styryl dyes from single synaptic vesicles in hippocampal neurons. J Neurosci *28*, 1894-1903

Chevaleyre, V., Heifets, B.D., Kaeser, P., Sudhof, T.C., Purpura, D.P., and Castillo, P.E. (2007). Endocannabinoid-mediated long-term plasticity requires cAMP/PKA signaling and RIM1alpha. Neuron *54*, 801-812

Collingridge, G.L., and Singer, W. (1990). Excitatory amino acid receptors and synaptic plasticity. Trends Pharmacol Sci *11*, 290-296

Contractor, A., Rogers, C., Maron, C., Henkemeyer, M., Swanson, G.T., and Heinemann, S.F. (2002). Trans-synaptic Eph receptor-ephrin signaling in hippocampal mossy fiber LTP. Science *296*, 1864-1869

Coppola, T., Magnin-Luthi, S., Perret-Menoud, V., Gattesco, S., Schiavo, G., and Regazzi, R. (2001). Direct interaction of the Rab3 effector RIM with Ca2+ channels, SNAP-25, and synaptotagmin. J Biol Chem *276*, 32756-32762

Costa-Mattioli, M., Gobert, D., Stern, E., Gamache, K., Colina, R., Cuello, C., Sossin, W., Kaufman, R., Pelletier, J., Rosenblum, K., Krnjevic, K., Lacaille, J.C., Nader, K., and Sonenberg, N. (2007). eIF2alpha phosphorylation bidirectionally regulates the switch from short- to long-term synaptic plasticity and memory. Cell *129*, 195-206

Craxton, M. (2001). Genomic analysis of synaptotagmin genes. Genomics *77*, 43-49

Craxton, M. (2004). Synaptotagmin gene content of the sequenced genomes. BMC Genomics *5*, 43

Crippa, D., Schenk, U., Francolini, M., Rosa, P., Verderio, C., Zonta, M., Pozzan, T., Matteoli, M., and Carmignoto, G. (2006). Synaptobrevin2-expressing vesicles in rat astrocytes: insights into molecular characterization, dynamics and exocytosis. J Physiol *570*, 567-582

Dahm, L.M., and Landmesser, L.T. (1991). The regulation of synaptogenesis during normal development and following activity blockade. J Neurosci *11*, 238-255

Dai, H., Shin, O.H., Machius, M., Tomchick, D.R., Sudhof, T.C., and Rizo, J. (2004). Structural basis for the evolutionary inactivation of Ca2+ binding to synaptotagmin 4. Nat Struct Mol Biol *11*, 844-849

Dam, M. (1992). Quantitative neuropathology in epilepsy. Acta Neurol Scand Suppl *137*, 51-54

Deak, F., Xu, Y., Chang, W.P., Dulubova, I., Khvotchev, M., Liu, X., Sudhof, T.C., and Rizo, J. (2009). Munc18-1 binding to the neuronal SNARE complex controls synaptic vesicle priming. J Cell Biol *184*, 751-764

Dean, C., Liu, H., Dunning, F.M., Chang, P.Y., Jackson, M.B., and Chapman, E.R. (2009). Synaptotagmin-IV modulates synaptic function and long-term potentiation by regulating BDNF release. Nat Neurosci *12*, 767-776

Deguchi-Tawarada, M., Inoue, E., Takao-Rikitsu, E., Inoue, M., Kitajima, I., Ohtsuka, T., and Takai, Y. (2006). Active zone protein CAST is a component of conventional and ribbon synapses in mouse retina. J Comp Neurol *495*, 480-496

Deken, S.L., Vincent, R., Hadwiger, G., Liu, Q., Wang, Z.W., and Nonet, M.L. (2005). Redundant localization mechanisms of RIM and ELKS in Caenorhabditis elegans. J Neurosci *25*, 5975-5983

Dick, O., tom Dieck, S., Altrock, W.D., Ammermuller, J., Weiler, R., Garner, C.C., Gundelfinger, E.D., and Brandstatter, J.H. (2003). The presynaptic active zone protein bassoon is essential for photoreceptor ribbon synapse formation in the retina. Neuron *37*, 775-786

Dickinson, B.A., Jo, J., Seok, H., Son, G.H., Whitcomb, D.J., Davies, C.H., Sheng, M., Collingridge, G.L., and Cho, K. (2009). A novel mechanism of hippocampal LTD involving muscarinic receptor-triggered interactions between AMPARs, GRIP and liprin-alpha. Mol Brain *2*, 18

Dong, H., Wade, M., Williams, A., Lee, A., Douglas, G.R., and Yauk, C. (2005). Molecular insight into the effects of hypothyroidism on the developing cerebellum. Biochem Biophys Res Commun *330*, 1182-1193

Dulubova, I., Sugita, S., Hill, S., Hosaka, M., Fernandez, I., Sudhof, T.C., and Rizo, J. (1999). A conformational switch in syntaxin during exocytosis: role of munc18. Embo J *18*, 4372-4382

Dulubova, I., Lou, X., Lu, J., Huryeva, I., Alam, A., Schneggenburger, R., Sudhof, T.C., and Rizo, J. (2005). A Munc13/RIM/Rab3 tripartite complex: from priming to plasticity? Embo J *24*, 2839-2850

Dunah, A.W., Hueske, E., Wyszynski, M., Hoogenraad, C.C., Jaworski, J., Pak, D.T., Simonetta, A., Liu, G., and Sheng, M. (2005). LAR receptor protein tyrosine phosphatases in the development and maintenance of excitatory synapses. Nat Neurosci *8*, 458-467

Enoki, R., Hu, Y.L., Hamilton, D., and Fine, A. (2009). Expression of long-term plasticity at individual synapses in hippocampus is graded, bidirectional, and mainly presynaptic: optical quantal analysis. Neuron *62*, 242-253

Estable, C., Reissig, M., and De Robertis, E. (1954). Microscopic and submicroscopic structure of the synapsis in the ventral ganglion of the acoustic nerve. Exp Cell Res *6*, 255-262

Felsenstein, J. (1985). Confidence limits on phylogenetics: an approach using the bootstrap. Evol *39*, 783-791

Fenster, S.D., Chung, W.J., Zhai, R., Cases-Langhoff, C., Voss, B., Garner, A.M., Kaempf, U., Kindler, S., Gundelfinger, E.D., and Garner, C.C. (2000). Piccolo, a presynaptic zinc finger protein structurally related to bassoon. Neuron *25*, 203-214

Fenster, S.D., Kessels, M.M., Qualmann, B., Chung, W.J., Nash, J., Gundelfinger, E.D., and Garner, C.C. (2003). Interactions between Piccolo and the actin/dynamin-binding protein Abp1 link vesicle endocytosis to presynaptic active zones. J Biol Chem *278*, 20268-20277

Ferguson, G.D., Herschman, H.R., and Storm, D.R. (2004). Reduced anxiety and depression-like behavior in synaptotagmin IV (-/-) mice. Neuropharmacology *47*, 604-611

Fernandez-Chacon, R., Konigstorfer, A., Gerber, S.H., Garcia, J., Matos, M.F., Stevens, C.F., Brose, N., Rizo, J., Rosenmund, C., and Sudhof, T.C. (2001). Synaptotagmin I functions as a calcium regulator of release probability. Nature *410*, 41-49

Fourcaudot, E., Gambino, F., Humeau, Y., Casassus, G., Shaban, H., Poulain, B., and Luthi, A. (2008). cAMP/PKA signaling and RIM1alpha mediate presynaptic LTP in the lateral amygdala. Proc Natl Acad Sci U S A *105*, 15130-15135

Fox, M.A., and Sanes, J.R. (2007). Synaptotagmin I and II are present in distinct subsets of central synapses. J Comp Neurol *503*, 280-296

Fukuda, M., Kanno, E., and Mikoshiba, K. (1999). Conserved N-terminal cysteine motif is essential for homo- and heterodimer formation of synaptotagmins III, V, VI, and X. J Biol Chem *274*, 31421-31427

Fukuda, M. (2003a). Molecular cloning and characterization of human, rat, and mouse synaptotagmin XV. Biochem Biophys Res Commun *306*, 64-71

Fukuda, M. (2003b). Molecular cloning, expression, and characterization of a novel class of synaptotagmin (Syt XIV) conserved from Drosophila to humans. J Biochem *133*, 641-649

Fukuda, M., and Yamamoto, A. (2004). Effect of forskolin on synaptotagmin IV protein trafficking in PC12 cells. J Biochem (Tokyo) *136*, 245-253

Fukuda, M., Kanno, E., Satoh, M., Saegusa, C., and Yamamoto, A. (2004). Synaptotagmin VII is targeted to dense-core vesicles and regulates their Ca2+ - dependent exocytosis in PC12 cells. J Biol Chem *279*, 52677-52684

Gao, Z., Reavey-Cantwell, J., Young, R.A., Jegier, P., and Wolf, B.A. (2000). Synaptotagmin III/VII isoforms mediate Ca2+-induced insulin secretion in pancreatic islet beta -cells. J Biol Chem *275*, 36079-36085

Garcia, J., Gerber, S.H., Sugita, S., Sudhof, T.C., and Rizo, J. (2004). A conformational switch in the Piccolo C2A domain regulated by alternative splicing. Nat Struct Mol Biol *11*, 45-53

Gauthier, B.R., Duhamel, D.L., Iezzi, M., Theander, S., Saltel, F., Fukuda, M., Wehrle-Haller, B., and Wollheim, C.B. (2008). Synaptotagmin VII splice variants alpha, beta, and delta are expressed in pancreatic beta-cells and regulate insulin exocytosis. FASEB J *22*, 194-206

Geppert, M., Goda, Y., Hammer, R.E., Li, C., Rosahl, T.W., Stevens, C.F., and Sudhof, T.C. (1994). Synaptotagmin I: a major Ca2+ sensor for transmitter release at a central synapse. Cell *79*, 717-727

Glisovic, S., Glavan, G., Saghafi, M.M., and Zivin, M. (2007). Upregulation of synaptotagmin IV protein in kainate-induced seizures. Neuroreport *18*, 831-835

Goll, C.M., Pastore, A., and Nilges, M. (1998). The three-dimensional structure of a type I module from titin: a prototype of intracellular fibronectin type III domains. Structure *6*, 1291-1302

Green, J.B., Gardner, C.D., Wharton, R.P., and Aggarwal, A.K. (2003). RNA recognition via the SAM domain of Smaug. Mol Cell *11*, 1537-1548

Grimberg, E., Peng, Z., Hammel, I., and Sagi-Eisenberg, R. (2003). Synaptotagmin III is a critical factor for the formation of the perinuclear endocytic recycling compartment and determination of secretory granules size. J Cell Sci *116*, 145-154

Guan, R., Dai, H., and Rizo, J. (2008). Binding of the Munc13-1 MUN domain to membrane-anchored SNARE complexes. Biochemistry *47*, 1474-1481

Guindon, S., and Gascuel, O. (2003). A simple, fast, and accurate algorithm to estimate large phylogenies by maximum likelihood. Syst Biol *52*, 696-704

Guindon, S., Lethiec, F., Duroux, P., and Gascuel, O. (2005). PHYML Online--a web server for fast maximum likelihood-based phylogenetic inference. Nucleic Acids Res *33*, W557-559

Gustavsson, N., Wei, S.H., Hoang, D.N., Lao, Y., Zhang, Q., Radda, G.K., Rorsman, P., Sudhof, T.C., and Han, W. (2009). Synaptotagmin-7 is a principal Ca2+ sensor for Ca2+ -induced glucagon exocytosis in pancreas. J Physiol *587*, 1169-1178

Han, W., Rhee, J.S., Maximov, A., Lao, Y., Mashimo, T., Rosenmund, C., and Sudhof, T.C. (2004). N-glycosylation is essential for vesicular targeting of synaptotagmin 1. Neuron *41*, 85-99

Harata, N.C., Choi, S., Pyle, J.L., Aravanis, A.M., and Tsien, R.W. (2006). Frequency-dependent kinetics and prevalence of kiss-and-run and reuse at hippocampal synapses studied with novel quenching methods. Neuron *49*, 243-256

Harlow, M.L., Ress, D., Stoschek, A., Marshall, R.M., and McMahan, U.J. (2001). The architecture of active zone material at the frog's neuromuscular junction. Nature *409*, 479-484

Harris, A.J., and McCaig, C.D. (1984). Motoneuron death and motor unit size during embryonic development of the rat. J Neurosci *4*, 13-24

Hay, J.C. (2007). Calcium: a fundamental regulator of intracellular membrane fusion? EMBO Rep *8*, 236-240

Hebb, D.O. (1949). The Organization of Behavior (New York: Wiley)

Hebert, J.M., and McConnell, S.K. (2000). Targeting of cre to the Foxg1 (BF-1) locus mediates loxP recombination in the telencephalon and other developing head structures. Dev Biol *222*, 296-306

Herrick, D.Z., Kuo, W., Huang, H., Schwieters, C.D., Ellena, J.F., and Cafiso, D.S. (2009). Solution and membrane-bound conformations of the tandem C2A and C2B domains of synaptotagmin 1: Evidence for bilayer bridging. Journal of molecular biology *390*, 913-923

Hibino, H., Pironkova, R., Onwumere, O., Vologodskaia, M., Hudspeth, A.J., and Lesage, F. (2002). RIM binding proteins (RBPs) couple Rab3-interacting molecules (RIMs) to voltage-gated Ca(2+) channels. Neuron *34*, 411-423

Hoogenraad, C.C., Feliu-Mojer, M.I., Spangler, S.A., Milstein, A.D., Dunah, A.W., Hung, A.Y., and Sheng, M. (2007). Liprinalpha1 degradation by calcium/calmodulin-dependent protein kinase II regulates LAR receptor tyrosine phosphatase distribution and dendrite development. Dev Cell *12*, 587-602

Huang, Y.Y., and Kandel, E.R. (1994). Recruitment of long-lasting and protein kinase A-dependent long-term potentiation in the CA1 region of hippocampus requires repeated tetanization. Learn Mem *1*, 74-82

Huang, Y.Y., Zakharenko, S.S., Schoch, S., Kaeser, P.S., Janz, R., Sudhof, T.C., Siegelbaum, S.A., and Kandel, E.R. (2005). Genetic evidence for a protein-kinase-A-mediated presynaptic component in NMDA-receptor-dependent forms of long-term synaptic potentiation. Proc Natl Acad Sci U S A *102*, 9365-9370

Hui, E., Bai, J., Wang, P., Sugimori, M., Llinas, R.R., and Chapman, E.R. (2005). Three distinct kinetic groupings of the synaptotagmin family: candidate sensors for rapid and delayed exocytosis. Proc Natl Acad Sci U S A *102*, 5210-5214

Humeau, Y., Shaban, H., Bissiere, S., and Luthi, A. (2003). Presynaptic induction of heterosynaptic associative plasticity in the mammalian brain. Nature *426*, 841-845

Hutt, D.M., Baltz, J.M., and Ngsee, J.K. (2005). Synaptotagmin VI and VIII and syntaxin 2 are essential for the mouse sperm acrosome reaction. J Biol Chem *280*, 20197-20203

Ibata, K., Fukuda, M., and Mikoshiba, K. (1998). Inositol 1,3,4,5-tetrakisphosphate binding activities of neuronal and non-neuronal synaptotagmins. Identification of conserved amino acid substitutions that abolish inositol 1,3,4,5-tetrakisphosphate binding to synaptotagmins III, V, and X. J Biol Chem *273*, 12267-12273

Iezzi, M., Regazzi, R., and Wollheim, C.B. (2000). The Rab3-interacting molecule RIM is expressed in pancreatic beta-cells and is implicated in insulin exocytosis. FEBS Lett *474*, 66-70

Jiang, X., Litkowski, P.E., Taylor, A.A., Lin, Y., Snider, B.J., and Moulder, K.L. (2010). A role for the ubiquitin-proteasome system in activity-dependent presynaptic silencing. J Neurosci *30*, 1798-1809

Johnson, S., Halford, S., Morris, A.G., Patel, R.J., Wilkie, S.E., Hardcastle, A.J., Moore, A.T., Zhang, K., and Hunt, D.M. (2003). Genomic organisation and alternative splicing of human RIM1, a gene implicated in autosomal dominant cone-rod dystrophy (CORD7). Genomics *81*, 304-314

Jorgensen, E.M., Hartwieg, E., Schuske, K., Nonet, M.L., Jin, Y., and Horvitz, H.R. (1995). Defective recycling of synaptic vesicles in synaptotagmin mutants of Caenorhabditis elegans. Nature *378*, 196-199

Junge, H.J., Rhee, J.S., Jahn, O., Varoqueaux, F., Spiess, J., Waxham, M.N., Rosenmund, C., and Brose, N. (2004). Calmodulin and Munc13 form a Ca2+ sensor/effector complex that controls short-term synaptic plasticity. Cell *118*, 389-401

Kaeser, P.S., Kwon, H.B., Chiu, C.Q., Deng, L., Castillo, P.E., and Sudhof, T.C. (2008a). RIM1alpha and RIM1beta are synthesized from distinct promoters of the RIM1 gene to mediate differential but overlapping synaptic functions. J Neurosci *28*, 13435-13447

Kaeser, P.S., Kwon, H.B., Blundell, J., Chevaleyre, V., Morishita, W., Malenka, R.C., Powell, C.M., Castillo, P.E., and Sudhof, T.C. (2008b). RIM1alpha phosphorylation at serine-413 by protein kinase A is not required for presynaptic long-term plasticity or learning. Proc Natl Acad Sci U S A *105*, 14680-14685

Kaeser, P.S., Deng, L., Chavez, A.E., Liu, X., Castillo, P.E., and Sudhof, T.C. (2009). ELKS2alpha/CAST deletion selectively increases neurotransmitter release at inhibitory synapses. Neuron *64*, 227-239

Kalla, S., Stern, M., Basu, J., Varoqueaux, F., Reim, K., Rosenmund, C., Ziv, N., and Brose, N. (2006). Molecular Dynamics of a Presynaptic Active Zone Protein Studied in Munc13-1-Enhanced Yellow Fluorescent Protein Knock-In Mutant Mice. Journal of Neuroscience *26*, 13054-13066

Kamikubo, Y., Tabata, T., Kakizawa, S., Kawakami, D., Watanabe, M., Ogura, A., Iino, M., and Kano, M. (2007). Postsynaptic GABAB receptor signalling enhances LTD in mouse cerebellar Purkinje cells. J Physiol *585*, 549-563

Kamiya, H., Umeda, K., Ozawa, S., and Manabe, T. (2002). Presynaptic Ca2+ entry is unchanged during hippocampal mossy fiber long-term potentiation. J Neurosci *22*, 10524-10528

Kandel, E.R. (2001). The molecular biology of memory storage: a dialogue between genes and synapses. Science *294*, 1030-1038

Kashima, Y., Miki, T., Shibasaki, T., Ozaki, N., Miyazaki, M., Yano, H., and Seino, S. (2001). Critical role of cAMP-GEFII--Rim2 complex in incretin-potentiated insulin secretion. J Biol Chem *276*, 46046-46053

Katz, B. (1969). The release of neural transmitter substances (Springfield, Ill: Thomas)

Kaufmann, N., DeProto, J., Ranjan, R., Wan, H., and Van Vactor, D. (2002). Drosophila liprin-alpha and the receptor phosphatase Dlar control synapse morphogenesis. Neuron *34*, 27-38

Kelly, L., Farrant, M., and Cull-Candy, S.G. (2009). Synaptic mGluR activation drives plasticity of calcium-permeable AMPA receptors. Nat Neurosci *12*, 593-601

Khimich, D., Nouvian, R., Pujol, R., Tom Dieck, S., Egner, A., Gundelfinger, E.D., and Moser, T. (2005). Hair cell synaptic ribbons are essential for synchronous auditory signalling. Nature *434*, 889-894

Kittel, R.J., Wichmann, C., Rasse, T.M., Fouquet, W., Schmidt, M., Schmid, A., Wagh, D.A., Pawlu, C., Kellner, R.R., Willig, K.I., Hell, S.W., Buchner, E., Heckmann, M., and Sigrist, S.J. (2006). Bruchpilot Promotes Active Zone Assembly, Ca2+-Channel Clustering, and Vesicle Release. Science

Kiyonaka, S., Wakamori, M., Miki, T., Uriu, Y., Nonaka, M., Bito, H., Beedle, A.M., Mori, E., Hara, Y., De Waard, M., Kanagawa, M., Itakura, M., Takahashi, M., Campbell, K.P., and Mori, Y. (2007). RIM1 confers sustained activity and neurotransmitter vesicle anchoring to presynaptic Ca2+ channels. Nat Neurosci *10*, 691-701

Knott, G., and Holtmaat, A. (2008). Dendritic spine plasticity--current understanding from in vivo studies. Brain Res Rev *58*, 282-289

Ko, J., Na, M., Kim, S., Lee, J.R., and Kim, E. (2003). Interaction of the ERC family of RIM-binding proteins with the liprin-alpha family of multidomain proteins. J Biol Chem *278*, 42377-42385

Koch, H., Hofmann, K., and Brose, N. (2000). Definition of Munc13-homology-domains and characterization of a novel ubiquitously expressed Munc13 isoform. Biochem J *349*, 247-253

Koushika, S.P., Richmond, J.E., Hadwiger, G., Weimer, R.M., Jorgensen, E.M., and Nonet, M.L. (2001). A post-docking role for active zone protein Rim. Nat Neurosci *4*, 997-1005

Kuo, W., Herrick, D.Z., Ellena, J.F., and Cafiso, D.S. (2009). The calcium-dependent and calcium-independent membrane binding of synaptotagmin 1: two modes of C2B binding. J Mol Biol *387*, 284-294

Lachamp, P.M., Liu, Y., and Liu, S.J. (2009). Glutamatergic modulation of cerebellar interneuron activity is mediated by an enhancement of GABA release and requires protein kinase A/RIM1alpha signaling. J Neurosci *29*, 381-392

Laemmli, U.K. (1970). Cleavage of structural proteins during the assembly of the head of bacteriophage T4. Nature *227*, 680-685

Lauri, S.E., Bortolotto, Z.A., Bleakman, D., Ornstein, P.L., Lodge, D., Isaac, J.T., and Collingridge, G.L. (2001). A critical role of a facilitatory presynaptic kainate receptor in mossy fiber LTP. Neuron *32*, 697-709

Li, C., Ullrich, B., Zhang, J.Z., Anderson, R.G., Brose, N., and Sudhof, T.C. (1995a). Ca(2+)-dependent and -independent activities of neural and non-neural synaptotagmins. Nature *375*, 594-599

Li, C., Davletov, B.A., and Sudhof, T.C. (1995b). Distinct Ca2+ and Sr2+ binding properties of synaptotagmins. Definition of candidate Ca2+ sensors for the fast and slow components of neurotransmitter release. J Biol Chem *270*, 24898-24902

Li, S.S. (2005). Specificity and versatility of SH3 and other proline-recognition domains: structural basis and implications for cellular signal transduction. Biochem J *390*, 641-653

Linden, D.J. (1997). Long-term potentiation of glial synaptic currents in cerebellar culture. Neuron *18*, 983-994

Liu, Y., Krantz, D.E., Waites, C., and Edwards, R.H. (1999). Membrane trafficking of neurotransmitter transporters in the regulation of synaptic transmission. Trends Cell Biol *9*, 356-363

Llinas, R., Sugimori, M., and Silver, R.B. (1992). Microdomains of high calcium concentration in a presynaptic terminal. Science *256*, 677-679

Lonart, G., Schoch, S., Kaeser, P.S., Larkin, C.J., Sudhof, T.C., and Linden, D.J. (2003). Phosphorylation of RIM1alpha by PKA triggers presynaptic long-term potentiation at cerebellar parallel fiber synapses. Cell *115*, 49-60

Lu, H.C., Butts, D.A., Kaeser, P.S., She, W.C., Janz, R., and Crair, M.C. (2006). Role of efficient neurotransmitter release in barrel map development. J Neurosci *26*, 2692-2703

Mackler, J.M., Drummond, J.A., Loewen, C.A., Robinson, I.M., and Reist, N.E. (2002). The C(2)B Ca(2+)-binding motif of synaptotagmin is required for synaptic transmission in vivo. Nature *418*, 340-344

Majores, M., Schoch, S., Lie, A., and Becker, A.J. (2007). Molecular neuropathology of temporal lobe epilepsy: complementary approaches in animal models and human disease tissue. Epilepsia *48 Suppl 2*, 4-12

Malinow, R., and Malenka, R.C. (2002). AMPA receptor trafficking and synaptic plasticity. Annual review of neuroscience *25*, 103-126

Marqueze, B., Boudier, J.A., Mizuta, M., Inagaki, N., Seino, S., and Seagar, M. (1995). Cellular localization of synaptotagmin I, II, and III mRNAs in the central nervous system and pituitary and adrenal glands of the rat. J Neurosci *15*, 4906-4917

Martinez, I., Chakrabarti, S., Hellevik, T., Morehead, J., Fowler, K., and Andrews, N.W. (2000). Synaptotagmin VII regulates Ca(2+)-dependent exocytosis of lysosomes in fibroblasts. J Cell Biol *148*, 1141-1149

Maruyama, I.N., and Brenner, S. (1991). A phorbol ester/diacylglycerol-binding protein encoded by the unc-13 gene of Caenorhabditis elegans. Proc Natl Acad Sci U S A *88*, 5729-5733

Masztalerz, A., Zeelenberg, I.S., Wijnands, Y.M., de Bruijn, R., Drager, A.M., Janssen, H., and Roos, E. (2007). Synaptotagmin 3 deficiency in T cells impairs recycling of the chemokine receptor CXCR4 and thereby inhibits CXCL12 chemokine-induced migration. J Cell Sci *120*, 219-228

Matthias, K., Kirchhoff, F., Seifert, G., Huttmann, K., Matyash, M., Kettenmann, H., and Steinhauser, C. (2003). Segregated expression of AMPA-type glutamate receptors and glutamate transporters defines distinct astrocyte populations in the mouse hippocampus. J Neurosci *23*, 1750-1758

Maximov, A., and Sudhof, T.C. (2005). Autonomous function of synaptotagmin 1 in triggering synchronous release independent of asynchronous release. Neuron *48*, 547-554

Maximov, A., Shin, O.H., Liu, X., and Sudhof, T.C. (2007). Synaptotagmin-12, a synaptic vesicle phosphoprotein that modulates spontaneous neurotransmitter release. J Cell Biol *176*, 113-124

Maximov, A., Lao, Y., Li, H., Chen, X.N., Rizo, J., Sørensen, J.B., and Sudhof, T.C. (2008). Genetic analysis of synaptotagmin-7 function in synaptic vesicle exocytosis. Proc Natl Acad Sci USA

Maximov, A., Tang, J., Yang, X., Pang, Z.P., and Sudhof, T.C. (2009). Complexin controls the force transfer from SNARE complexes to membranes in fusion. Science *323*, 516-521

Mello, L.E., Cavalheiro, E.A., Tan, A.M., Pretorius, J.K., Babb, T.L., and Finch, D.M. (1992). Granule cell dispersion in relation to mossy fiber sprouting, hippocampal cell loss, silent period and seizure frequency in the pilocarpine model of epilepsy. Epilepsy Res Suppl *9*, 51-59; discussion 59-60

Mello, L.E., Cavalheiro, E.A., Tan, A.M., Kupfer, W.R., Pretorius, J.K., Babb, T.L., and Finch, D.M. (1993). Circuit mechanisms of seizures in the pilocarpine model of chronic epilepsy: cell loss and mossy fiber sprouting. Epilepsia *34*, 985-995

Michaut, M., De Blas, G., Tomes, C.N., Yunes, R., Fukuda, M., and Mayorga, L.S. (2001). Synaptotagmin VI participates in the acrosome reaction of human spermatozoa. Dev Biol *235*, 521-529

Miller, K.E., DeProto, J., Kaufmann, N., Patel, B.N., Duckworth, A., and Van Vactor, D. (2005). Direct observation demonstrates that Liprin-alpha is required for trafficking of synaptic vesicles. Curr Biol *15*, 684-689

Misgeld, T., Burgess, R.W., Lewis, R.M., Cunningham, J.M., Lichtman, J.W., and Sanes, J.R. (2002). Roles of neurotransmitter in synapse formation: development of neuromuscular junctions lacking choline acetyltransferase. Neuron *36*, 635-648

Mittelstaedt, T., Seifert, G., Alvarez-Baron, E., Steinhauser, C., Becker, A.J., and Schoch, S. (2009). Differential mRNA expression patterns of the synaptotagmin gene family in the rodent brain. J Comp Neurol *512*, 514-528

Moore, S.J., Cooper, D.C., and Spruston, N. (2009). Plasticity of burst firing induced by synergistic activation of metabotropic glutamate and acetylcholine receptors. Neuron *61*, 287-300

Morgenstern, B. (2004). DIALIGN: multiple DNA and protein sequence alignment at BiBiServ. Nucleic Acids Res *32*, W33-36

Mori, Y., Higuchi, M., Hirabayashi, Y., Fukuda, M., and Gotoh, Y. (2008). JNK phosphorylates synaptotagmin-4 and enhances Ca2+-evoked release. Embo J *27*, 76-87

Morimoto, K., Fahnestock, M., and Racine, R.J. (2004). Kindling and status epilepticus models of epilepsy: rewiring the brain. Prog Neurobiol *73*, 1-60

Moulder, K.L., Cormier, R.J., Shute, A.A., Zorumski, C.F., and Mennerick, S. (2003). Homeostatic effects of depolarization on Ca2+ influx, synaptic signaling, and survival. J Neurosci *23*, 1825-1831

Moulder, K.L., Meeks, J.P., Shute, A.A., Hamilton, C.K., de Erausquin, G., and Mennerick, S. (2004). Plastic elimination of functional glutamate release sites by depolarization. Neuron *42*, 423-435

Moulder, K.L., Meeks, J.P., and Mennerick, S. (2006a). Homeostatic regulation of glutamate release in response to depolarization. Mol Neurobiol *33*, 133-153

Moulder, K.L., Jiang, X., Taylor, A.A., Olney, J.W., and Mennerick, S. (2006b). Physiological activity depresses synaptic function through an effect on vesicle priming. J Neurosci *26*, 6618-6626

Moulder, K.L., Jiang, X., Chang, C., Taylor, A.A., Benz, A.M., Conti, A.C., Muglia, L.J., and Mennerick, S. (2008). A specific role for Ca2+-dependent adenylyl cyclases in recovery from adaptive presynaptic silencing. J Neurosci *28*, 5159-5168

Nagy, G., Kim, J.H., Pang, Z.P., Matti, U., Rettig, J., Sudhof, T.C., and Sorensen, J.B. (2006). Different effects on fast exocytosis induced by synaptotagmin 1 and 2 isoforms and abundance but not by phosphorylation. J Neurosci *26*, 632-643

Newpher, T.M., and Ehlers, M.D. (2008). Glutamate receptor dynamics in dendritic microdomains. Neuron *58*, 472-497

Nicoll, R.A., Kauer, J.A., and Malenka, R.C. (1988). The current excitement in long-term potentiation. Neuron *1*, 97-103

Nicoll, R.A., and Malenka, R.C. (1995). Contrasting properties of two forms of long-term potentiation in the hippocampus. Nature *377*, 115-118

Nicoll, R.A., and Schmitz, D. (2005). Synaptic plasticity at hippocampal mossy fibre synapses. Nat Rev Neurosci *6*, 863-876

Notredame, C., Higgins, D.G., and Heringa, J. (2000). T-Coffee: A novel method for fast and accurate multiple sequence alignment. J Mol Biol *302*, 205-217

O'Brien, R.J., Kamboj, S., Ehlers, M.D., Rosen, K.R., Fischbach, G.D., and Huganir, R.L. (1998). Activity-dependent modulation of synaptic AMPA receptor accumulation. Neuron *21*, 1067-1078

O'Gorman, S., Dagenais, N.A., Qian, M., and Marchuk, Y. (1997). Protamine-Cre recombinase transgenes efficiently recombine target sequences in the male germ line of mice, but not in embryonic stem cells. Proc Natl Acad Sci U S A *94*, 14602-14607

Ohtsuka, T., Takao-Rikitsu, E., Inoue, E., Inoue, M., Takeuchi, M., Matsubara, K., Deguchi-Tawarada, M., Satoh, K., Morimoto, K., Nakanishi, H., and Takai, Y. (2002). Cast: a novel protein of the cytomatrix at the active zone of synapses that forms a ternary complex with RIM1 and munc13-1. J Cell Biol *158*, 577-590

Okada, Y., Yamazaki, H., Sekine-Aizawa, Y., and Hirokawa, N. (1995). The neuron-specific kinesin superfamily protein KIF1A is a unique monomeric motor for anterograde axonal transport of synaptic vesicle precursors. Cell *81*, 769-780

Oppenheim, R.W. (1991). Cell death during development of the nervous system. Annu Rev Neurosci *14*, 453-501

Ozaki, N., Shibasaki, T., Kashima, Y., Miki, T., Takahashi, K., Ueno, H., Sunaga, Y., Yano, H., Matsuura, Y., Iwanaga, T., Takai, Y., and Seino, S. (2000). cAMP-GEFII is a direct target of cAMP in regulated exocytosis. Nat Cell Biol *2*, 805-811

Paddock, B.E., Striegel, A.R., Hui, E., Chapman, E.R., and Reist, N.E. (2008). Ca2+-dependent, phospholipid-binding residues of synaptotagmin are critical for excitation-secretion coupling in vivo. J Neurosci *28*, 7458-7466

Pang, Z.P., Sun, J., Rizo, J., Maximov, A., and Sudhof, T.C. (2006a). Genetic analysis of synaptotagmin 2 in spontaneous and Ca2+-triggered neurotransmitter release. Embo J *25*, 2039-2050

Pang, Z.P., Melicoff, E., Padgett, D., Liu, Y., Teich, A.F., Dickey, B.F., Lin, W., Adachi, R., and Sudhof, T.C. (2006b). Synaptotagmin-2 is essential for survival and contributes to Ca2+ triggering of neurotransmitter release in central and neuromuscular synapses. J Neurosci *26*, 13493-13504

Parpura, V., Basarsky, T.A., Liu, F., Jeftinija, K., Jeftinija, S., and Haydon, P.G. (1994). Glutamate-mediated astrocyte-neuron signalling. Nature *369*, 744-747

Paxinos, G., Watson, C. (1988). the rat brain in sterotaxic coordinates, 4th ed. Academic Press)

Pelkey, K.A., Topolnik, L., Yuan, X.Q., Lacaille, J.C., and McBain, C.J. (2008). State-dependent cAMP sensitivity of presynaptic function underlies metaplasticity in a hippocampal feedforward inhibitory circuit. Neuron *60*, 980-987

Pelkey, K.A., and McBain, C.J. (2008). Target-cell-dependent plasticity within the mossy fibre-CA3 circuit reveals compartmentalized regulation of presynaptic function at divergent release sites. J Physiol *586*, 1495-1502

Pitsch, J., Schoch, S., Gueler, N., Flor, P.J., van der Putten, H., and Becker, A.J. (2007). Functional role of mGluR1 and mGluR4 in pilocarpine-induced temporal lobe epilepsy. Neurobiol Dis *26*, 623-633

Powell, C.M., Schoch, S., Monteggia, L., Barrot, M., Matos, M.F., Feldmann, N., Sudhof, T.C., and Nestler, E.J. (2004). The presynaptic active zone protein RIM1alpha is critical for normal learning and memory. Neuron *42*, 143-153

Prakash, S., McLendon, H.M., Dubreuil, C.I., Ghose, A., Hwa, J., Dennehy, K.A., Tomalty, K.M., Clark, K.L., Van Vactor, D., and Clandinin, T.R. (2009). Complex interactions amongst N-cadherin, DLAR, and Liprin-alpha regulate Drosophila photoreceptor axon targeting. Dev Biol *336*, 10-19

Priel, M.R., and Albuquerque, E.X. (2002). Short-term effects of pilocarpine on rat hippocampal neurons in culture. Epilepsia *43 Suppl 5*, 40-46

Regehr, W.G., and Tank, D.W. (1991). The maintenance of LTP at hippocampal mossy fiber synapses is independent of sustained presynaptic calcium. Neuron *7*, 451-459

Reid, C.A., Dixon, D.B., Takahashi, M., Bliss, T.V., and Fine, A. (2004). Optical quantal analysis indicates that long-term potentiation at single hippocampal mossy fiber synapses is expressed through increased release probability, recruitment of new release sites, and activation of silent synapses. J Neurosci *24*, 3618-3626

Remy, S., Urban, B.W., Elger, C.E., and Beck, H. (2003). Anticonvulsant pharmacology of voltage-gated Na+ channels in hippocampal neurons of control and chronically epileptic rats. Eur J Neurosci *17*, 2648-2658

Richmond, J.E., Weimer, R.M., and Jorgensen, E.M. (2001). An open form of syntaxin bypasses the requirement for UNC-13 in vesicle priming. Nature *412*, 338-341

Rickman, C., Craxton, M., Osborne, S., and Davletov, B. (2004). Comparative analysis of tandem C2 domains from the mammalian synaptotagmin family. Biochem J *378*, 681-686

Rizo, J., and Rosenmund, C. (2008). Synaptic vesicle fusion. Nat Struct Mol Biol *15*, 665-674

Robertson, J.D. (1953). Ultrastructure of two invertebrate synapses. Proc Soc Exp Biol Med *82*, 219-223

Roggero, C.M., De Blas, G.A., Dai, H., Tomes, C.N., Rizo, J., and Mayorga, L.S. (2007). Complexin/synaptotagmin interplay controls acrosomal exocytosis. J Biol Chem *282*, 26335-26343

Rosahl, T.W., Spillane, D., Missler, M., Herz, J., Selig, D.K., Wolff, J.R., Hammer, R.E., Malenka, R.C., and Sudhof, T.C. (1995). Essential functions of synapsins I and II in synaptic vesicle regulation. Nature *375*, 488-493

Rosenmund, C., Sigler, A., Augustin, I., Reim, K., Brose, N., and Rhee, J.S. (2002). Differential control of vesicle priming and short-term plasticity by Munc13 isoforms. Neuron *33*, 411-424

Rosenmund, C., Rettig, J., and Brose, N. (2003). Molecular mechanisms of active zone function. Curr Opin Neurobiol *13*, 509-519

Sabatini, B.L., and Regehr, W.G. (1996). Timing of neurotransmission at fast synapses in the mammalian brain. Nature *384*, 170-172

Sakharkar, M.K., and Kangueane, P. (2004). Genome SEGE: a database for 'intronless' genes in eukaryotic genomes. BMC Bioinformatics *5*, 67

Salin, P.A., Malenka, R.C., and Nicoll, R.A. (1996). Cyclic AMP mediates a presynaptic form of LTP at cerebellar parallel fiber synapses. Neuron *16*, 797-803

Santos, M.S., Li, H., and Voglmaier, S.M. (2009). Synaptic vesicle protein trafficking at the glutamate synapse. Neuroscience *158*, 189-203

Scharfman, H.E. (2007). The neurobiology of epilepsy. Curr Neurol Neurosci Rep *7*, 348-354

Schluter, O.M. (2004). A Complete Genetic Analysis of Neuronal Rab3 Function. Journal of Neuroscience *24*, 6629-6637

Schmitz, D., Mellor, J., Breustedt, J., and Nicoll, R.A. (2003). Presynaptic kainate receptors impart an associative property to hippocampal mossy fiber long-term potentiation. Nat Neurosci *6*, 1058-1063

Schneggenburger, R., and Neher, E. (2005). Presynaptic calcium and control of vesicle fusion. Curr Opin Neurobiol *15*, 266-274

Schoch, S., Deak, F., Konigstorfer, A., Mozhayeva, M., Sara, Y., Sudhof, T.C., and Kavalali, E.T. (2001). SNARE function analyzed in synaptobrevin/VAMP knockout mice. Science *294*, 1117-1122

Schoch, S., Castillo, P.E., Jo, T., Mukherjee, K., Geppert, M., Wang, Y., Schmitz, F., Malenka, R.C., and Sudhof, T.C. (2002). RIM1alpha forms a protein scaffold for regulating neurotransmitter release at the active zone. Nature *415*, 321-326

Schoch, S., and Gundelfinger, E.D. (2006). Molecular organization of the presynaptic active zone. Cell Tissue Res *326*, 379-391

Schoch, S., Mittelstaedt, T., Kaeser, P.S., Padgett, D., Feldmann, N., Chevaleyre, V., Castillo, P.E., Hammer, R.E., Han, W., Schmitz, F., Lin, W., and Sudhof, T.C. (2006). Redundant functions of RIM1alpha and RIM2alpha in Ca(2+)-triggered neurotransmitter release. Embo J *25*, 5852-5863

Schonn, J.S., Maximov, A., Lao, Y., Sudhof, T.C., and Sorensen, J.B. (2008). Synaptotagmin-1 and -7 are functionally overlapping Ca2+ sensors for

exocytosis in adrenal chromaffin cells. Proc Natl Acad Sci U S A *105*, 3998-4003

Serra-Pages, C., Medley, Q.G., Tang, M., Hart, A., and Streuli, M. (1998). Liprins, a family of LAR transmembrane protein-tyrosine phosphatase-interacting proteins. J Biol Chem *273*, 15611-15620

Serra-Pages, C., Streuli, M., and Medley, Q.G. (2005). Liprin Phosphorylation Regulates Binding to LAR: Evidence for Liprin Autophosphorylation. Biochemistry *44*, 15715-15724

Shaban, H., Humeau, Y., Herry, C., Cassasus, G., Shigemoto, R., Ciocchi, S., Barbieri, S., van der Putten, H., Kaupmann, K., Bettler, B., and Luthi, A. (2006). Generalization of amygdala LTP and conditioned fear in the absence of presynaptic inhibition. Nat Neurosci *9*, 1028-1035

Shin, H., Wyszynski, M., Huh, K.H., Valtschanoff, J.G., Lee, J.R., Ko, J., Streuli, M., Weinberg, R.J., Sheng, M., and Kim, E. (2003). Association of the kinesin motor KIF1A with the multimodular protein liprin-alpha. J Biol Chem *278*, 11393-11401

Shin, O.-H., Xu, J., Rizo, J., and Sudhof, T.C. (2009). Differential but convergent functions of Ca2+ binding to synaptotagmin-1 C2 domains mediate neurotransmitter release. Proceedings of the National Academy of Sciences of the United States of America *106*, 16469-16474

Siksou, L., Rostaing, P., Lechaire, J.P., Boudier, T., Ohtsuka, T., Fejtova, A., Kao, H.T., Greengard, P., Gundelfinger, E.D., Triller, A., and Marty, S. (2007). Three-dimensional architecture of presynaptic terminal cytomatrix. J Neurosci *27*, 6868-6877

Siksou, L., Triller, A., and Marty, S. (2009). An emerging view of presynaptic structure from electron microscopic studies. J Neurochem *108*, 1336-1342

Simsek-Duran, F., Linden, D.J., and Lonart, G. (2004). Adapter protein 14-3-3 is required for a presynaptic form of LTP in the cerebellum. Nat Neurosci *7*, 1296-1298

Spangler, S.A., and Hoogenraad, C.C. (2007). Liprin-alpha proteins: scaffold molecules for synapse maturation. Biochem Soc Trans *35*, 1278-1282

Spencer, J.P., and Murphy, K.P. (2002). Activation of cyclic AMP-dependent protein kinase is required for long-term enhancement at corticostriatal synapses in rats. Neurosci Lett *329*, 217-221

Steinhauser, C., Jabs, R., and Kettenmann, H. (1994). Properties of GABA and glutamate responses in identified glial cells of the mouse hippocampal slice. Hippocampus *4*, 19-35

Stenovec, M., Kreft, M., Grilc, S., Potokar, M., Kreft, M.E., Pangrsic, T., and Zorec, R. (2007). Ca2+-dependent mobility of vesicles capturing anti-VGLUT1 antibodies. Exp Cell Res *313*, 3809-3818

Stevens, D.R., Wu, Z.X., Matti, U., Junge, H.J., Schirra, C., Becherer, U., Wojcik, S.M., Brose, N., and Rettig, J. (2005). Identification of the minimal protein domain required for priming activity of Munc13-1. Curr Biol *15*, 2243-2248

Stryker, E., and Johnson, K.G. (2007). LAR, liprin alpha and the regulation of active zone morphogenesis. Journal of Cell Science *120*, 3723-3728

Sudhof, T.C. (2002). Synaptotagmins: why so many? J Biol Chem *277*, 7629-7632

Sugita, S., Han, W., Butz, S., Liu, X., Fernandez-Chacon, R., Lao, Y., and Sudhof, T.C. (2001). Synaptotagmin VII as a plasma membrane Ca(2+) sensor in exocytosis. Neuron *30*, 459-473

Sugita, S., Shin, O.H., Han, W., Lao, Y., and Sudhof, T.C. (2002). Synaptotagmins form a hierarchy of exocytotic Ca(2+) sensors with distinct Ca(2+) affinities. Embo J *21*, 270-280

Sun, J., Pang, Z.P., Qin, D., Fahim, A.T., Adachi, R., and Sudhof, T.C. (2007). A dual-Ca2+-sensor model for neurotransmitter release in a central synapse. Nature *450*, 676-682

Sun, L., Bittner, M.A., and Holz, R.W. (2003). Rim, a component of the presynaptic active zone and modulator of exocytosis, binds 14-3-3 through its N terminus. J Biol Chem *278*, 38301-38309

Sutton, M.A., and Schuman, E.M. (2006). Dendritic protein synthesis, synaptic plasticity, and memory. Cell *127*, 49-58

Takamori, S., Holt, M., Stenius, K., Lemke, E.A., Gronborg, M., Riedel, D., Urlaub, H., Schenck, S., Brugger, B., Ringler, P., Muller, S.A., Rammner, B., Grater, F., Hub, J.S., De Groot, B.L., Mieskes, G., Moriyama, Y., Klingauf, J., Grubmuller, H., Heuser, J., Wieland, F., and Jahn, R. (2006). Molecular anatomy of a trafficking organelle. Cell *127*, 831-846

Takao-Rikitsu, E., Mochida, S., Inoue, E., Deguchi-Tawarada, M., Inoue, M., Ohtsuka, T., and Takai, Y. (2004). Physical and functional interaction of the active zone proteins, CAST, RIM1, and Bassoon, in neurotransmitter release. J Cell Biol *164*, 301-311

Thompson, C.C. (1996). Thyroid hormone-responsive genes in developing cerebellum include a novel synaptotagmin and a hairless homolog. J Neurosci *16*, 7832-7840

Ting, J.T., Kelley, B.G., and Sullivan, J.M. (2006). Synaptotagmin IV does not alter excitatory fast synaptic transmission or fusion pore kinetics in mammalian CNS neurons. J Neurosci *26*, 372-380

Tocco, G., Bi, X., Vician, L., Lim, I.K., Herschman, H., and Baudry, M. (1996). Two synaptotagmin genes, Syt1 and Syt4, are differentially regulated in adult brain and during postnatal development following kainic acid-induced seizures. Brain Res Mol Brain Res *40*, 229-239

Tokuoka, H., and Goda, Y. (2008). Activity-dependent coordination of presynaptic release probability and postsynaptic GluR2 abundance at single synapses. Proc Natl Acad Sci U S A *105*, 14656-14661

tom Dieck, S., Sanmarti-Vila, L., Langnaese, K., Richter, K., Kindler, S., Soyke, A., Wex, H., Smalla, K.H., Kampf, U., Franzer, J.T., Stumm, M., Garner, C.C., and Gundelfinger, E.D. (1998). Bassoon, a novel zinc-finger CAG/glutamine-repeat protein selectively localized at the active zone of presynaptic nerve terminals. J Cell Biol *142*, 499-509

Towbin, H., Staehelin, T., and Gordon, J. (1979). Electrophoretic transfer of proteins from polyacrylamide gels to nitrocellulose sheets: procedure and some applications. Proc Natl Acad Sci U S A *76*, 4350-4354

Tucker, W.C., and Chapman, E.R. (2002). Role of synaptotagmin in Ca2+-triggered exocytosis. Biochem J *366*, 1-13

Turrigiano, G.G., Leslie, K.R., Desai, N.S., Rutherford, L.C., and Nelson, S.B. (1998). Activity-dependent scaling of quantal amplitude in neocortical neurons. Nature *391*, 892-896

Turski, W.A., Cavalheiro, E.A., Schwarz, M., Czuczwar, S.J., Kleinrok, Z., and Turski, L. (1983). Limbic seizures produced by pilocarpine in rats: behavioural, electroencephalographic and neuropathological study. Behav Brain Res *9*, 315-335

Ullrich, B., Li, C., Zhang, J.Z., McMahon, H., Anderson, R.G., Geppert, M., and Sudhof, T.C. (1994). Functional properties of multiple synaptotagmins in brain. Neuron *13*, 1281-1291

Ullrich, B., and Sudhof, T.C. (1995). Differential distributions of novel synaptotagmins: comparison to synapsins. Neuropharmacology *34*, 1371-1377

Varoqueaux, F., Sigler, A., Rhee, J.S., Brose, N., Enk, C., Reim, K., and Rosenmund, C. (2002). Total arrest of spontaneous and evoked synaptic transmission but normal synaptogenesis in the absence of Munc13-mediated vesicle priming. Proc Natl Acad Sci U S A *99*, 9037-9042

Varoqueaux, F., Sons, M.S., Plomp, J.J., and Brose, N. (2005). Aberrant morphology and residual transmitter release at the munc13-deficient mouse neuromuscular synapse. Mol Cell Biol *25*, 5973-5984

Vician, L., Lim, I.K., Ferguson, G., Tocco, G., Baudry, M., and Herschman, H.R. (1995). Synaptotagmin IV is an immediate early gene induced by depolarization in PC12 cells and in brain. Proc Natl Acad Sci U S A *92*, 2164-2168

Virmani, T., Han, W., Liu, X., Sudhof, T.C., and Kavalali, E.T. (2003). Synaptotagmin 7 splice variants differentially regulate synaptic vesicle recycling. Embo J *22*, 5347-5357

Volterra, A., and Meldolesi, J. (2005). Astrocytes, from brain glue to communication elements: the revolution continues. Nat Rev Neurosci *6*, 626-640

von Poser, C., Ichtchenko, K., Shao, X., Rizo, J., and Sudhof, T.C. (1997). The evolutionary pressure to inactivate. A subclass of synaptotagmins with an amino acid substitution that abolishes Ca2+ binding. J Biol Chem *272*, 14314-14319

von Poser, C., and Sudhof, T.C. (2001). Synaptotagmin 13: structure and expression of a novel synaptotagmin. Eur J Cell Biol *80*, 41-47

Wagh, D.A., Rasse, T.M., Asan, E., Hofbauer, A., Schwenkert, I., Durrbeck, H., Buchner, S., Dabauvalle, M.C., Schmidt, M., Qin, G., Wichmann, C., Kittel, R., Sigrist, S.J., and Buchner, E. (2006). Bruchpilot, a protein with homology to ELKS/CAST, is required for structural integrity and function of synaptic active zones in Drosophila. Neuron *49*, 833-844

Wang, C.T., Grishanin, R., Earles, C.A., Chang, P.Y., Martin, T.F., Chapman, E.R., and Jackson, M.B. (2001a). Synaptotagmin modulation of fusion pore kinetics in regulated exocytosis of dense-core vesicles. Science *294*, 1111-1115

Wang, C.T., Lu, J.C., Bai, J., Chang, P.Y., Martin, T.F., Chapman, E.R., and Jackson, M.B. (2003). Different domains of synaptotagmin control the choice between kiss-and-run and full fusion. Nature *424*, 943-947

Wang, P., Chicka, M.C., Bhalla, A., Richards, D.A., and Chapman, E.R. (2005). Synaptotagmin VII is targeted to secretory organelles in PC12 cells, where it functions as a high-affinity calcium sensor. Mol Cell Biol *25*, 8693-8702

Wang, X., Hu, B., Zimmermann, B., and Kilimann, M.W. (2001b). Rim1 and rabphilin-3 bind Rab3-GTP by composite determinants partially related through N-terminal alpha -helix motifs. J Biol Chem *276*, 32480-32488

Wang, Y., Okamoto, M., Schmitz, F., Hofmann, K., and Sudhof, T.C. (1997). Rim is a putative Rab3 effector in regulating synaptic-vesicle fusion. Nature *388*, 593-598

Wang, Y., Sugita, S., and Sudhof, T.C. (2000). The RIM/NIM family of neuronal C2 domain proteins. Interactions with Rab3 and a new class of Src homology 3 domain proteins. J Biol Chem *275*, 20033-20044

Wang, Y., Liu, X., Biederer, T., and Sudhof, T.C. (2002). A family of RIM-binding proteins regulated by alternative splicing: Implications for the genesis of synaptic active zones. Proc Natl Acad Sci U S A *99*, 14464-14469

Wang, Y., and Sudhof, T.C. (2003). Genomic definition of RIM proteins: evolutionary amplification of a family of synaptic regulatory proteins(small star, filled). Genomics *81*, 126-137

Washbourne, P., Thompson, P.M., Carta, M., Costa, E.T., Mathews, J.R., Lopez-Bendito, G., Molnar, Z., Becher, M.W., Valenzuela, C.F., Partridge, L.D., and Wilson, M.C. (2002). Genetic ablation of the t-SNARE SNAP-25 distinguishes mechanisms of neuroexocytosis. Nat Neurosci *5*, 19-26

Weimer, R.M., and Jorgensen, E.M. (2003). Controversies in synaptic vesicle exocytosis. J Cell Sci *116*, 3661-3666

Weimer, R.M., Gracheva, E.O., Meyrignac, O., Miller, K.G., Richmond, J.E., and Bessereau, J.L. (2006). UNC-13 and UNC-10/rim localize synaptic vesicles to specific membrane domains. J Neurosci *26*, 8040-8047

Weninger, K., Bowen, M.E., Choi, U.B., Chu, S., and Brunger, A.T. (2008). Accessory proteins stabilize the acceptor complex for synaptobrevin, the 1:1 syntaxin/SNAP-25 complex. Structure *16*, 308-320

Whelan, S., and Goldman, N. (2001). A general empirical model of protein evolution derived from multiple protein families using a maximum-likelihood approach. Mol Biol Evol *18*, 691-699

Wierenga, C.J., Walsh, M.F., and Turrigiano, G.G. (2006). Temporal regulation of the expression locus of homeostatic plasticity. J Neurophysiol *96*, 2127-2133

Wieser, H.G., and Hane, A. (2004). Antiepileptic drug treatment in seizure-free mesial temporal lobe epilepsy patients with hippocampal sclerosis following selective amygdalohippocampectomy. Seizure *13*, 534-536

Wyszynski, M., Kim, E., Dunah, A.W., Passafaro, M., Valtschanoff, J.G., Serra-Pages, C., Streuli, M., Weinberg, R.J., and Sheng, M. (2002). Interaction between GRIP and liprin-alpha/SYD2 is required for AMPA receptor targeting. Neuron *34*, 39-52

Xiao, Z., Gong, Y., Wang, X.F., Xiao, F., Xi, Z.Q., Lu, Y., and Sun, H.B. (2009). Altered expression of synaptotagmin I in temporal lobe tissue of patients with refractory epilepsy. J Mol Neurosci *38*, 193-200

Xu, J., Mashimo, T., and Sudhof, T.C. (2007). Synaptotagmin-1, -2, and -9: Ca(2+) sensors for fast release that specify distinct presynaptic properties in subsets of neurons. Neuron *54*, 567-581

Xu, J., Pang, Z.P., Shin, O.H., and Sudhof, T.C. (2009). Synaptotagmin-1 functions as a Ca(2+) sensor for spontaneous release. Nat Neurosci

Xue, M., Ma, C., Craig, T.K., Rosenmund, C., and Rizo, J. (2008). The Janus-faced nature of the C(2)B domain is fundamental for synaptotagmin-1 function. Nat Struct Mol Biol *15*, 1160-1168

Yao, I., Takagi, H., Ageta, H., Kahyo, T., Sato, S., Hatanaka, K., Fukuda, Y., Chiba, T., Morone, N., Yuasa, S., Inokuchi, K., Ohtsuka, T., Macgregor, G.R., Tanaka, K., and Setou, M. (2007). SCRAPPER-dependent ubiquitination of active zone protein RIM1 regulates synaptic vesicle release. Cell *130*, 943-957

Yokota, T., Nakata, T., Minami, S., Inazawa, J., and Emi, M. (2000). Genomic organization and chromosomal mapping of ELKS, a gene rearranged in a papillary thyroid carcinoma. J Hum Genet *45*, 6-11

Yoshihara, M., and Littleton, J.T. (2002). Synaptotagmin I functions as a calcium sensor to synchronize neurotransmitter release. Neuron *36*, 897-908

Yoshihara, M., and Montana, E.S. (2004). The synaptotagmins: calcium sensors for vesicular trafficking. Neuroscientist *10*, 566-574

Yudowski, G.A., Puthenveedu, M.A., Leonoudakis, D., Panicker, S., Thorn, K.S., Beattie, E.C., and von Zastrow, M. (2007). Real-time imaging of discrete exocytic events mediating surface delivery of AMPA receptors. J Neurosci *27*, 11112-11121

Zhai, R.G., and Bellen, H.J. (2004). The architecture of the active zone in the presynaptic nerve terminal. Physiology (Bethesda) *19*, 262-270

Zhang, Q., Fukuda, M., Van Bockstaele, E., Pascual, O., and Haydon, P.G. (2004). Synaptotagmin IV regulates glial glutamate release. Proc Natl Acad Sci USA *101*, 9441-9446

Zhang, Q., Li, Y., and Tsien, R.W. (2009). The dynamic control of kiss-and-run and vesicular reuse probed with single nanoparticles. Science *323*, 1448-1453

Zhen, M., and Jin, Y. (1999). The liprin protein SYD-2 regulates the differentiation of presynaptic termini in C. elegans. Nature *401*, 371-375

Zhou, J., Du, Y.R., Qin, W.H., Hu, Y.G., Huang, Y.N., Bao, L., Han, D., Mansouri, A., and Xu, G.L. (2009). RIM-BP3 is a manchette-associated protein essential for spermiogenesis. Development *136*, 373-382

Zurner, M., and Schoch, S. (2009). The mouse and human Liprin-alpha family of scaffolding proteins: genomic organization, expression profiling and regulation by alternative splicing. Genomics *93*, 243-253

Erklärung

Hiermit erkläre ich, dass ich die vorliegende Dissertation selbständig angefertigt habe. Es wurden nur die in der Arbeit ausdrücklich benannten Quellen und Hilfsmittel benutzt. Wörtlich oder sinngemäß übernommenes Gedankengut habe ich als solches kenntlich gemacht.

_____

Ort, Datum

_____

Unterschrift